KUNGL TEKNISKA HÖGSKOLAN

ISBN 91-7170-540-6
ISRN KTH/KRV/R-00/3-SE
TRITA-KRV-2000-3
ISSN 110-7990

Significance of Loss Models in Aerothermodynamic Simulation for Axial Turbines

Ning WEI

Doctoral Thesis
2000

Department of Energy Technology
Division of Heat and Power Technology
Royal Institute of Technology

KUNGL
TEKNISKA
HÖGSKOLAN

ISBN 91-7170-540-6
ISRN KTH/KRV/R-00/3-SE
TRITA-KRV-2000-3
ISSN 110-7990

Significance of Loss Models in Aerothermodynamic Simulation for Axial Turbines

Ning WEI

Doctoral Thesis
2000

Department of Energy Technology
Division of Heat and Power Technology
Royal Institute of Technology

Akademisk avhandling som med tillstånd från Kungliga Tekniska Högskolan (Royal Institute of Technology) i Stockholm framläggas till offentlig granskning för avläggande av teknisk doktorsexamen i Energiteknik, fredag den 26 maj 2000 i sal M3, Kungliga Tekniska Högskolan, Brinellvägen 64, Stockholm.

ABSTRACT

This thesis deals with a study of the significance of loss models and their applications in simulation and optimisation of axial turbines. The design of a turbomachine system is a very complex engineering operation which can be looked upon as an iterative procedure made of various steps. Computational tools for simulating and optimising turbomachines are needed nowadays in order to design turbines more effectively and efficiently. In order to use the tools to analyse elaborate thermodynamic cycles and optimise the cycles for different assignments, aerothermodynamic performances over each blade row in turbines have to be predicted in a correct trend and reasonable accurate in a wide operating range. Because the flow in a turbine is complex and many mechanisms of the flow losses in turbine have not be known well, loss models are needed, not only in the preliminary process of mean line prediction but also in the further process of through flow calculation, in the simulation and optimisation of turbines. Most of the loss models are empirical while some of them are established with combination of test data and analysis of physical origins of the losses.

The objectives of this thesis are to further understand and develop loss models and therefore to achieve useful guides for applying the models properly in turbine aerothermodynamic simulation and optimisation.

In this thesis, concepts of the flow field, loss mechanisms and classification and definition of loss coefficient in axial turbines are introduced in Chapter 1. In Chapter 2, some loss models published in the literature for axial turbines are reviewed and studied in detail. An effort is also made, in this chapter, to develop a simple method for approximately predicting overall film cooling losses in a turbine blade row based on equation of mass, momentum and energy conservation in mixing flows. In Chapter 3, five axial turbine stages, which have been used for the study, are introduced. These turbine stages are with different geometrical parameters, with impulse and reaction and untwisted and free vortex blading, and work at different flow conditions, in subsonic and supersonic flow and cooling and non-cooling conditions. In Chapter 4, mean line performances of these turbine stages were simulated with different loss models which are the models by Ainley/Mathieson/Dunham/Came (AMDC), Kacker/Okapuu, Craig/Cox and Moustaph/Kacker supplemented with the new developed cooling loss prediction method. The simulations were performed within large operating ranges which cover design and off-design points. The predicted results from the mean line performance calculation in the loss models were compared with the experimental data. In Chapter 5, an analysis of the optimum pitch/chord ratio for both the stator and rotor in one of these turbine stages was made through studying the total losses predicted in the loss models.

It was found that all these loss models give the same trend of overall performance compared with the trend of experimental results on the turbine stages. For the impulse turbine stages, it was showed that all these loss models seem to overestimate losses in the whole operation range and the AMDC model is one which most overestimates the losses while the Craig/Cox model gives the loss closest to the experimental results at and near the design point. When the aspect ratios in the impulse turbine stages increase about 25%, the results showed that the models give about 15-30% lower total losses. For the free vortex blading turbine, it was found that the losses are underpredicted in all the models, especially on the off-design operation points, because the high losses at the hub wall caused by the blading of free vortex are underestimated by using the parameters at mean line. For the high pressure and

temperature cooled turbine stage, the predicted results showed that all these models predict higher efficiencies than the experiments because the lack of cooling loss calculation in the models. The AMDC and Craig/Cox models seem to give close results to the experiments in this cooling turbine stage because of the fortuity of overestimated uncooled turbine losses. After adding the cooling losses predicted with the new developed method in the thesis, the trends of simulated performances in this turbine stage have better agreement with the trend of experimental data. In the analysis of the optimum pitch/chord ratio, the results showed that the pitch/chord ratio evaluated by total losses is not very critical and all the models gave similar low loss regions of pitch/chord ratios in which the total losses do not change significantly. This implies there will be no significant difference between these loss models if they are employed to obtain the optimum pitch/chord ratio in turbine optimisation process.

ACKNOWLEDGEMENT

I would like to express thanks to my supervisor, professor Torsten Fransson, for his supervision and guidance in this research work.

I would like to thank Volvo Aero Corporation, in Sweden, for their financial support of the research and the support of technical information. The thanks also go to Dr. Anders Lundbladh, Thomas Johansson and Thomas Grönstedt, who are personnel working in Volvo Aero Corporation, for their kindly help and advice.

I would also like to thank ABB-STAL in Sweden for the support of experimental information to this research.

I would like to acknowledge professor Ulf Håll, Chalmers University of Technology, Sweden, for his advice and help on the understanding of the loss models and establishment of the turbine performance calculating program.

I would also like to acknowledge professor Björn Kjellström, now at Luleå University of Technology in Sweden, for that he took me in the Department of Energy Technology of the Royal Institute of Technology, and gave me a chance to initiate my Ph.D. program here.

Finally, I would like to thank my wife, Zhang Yi, and my sons, Sibo and Boyang, for their encouraging, supporting and understanding when I performed this thesis.

Content

NOMENCLATURE

Latin characters

A	Flow channel area	[m^2]
A_w	Endwall surface area between stator and rotor	[m^2]
Δ_a	Tangential trailing edge projection	[-]
C_d	Blade surface dissipation coefficient	[-]
C_p	Specific heat capacity (at constant pressure)	[kJ/kgK]
C_s	Blade surface length counted from the leading edge to the trailing edge	[-]
C_x	Blade axial chord	[m]
c_f	Friction factor	[-]
c_0	Absolute velocity upstream the stator	[m/s]
c	Flow absolute velocity	[m/s]
$\bar{c}$	Absolute velocity at Euler radius	[m/s]
c_M	Torque coefficient	[-]
c_x	Axial component of the flow absolute velocity	[m/s]
D	Diameter	[m]
F	Lift factor	[-]
f_{sp}	Leakage area	[m^2]
H	Blade span	[m]
h	Specific enthalpy	[kJ/kg]
h_R	Specific rothalpy, $h_R = h+w^2/2-u^2/2$	[kJ/kg]
$\Delta h'_S$	Enthalpy drop over the stator	[kJ/kg]
$\Delta h_{is,S}$	Isentropic enthalpy drop over the stator	[kJ/kg]
$\Delta h''_S$	enthalpy drop over the rotor	[kJ/kg]
$\Delta h_{is,R}$	Isentropic enthalpy drop over the rotor	[kJ/kg]
Δh	Real enthalpy drop over the stage	[kJ/kg]
Δh_{is}	Isentropic enthalpy drop over the stage	
$i+$	Positive incidence angle	[deg]
$i-$	Negative incidence angle	[deg]
k_s	Surface sand roughness	[m]
l	Blade chord	[m]
l_1	Stator outlet blade span	[m]
l_2	Rotor outlet blade span	[m]
l_r	Rotor chord	[m]
l_s	Stator chord	[m]
M	Mach number	[-]
$\dot{m}$	Mass flow	[kg/s]
$\dot{m}$	Rotor tip clearance leakage mass flow	[kg/s]
$\dot{m}$	Main mass flow through the rotor cascade	[kg/s]
n	Rotational speed	[rpm]
o	Blade throat width	
p	Static pressure	[Pa]
$p_{b,N}$	Stator base pressure	[Pa]
$p_{b,R}$	Rotor base pressure	[Pa]
p_c	Stagnation pressure	[Pa]

Δp	Static pressure drop	[Pa]
R	Specific gas constant for air	[J/kgK]
R	Degree of reaction	[-]
Re	Reynolds number	[-]
r	Radius	[m]
$\bar{r}$	Euler radius	[m]
$\Delta S_{Bb,N}$	Entropy rate created during growth of the boundary layer on the stator blade surfaces	[kJ/kgK]
$\Delta S_{Bb,R}$	Entropy rate created during growth of the boundary layer on the rotor blade surfaces	[kJ/kgK]
$\Delta S_{Eb,Bt}$	Entropy rate created during growth of the endwall boundary layer between stator and rotor	[kJ/kgK]
ΔS	Entropy rate created during growth of the stator endwall boundary layer	[kJ/kgK]
ΔS	Entropy rate created during growth of the rotor endwall boundary layer	[kJ/kgK]
s	Blade chord	[m]
s	Specific entropy	[kJ/kgK]
s	Distance on blade surface	[m]
T_0	Temperature before the stator, static	[K]
T_1	Temperature after the stator, static	[K]
T_2	Temperature after the rotor, static	[K]
t	Pitch	[m]
t'_{max}	Maximum blade thickness	[m]
t'_N	Stator trailing edge thickness	[m]
t'_R	Rotor trailing edge thickness	[m]
u	Blade speed	[m/s]
w	Flow relative velocity	[m/s]
x	Distance in axial direction	[m]
y	Distance in tangential direction	[m]
y_N	Local gap between the stator pressure and suction surfaces	[m
y_R	Local gap between the rotor pressure and suction surfaces	[m]
Y	Pressure loss coefficient	[-]
Y_{fc}	Film cooling loss coefficient	[-]
Y_P	Profile loss component of pressure loss coefficient	[-]
Y_S	Secondary loss component of pressure loss coefficient	[-]
Y_{te}	Tailing edge loss component of pressure loss coefficient	[-]
Y_{Tl}	Tip leakage loss component of pressure loss coefficient	[-]
z	Number of labyrinth strips	[-]

<u>Greek characters</u>

α	Leakage ratio	[-]
α	Flow angle	[deg]
α'	Blade angle	[deg]
α_0	Stator absolute inlet flow angle	[deg]
α_1	Stator absolute outlet flow angle	[deg]
β_1	Rotor relative inlet flow angle	[deg]

β_2	Rotor relative outlet flow angle	[deg]
χ_M	Mach number correction factor	[-]
χ_R	Reynolds number correction factor	[-]
δ	Trailing edge thickness	[m]
δ_{a1}	Axial tip gap between rotor and upstream stator [	[m]
δ_{a2}	Axial tip gap between rotor and downstream stator	[m]
δ^*_N	Stator trailing edge total boundary layer momentum thickness	[m]
δ^*_R	Rotor trailing edge total boundary layer momentum thickness	[m]
ε	Blade deflection (blade turning angle)	[deg]
ϕ^2	Kinetic energy loss coefficient (actual gas exit velocity/ideal gas exit velocity)	
γ	Isentropic exponent	[-]
γ	Stagger angle	[deg]
η	Efficiency	[-]
φ	Flow number	[-]
θ_N	Stator trailing edge total boundary layer displacement thickness	[m]
θ_R	Rotor trailing edge total boundary layer displacement thickness	[m]
ρ	Density	[kg/m^3]
π	Pressure ratio	[-]
υ	Kinematic viscosity	[m^2/s]
μ	Dynamic viscosity	[kg/sm]
μ	Relative mass flow	[-]
ν	Velocity ratio	[-]
$n(a_0^*)$	Velocity ratio at nominal conditions	[-]
$n(b_1^*)$	Velocity ratio at nominal conditions	[-]
ξ	Enthalpy loss coefficient referred to the isentropic velocity	[-]
τ	Tip clearance distance	[m]
ψ	Pressure number	[-]
ζ	Enthalpy loss coefficient	[-]
ζ_a	Axial distance loss coefficient	[-]
$\zeta_{Bb,N}$	Stator blade surface boundary layer loss coefficient	[-]
$\zeta_{Bb,R}$	Rotor blade surface boundary layer loss coefficient	[-]
ζ_c	Carnot shock loss coefficient	[-]
ζ_D	Loss coefficient according to Denton	[-]
$\zeta_{Eb,Bt}$	Endwall boundary layer loss coefficient between stator and rotor	[-]
$\zeta_{Ebi,N}$	Stator endwall boundary layer loss coefficient	[-]
$\zeta_{Ebi,R}$	Rotor endwall boundary layer loss coefficient	[-]
ζ_F	Humidity loss coefficient	[-]
ζ_f	Fan loss coefficient	[-]
ζ_{fc}	Film cooling loss coefficient	[-]
ζ_h	Trailing edge loss coefficient	[-]

ζ_N	Stator loss coefficient	[-]
ζ_p	Profile loss coefficient	[-]
ζ_{p0}	Basic profile loss coefficient	[-]
ζ_R	Rotor loss coefficient	[-]
ζ_s	Secondary loss coefficient	[-]
ζ_{sp}	Tip leakage loss coefficient	[-]
ζ_T	Loss coefficient according to Traupel	[-]
$\zeta_{Te,N}$	Stator trailing edge loss coefficient	[-]
$\zeta_{Te,R}$	Rotor trailing edge loss coefficient	[-]
$\zeta_{Tl,R}$	Rotor tip leakage loss coefficient	[-]
ζ_V	Ventilation loss coefficient	[-]
ζ_z	Other loss coefficient	[-]
Ω	Blade channel annulus area	[m^2]

Suffix

0	Upstream the stator
1	Upstream the rotor
2	Downstream the rotor
a	Axial
b	Base pressure
c	Stagnation values in absolute reference frame
hub	Hub
in	Inlet
is	Isentropic
m	Mean value
m	Mechanically
N	Stator (Nozzle)
out	Outlet
p	Pressure surface
R	Rotor
r	Rotor
s	Stator
s	Suction surface
tip	Tip, Casing
tot	Total
ts	Total-to-static
tt	Total-to-total
w	Stagnation values in relative reference frame

Superscripts

*	Nominal condition, design point

1 INTRODUCTION

1.1 General Introduction

Of the various means of producing mechanical power, Turbomachine is in many respects the most satisfactory. The absence of reciprocating and rubbing members means that balancing problems are few, that the lubricating oil consumption is exceptionally low, and that reliability can be high. Turbomachines are widely used today through the world as power generators, mechanical drives, marine and aircraft engines. The demand for turbomachines in the future will certainly increase. For example, the total demand for gas turbines in the world is estimated to be 750-900 GW by the year 2010 [Franus, 1994]. In order to use the existing energy resources, such as coal, oil, gas and biomass fuel, efficiently, turbomachine designs with low losses, high efficiency and desirable performance are needed.

The design procedure of a turbomachine is a very complex engineering operation, involving thermodynamic, aerodynamic, technological, structural and economic aspects. Thermo and aerodynamic designs in turbomachines can be looked upon as an iterative procedure made of various steps, in which the previously assumed (or computed) values are progressively modified according to the results of more refined flow calculations. A typical structure of the design system for an axial flow turbomachine is represented in Fig. 1.1.1.

The designs are usually performed by starting from focusing on simple performance predictions of the flow at the mean line of blade height (see the part in the dot line rectangular in Fig. 1.1.1). In choosing the gas path for a new turbine, the designer has to carry out an optimization study which involves the calculation of velocity triangles in order to obtain the minimum losses. Blade lengths and radii are thereby determined early in the design cycle before blade shapes are known. This is done by means of a mean line velocity triangle calculation, which is based on the assumption that the thermodynamic processes undergone by the working fluid can be represented by velocity triangle at midspan. This mean line calculation is just the very preliminary step in the design of a turbomachine. However, the importance of this phase should not be underestimated. For instance, it is known that the efficiency of a properly designed axial flow turbine can be predicted with fair accuracy (1 or 2%) by the adoption of simple mean line analysis methods which incorporate proper loss and flow angle correlations [Macchi, 1985]. This implies, if it is correct, that the efficiency of a turbine is set, within a narrow range, simply by the selection of the basic design parameters. The increase of the efficiency by all other design phases is limited. Obviously, one should not underestimate the importance of the role played by very accurate blade design procedures or flow analysis made nowadays possible by computational fluid dynamics. However the first predictions on turbomachine main characteristics by mean line calculation, which are input data to subsequent calculations, are of great importance too.

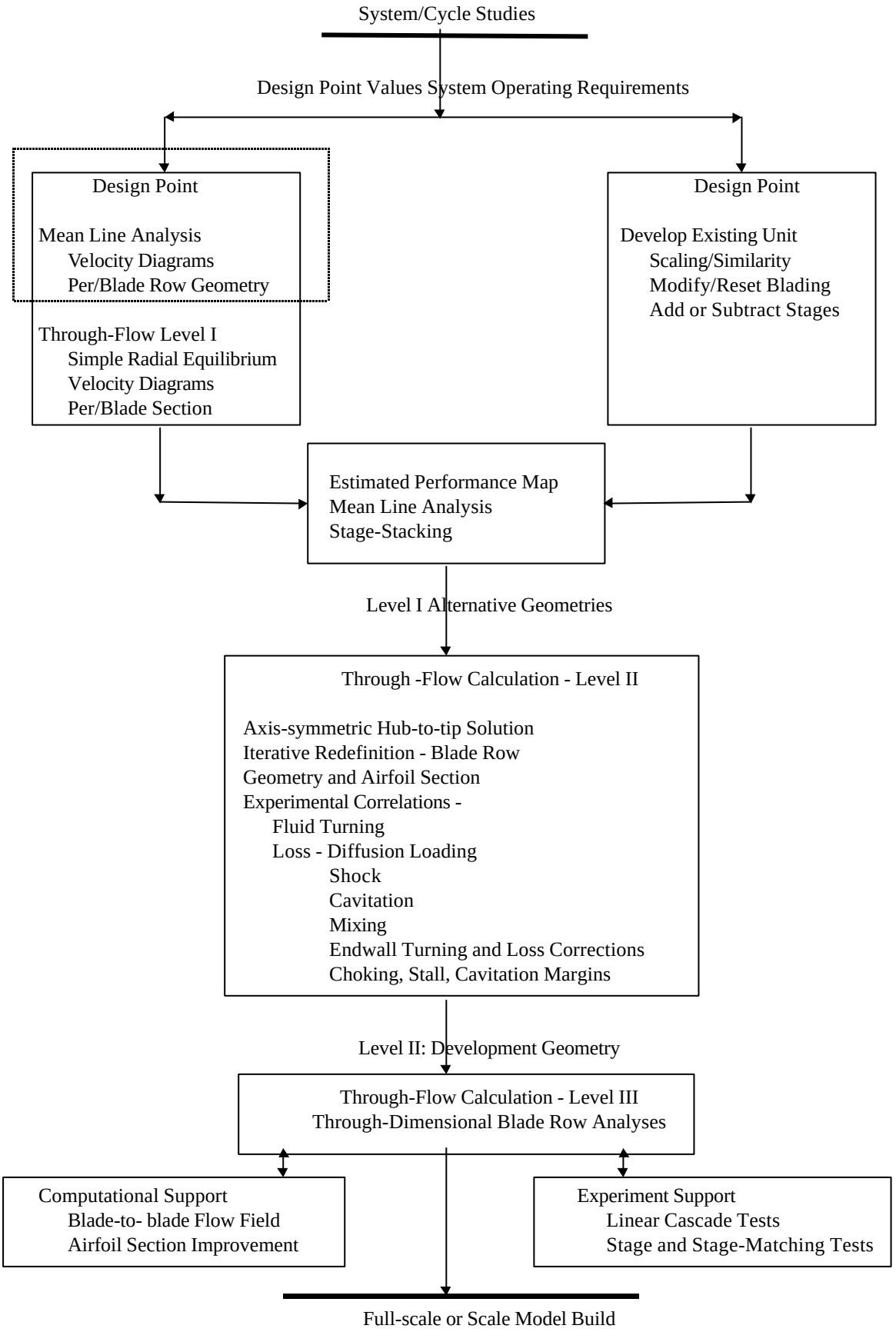
System/Cycle Studies
Design Point Values System Operating Requirements
Design Point
Mean Line Analysis
Velocity Diagrams
Per/Blade Row Geometry
Through-Flow Level I
Simple Radial Equilibrium
Velocity Diagrams
Per/Blade Section
Design Point
Develop Existing Unit
Scaling/Similarity
Modify/Reset Blading
Add or Subtract Stages
Estimated Performance Map
Mean Line Analysis
Stage-Stacking
Level I Alternative Geometries
Through -Flow Calculation - Level II
Axis-symmetric Hub-to-tip Solution
Iterative Redefinition - Blade Row
Geometry and Airfoil Section
Experimental Correlations -
Fluid Turning
Loss - Diffusion Loading
Shock
Cavitation
Mixing
Endwall Turning and Loss Corrections
Choking, Stall, Cavitation Margins
Level II: Development Geometry
Through-Flow Calculation - Level III
Through-Dimensional Blade Row Analyses
Computational Support
Blade-to- blade Flow Field
Airfoil Section Improvement
Experiment Support
Linear Cascade Tests
Stage and Stage-Matching Tests
Full-scale or Scale Model Build

Fig. 1.1.1: *Typical structure of a design system for axial flow turbomachines [Macchi, 1985, Fig. 1].*

To produce an optimum gas path such calculation must incorporate parameters of aerodynamic losses. As the loss mechanisms in turbomachines are very complex (a brief discussion of the origins of the losses in an axial turbine passage will be made in the following section of this chapter) and the full scale tests are rarely possible, the losses must be predicted by using empirical models. This prediction with empirical loss models will yield useful indications about the losses breakdown and about the way to follow in the optimisations.

Computational tools for analysing and optimising aeroengines are needed by any aeroengine industry. It is required that the tools can be used to analyse elaborate engine cycles, including simulation of the off-design conditions, and optimise the cycles for different assignments. For these purposes, the turbine and compressor in the engine have to be optimised and analysed, therefore methods for predicting losses through compressor and turbine components in engines are greatly needed. A number of empirical loss prediction methods for prediction total losses in turbomachines have been described in the open literature. A detailed discussion on the loss models for axial turbines will be performed in Chapter 2. In order to apply the loss models properly, it is needed to see what are the different characteristics of various loss prediction methods in applications and what are the physical concepts behind the different methods. However, a limited amount of such work has been found in open literature.

The objective of this thesis is to make a detailed systematic analysis of the turbine performance prediction with different loss models in various blade geometrical parameters at both the design and off-design conditions and to further understand the significance of the models in order to apply them properly in turbine aerothermodynamic simulation and optimisation.

In this thesis, mean line performance simulations on 5 turbine stages with different geometrical parameters, impulse and reaction stages, and flow conditions, sub- and supersonic flow, are made with different loss models. The calculations are within a large operating range which covers both design and off-design points. The loss models applied in the calculations are the models by Ainley/Mathieson, Dunham/Came, Kacker/Okapuu, Craig/Cox, Moustaph/Kacker. In the calculation, the main input data are the stage inlet stagnation pressure and temperature, mass flow, turbine speed and geometric parameters of the stator and the rotor. These data are taken from experiments and the original design of the stage. Then the flow parameters at each section and the overall performance parameters of the stage are predicted row by row. The calculations are based on the principle of conservation of mass, momentum and energy over every blade row. In this approach, loss models have to be used to determine the entropy increase across each section in the turbine stage. Finally, the analysis and comparisons between the calculated results and experimental data are performed.

1.2 Flow Field and Loss Mechanisms in Axial Turbines

Flows through a turbine blade passage are very complex. Both the geometric description of the fluid flow domain and the physical processes present are extremely complicated. In axial turbines, flows are always three-dimensional, viscous, and unsteady. They may be incompressible or compressible, with subsonic, transonic, and supersonic regimes which may be present simultaneously in different regions. The viscous flow usually has high free-stream turbulence which may include multiple length and time scales. Regions of laminar, transitional and turbulent flows, separated flows and fully developed viscous profiles may all be present simultaneously due to the multiplicity of length scales introduced by the complicated geometry of the flow field. The viscous and turbulent regions encounter complex stress and strain due to the presence of three-dimensionality, large pressure gradients in all directions, rotation, curvature, shock waves, shock wave-boundary layer interaction, interacting boundary layers and wakes and heat transfer. A schematic representation of the flow field through an axial turbine blade passage is shown in Fig. 1.2.1.

The geometric description of the flow regions includes many parameters having different length scales. Associated with the blade profile are stagger angle, blade camber, chord, blade spacing, maximum thickness, thickness distribution, leading and trailing edge radii, surface roughness and cooling hole distribution. Associated with the flow path are radial distribution of stagger angle, camber and thickness, lean, twist, sweep, skew, flare, aspect ratio, hub/tip ratio, tip clearance, endwall curvature, flow path area change, axial spacing between blade rows and radial distribution of cooling holes.

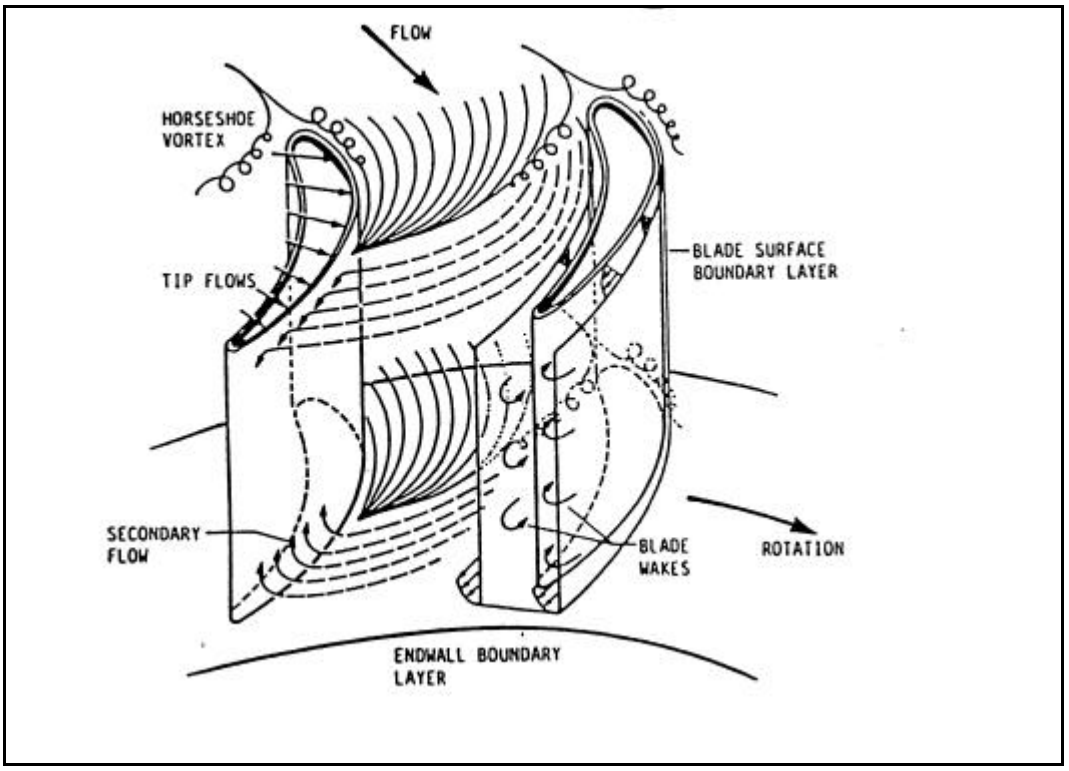

Fig. 1.2.1: *Flow structure in a turbine cascade [Denton, 1994]*

When the flow on a turbine blade surface is laminar, transitional flows are often encountered. An understanding of the transition and its effect on aerodynamics and heat transfer is

important in turbines. Laminar flows with laminar separation bubbles are often encountered in these accelerating flows. Turbine flow with a laminar separation bubble is illustrated in Fig. 1.2.2. The laminar flow may separate because of the local adverse pressure gradient. This separation bubble will reattach, and this may in turn initiate transition result in turbulent flow downstream. The presence of these separation bubbles results in increased losses. Transitional flow depends on inlet turbulence levels, flow acceleration, blade surface roughness and, most importantly, Reynolds number.

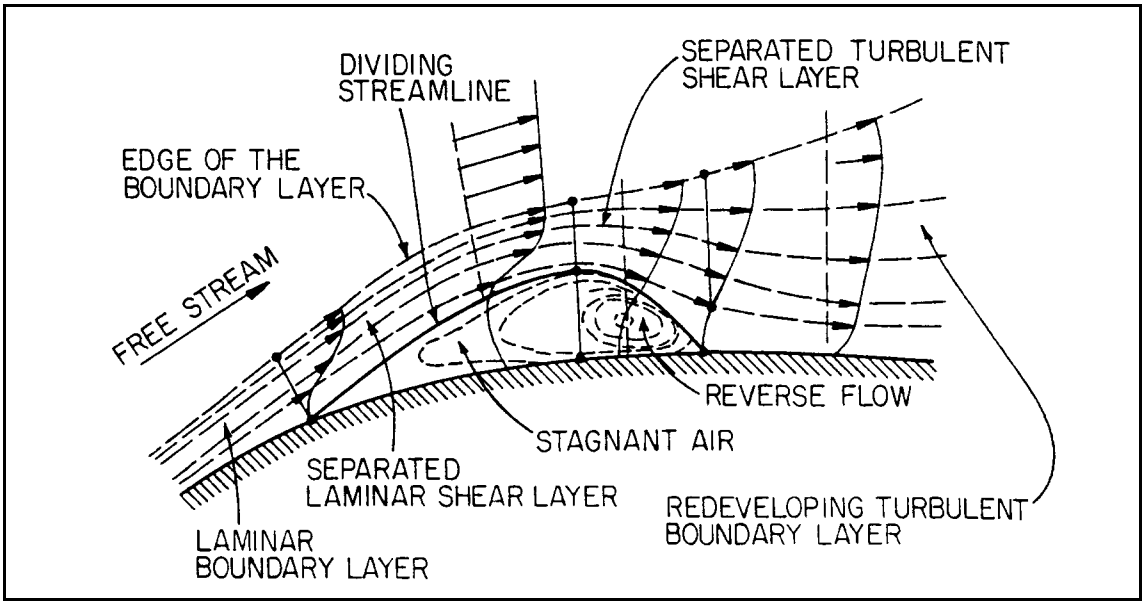

Fig. 1.2.2: *Scheme of laminar separation bubble on a turbine blade [Lakshminarayana, 1996, Fig. 6.18]*

The another important and complex flow phenomenon in a turbine is the secondary flow. In the turbine, flow used to have larger turning and the leading edge is thicker than a compressor. Sieverding [1984] and Gregory-Smith [1988] gave detailed descriptions about the secondary flow creation. The phenomenon is shown schematically in Fig. 1.2.3. When the flow passes through a curved turbine passage, it is theoretically balanced, in the normal direction, between the centripetal acceleration along the stream line and the pressure gradient normal to the stream line from the pressure to suction sides. But the blade row causes radially nonuniform velocity, stagnation pressure and stagnation enthalpy profiles, especially in the endwall boundary layer there is a great radial gradient of the flow parameters. Because the flow in the endwall boundary layer has lower velocity and kinetic energy than the main stream, there is an imbalance between the normal pressure gradient (normal to the stream lines) and the centripetal acceleration and thus the flow in the endwall boundary layer will move towards the suction side of the blade. Thereby a cross-flow, secondary flow shown in Fig. 1.2.1, is generated. The secondary flow gives a secondary vorticity flow which is circulated in the endwall region. It is also called passage vortex in Fig. 1.2.3. Generation of the secondary flow and vortex in turbomachinery have been discussed in incompressible fluid theory by Lakshminarayana [1996].

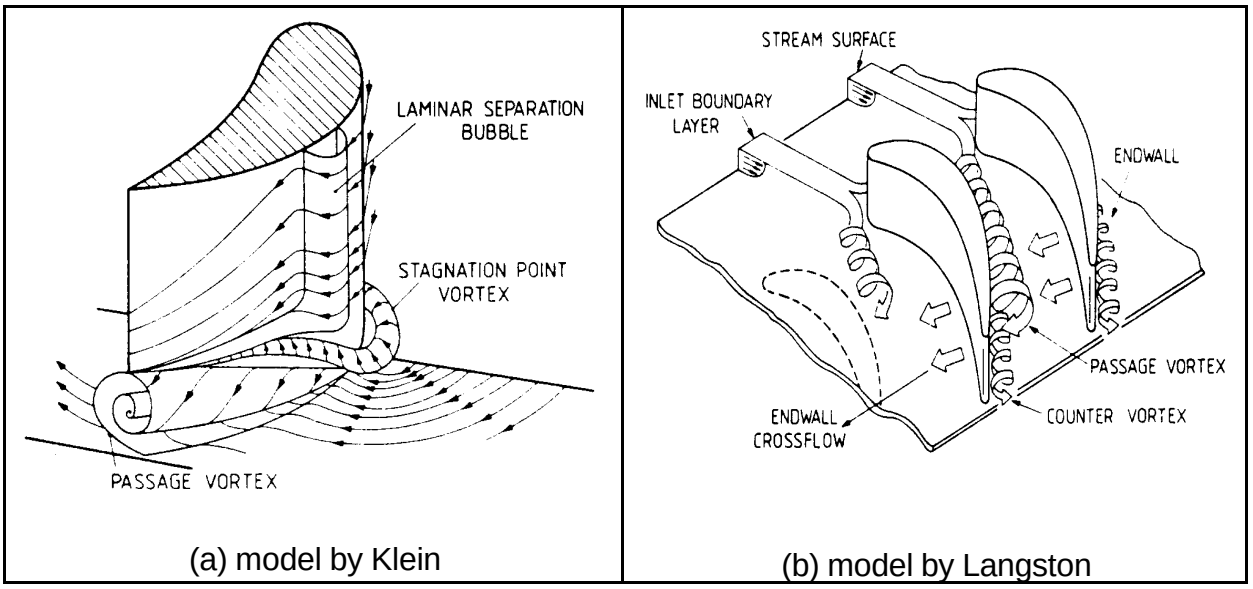

Fig. 1.2.3: *Endwall flow models for turbine cascades* [Sieverding, 1984]

The curvature of the streamline upstream of the leading edge introduces pitchwise motions oriented away from the blade, along with spanwise motion toward the wall along the blade surfaces resulting in the counter vortex shown in Fig. 1.2.3 (b). This vortex interacts with the corner boundary layer and entrains the fluid from this viscous layer to produce a strong vortex which may persist along the passage depending on Reynolds number, leading edge radius, turning angle and initial boundary layer thickness. Even though the formation of a horseshoe vortex can be explained on the basis of inviscid secondary flow theory (see [Lakshminarayana, 1996, section 4.2.6]), the subsequent roll-up, increased size and flow separation associated with it is predominantly a viscous phenomenon. Thus two distinct (but arising from the same physical phenomena) vortices are present on the suction blade side, as shown in Fig. 1.2.3 (b). They may merge, interact or stay separate. The secondary or passage vortex (arising from the turning of the flow inside the passage) occurs near the suction surface due to transverse fluid motion from the pressure to the suction surface along the endwall. Endwall flow models suggested by Klein [1966] and Langston [1980] are shown in the Fig. 1.2.3 (a) and (b) respectively. Klein´s " stagnation point vortex" is the same as the terminology "counter vortex" by Langston. This is also called " leading edge vortex " or "horseshoe vortex" by many authors. Langston et al [1977] observed that the pressure side of the horseshoe vortex merges with the passage vortex near the suction surface (both have the same sense of rotation). They observed that the suction leg of the horseshoe vortex (which is opposite in direction to passage vortex) continues on the suction side. Klein [1966] showed that this suction leg of the horseshoe vortex is diffused and dissipated by the time it reaches the trailing edge. Yamamoto [1989] indicated that the secondary vortex interacts with the blade wake in the endwall flow region to generate an additional vortex, which hugs the secondary flow [Lakshminarayana, 1996].

Because the blade loading is usually high in turbines, the tip clearance plays a major role and increase losses and three-dimensionality in turbines. The tip clearance flow field measured by Yamamoto [1989] in an unshrouded turbine cascade is shown in Fig. 1.2.4. It can be seen that the flow passes though the tip clearance driven by the pressure gradients between the pressure and suction surfaces at the tip. This tip leakage flow rolls up into a vortex and interacts with the secondary flow. The secondary flow and tip leakage flow interaction

produces a distinct interface. The most critical parameters controlling the magnitude of the leakage flow are the blade clearance and the blade loading (local pressure difference between the pressure and the suction surface)

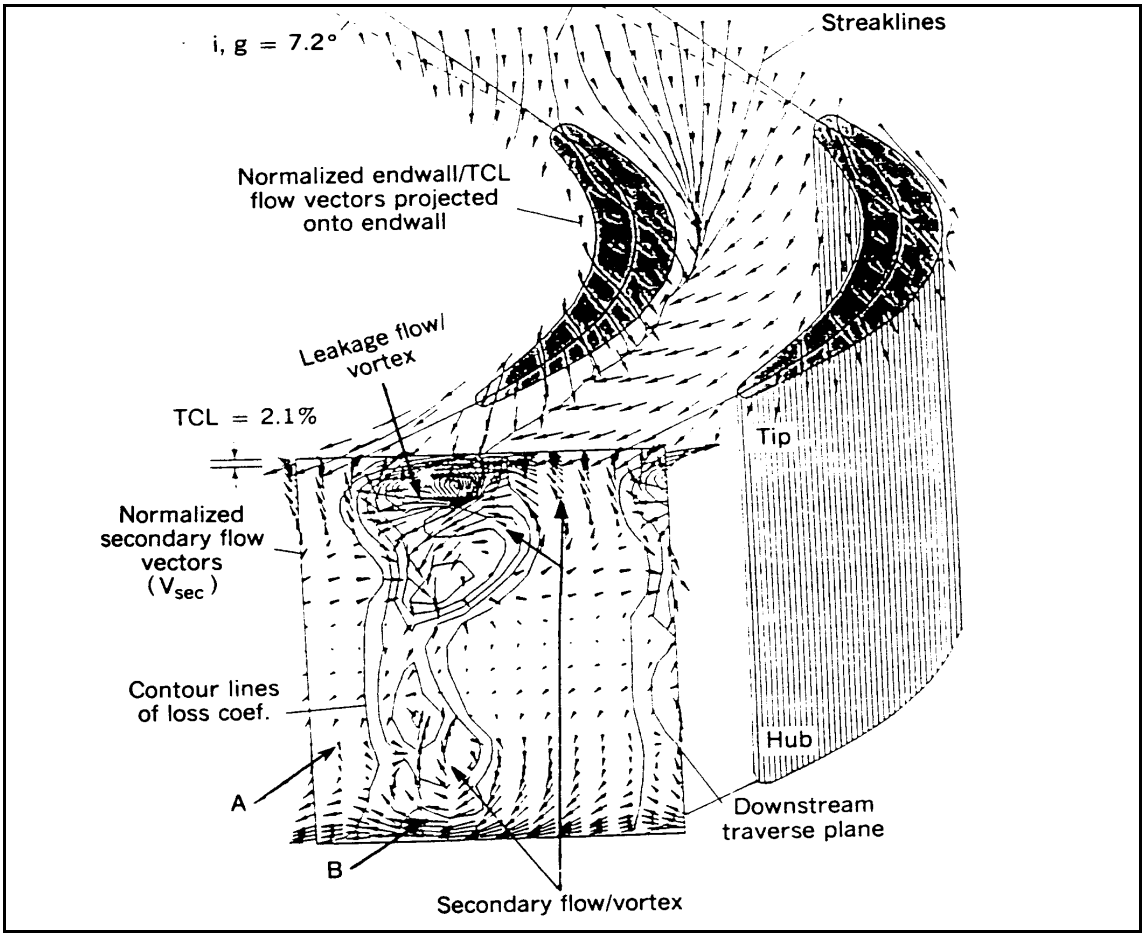

***Fig. 1.2.4**: Tip clearance effect in a unshrouded turbine rotor row [Yamamoto, 1989]*

Fig. 1.2.5 shows the schematic illustration of the tip leakage flow in a shrouded turbine given by Denton [1993]. The tip leakage flow go though the tip clearance driven by the different pressure between the up- and downstream pressures at tip. The leakage flow jet mixes out firstly in the clearance space and this mixing process is irreversible. Then the leakage flow must be re-injected into the main flow where the difference in both the meridional velocity and the swirl velocity of the two flows will generate further mixing. The critical parameters controlling the magnitude of the this leakage flow are blade clearance, blade turning and the pressure ratio over the blade row.

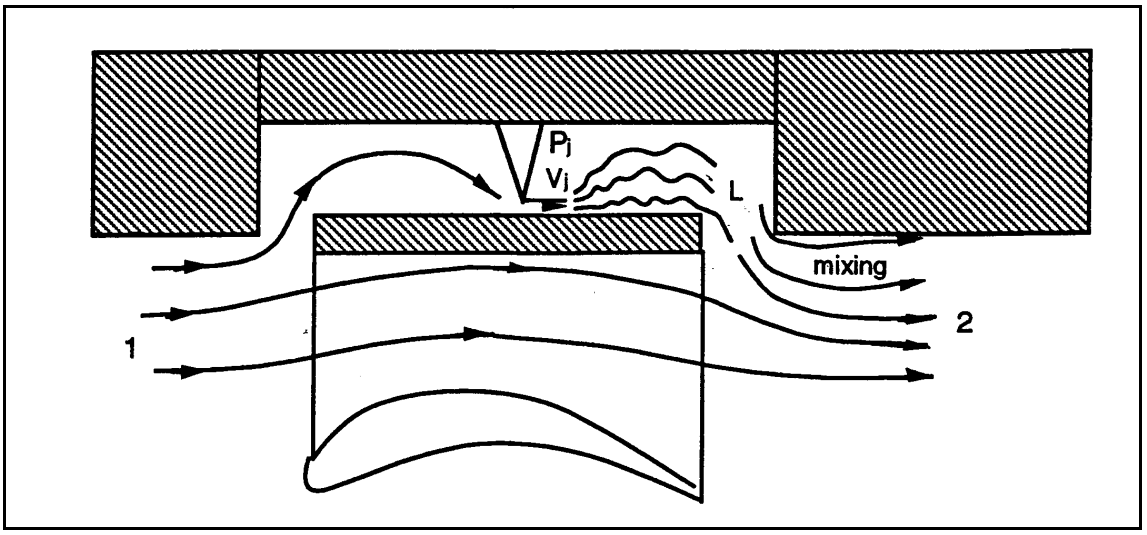

***Fig. 1.2.5**: Tip clearance effect over a shrouded turbine rotor row [Denton ,1994, p. 6]*

Flow in the turbine passage is irreversible. Hence the entropy will increase in the flow. For example, in boundary layers, the viscous dissipation would increase the entropy, and hence is not available for performing useful work. We thus call it a loss. Likewise, viscous and turbulent dissipative mechanisms of vortices and shocks result in an increase in the entropy of flow and hence they are also a source of losses. For viscous layers and vortices, the interest usually lies in overall or integrated losses rather than local losses. An estimation of the local loss involves the solution of the Navier-Stokes equations with a suitable turbulence model. For the overall losses, suitable loss models or correlations are well used in turbomachinery engineering.

Profile Losses

The losses due to blade boundary layers (including separated flow) on blade surfaces and wake through viscous and turbulent dissipation are classified “profile losses”. The mechanical energy is dissipated into heat within the boundary layer. This increases the entropy and results in stagnation pressure loss, even though the stagnation enthalpy is constant for adiabatic flow. In addition, the non-uniform velocity profiles in both the boundary layer and the wake (bounded and shear flows) are smoothed out by viscous and turbulence effects. Furthermore, the trailing vortex systems in the blade wake and its eventual mixing and dissipation give rise to additional losses. The magnitude of the profile loss mainly depends on the flow velocity in free stream, roughness of the blade surfaces, Reynolds number and the surface areas. The difficulty of predicting transition of the boundary layer remains a major limitation to accurate prediction of this loss.

In many instance, a separate category called “trailing edge loss” is included to account for losses due to the finite thickness of the blade trailing edge, which causes flow separation (mixing of jets) and shock-expansion-wave interactions due to sharp corners. This loss could be appreciable in transonic and supersonic turbines. In subsonic turbines, this loss is used to be classified and taken account inside the profile losses.

Shock Losses

The losses due to viscous dissipation across the shock is called “shock losses”. This loss, in principle, could be estimated theoretically (e.g. [Shapiro, 1953]), but the estimate of indirect losses associated with boundary-layer-shock interaction has to be based on computation or correlations. Sudden jump in static pressure across the shock results in thickening of the boundary layer and flow separation. This loss could be a substantial portion of total profile losses, depending on Mach number and Reynolds number.

Tip Leakage Losses

The loss due to the clearance between the blade tip and the casing is called the “tip leakage loss”. This loss is considered in different ways depending on whether the blade is shrouded or unshrouded. The blades shown in Fig. 1.2.1 are unshrouded. The tip flow goes through the tip clearance gap from the pressure side to the suction side of the blade. The loss will be caused by the mixing of this leakage flow with the main flow near the suction surface and even downstream of the blade. The leakage flow and main flow in the tip clearance region are at different angles and velocities and mixing of these two dissimilar flows results in dissipation account for losses. In addition, the formation of a leakage vortex and its eventual dissipation (viscous and turbulent) along with its interaction with the main flow result in losses. The main factors influencing the tip leakage loss are the clearance gap size, the cascade incidence and the pressure difference between the pressure and suction surface [Bindon, 1989].

The tip leakage losses include also the loss due to the tip leakage flow through the clearance. The flow in the clearance space undergoes no change in angular momentum, and thus it is not available for doing work. This loss can be estimated from a knowledge of inlet boundary layer thickness and the clearance height. The fraction of mass flow through the gap does not participate in the pressure drop.

Endwall Losses

The secondary flow and formation of vortex result in mixing and dissipation of energy similar to those described under “tip clearance losses”. The losses will be caused by the mixing of the secondary flow with the main flow, formation of the secondary vortex and the counter vortex and interaction between the vortices. In addition, the indirect effect such as interaction of secondary flow with the wall and the blade boundary layer and wake results in additional losses. The losses due to this source are usually lumped together with the annulus wall boundary layer losses and budgeted under “endwall losses”. The source of loss mechanisms is viscous and turbulent mixing and dissipation.

“Endwall losses” usually include losses due to annulus wall boundary layer which are almost invariable three-dimensional in nature. The three-dimensional boundary layer does account for the secondary flow. The growth of endwall boundary layer and mixing, along with the dissipative mechanisms associated with them, result in additional losses.

Cooling Losses

The performance of a gas turbine increases in general with increasing inlet temperature. However, the attainable temperature of the structural components is restricted because of the potential of mechanical failure. This holds especially for the turbine blades and vanes. Cooling methods are now widely used to maintain the skin of blades at acceptable temperatures.

Various techniques of cooling in the blades have been proposed over the years: air cooling, water cooling, steam cooling, fuel cooling, liquid metal cooling, and so on. Air cooling is by far the most common method especially in aerospace turbines. The air cooling technique can be classified as follows (LeGrives, 1986)

- Internal cooling (for external stream temperatures of 1300-1600 K): convection cooling, impingement cooling and internally air-cooled thermal barrier

- External cooling (for external stream temperatures more than 1600 K): local film cooling, full-coverage film cooling and transpiration cooling

Convection cooling is the simplest and one of the earliest techniques used. The coolant is passed through a multipass circuit from hub to tip and ejected at the trailing edge or the blade tip. In impingement cooling, the cold air from one row or many rows of small holes ejected from insert within a blade impacts the blade wall and reduces its temperature. The mean blade temperature will be at a lower temperature than the gas, thus enabling a higher turbine inlet temperature to be used. Another method of keeping the blade cool is through a thermal barrier, which is a low-conductivity ceramic coating. Internal cooling is not as effective as external cooling, so its use is limited to a temperature range of 1300-1600 K.

Modern gas turbines employed a combination of convective cooling and film cooling to achieve higher turbine inlet temperature. In film cooling, a thin layer of cool air insulates the blade from the hot gas stream, especially near the leading edge regions where high temperatures are encountered. A more efficient technique is the full-coverage film cooling which utilises a large number of closely spaced holes. The temperature range where this technique is employed is 1560-1800 K. One of the most efficient techniques, which is only in the conceptual stage, is transpiration cooling, where a layer of cool air is deposited on the surface after passing through porous or woven material. It is useful when inlet temperature is in excess of 1800 K [Lakshminarayana, 1996].

All of the cooling techniques involve increased aerodynamic losses, in addition to the conventional losses introduced before in this chapter, and decreased efficiency. The losses associated with turbine cooling include: the lost work or power of the coolant flow; increased profile losses due to thicker blade profiles arising from coolant holes, interaction of coolant film with the blade boundary layer, mixing losses between coolant and main flows and the modification of transition, boundary layer and wakes. The endwall losses are also affected through both convective and film cooling. In view of the complexity of the geometry and numerous parameters involved, a systematic method is yet to evolve for the prediction of

cooled turbine efficiency. At the present time, testing is the only reliable method of determining the aerodynamic performance. It is necessary to optimise the thermal gain (increased turbine inlet temperature, cycle efficiency, etc.) with aerodynamic losses and decreased efficiency. Denton [1993] made an analysis of the thermal cycle efficiency of a turbine system affected by variations of the turbine inlet temperature, coolant flow rate and efficiency of turbine component. He noted that, compared with the other two items, the rate of loss of turbine efficiency with cooling flow has a larger effect on the overall cycle efficiency. An understanding of the losses due to the cooling is very important. Loss analysis plays a significant role in the selection of the technique, location of the coolant holes, geometry of the coolant hole, coolant mass flow rate and so on.

In many instances, it is difficult to distinguish between various sources of losses. For example, the tip leakage and secondary flow loss can not be separated due to intense interaction and mixing of these two flows.

Besides the losses caused by the flow shown in Fig. 1.2.1, there are some other losses such as unsteady loss, windage loss, partial admission loss, lacing wires loss and exhaust loss etc. Theses are many minor sources of loss which are small in most applications on turbomachinery but can become significant in special cases.

There are have been many papers published on sources of losses, loss correlations and methods of predicting axial turbine performance. Some of these will be reviewed in the next chapter.

1.3 Basic Definition and Relationship of Efficiencies and Loss Coefficients in Axial Flow Turbines

1.3.1 Turbine Efficiencies

In conventional turbines, the flow through a stage can be regarded as adiabatic since heat losses are usually small in relation to work outputs. The performance of the flow can be represented in an enthalpy-entropy diagram in Fig. 1.3.1. A scheme of an axial turbine stage corresponding to the thermodynamic processes in this figure is shown in Fig 1.3.2. In Fig. 1.3.1, an ideal process (no losses) through the turbine stage is from the point 0 to 2_{ss} and a real process (with losses) is from the point 0 to 2. The difference between the ideal and real points 2_{ss} and 2 at the exit of the turbine stage is mainly caused by the losses in the flow described in the previous section. In turbines, efficiencies are used to evaluate quantitatively that how the flow works efficiently through the turbine or, in the another word, how much percent of work can really be achieved after considering the losses.

Traditionally the efficiencies used in turbines are classified as total-to-total, total-to-static and static-to-static efficiencies:

total-to-total efficiency: $$h_{tt} = \frac{h_{co} - h_{c2}}{h_{co} - h_{c2ss}} \qquad \text{(eq. 1.3.1.1)}$$

total-to-static efficiency: $h_{ts} = \frac{h_{co} - h_{c2}}{h_{co} - h_{2ss}}$ (eq. 1.3.1.2)

static-to-static efficiency: $h_{ss} = \frac{h_o - h_2}{h_o - h_{2ss}}$ (eq. 1.3.1.3)

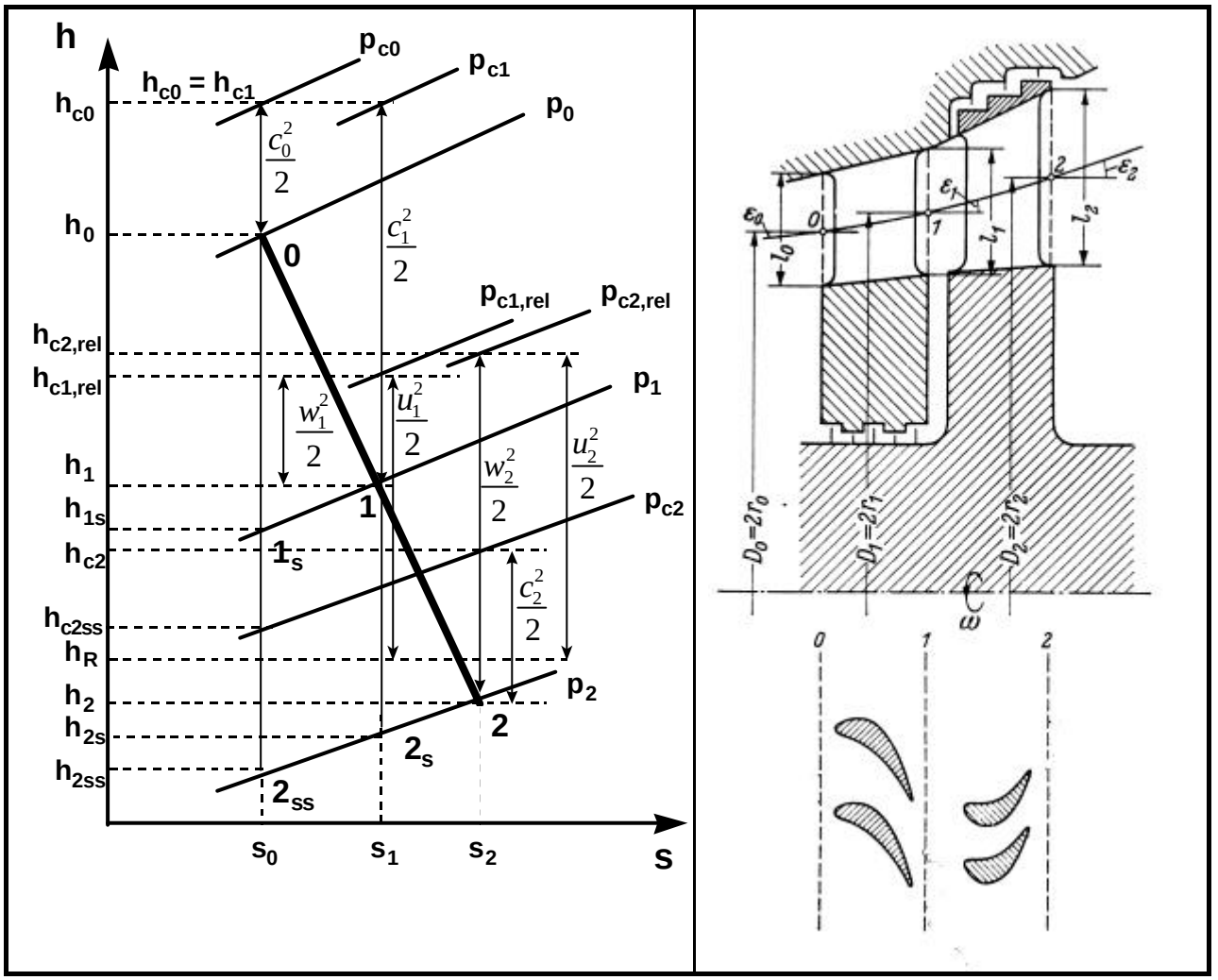

Fig. 1.3.1: *Enthalpy-entropy diagram for one process in a turbine stage (by reference to [Bölcs,1993, Fig. 3.1, p. 70])*

Fig. 1.3.2: *A scheme of an axial turbine stage [Traupel,1977, Fig. 3.2.1]*

The total-to-total efficiency should general be used in multi-stage turbines where the exhaust velocity from a stage is not lost. The total-to-static efficiency is used when the exit velocity is not recovered, such as the single stage turbine and the last stage in a multi-stage turbine. For a turbine stage where the inlet and outlet velocities are approximately the same, the total-to-total efficiency can be regarded as the same as the static-to-static efficiency. The detailed discussions concerning the turbine efficiencies can be found in text books for turbines, such as [Horlock, 1966], [Dixon, 1989] and [Cohen et al, 1996].

1.3.2 Loss Coefficients

Losses in turbines are used to be expressed in terms of loss coefficients. They are manifested by a decrease in stagnation enthalpy, and a variation in static pressure and temperature, compared to the isentropic flow. Usually the following loss coefficients are used in turbines (see Fig 1.3.1: h-s diagram).

Enthalpy loss coefficient:

Stator; $$z_N = \frac{h_1 - h_{1s}}{h_{co} - h_1} = \frac{h_1 - h_{1s}}{\frac{1}{2}c_1^2}$$ (eq. 1.3.2.1)

Rotor; $$z_R = \frac{h_2 - h_{2s}}{h_{c1,rel} - h_2} = \frac{h_2 - h_{2s}}{\frac{1}{2}w_2^2}$$ (eq. 1.3.2.2)

The enthalpy loss coefficient shown in equation 1.3.2.1 and 1.3.2.2 are most useful for design of the turbines [Denton, 1993]. In these equations, the isentropic final enthalpy, h_{1s} for stator and h_{2s} for rotor, are the values obtained in isentropic expansions to the same final static pressure, p_1 and p_2 respectively, as the actual processes. We can define an entropy loss coefficient by:

$$z_N \cong \frac{T_1(s_0 - s_1)}{\frac{1}{2}c_1^2}$$ (eq. 1.3.2.3)

$$z_R \cong \frac{T_2(s_1 - s_2)}{\frac{1}{2}w_2^2}$$ (eq. 1.3.2.4)

So the relationships between the loss coefficients and entropy increase, which is the useful parameter to present the irreversibilities of the flow though turbine rows, is established. It has been proved by Denton [1993, p. 4] that the error between the enthalpy and entropy loss coefficients is of order 10^{-3} and is always negligible.

Sometimes the enthalpy loss coefficient referred to the isentropic velocity is used. It is defined as:

Stator; $$x_N = \frac{h_1 - h_{1s}}{h_{co} - h_{1s}} = \frac{h_1 - h_{1s}}{\frac{1}{2}c_{1s}^2}$$ (eq. 1.3.2.5)

Rotor; $$x_R = \frac{h_2 - h_{2s}}{h_{c1,rel} - h_{2s}} = \frac{h_2 - h_{2s}}{\frac{1}{2}w_{2s}^2}$$ (eq. 1.3.2.6)

The relationship between the ξ and ζ is

Stator; $$x_N = \frac{z_N}{1+z_N}$$ (eq. 1.3.2.7)

Rotor; $$x_R = \frac{z_R}{1+z_R}$$ (eq. 1.3.2.8)

The derivation of this relationship can be found from [Horlock, 1966] and [Wei & Svensdotter, 1995].

The another commonly used loss coefficient is the stagnation pressure loss coefficient. It is defined as:

Stator; $$Y_N = \begin{cases} \dfrac{p_{c0} - p_{c1}}{p_{c1} - p_1} & \text{in compressible flow} \\ \dfrac{p_{c0} - p_{c1}}{\frac{1}{2} r c_1^2} & \text{in incompressible flow} \end{cases}$$ (eq. 1.3.2.9)

Rotor; $$Y_N = \begin{cases} \dfrac{p_{c1,rel} - p_{c2,rel}}{p_{c2,rel} - p_2} & \text{in compressible flow} \\ \dfrac{p_{c1,rel} - p_{c2,rel}}{\frac{1}{2} r w_2^2} & \text{in incompressible flow} \end{cases}$$ (eq. 1.3.2.10)

The reason that the stagnation pressure loss coefficient is so common is that it is easily calculated from cascade test data.

The relationship between the stagnation pressure and enthalpy (or entropy) loss coefficients was given by Horlock [1966, p. 64].

$$Y_N \begin{cases} = \dfrac{(z_N g M_1^2/2)}{1-(z_N g M_1^2/2)} \left\{ \dfrac{1}{1-\left[1\Big/\left(1+\dfrac{g-1}{2} M_{2s}^2\right)^{g/(g-1)}\right]} \right\} \\ \cong z_N \left(1+\dfrac{g\ M_1^2}{2}\right) & \text{for compressible flow, } M_1 < 1 \\ \cong z_N & \text{for incompressible flow} \end{cases} \qquad \text{(eq. 1.3.2.11)}$$

$$Y_R \begin{cases} = \dfrac{(z_R g M_{2,rel}^2/2)}{1-(z_R g M_{2,rel}^2/2)} \left\{ \dfrac{1}{1-\left[1\Big/\left(1+\dfrac{g-1}{2} M_{2s,rel}^2\right)^{g/(g-1)}\right]} \right\} \\ \cong z_R \left(1+\dfrac{g\ M_{2,rel}^2}{2}\right) & \text{for compressible flow, } M_{2,rel} < 1 \\ \cong z_R & \text{for incompressible flow} \end{cases} \qquad \text{(eq. 1.3.2.12)}$$

Entropy is a useful thermodynamic parameter for expressing the irreversiability of the process but it can not be seen or measured directly. Its value can only be inferred by measuring other properties. Basic thermodynamics tells us that for a single phase fluid entropy is a function of any two other thermodynamic properties such as temperature, and pressure. For a perfect gas, two of the relations between specific entropy and more familiar quantities are

$$s - s_{ref} = c_p \ln\left(\frac{T}{T_{ref}}\right) - R \ln\left(\frac{p}{p_{ref}}\right) \qquad \text{(eq. 1.3.2.13)}$$

and $$s - s_{ref} = c_v \ln(\frac{T}{T_{ref}}) + R\ln(\frac{r}{r_{ref}})$$ (eq. 1.3.2.14)

The temperatures, pressures and densities used in these equations may be either all static values or all stagnation values because by definition the change from static to stagnation conditions is isentropic.

If applying equation 1.3.2.13 to the processes in a turbine stage shown in Fig. 1.3.1 and because of $T_{c0}=T_{c1}$ and $T_{c1,rel}=T_{c2,rel}$, we have

stator $$s_0 - s_1 = -R\ln(\frac{p_{c1}}{p_{c0}}) = -R\ln(1-\frac{p_{c0}-p_{c1}}{p_{c0}})$$ (eq. 1.3.2.15)

rotor $$s_1 - s_2 = -R\ln(\frac{p_{c2,rel}}{p_{c1,rel}}) = -R\ln(1-\frac{p_{c1,rel}-p_{c2,rel}}{p_{c1.rel}})$$ (eq. 1.3.2.16)

These equations show the relationship between the increase of the entropy and decrease of the stagnation pressure, which are caused by the losses, in the irreversible processes through the turbine stator and rotor respectively. These equations are very commonly used in the performance calculations for gas turbines.

1.4 Objectives

As introduced in this chapter, flow is irreversible and losses exist in the turbine passage. For example, in boundary layers, the viscous dissipation would increase the entropy, and hence is not available for performing useful work. Likewise, viscous and turbulent dissipative mechanisms of vortices and shocks result in an increase in the entropy of flow and hence they are also a source of losses. For viscous layers and vortices, the interest usually lies in overall or integrated losses rather than local losses. For the overall losses, suitable loss models are well used in turbomachinery engineering. Such loss models are needed in not only the mean line prediction but also the through flow calculation processes in turbine optimisation and analysis (see Fig. 1.1.1). A number of empirical loss models for prediction total losses in turbines have been described in the open literature (A detailed discussion on the loss models for axial turbines will be performed in the next chapter). In order to apply the loss models properly, it is needed to see what are the different characteristics of various loss prediction methods in applications and what are the physical concepts behind the different methods. However, a limited amount of such work has been found in open literature.

The objectives of this thesis are to make a detailed systematic analysis of the turbine performance prediction with different loss models in various blade geometrical parameters at both the design and off-design conditions, to further understand the significance of the models and to develop them in order to apply loss models properly in turbine aerothermodynamic simulation and optimisation.

2 REVIEW AND DEVELOPMENT OF LOSS PREDICTION MODELS IN AXIAL TURBINES

Many loss prediction methods exist to predict losses in turbomachines. Concerning axial turbines, methods for predicting total losses in the cascades have been developed such as Soderberg [1949], Ainley & Mathieson [1951], Steward [1960], Smith [1965], Baljé & Binsley [1968], Mukhtarov & Krichakin [1969], Craig & Cox [1970], Dunham & Came [1970], Kroon & Tobiasz [1971], Traupel [1977], Kacker & Okapuu [1982], Moustapha et al [1990], Denton [1987, 1990, 1993] and Schobeiri & Abouelkheir [1992]. There are also some methods which are for predicting the individual loss components, especially secondary and tip clearance losses, in turbines. These methods were given by Ehrich & Detra [1954], Scholz [1954], Hawthorne [1955], Boulter [1962], Sharma & Butler [1987], Dunham [1970], Lakshminarayana [1970], Okan & Gregory-Smith [1992], Yaras & Sjolander [1992], Cecco et al [1995], Kim & Chung [1997] and Wehner et al [1997].

In this chapter, the concentration will be put on the descriptions of the loss models which were created to predict total losses including off-design losses in turbine cascade rows. The details of these loss models are introduced one by one. Then a overview comparison of the loss models is summarised. All equations of the models discussed in this chapter are listed in Appendix 1. The information of models for predicting individual loss components, secondary and tip leakage losses, is listed in Appendix 2.

As cooling techniques are more and more used in high temperature turbines nowadays, prediction of cooling losses, especially film cooling loss, is significantly important in turbine simulation and optimisation. There are a few methods published for predicting film cooling loss in turbines. In this chapter, film cooling loss models given by Ito et al [1980] and Lakshminarayana [1996] are reviewed. A study of the film cooling loss in a turbine blade row is made by means of analysing equations of the conservation of mass, momentum and energy in an one dimensional channel with injected additional flow. Then a development of the film cooling loss model is acquired in this chapter for approximately estimating the overall film cooling loss in a turbine blade row.

2.1 Soderberg

Soderberg [1949] gave the total loss coefficient as:

for stators $$\zeta_N = \left(\frac{10^5}{R_e}\right)^{1/4} \left[(1+\xi^*)\left(0.993 + 0.075\frac{l}{H}\right) - 1\right] \qquad \text{(eq. 2.1.1)}$$

for rotors $$\zeta_R = \left(\frac{10^5}{R_e}\right)^{1/4} \left[(1+\xi^*)\left(0.975 + 0.075\frac{l}{H}\right) - 1\right] \qquad \text{(eq. 2.1.2)}$$

In (eq. 2.1.1) and (eq. 2.1.2), ξ^* is the nominal loss coefficient and main function of blade deflection, (see [Dixon, 1989, Fig. 4.3]). From Dixon [1989, p. 99]), It can be simplified as a equation

$$\xi^* = 0.04 + 0.06\left(\frac{\varepsilon}{100}\right)^2 \qquad \text{(eq. 2.1.3)}$$

Soderberg's model includes profile and secondary flow loss but not tip clearance loss. The profile loss was considered mainly as a function of blade deflection, ε. A large deflection indicates a high turning of blades therefore the profile loss is high. The secondary loss in this model depends mainly on the blade aspect ratio, l/H, which is the most important factor for the secondary loss. The tip clearance loss can be considered by the simple expedient of multiplying the final calculated stage efficiency by the ratio of "blade" area to total area (i.e. "blade area + clearance area) [Dixon, 1989, p. 100].

This loss model is based on the work of Zweifel [1945] to obtain the optimum pitch/chord ratio for a given change in direction through a cascade. From a series of cascade tests, Zweifel [1945] suggested that the optimum lift coefficient based on the tangential loading

$$C_y = 2(t/l_x)(\tan a_{out} + \tan a_{in})\cos^2 a_{out} \qquad \text{(eq. 2.1.4)}$$

should be approximately 0.8, where l_x is the axial chord. For given gas flow angles α_{in} and α_{out}, the optimum pitch/chord ratio is obtained from this equation.

The nominal loss coefficient calculated with equation 2.1.3 is based on the design force coefficient from equation 2.1.4 and valid at the Reynolds number of 10^5 and with aspect ratio of 3:1. For the case of other Reynolds number and aspect ratio, the losses are calculated with equations 2.1.1-2.

It can be seen that Soderberg's model implies that the effect of profile shape on the losses is limited. Further, it is implied that the degree of reaction (or stagger) is unimportant, so as the optimum pitch/chord ratio is chosen. In addition, the aspect ratio is expected to be the only important parameter in the correlation of secondary loss without considering of the inlet boundary layer and the blade geometry. The neglect of these parameters renders Soderberg's loss model open to criticism. However, the model is useful for obtaining quick and preliminary estimates of turbine performance.

2.2 Traupel

Traupel [1977] has developed an one-dimensional, empirical model, where various flow disturbances are generated by the presence of the blades. Extensive testing has been the base for empirical diagrams, where the influence of the blade geometry (including shrouds, damping wires, seals etc.) on the part-losses has been represented. These experimental results are then interpreted in a physical sense to be interpolated/extrapolated also for other flow and geometrical conditions.

Total Loss Coefficient

The total losses by Traupel consists of profile losses, secondary losses (rest losses), tip leakage losses and fan losses.

stator $\zeta_N = \zeta_{p,N} + \zeta_{f,N} + \zeta_{r,N} + \zeta_{Tl,N}$ (eq. 2.2.1)

rotor $\zeta_R = \zeta_{p,R} + \zeta_{f,R} + \zeta_{r,R} + \zeta_{Tl,R}$

Profile Loss

The profile losses are due to the friction on the profile surfaces and the separation of the boundary layers on the blade. The profile losses can be calculated as:

$\zeta_p = \chi_R \chi_M \zeta_{p0} + \zeta_{Te} + \zeta_c$ (eq. 2.2.2)

ζ_{p0} --- the basic profile loss, decided by the inlet and outlet flow angles.
χ_R --- the Reynolds number correction factor based on the influence of Reynolds number and surface roughness.
χ_M --- the Mach number correction factor, where the free stream velocity is taken into account.
ζ_{Te} --- the trailing edge loss, caused by the wake after the trailing edge and
ζ_c --- the Carnot shock loss which appears in a fluid that is undergoing a sudden expansion, for example after the trailing edge.

The basic profile loss, ζ_{p0}, can obtained from an empirical correlation given in Fig. 2.2.1. It is intuitively clear that a blade with a higher camber can have thicker boundary layers and even separation in zones of fast deceleration, and thus higher losses on the suction surface. On the pressure surface the flow does not separate as easily, and thus the losses are smaller. In a similar way, the importance of the inlet and outlet flow angles, that is the blade camber, is illustrated in Fig. 2.2.1. When reading from the diagram in Fig. 2.2.1, it should be noted that the definition of the flow angles is made from the tangential direction.

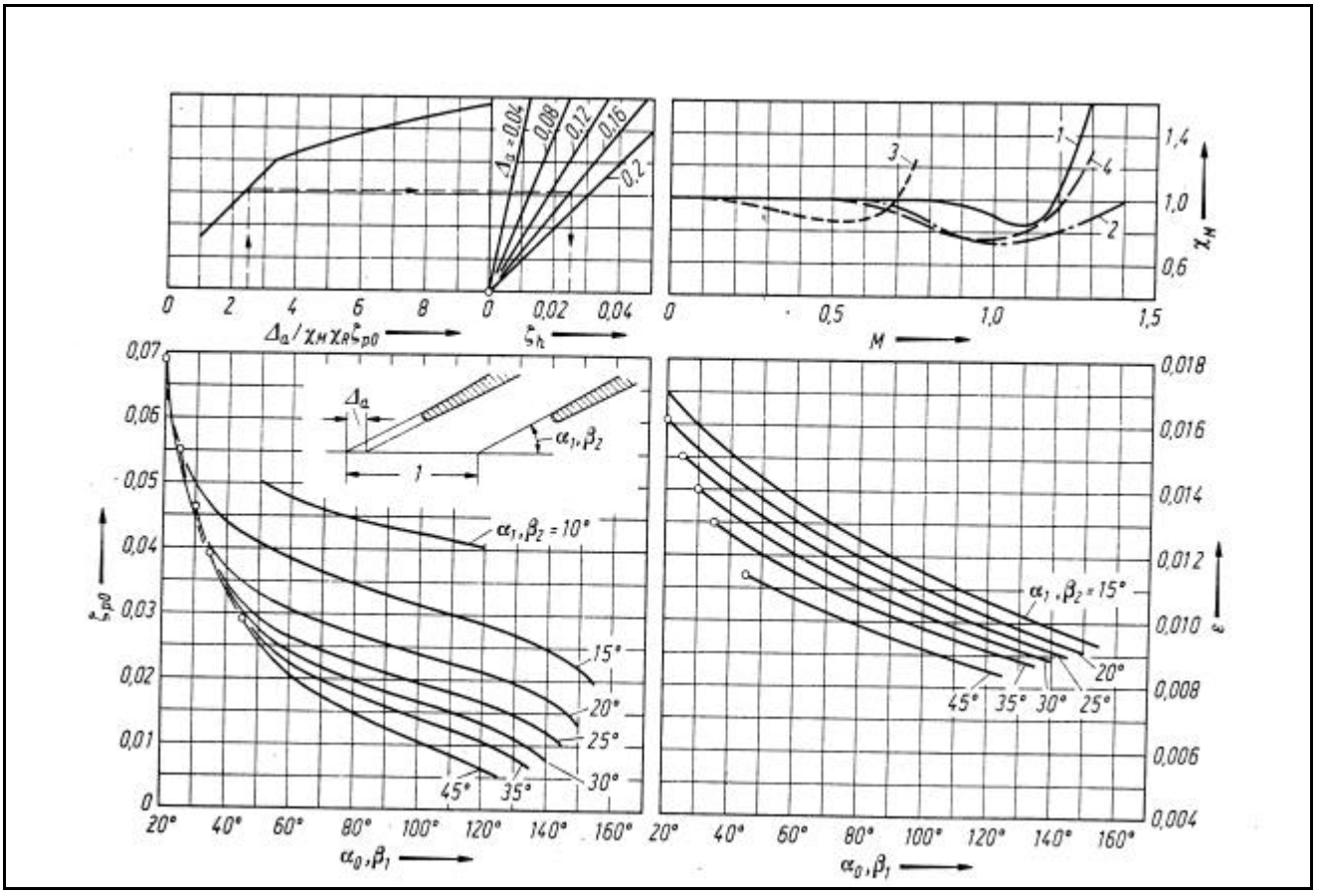

Fig. 2.2.1 *Correlations of the profile losses by Traupel [1977, Fig. 8.4.5].*

The Mach number correction factor, χ_M, takes into account how the outlet Mach number affects the profile losses. It is read from Fig. 2.2.1 [Traupel, 1977, Fig 8.4.5]. In the figure , curve 1 is for axial entry nozzle blades and curve 3 is for impulse blades for subsonic turbine, curves 2 and 4 are for axial entry nozzle and impulse blades respectively for supersonic turbine [Dejc, Trojanovskij, 1973].

Traupel [1977] gave the trailing edge loss, ζ_{Te}, (which is presented as ζ_h in Fig. 2.2.1) as the function of the trailing edge thickness, outlet flow angle, basic profile loss, Reynolds and Mach number corrections (see Fig. 2.2.1). At the trailing edge, a wake appears after the profile with a static pressure lower than in the free stream flow downstream of the cascade. The mixing of the low pressure fluid with the free stream fluid produces a loss called the trailing edge loss. The trailing edge loss is affected mainly by the trailing edge tangential projection, which is the trailing edge thickness divided with the sine of the outlet flow angle and unified with the pitch. The larger the projection, i.e. the thicker profile or the smaller outlet flow angle, the larger the loss due to the broader wake.

The Carnot shock loss is caused by a Carnot shock after the trailing edge. This is a shock that appears in a fluid that is undergoing a sudden expansion, for example after the trailing edge. The Carnot shock loss is a function of the trailing edge thickness and flow angle

(absolute angle for stators and relative angle for rotors) at outlet of cascades. It is shown as formula (eq. 2.2.3) and (eq. 2.2.4).

stator $$\zeta_{c,N} = \left\langle \frac{\Delta_{a,N}}{1-\Delta_{a,N}} \right\rangle^2 sin^2\alpha_1 \quad \text{and} \quad \Delta_{a,N} = \frac{t'_N}{t_N \, sin\left(90^0 - \alpha_1\right)} \qquad \text{(eq. 2.2.3)}$$

rotor $$\zeta_{c,R} = \left\langle \frac{\Delta_{a,R}}{1-\Delta_{a,R}} \right\rangle^2 sin^2\beta_2 \quad \text{and} \quad \Delta_{a,R} = \frac{t'_R}{t_R \, sin\left(90^0 - \beta_2\right)} \qquad \text{(eq. 2.2.4)}$$

The Reynolds number correction, χ_R, can be found from the diagrams shown in Fig. 2.2.2 [Traupel, 1977, Fig 8.4.6]. Line "a" is for turbines, lines "b" and "c" are for compressors. As can be seen in the figure, a high Reynolds number (above $2x10^5$) has no effect on the profile loss, while a low Reynolds number will increase the profile loss. This is similar to the skin friction for flow over a flat plate, where measurements and classical theory both indicate a decreasing skin friction for increasing Re. The obvious causes for the increase of the losses at reduced Reynolds number are a general thickening of the laminar boundary layers and a gradual increase of separated laminar flow regions.

The surface roughness has a larger impact on the Reynolds number correction factor; the higher relative surface roughness, the higher correction factor. A higher surface roughness gives higher friction and turbulence to the flow and is thereby increasing the loss, as can be seen in Fig. 2.2.2.

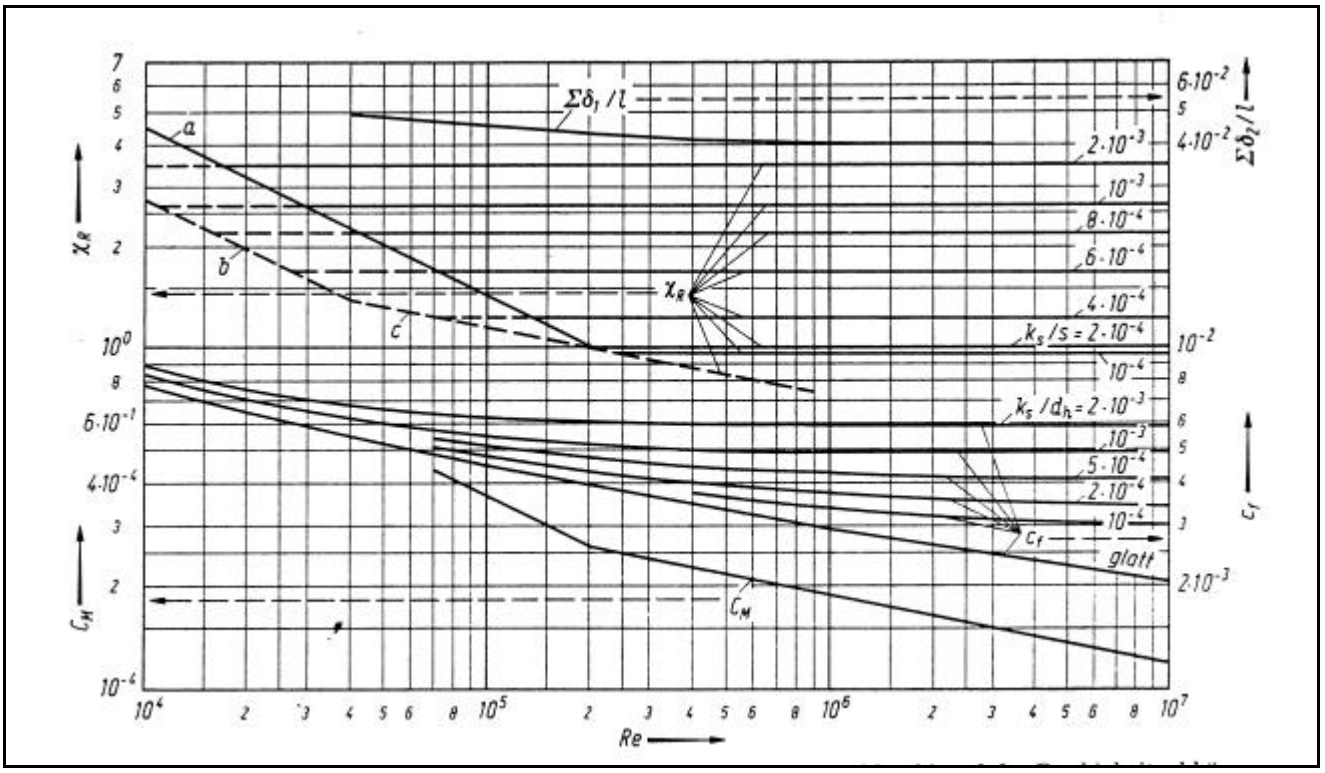

Fig. 2.2.2 *Reynolds number correlation factor given by Traupel [1977, Fig. 8.4.6].*

Secondary loss

The structure of the secondary losses given by Traupel was obtained from measured data on straight cascades. However, the quantitative values were obtained by comparison with turbine performance measurements at ETH Zurich [Sieverding, 1985]. As long as no interference between the secondary loss regions from both endwalls occurs, the losses are expressed as:

a) If $H/t \geq (H/t)_k$

$$\zeta_S = \frac{\zeta_p}{\zeta_{p0}} F\left(\frac{t}{H}\right) + \zeta_a$$

for stator resp. rotor

b) If $H/t < (H/t)_k$

$$\zeta_S = \frac{\zeta_p}{\zeta_{p0}} F\left(\frac{t}{H}\right)_k + \zeta_a + A\left(\frac{l}{H} - \frac{l/t}{(H/t)_k}\right)$$

for stator resp. rotor

(eq. 2.2.5)

The first term is the loss from the secondary flow in the blade channel, ζ_a is representing the losses from the endwalls between the stator and the rotor disk, and the unsteady effects due to the rotor-stator interaction. The third term, in equation 2.2.5 is a correction factor due to the fact that there is no undisturbed flow core in the blade channel. The factor of ζ_p/ζ_{p0} in equation 2.2.5 (ratio of losses at given Reynolds number Mach number and trailing edge thickness to losses at reference conditions) indicates that the secondary losses are affected by the same parameters, such as blade angles, trailing edge, Mach and Reynolds numbers, as the profile losses. The span/pitch ratio, H/t, is considered in this model. It is obvious that a small value of the ratio will make the secondary flow strong and the losses will be large. When this ratio is more than the critical value, there will be the risk of the interaction between the secondary vortex on at two endwalls, therefore the third term of loss is added in equation 2.2.5. The critical span/pitch ratio is:

$$(H/t)_k = B \cdot \sqrt{\zeta_p} \quad , \quad \text{B= 7 for stator and B=10 for rotor} \qquad \text{(eq. 2.2.6)}$$

The parameter **F** in equation 2.2.5 represents how the secondary flow in the blade channel is affected by the flow turning, i.e. the difference between the inlet and the outlet flow angle, and the velocity ratio, i.e. how the flow is accelerated through the blade channel. The more turning and less acceleration, the higher **F** and thus higher secondary losses. The variation of **F** with the blade turning was given in Fig. 2.2.3 [Traupel, 1977, Fig. 8.4.8].

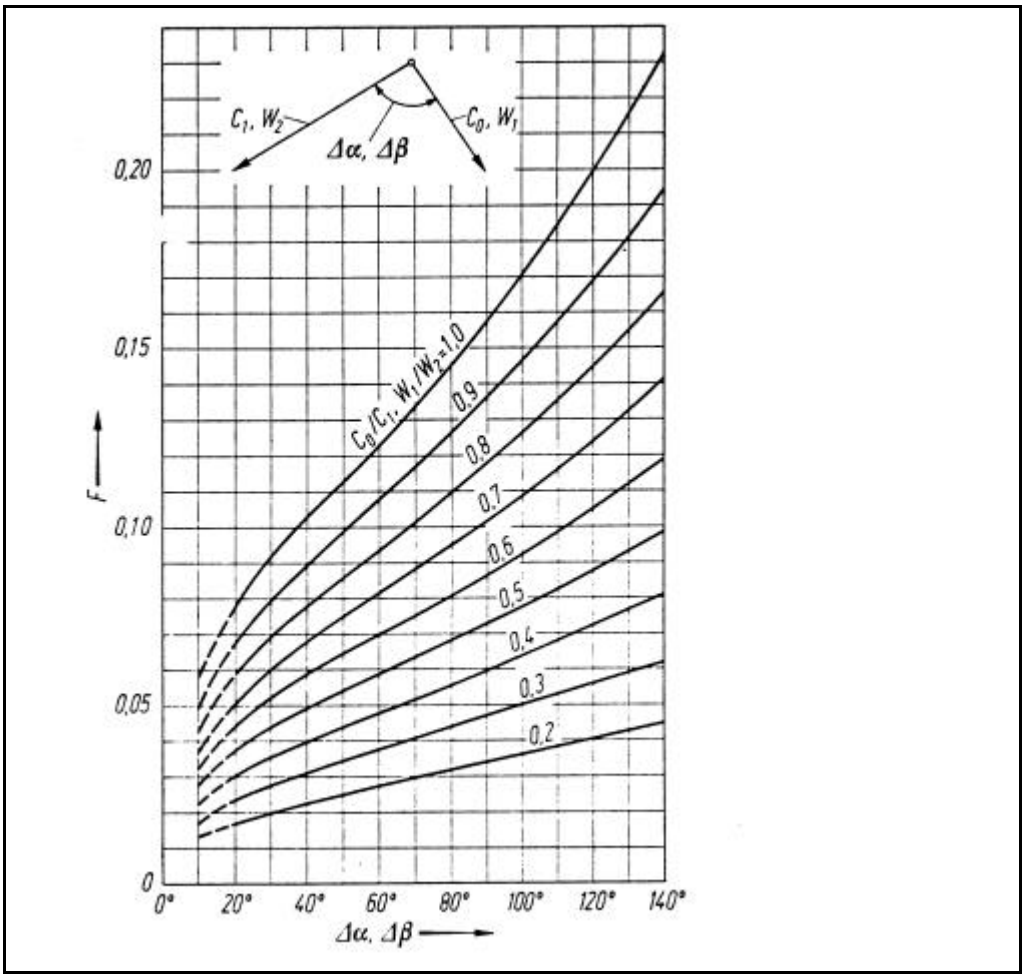

Fig. 2.2.3 *Factor F for secondary losses given by Traupel [1977, Fig. 8.4.8].*

The losses from the endwalls between stator and rotor are caused by the state of the boundary layers at the endwalls. It can be predicted as:

$$\zeta_{a,N} = \frac{c_f \cdot \delta_{a1}}{sin\left(90^0 - \alpha_1\right) \cdot l_1} \qquad \zeta_{a,R} = \frac{c_f \cdot \delta_{a2}}{\sin\left(90^0 - \beta_2\right) \cdot l_2} \qquad \text{(eq. 2.2.7)}$$

l_1, l_2, are the height of the cascade casing. δ_{a1} and δ_{a2} are the axial gaps between cascades. The definitions of these parameters were given in a figure by Traupel [1977, Fig 8.4.9b].

Fan loss

The fan losses is due to the fact that the blade spacing is not constant over the radius. It is read from a figure [Traupel, 1977, Fig 8.4.7].

The fan loss is highly affected by the blade span to diameter ratio and is increasing with increasing span to diameter ratio. It is also affected by the velocity ratio and is decreasing with increasing velocity ratio.

Tip leakage loss

Traupel [1977, p. 415ff] has put up different empirical formulas for shrouded and unshrouded blades.

The tip leakage losses for shrouded blades

The tip leakage losses for shrouded blades can be divided into two parts: one caused by the energy dissipation of the fluid and one from mixing of the tip leakage flow with the main flow. The shrouded tip leakage loss is calculated from (eq. 2.2.8) and (eq. 2.2.9) [Traupel, 1977, p 418].

stator $$\zeta_{Tl,N} = 2\cdot(1-R_H)\cdot\mu_N\cdot\left[1-\left(\frac{\nu-\nu(\alpha_0{}^*)}{\nu(\alpha_0{}^*)}\right)^2\right] \qquad \text{(eq. 2.2.8)}$$

rotor $$\zeta_{Tl,R} = \mu_R\cdot\left[1-\left(\frac{\nu-\nu(\beta_1{}^*)}{\nu(\beta_1{}^*)}\right)^2\right] \qquad \text{(eq. 2.2.9)}$$

In the equation above, μ is the ratio of mass flow going through the seals on the shrouds, here called the relative mass flow. This is depending on various factors such as degree of reaction at the hub and at the casing, inlet and outlet velocities, flow areas, amount of seals etc.

$u(a_0^*)$ and $u(b_1^*)$ are the velocity ratios at the design point. In this text, the term $\left[1-\left(\frac{n-n(b_1{}^*)}{n(b_1{}^*)}\right)^2\right]$ is called the relative velocity ratio. It has the strongest impact on the tip leakage losses.

The tip leakage losses for unshrouded blades

Traupel proposes two sets of equations depending on whether the tip leakage losses are or are not to be included in the aerodynamic blade efficiency. In the case the losses are included, the blade efficiency has to be diminished by Δh_{Tl}, which is a function of the tip clearance, blade span, blade chord and blade diameter at the tip and the mean diameter of blades. Eq. 2.2.10 was given by Traupel [1977, p. 416] for calculating the tip leakage loss, Δh_{Tl}, in unshrouded blade rows.

$$\Delta\eta_{Tl} = K_\delta\,\frac{(\tau-0.002\,l)D}{HD_m} \qquad \text{(eq. 2.2.10)}$$

In equation (eq. 2.2.10), the coefficient K_d can be obtained form [Traupel, 1977, p. 417, Fig. 8.4.16]

2.3 Ainley & Mathieson

A method for predicting losses through a turbine cascade was given by Ainley & Mathieson [1951]. The method has been used for many years in turbine performance predictions. This method is based on several broad assumptions and a correlation of the data then is available on blade losses. The method can be used to predict the performance of an axial flow turbine with conventional blades over a wide part of its full operating range [Ainley & Mathieson, 1951, p. 1].

In the method, Ainley & Mathieson [1951] assumed that the pressure loss coefficients are not influenced by the flow Mach numbers and that the flow outlet angles from a blade row are not influenced by the flow incidence angle range [Ainley & Mathieson, 1951, p. 3].

Ainley & Mathieson [1951] estimated that the tolerance on the absolute values of gas mass flow and peak efficiency would be in the region of +/- 2.0% for efficiency and +/- 3% for gas mass flow.

Total Loss Coefficient

The total losses in a turbine cascade by Ainley-Mathieson consists of profile loss, secondary losses, tip leakage loss. It can be written as eq. 2.3.1.

$$Y = (Y_p + Y_s + Y_{Tl})\,\chi_{Te} \qquad \text{(eq. 2.3.1)}$$

χ_{Te} is the trailing edge coefficient. It can be obtained from a figure by Ainley & Mathieson [1951, p. 26, Fig. 9]. The figure shows that χ_{Te} will be from 1.0 to 1.8 when the ratio of trailing edge thickness to pitch is from 0.02 to 0.12.

Profile Loss

Ainley/Mathieson gave profile loss model based on overall tests on a variety of turbine stages. The data refer to blade profiles designed prior to 1950, i.e., either blade profiles with contours composed of circular arc and straight lines or blades which made use of the British blade profile series with circular or parabolic camber lines. The maximum blade thickness varies between t_{max}/l=0.15 to 0.25. The correlation is based on a series of graphs of total pressure losses versus pitch/chord ratio for nozzle and impulse blades (see Fig. 2.3.1 and 2.3.2). For any other combination of angles, the profile losses at design point, $\mathbf{Y_{P(i=0)}}$, are calculated as

$$Y_{P(i=0)} = \left\{ Y_{P(\alpha'_{in}=0)} + \left(\frac{\alpha'_{in}}{\alpha_{out}}\right)^2 \left[Y_{P(\alpha'_{in}=\alpha_{out})} - Y_{P(\alpha'_{in}=0)} \right] \right\} \left(\frac{t'_{max}/l}{0.2} \right)^{\frac{\alpha'_{in}}{\alpha_{out}}} \qquad \text{(eq. 2.3.2)}$$

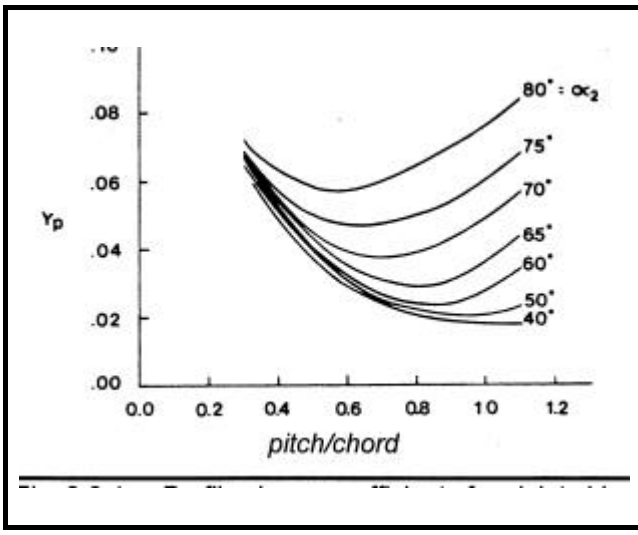

Fig. 2.3.1: Profile loss coefficient for inlet blade angle, α'_{in}=0, Ainley and Mathieson [1951, Fig. 4a]

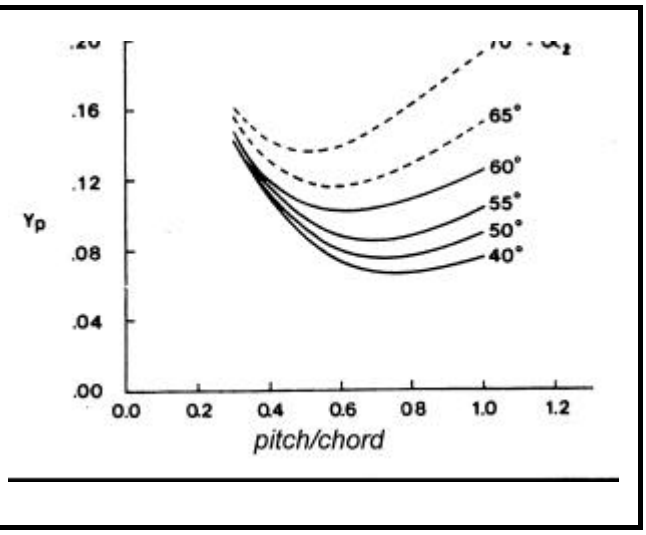

Fig. 2.3.2: Profile loss coefficient for inlet blade angle, $\alpha'_{in}= \alpha_{out}$, Ainley and Mathieson [1951, Fig. 4b]

The curves in Fig. 2.3.1 and 2.3.2 are established for a trailing edge thickness of t'/t=0.02 and Re=$2x10^5$ (based on chord and outlet velocity)

The final profile loss is equal to the profile loss at zero incidence, multiplied by an incidence coefficient, χ_i.

$Y_p= \chi_i \, Y_{P(i=0)}$ (eq. 2.3.3)

To obtain χ_i, it is needed to calculate the stalling incidence first. Ainley/Mathieson found that the positive stalling incidence on turbine blades can be correlated with pitch to chord ratio, **t/l**, exit flow angle, $\mathbf{a}_{out}$, and $\mathbf{a'_{in}/a_{out}}$. The stalling incidence for an equivalent cascade of pitch to chord ratio of 0.75 is determined from Fig. 7.3.3(a), the correction on exit angle for the t/l=0.75 equivalent cascade being determined from Fig. 2.3.3(b). For the actual value of t/l, the stalling incidence is then obtained from Fig. 2.3.3.(c). After knowing the stall incidence, $\mathbf{i_{(stall)}}$, and the incidence, **i**, the off-design profile loss coefficient, $\mathbf{c_i=Y_p/Y_{P(i=0)}}$, can be obtained from Fig. 2.3.4.

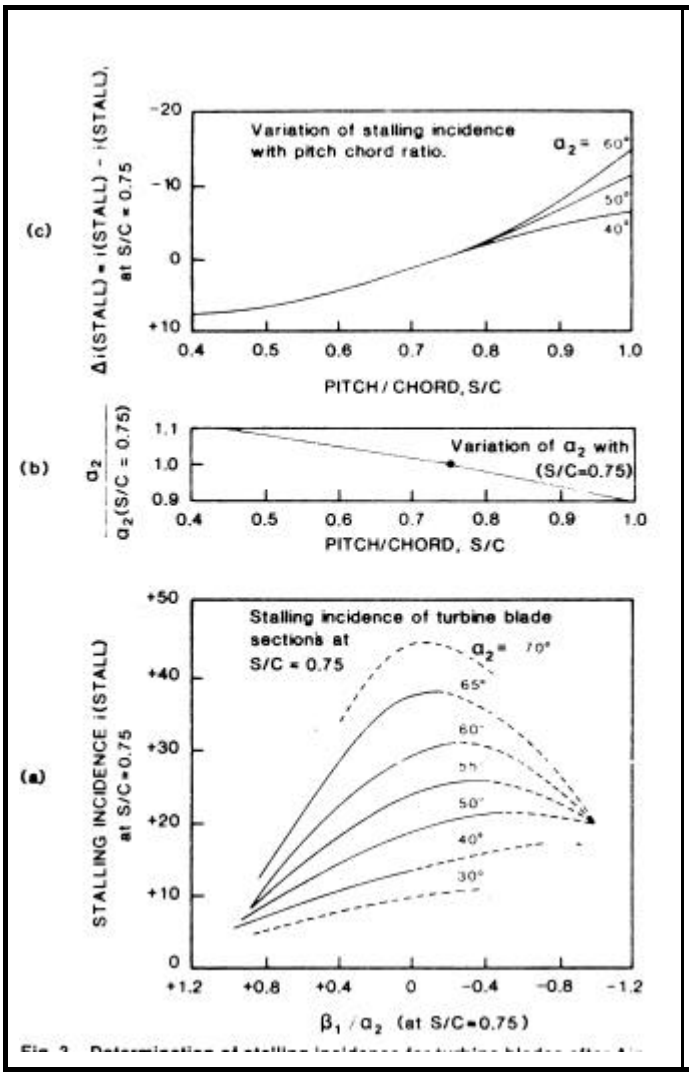

Fig.2.3.3: Determination of stalling incidence for turbine [Ainley & Mathieson, 1951, Fig. 7]

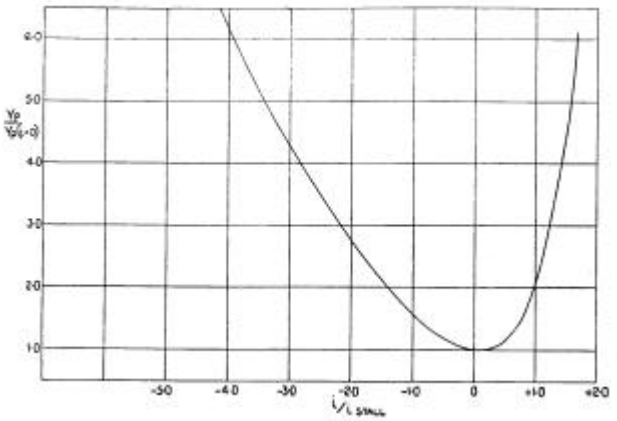

Fig.2.3.4: Variation of profile loss with incidence [Ainley & Mathieson, 1951, Fig. 6]

This method is valid in the condition of a trailing edge thickness to pitch ratio of 0.02, Reynolds number of 2×10^5 and Mach number less than 0.6.

Secondary Loss

The basic equation for secondary loss coefficient given by Ainley & Mathieson [1951] was derived from performance measurements on conventional blades using the correlation already established for profile losses [Sieverding, 1985]. It is calculated in based on the blade loading which is considered as a main function of the blade turning. This secondary loss coefficient can be calculated with eq. 2.3.4 [Ainley & Mathieson, 1951, p. 5].

$$Y_S = l\left(\frac{C_L}{t/l}\right)^2\left(\frac{\cos^2 a_{out}}{\cos^3 a_m}\right) \qquad \text{(eq. 2.3.4)}$$

In the equation 2.3.4, Ψ is a parameter which is function of the flow acceleration through the blade row and can be found in a figure [Ainley & Mathieson, 1951, p. 26]. α_m is the average flow angle in the cascade and can be calculated with eq. 2.3.5 [Ainley & Mathieson, 1951, p. 5].

$$\alpha_m = \tan^{-1}[(\tan\alpha_{in} + \tan\alpha_{out})/2] \qquad \text{(eq. 2.3.5)}$$

C_L is the lift coefficient of the blade which was defined by Lakshminarayana [1996] with equation 2.3.6:

$$C_L = 2\frac{t}{l}(\tan\alpha_{in} - \tan\alpha_{out})\cos\alpha_m \qquad \text{(eq. 2.3.6)}$$

Then finally, the secondary loss can be calculated with equation 2.3.7

$$Y_S = \Psi 4(\tan\alpha_{in} - \tan\alpha_{out})^2\left(\frac{\cos^2\alpha_{out}}{\cos\alpha_m}\right) \qquad \text{(eq. 2.3.7)}$$

It is a function of the flow inlet and outlet angle and the coefficient Ψ.

Tip Leakage Loss

The tip leakage loss is also considered, with the same principle as the secondary loss, as a function of blade loading supplemented with the ratio of tip clearance to the blade height. It can be calculated with eq. 2.3.8 [Ainley & Mathieson, 1951, p. 5].

$$Y_{Tl} = B\frac{\tau}{h}4(\tan\alpha_{in} - \tan\alpha_{out})^2\left(\frac{\cos^2\alpha_{out}}{\cos\alpha_m}\right) \qquad \text{(eq. 2.3.8)}$$

τ -- radial tip clearance
h -- annulus height (equals blade height if radial tip clearance is zero)
B -- coefficient, 0.25 for shrouded blades or 0.5 for unshrouded blades

The variation of incidence was not considered by Ainley & Mathieson [1951] in the tip leakage loss.

2.4 Dunham & Came

The loss prediction method by Ainley & Mathieson [1951] was improved by Dunham & Came [1970]. The developments were based on, at that time, more recent data. Dunham & Came tested the Ainley-Mathieson method against experimental data from 25 turbines. They found that Ainley-Mathieson method was satisfactory for typical aircraft turbines but was misleading for small turbines. Thereafter they corrected the Ainley-Mathieson method by changing some of the loss correlations.

Total Loss Coefficient

The total losses in a turbine cascade by Dunham & Came [1970] is based on the loss model by Ainley-Mathieson [1951] and with additional consideration of the influence of Reynolds number on the profile and secondary losses (see eq. 2.4.1).

$$Y = \left[\left(Y_P + Y_S \right) \left(\frac{\mathrm{Re}}{2 \times 10^5} \right)^{-0.2} + Y_{Tl} \right] c_{Te} \qquad \text{(eq. 2.4.1)}$$

χ_{Te} is the trailing edge correction factor. It is the same as the one given by Ainley & Mathieson.

Profile loss

Dunham and Came developed the profile loss model from Ainley/Mathieson by taking the factor of Mach number into account. It is calculated with eq. 2.4.2.

$$Y_P = \left[1 + 60 \left(M_{out} - 1 \right)^2 \right] \chi_i Y_{P(i=0)} \qquad \text{(eq. 2.4.2)}$$

$\mathbf{Y_{P(i=0)}}$ and $\mathbf{c_i}$ are the profile loss at zero incidence and the incidence correction factor respectively. They are calculated in the same way as in the model given by Ainley/Mathieson.

Secondary Loss

Dunham and Came found that the Ainley/Mathieson secondary loss model was not correct for blade of low aspect ratio, as in small turbines. They modified the Ainley/Mathieson model to include a better correlation with aspect ratio, **H/l**, and at the same time simplified the flow acceleration parameter, $\mathbf{l}$. The models given by Dunham and Came is:

$$Y_S = 0.0334 \left(\frac{l}{H} \right) \left[4 \left(\tan\alpha_{in} - \tan\alpha_{out} \right)^2 \right] \left(\frac{\cos^2 \alpha_{out}}{\cos \alpha_m} \right) \left(\frac{\cos \alpha_{out}}{\cos \alpha'_{in}} \right) \qquad \text{(eq. 2.4.3)}$$

Tip Leakage Loss

The tip leakage loss model given by Dunham and Came is based on the model from Ainley/Mathieson , i.e. the loss coefficient is the function of blade load and tip clearance. However, Dunham & Came [1970] calculate the coefficient as the power function of the tip clearance instead of the linear function by Ainley/Mathieson. The model is

$$Y_{Tl} = B\frac{l}{h}\left(\frac{\tau}{l}\right)^{0.78} 4\left(\tan\alpha_{in} - \tan\alpha_{out}\right)^2\left(\frac{\cos^2\alpha_{out}}{\cos\alpha_m}\right) \qquad \text{(eq. 2.4.4)}$$

τ -- tip clearance
h -- annulus height (equals blade height if radial tip clearance is zero)
B -- coefficient, 0.47 for unshrouded blades or 0.37 for shrouded blades

For some shrouded blades with multiple tip seals, the effective value of τ is used. It is calculated with eq. 2.4.5.

τ=(geometrical tip clearance) x (number of seals)$^{-0.42}$ (eq. 2.4.5)

2.5 Kacker & Okapuu

The loss prediction method by Kacker & Okapuu [1982] is mainly based on the method by Ainley & Mathieson [1951] and the modified method by Dunham & Came [1970]. It was shown to be able to predict the efficiencies of a wide range of axial turbines of conventional stage loading to within +/- 1.5 % [Kacker & Okapuu, 1982, p.111]. Compared with the prediction methods by Ainley/Mathieson and Dunham/Came, the major departure in this method is the restructuring of the loss system and the introduction of compressibility and shock losses into the calculation of profile and secondary loss coefficients.

Total Loss Coefficient

The total loss given by Kacker & Okapuu [1982] consists of profile loss, secondary loss, tip leakage loss and trailing edge loss. The model is

$$Y = \chi_{Re} Y_p + Y_s + Y_{Tl} + Y_{Te} \qquad \text{(eq. 2.5.1)}$$

χ_{Re} is the Reynolds number correction factor. Comparing with the models by Ainley/Mathieson and Dunham/Came, they considered that the Reynolds number affects only the profile loss and the trailing edge loss is a separated from the other loss components. The Reynolds number is based on true chord and cascade exit flow conditions. χ_{Re} is calculated with the following equation.

$$c_{\mathrm{Re}} = \begin{cases} \left(\dfrac{\mathrm{Re}}{2\times10^5}\right)^{-0.4} & \mathrm{Re} \le 2\times10^5 \\ 1.0 & 2\times10^5 > \mathrm{Re} < 10^6 \\ \left(\dfrac{\mathrm{Re}}{10^6}\right)^{-0.2} & \mathrm{Re} > 10^6 \end{cases} \qquad \text{(eq. 2.5.2)}$$

Profile loss

The profile loss model given by Kacker & Okapuu [1982] is

$$Y_P = 0.914\left(\frac{2}{3}K_P\, c_i\, Y_{P(i=0)} + Y_{shock}\right) \qquad \text{(eq. 2.5.3)}$$

$Y_{P(i=0)}$ is the profile loss at zero incidence, which is mainly based on the one given by Ainley/Mathieson [1951] and calculated with

$$Y_{P(i=0)} = \left\{Y_{P(\alpha'_{in}=0)} + \left|\frac{\alpha'_{in}}{\alpha_{out}}\right|\left(\frac{\alpha'_{in}}{\alpha_{out}}\right)\left[Y_{P(\alpha'_{in}=\alpha_{out})} - Y_{P(\alpha'_{in}=0)}\right]\right\}\left(\frac{t'_{max}/l}{0.2}\right)^{\frac{\alpha'_{in}}{\alpha_{out}}} \qquad \text{(eq. 2.5.4)}$$

$\mathbf{c_i}$ is the incidence coefficient which is the same as one used by Ainley/Mathieson and Dunham/Came. The foregoing equation is similar to the equation given by Ainley/Mathieson except for the term $|\alpha'_{in}/\alpha_{out}|$, which was introduced to allow for negative inlet angle.

Kacker & Okapuu realised that the profile loss coefficient given by Ainley/Mathieson were derived from cascade tests carried out at low subsonic velocities and are therefore conservative when applied to turbines operating at higher Mach number levels. To correct this, they gave a Mach number correction factor K_p in the foregoing equation. It is calculated with

$$K_p = 1 - 1.25\left(M_{out} - 0.2\right)\left(\frac{M_{in}}{M_{out}}\right)^2 \qquad \text{for } M_{out} > 0.2 \qquad \text{(eq. 2.5.5)}$$

Y_{shock} is the loss coefficient concerning the loss caused by shocks. It is calculated with

$$Y_{shock} = 0.75\left(M_{in,H} - 0.4\right)^{1.75}\left(\frac{r_H}{r_T}\right)\left(\frac{p_{in}}{p_{out}}\right)\frac{1-\left(1+\frac{\gamma-1}{2}M_{in}^2\right)^{\gamma/\gamma-1}}{1-\left(1+\frac{\gamma-1}{2}M_{out}^2\right)^{\gamma/\gamma-1}} \qquad \text{(eq. 2.5.6)}$$

In equation (2.5.6), $\mathbf{M_{in,H}}$ is the inlet Mach number at the hub. It can be obtained from the correlation between the inlet average Mach number and the ratio of the hub radius to the tip radius [Kacker & Okapuu, 1982, p.113, Fig. 6]. According to Håll [1990], $\mathbf{M_{in,H}}$ can be calculated with equation (eq. 2.5.7).

$$M_{in,H} = M_{in}\left(1 + K\left|\frac{r_H}{r_T} - 1\right|^{2.2}\right) \qquad \text{(eq. 2.5.7)}$$

In equation (2.5.6), **K** is a constant. It is 1.8 for stators and 5.2 for rotors.

Secondary Loss

Kacker & Okapuu [1982] revised the secondary loss model from Dunham & Came [1970] based on some test results by considering the influence of blade aspect ratio and flow compressibility, which is expressed as the χ_{AR} and the last item respectively in the following equation. The secondary loss model given by Kacker/Okapuu is

$$Y_S = 0.04\left(\frac{l}{H}\right)\chi_{AR}\left[4\left(\tan\alpha_{in} - \tan\alpha_{out}\right)^2\right]\left(\frac{\cos^2\alpha_{out}}{\cos\alpha_m}\right)\left(\frac{\cos\alpha_{out}}{\cos\alpha'_{in}}\right)\left[1-\left(\frac{l_x}{H}\right)^2\left(1-K_P\right)\right] \qquad \text{(eq. 2.5.8)}$$

K_p is the same as one calculated with eq. 2.5.5.

χ_{AR} is the aspect ratio coefficient. It is:

$$\chi_{AR} = \begin{cases} 1 - 0.25\sqrt{2 - H/l} & \text{for } H/l \le 2 \\ 1 & \text{for } H/l > 2 \end{cases} \qquad \text{(eq. 2.5.9)}$$

Tailing Edge Loss

Kacker & Okapuu [1982] considered that the pressure tailing edge loss coefficient is a function of outlet Mach number and energy trailing edge loss coefficient. It can be calculated with

$$Y_{Te} = \frac{\left[1+\frac{\gamma-1}{2}M_{out}^2\left(\frac{1}{1-\Delta E_{Te}}-1\right)\right]^{-\gamma/(\gamma-1)} - 1}{1-\left(1+\frac{\gamma-1}{2}M_{out}^2\right)^{-\gamma/(\gamma-1)}} \qquad \text{(eq. 2.5.10)}$$

ΔE_{Te} is the energy loss coefficient at trailing edge. It should be the same definition as the enthalpy loss coefficient, ξ, based on the isentropic exit velocity shown in chapter 1 (see [Sieverding, 1985, p. 751 and Fig. 16]). It is a main function of the ratio of trailing edge thickness, **t'**, to the throat distance of blade passage, **o**. From an extensive survey of published and in-house cascade results, Kacker & Okapuu [1982] gave relations between the ratio **t'/o** and the trailing edge loss coefficient for axial entry blades, $\Delta E_{Te(\alpha'_{in}=0)}$, and the coefficient for impulse blades, $\Delta E_{Te(\alpha'_{in}=\alpha_{out})}$ (see Fig. 2.5.1)

For blades other than these two types, the trailing edge energy loss coefficient are interpolated in eq. 2.5.11 [Kacker & Okapuu, 1982, p. 116].

$$\Delta E_{Te} = \Delta E_{Te(\alpha'_{in}=0)} + \left|\frac{\alpha'_{in}}{\alpha_{out}}\right|\left(\frac{\alpha'_{in}}{\alpha_{out}}\right)\left[\Delta E_{Te(\alpha'_{in}=\alpha_{out})} - \Delta E_{Te(\alpha'_{in}=0)}\right] \qquad \text{(eq. 2.5.11)}$$

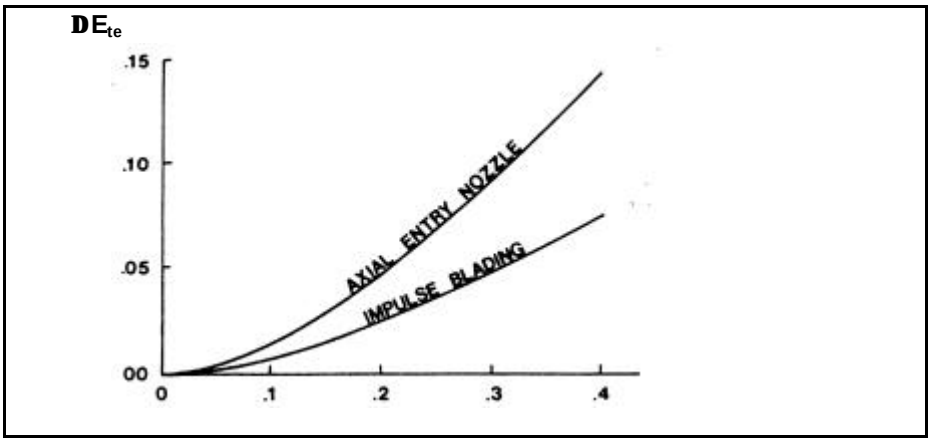

Fig. 2.5.1: *Trailing edge loss given by Kacker & Okapuu [1982, Fig. 14].*

Tip Leakage Loss

Tip Leakage Loss for Unshrouded Blades

The tip leakage loss given by Kacker & Okapuu [1982] is based on a large body of experimental data. Instead of giving directly the equation for calculating the loss coefficient, they derived the relation between the variation of total to total stage efficiency and the variation of tip clearance of unshrouded blades in eq. 2.5.12 (see [Kacker & Okapuu.1982, p. 116]).

$$\Delta h_{tt} = 0.93\left(\frac{r_T}{r_m}\right)\left(\frac{1}{H\cos\alpha_{out}}\right)h_{tt,0}\,\Delta t \qquad \text{(eq. 2.5.12)}$$

$\eta_{tt,0}$ is the total to total stage efficiency when the tip clearance is assumed as zero. Δt is the variation of the tip clearance. $\Delta\eta_{tt}$ is the variation of the total to total stage efficiency, the value of which depends on the $\eta_{tt,0}$, the ratio of tip radius to mean radius r_t/r_m, the outlet flow angle α_{out} and the variation of tip clearance Δt.

The tip leakage pressure loss coefficient Y_{Tl} by Kacker & Okapuu [1982] can be obtained by iterative calculating with eq. 2.5.12, eq. 2.5.1 and equation for total to total stage efficiency. Kacker & Okapuu [1982] did not give the detailed process of the iterative calculations.

Tip Leakage Loss for shrouded Blades

The tip leakage loss model for shrouded blades given by Kacker & Okapuu [1982] is based on the model from Dunham & Came [1970] (see equation 5.4). It is

$$Y_{Tl} = 0.37\frac{l}{h}\left(\frac{t'}{l}\right)^{0.78} 4\left(\tan a_{in} - \tan a_{out}\right)^2\left(\frac{\cos^2 a_{out}}{\cos a_m}\right) \qquad \text{(eq. 2.5.13)}$$

t' is the effective value of tip clearance **t**. It is calculated with eq. 2.5.14.

τ'=(geometrical tip clearance, τ) / (number of seals)$^{-0.42}$ (eq. 2.5.14)

2.6 Craig & Cox

Craig & Cox [1970] presented a method for predicting losses in an axial turbine stage. The method is based on analysis of linear cascade tests on blading, on a number of turbine test results, and on air tests of model casings [Craig & Cox, 1970, p. 407]. They showed that the method was allowed to be used for predicting performance of actual machines over a wide range of Reynolds number, Mach number, aspect ratio and other relevant variables with the accuracy less than +/- 1.25% on the overall efficiency.

Total Loss Coefficient

The total loss coefficient over a turbine cascade by Craig & Cox [1970] is split in the profile losses, secondary loss and annulus loss. It can be shown in eq. 2.6.1.

$$\zeta = \zeta_p + \zeta_s + \zeta_A \qquad \text{(eq. 2.6.1)}$$

Profile Loss

The profile loss model given by Craig & Cox [1970] is based on experimental data from straight cascade from prior to 1970. It is likely that this model relies to a great extent on conventional blade design with profiles made up of circles and straight lines [Sieverding, 1985].

The profile losses consist of an incompressible basic profile loss corrected by multiplying factors of Reynolds number, incidence and trailing edge. Further the effect of Mach number, suction trailing side curvature and trailing edge thickness are added. It is presented in eq. 2.6.2.

$$\zeta_p = \chi_R\, \chi_{Te}\, \chi_i\, \zeta_{P0} + \Delta\zeta_{P,M} + \Delta\zeta_{P,Se} + \Delta\zeta_{P,Tt} \qquad \text{(eq. 2.6.2)}$$

The basic profile loss parameter, $\zeta_{P0}\, t/b \sin a_{out}$, was given in a diagram by Craig & Cox [1970, Fig. 5] (see Fig. 2.6.1). It is based on a modified blade lift parameter, F_L, and a contraction ratio, **CR**. The lift parameter, F_L, depends on the flow turning and the cascade solidity (see Fig. 2.6.2). The contraction ratio denotes the internal blade passage with ratio of the particular cascade based on inlet to throat. This value can be measured for a known cascade. Craig & Cox [1970, p. 412, Fig 7] gave a correlation of this contraction ratio, **CR**

(see Fig. 2.6.3). In Fig. 2.6.1, **s** is pitch, **b** is blade backbone length and **B** is outlet flow angle.

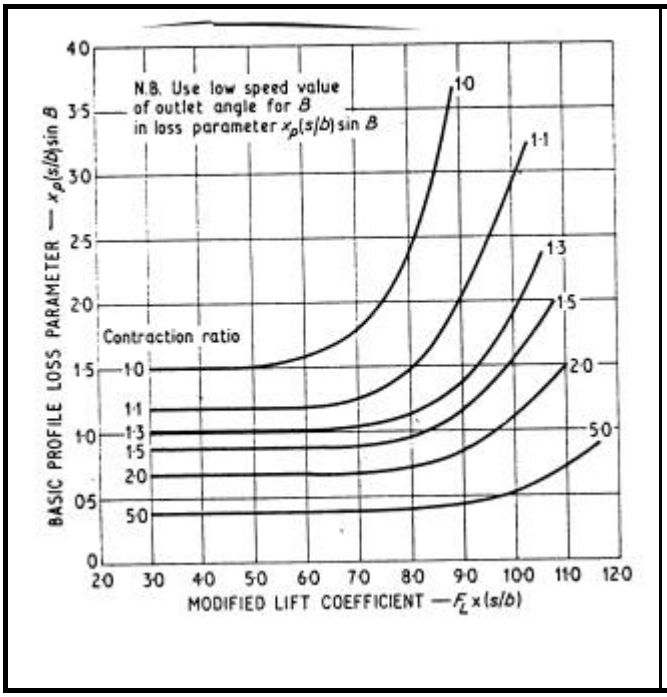

Fig. 2.6.1: Basic profile loss given by Craig and Cox [1970, Fig. 5]

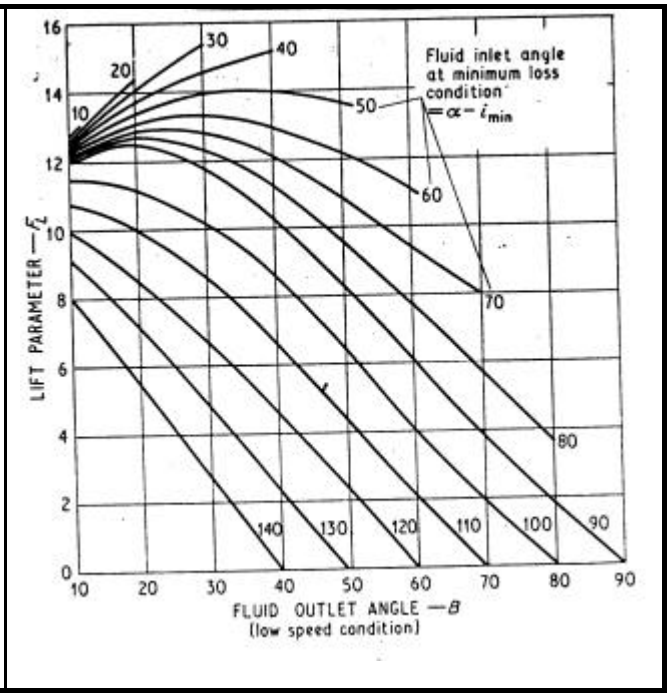

Fig. 2.6.2: Lift parameter, F_l, given by Craig & Cox, [1970, Fig 4].

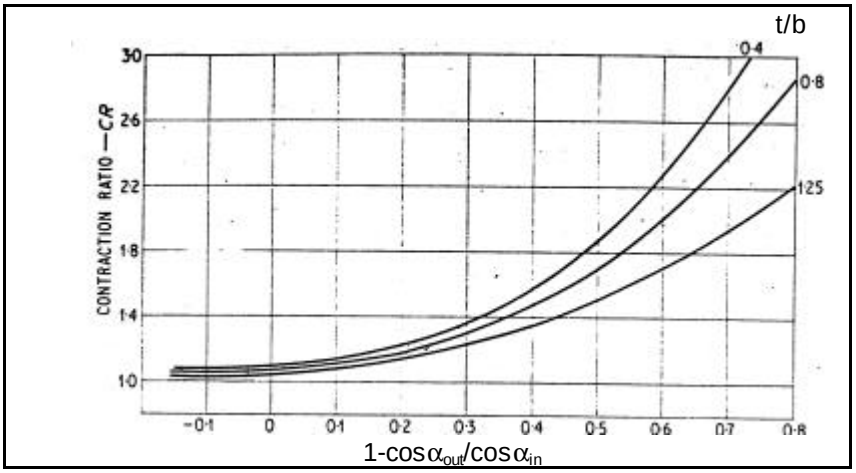

Fig. 2.6.3: *Contraction ratio given by Craig & Cox [1970, Fig.7]*

The loss multiplication factor due to Reynolds number, $\mathbf{c_R}$, was given in a figure by Craig & Cox [1970, p. 411, Fig 3] (see Fig. 2.6.4). In the figure, the Reynolds number factor is represented as $\mathbf{N_{pr}}$. Similar to the Reynolds number factor given by Traupel in Fig. 2.2.2, this figure also shows that a high Reynolds number (above $2x10^5$) has no effect on the profile loss, while a low Reynolds number will increase the profile loss caused by a general thickening of the laminar boundary layers and a gradual increase of separated laminar flow regions.

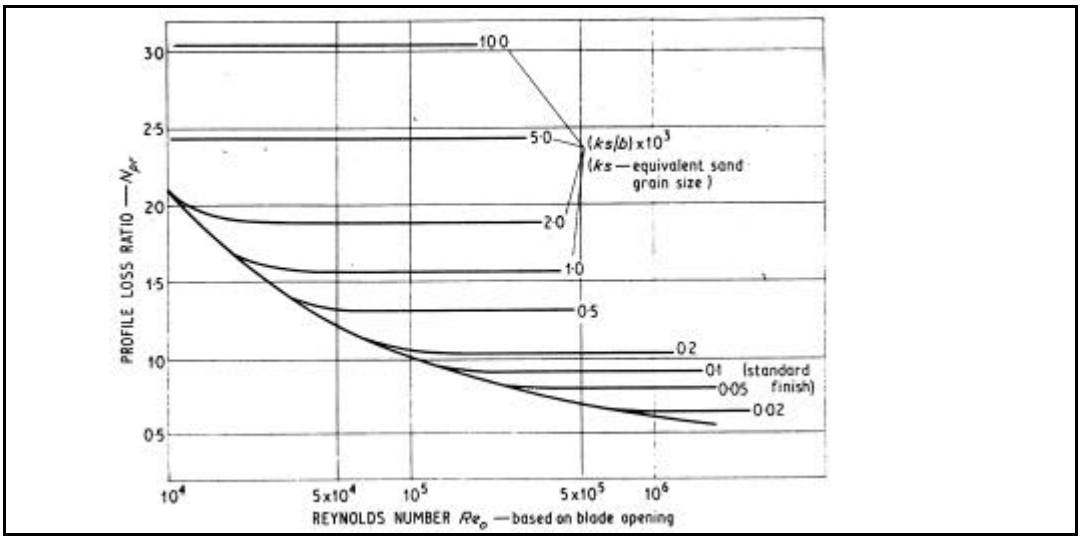

Fig. 2.6.4: *Reynolds number factor on the profile loss by Craig & Cox [1970, Fig. 3.]*

The multiplication factor due to trailing edge thickness, ζ_{Te}, is a function of the fluid outlet angle and the ratio of trailing edge thickness to pitch [Craig & Cox, 1970, p. 412, Fig 6].

At off design conditions, the profile loss are altered by the incidence losses. Craig & Cox [1970] introduced these incidence losses as a multiplying factor, ζ_i, to the basic profile loss. ζ_i can be obtained from several relations with the incidence angle, blade inlet angle, blade pitch, blade throat distance and length of blade camber line, showed in figures by Craig & Cox [1970, Fig. 10-15]. Fig. 2.6.5 shows the off-design profile loss distribution given by Craig/Cox.

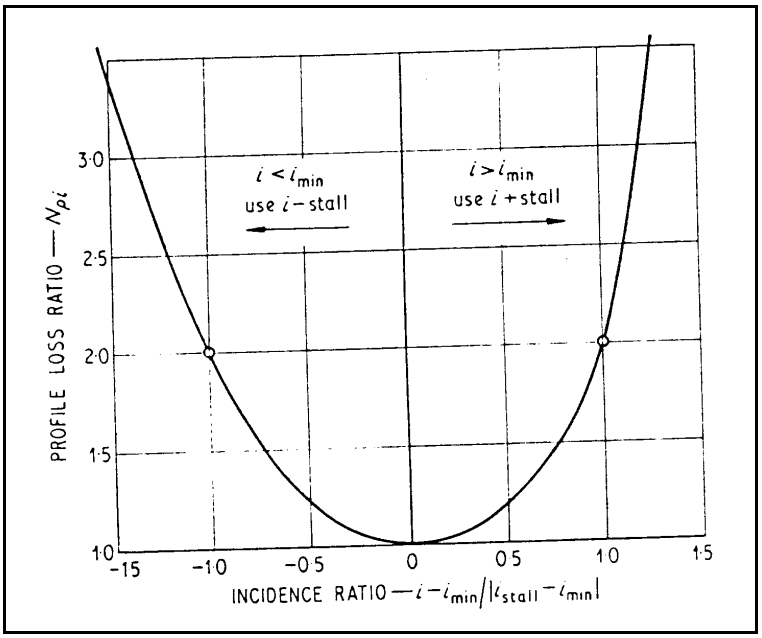

Fig. 2.6.5: *Off-design profile loss by Craig & Cox* [1970, Fig. 10].

The loss increment, $\Delta\zeta_{P,M}$, due to outlet Mach number for supersonic flow depends on the outlet Mach number, blade pitch, blade throat width and trailing edge thickness. The relations were given in a figure by Craig & Cox [1970, p. 413, Fig. 8] (see Fig. 2.6.6).

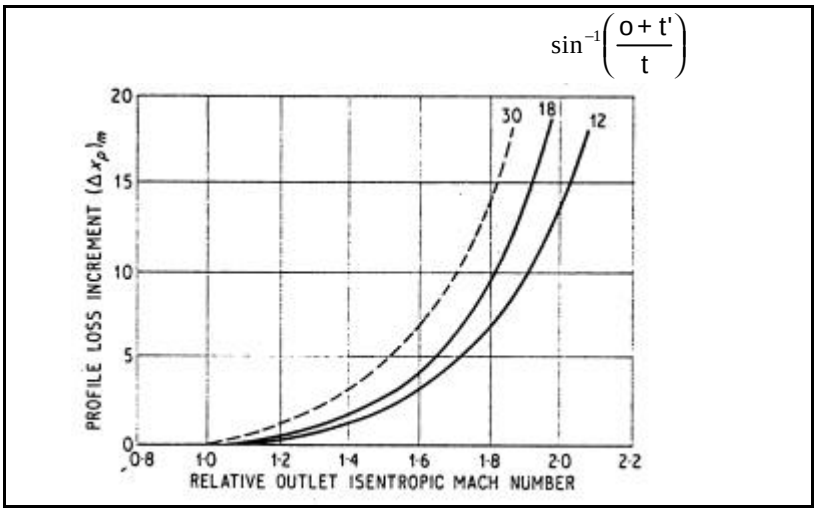

Fig. 2.6.6: *Mach number loss [Craig & Cox 1970, Fig. 8]*

A basic profiles is supposed to have a straight suction back. For the blades with curvature suction surfaces near trailing edges, the loss increment due to the trailing edge curvature, $\Delta\zeta_{P,Se}$, is needed. $\Delta\zeta_{P,Se}$ depends on the outlet Much number, blade pitch and length of blade camber line. This relation was given in a figure by Craig & Cox [1970, p. 413, Fig. 9].

The loss increment due to trailing edge thickness, $\Delta\zeta_{P,Tt}$, is a function of the blade pitch and trailing edge thickness (see [Craig & Cox, 1970, p. 413, Fig. 6]).

Secondary Loss

The total secondary loss coefficient given by Craig & Cox [1970] is based on experimental data from straight cascades. From a comparison of calculated and measured turbine performance data, the authors concluded that their cascade secondary loss data did not need to be corrected for use in turbine stage calculation. The secondary loss coefficient is a function of the basic secondary loss, ζ_{S0}, multiplied by factors due to Reynolds number, χ_R, and blade aspect ratio, χ_{AR}. It is showed in eq. 2.6.3.

$$\zeta_S = \chi_R \chi_{AR} \zeta_{S0} \qquad \text{(eq. 2.6.3)}$$

The basic secondary loss is a function of the lift parameter, F_L, and the ratio of the flow inlet velocity to the outlet velocity (see Fig. 2.6.7 [Craig & Cox, 1970, Fig. 18]). The multiplied factor due to Reynolds number, χ_R, was not given by Craig & Cox. The factor due to blade aspect ratio, χ_{AR}, is just a function of the aspect ratio (see Fig. 2.6.8 [Craig & Cox , 1970, p.417, Fig. 17]).

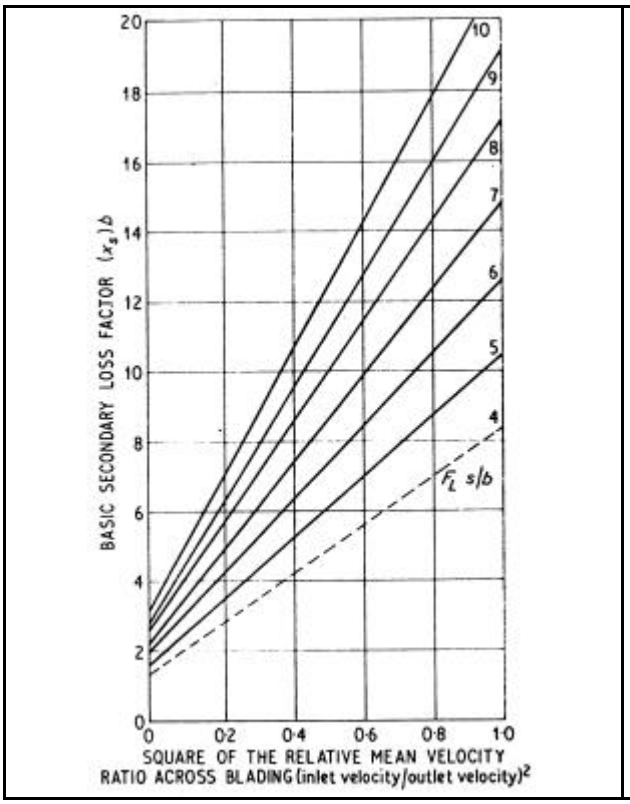

Fig. 2.6.7: *Basic secondary loss* [Craig & Cox, Fig. 18].

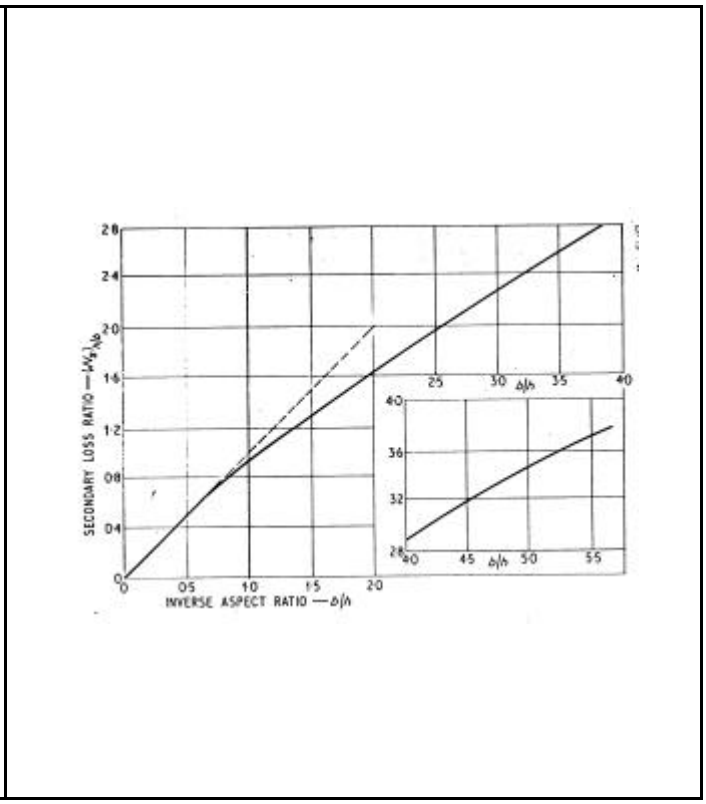

Fig. 2.6.8: *Aspect ratio factor of the secondary loss* [Craig & Cox, Fig. 17].

Tip leakage loss

The tip leakage loss in the C-C models is calculated with equation 2.6.4, in which the variation of the cascade efficiency caused by the tip leakage loss is a function of the leakage coefficient, ratio of the clearance to throat areas and the efficiency when the clearance is zero. The leakage coefficient F_k, in the equation is mainly a function of the ratio of the inlet and outlet velocity at the tip region (see [Craig & Cox, 1970, Fig. 21]). When this ratio is small, the leakage coefficient will be large. This actually imply the static pressure drop over the blade row. The small inlet and outlet velocities ratio means a high acceleration of the flow and large static pressure drop over the blade, which will drive more leakage flow through the clearance area and cause large tip clearance loss. A large inlet and outlet velocities ratio, for example when the ratio is close to unity, indicate a low acceleration of the flow and small static pressure drop. The mass flow through the leakage will be small therefore the tip leakage is small.

$$\Delta h_{Tl} = F_k \frac{A_k}{A_t} h_{Tl=0} \qquad \text{(eq. 2.6.4)}$$

Annulus loss

The annulus loss given by Craig & Cox occur when the annulus wall has an appreciable amount of diffusion between two stages or between the stator and rotor. The annulus loss

coefficient, ζ_A, is a function of detailed geometry of the annulus wall. This can be found in a figure by Craig & Cox [1970, p.418, Fig. 19].

Other losses

Some other kind losses were also mentioned by Craig & Cox, such as balance hole loss, lacing loss, wetness loss, disc windage loss and admission loss. These losses were considered by Craig & Cox when the stage efficiency was calculated but not included in the total cascade loss. Detailed methods for predicting these losses were not given by Craig & Cox.

2.7 Denton

The loss prediction method given by Denton [1987, 1990, 1993, 1994] is based on the fact that the physical origin of loss is the increase of entropy, which is created when there are viscous effects in boundary layers, viscous effects in mixing processes, shock waves and heat transfer within the fluid. The author performs studies on the entropy change through various flow disturbances. The loss models are established by means of applying boundary layer theories, basic thermodynamic equations and simplified equation of conservation of mass, momentum and energy on each specific loss condition. Some empirical parameter, such as base pressure coefficient, is also needed for the predictions.

Total Loss Coefficient

The total losses given by Denton [1994] concerning a turbine cascade is a sum of the all of the individual losses created in the cascade row, which consists of blade surface boundary layer losses, trailing edge losses, tip leakage losses, endwall boundary layer losses, endwall mixing losses, shock loss and other losses. It can be, in principle, shown in eq. 2.7.1.

$$\zeta = \sum \zeta_i \qquad \text{(eq. 2.7.1)}$$

However not all of the loss prediction models were given by Denton [1987, 1990, 1993, 1994] (see Eq. 2.7.2).

$$\zeta_N = \zeta_{Bb} + \zeta_{Te} + \zeta_{Tl} + \zeta_{Eb} + \zeta_{shock} \qquad \text{(eq. 2.7.2)}$$

Blade Surface Boundary Layer Losses

The blade surface boundary layer loss is associated with growth of the blade surface boundary layers. From Denton [1993a, p. 14, eq. 41 & 42] and [1993b], the blade surface boundary layer loss coefficient can be obtained as:

stator $$\zeta_{Bb,N} = \frac{T_1 \Delta S_{Bb,N}}{m c_1^2/2}$$ (eq. 2.7.3)

where $$\Delta S_{Bb,N} = \sum_s^p H C_s \int_0^1 \frac{C_d r c^3}{T} d(s/C_s)$$ (eq. 2.7.4)

rotor $$\zeta_{Bb,R} = \frac{T_2 \Delta S_{Bb,R}}{m w_2^2/2}$$ (eq. 2.7.5)

where $$\Delta S_{Bb,R} = \sum_s^p H C_s \int_0^1 \frac{C_d r w^3}{T} d(s/C_s)$$ (eq. 2.7.6)

The dissipation coefficient of the blade surface boundary layer, C_d, is assumed to be 0.002, if the boundary layer is in turbulent state [Denton, 1993a, p. 6] (For the laminar boundary layer, $C_d = 0.2\ Re_\theta^{-1}$ [Denton, 1994]). "p" and "s" on the sum symbols in eq. 2.7.4 and eq. 2.7.6 mean the sum over the pressure surface and suction surface. For a preliminary prediction, one can use a simple assumption of the velocity distribution suggested by Denton [1990, p. 2254].

From these equations, it can be seen that the blade boundary layer loss is in proportion to the cube of velocity.

Trailing Edge Loss

The trailing edge loss is the loss due to the finite thickness of the blade trailing edges. Denton [1993] considered that this loss is a function of the base pressure, flow angle at the outlet of cascade, blade pitch, thickness of the trailing edge, boundary layer displacement and momentum thickness at the trailing edge. It can be calculated with following equations:

stator: $$z_{Te,N} = -\frac{C_{pb} t'_N}{t_N \cos a_1} + \frac{2 q_N}{t_N \cos a_1} + \left(\frac{d^*_N + t'_N}{t_N \cos a_1}\right)^2$$ (eq. 2.7.7)

$$C_{pb} = (p_{b,N} - p_1)/(p_{c1} - p_1)$$ (eq. 2.7.8)

rotor: $$z_{Te,R} = -\frac{C_{pb} t'_R}{t_R \cos b_2} + \frac{2 q_R}{t_R \cos b_2} + \left(\frac{d^*_R + t'_R}{t_R \cos b_2}\right)^2$$ (eq. 2.7.9)

$$C_{pb} = (p_{b,R} - p_2)/(p_{c2} - p_2)$$ (eq. 2.7.10)

This trailing edge loss model was derived from an analysis of a flow mixing control volume in which the equations for conservation of mass, energy and momentum are applied between the blade throat and a far downstream boundary where the mixing process is assumed to

have restored the flow to a completely uniform condition. In eq. 2.7.7, the first term is the loss due to the low base pressure acting on the trailing edge, in general this must be obtained from empirical data. Denton suggested that the typical value of C_{pb} is in the range -0.1 to -0.2. Or this base pressure can, for example, be obtained from the correlation by Sieverding (see [Sieverding et al, 1980]. The second term is the mixed out loss of the boundary layers on the blade surface just before the trailing edge and the third term arises from the combined blockage of the trailing edge and the boundary layers.

For the case where the boundary layers are separated at the trailing edge, Denton gave a model to calculate this separation loss by

$$z_{sep} = \left(\frac{W}{t\cos\beta_2}\right)^2 \qquad \text{(eq. 2.7.11)}$$

In this model, W is a thickness of separation. This separation loss can be the extra loss to the equation 2.7.7. The loss calculated with equation 2.7.11 is surprisingly small, 1% loss for 10% blockage. In practice it is often found that the loss increases rapidly with trailing edge boundary layer separation, especially on the off-design operation points where the incidence to the blade row significant exists. Denton [1993, 1994] believed that this must be due to the separation reducing the base pressure and so increase the base pressure term in equation 2.7.7. From this point of view, to develop the Denton loss model to predict off-design losses, the relationship base pressure and incidence, $p_b=f(i)$, and separation thickness and incidence, $W=f(i)$, must be found out.

Tip Leakage Loss

The tip leakage loss is the loss due to leakage of flow around the ends of shrouded or unshrouded blades.

Shrouded Blades

The loss coefficient for shrouded turbine blades given by Denton [1993, p. 39, eq. A5.8] is a function of the inlet flow angle, outlet flow angle, leakage mass flow and main mass flow through the rotor blade passage as equation (2.7.12).

$$z_{Tl,R} = 2\frac{m_l}{m_m}\left(1-\frac{\tan\beta_1}{\tan\beta_2}\sin^2\beta_2\right) \qquad \text{(eq. 2.7.12)}$$

The tip leakage loss depends on two factors from eq. 2.7.11: one is the ratio of leakage flow to the main flow m_l/m_m; the other is the difference between direction of the leakage flow and the direction of the main flow through the rotor. The difference of the direction between the main and leakage flow is represented by β_1 and β_2 in eq. 2.7.11. The larger mass flow ratio m_l/m_m and angle between the leakage and main flow there are, the larger the leakage loss is.

Unshrouded Blades

The loss coefficient for unshrouded turbine blades given by Denton [1993, p. 39, eq. A5.8] is a function of the tip clearance, blade chord, blade span, blade pitch, outlet relative velocity and relative velocity distributions on the blade pressure surface and suction surface [Denton, 1993, p. 39].

$$\zeta_{Tl,R} = 1.5\frac{\tau l}{H t \cos\beta_2}\int_0^1\left(\frac{w_s}{w_2}\right)^3\left(1-\frac{w_p}{w_s}\right)\sqrt{\left(1-\left(\frac{w_p}{w_s}\right)^2\right)}\; d\left(s/l\right) \qquad \text{(eq. 2.7.13)}$$

In eq. 2.7.12, the integration is performed along the blade chord and from the leading edge to trailing edge. The velocity distribution on the blade surface used in eq. 2.7.12 can be determined in the same way as the calculation of blade boundary layer loss coefficient

Endwall Boundary Layer Loss

The endwall boundary layer loss is associated with the growth of boundary layers on the endwalls. These losses are separated into losses from boundary layers inside stator and rotor and losses from endwall boundary layers between cascades.

The endwall boundary loss coefficient can written as:

$$\zeta_{Eb} = \zeta_{Ebi} + \zeta_{Eb,Bt} \qquad \text{(eq. 2.7.14)}$$

Loss from Endwall Boundary Layer Inside Cascades

From the equation given by Denton [1993, p.23. eq. 50], the endwall boundary layer loss coefficient inside the cascade depends mainly on the entropy rate, ΔS_{Ebi}. The entropy rate is a function of the temperature, endwall area and velocity distributions on the pressure surface and suction surface of blade. The loss coefficient and entropy rate can be calculated with following equations.

inside stator:
$$z_{Ebi,N} = \frac{T_1 \Delta S_{Ebi,N}}{m\, c_1^2/2} \qquad \text{(eq. 2.7.15)}$$

$$\Delta S_{Ebi,N} = 0.25\int_0^{l_x}\frac{C_d}{T}\frac{(c_s^4 - c_p^4)}{(c_s - c_p)}\, r\, y_N\, dx \qquad \text{(eq. 2.7.16)}$$

inside rotor:
$$z_{Ebi,R} = \frac{T_2 \Delta S_{Ebi,R}}{m\, w_2^2/2} \qquad \text{(eq. 2.7.17)}$$

$$\Delta S_{Ebi,R} = 0.25\int_0^{l_x}\frac{C_d}{T}\frac{(w_s^4 - w_p^4)}{(w_s - w_p)}\, r\, y_R\, dx \qquad \text{(eq. 2.7.18)}$$

The velocity distribution on the blade surface used in eq. 2.7.15 and 2.7.17 can be determined in the same way as the calculation of blade boundary layer loss coefficient. Like the blade surface boundary layer, the endwall boundary layer inside a cascade from Denton's loss model is proportional to the cube of the flow velocity. The higher the velocity is, the larger endwall boundary layer loss the cascade has.

Loss from Endwall Boundary Layer Between Blade Rows

According to the basic equation for calculating loss due to the boundary layer [Denton, 1993, p. 7, eq. 20], the loss coefficient of the endwall boundary layer between the cascades can be calculated with the following equations.

$$z_{Eb,\,Bt} = \frac{T_1 \Delta S_{Eb,Bt}}{m c_1^2 / 2} \qquad \text{(eq. 2.7.19)}$$

$$\Delta S_{Eb,\,Bt} = \int_0^{A_w} \frac{C_d\, r\, c_1^3}{T} dA \qquad \text{(eq. 2.7.20)}$$

The endwall boundary layer between blade rows is proportional to the cube of the absolute velocity there. The loss is also proportional to the area of the endwall.

Endwall Mixing Losses

The endwall mixing losses include:
- Mixing loss of the upstream boundary layer approaching the blades within and downstream of the blade row
- Mixing loss of the complex secondary flow downstream
- Extra mixing loss due to separations by the complex endwall flows

The models for calculating the mixing loss coefficient above have not been given by Denton. Denton mentioned that the mixing loss of the upstream boundary layer is in the order of 20% of the loss present in the upstream boundary layer and the mixing loss of the secondary flow is of the order of 30% of the total endwall loss for turbines [Denton, 1994, p.35]. The magnitude of the extra mixing loss due to separation by the complex endwall flow has not been found.

Shock Loss

The shock loss is associated with the entropy creation which occurs due to heat conduction and high viscous normal stresses within the shock wave. Denton [1993, p.11] showed that the entropy creation by shock is a main function of the inlet Mach number. The shock loss coefficient and entropy creation due to the shock can be calculated with eq. 2.7.20 and 2.7.21 respectively.

$$\zeta_{shock} = \frac{T_{out}\Delta S_{shock}}{m\, V_{out}^2/2} \qquad \text{(eq. 2.7.21)}$$

$$\Delta S_{shock} = C_v \frac{2\gamma(\gamma-1)}{3(\gamma+1)^2}\left(M_{in}^2-1\right)^3 \qquad \text{(eq. 2.7.22)}$$

2.8 Stewart et al

Stewart et al [1960] presented the results of a number of investigations concerning the boundary layer characteristics of turbomachine blade rows and their relation to the overall blade loss. It is demonstrated how the overall blade loss can be obtained from the momentum boundary layer thickness. The momentum boundary layer thickness is in turn showed to be correlated by flow Reynolds number and total blade surface diffusion. By assuming Zweifel's form of blade-loading diagram the total blade surface diffusion parameter can be determined as a function of blade solidity and reaction across the blade row.

Total Loss Coefficient

The total losses were given as the combination of profile loss ζ_p, endwall loss ζ_e and trailing edge loss ζ_m (which is a kind of mixing loss at the trailing edge of blades).

$$z = z_p + z_e + z_m \qquad \text{(eq. 2.8.1)}$$

Profile Loss

The profile loss is associated with the boundary layer thickness. It was given as a fraction of the ratio of deficiency of momentum in the boundary layer to the ideal momentum in free-stream flow:

$$z_P = 1.8\frac{\frac{q}{l_c}\frac{l_c}{t\cos a_{out}}}{1-\frac{t'+d^*}{t\cos a_{out}}} \qquad \text{(eq. 2.8.2)}$$

l_c in the foregoing equation is the mean camber length of blade. To calculate this loss, the parameters of boundary layer momentum thickness, blade chord, blade pitch, outlet flow angle, camber line distance and boundary layer displacement thickness are needed. The boundary layer momentum thickness can be calculated with

$$\frac{q}{l_c} = \frac{0.003}{1-1.4D_t} \qquad \text{(eq. 2.8.3)}$$

D_t in equation 2.8.3 is the total diffusion parameter given by Stewart et al [1960].

Endwall Loss

The endwall loss was given just as simple factor multiplying to the profile loss (see eq. 2.8.4). This factor is a function of aspect ratio, solidity and blade stagger angle. The assumption for this is that the endwall loss is equal to the average loss occurring on the blade surfaces.

$$z_e = (1 + \frac{t \cos g}{H})\, z_p \qquad \text{(eq. 2.8.4)}$$

Mixing Loss

The mixing loss at trailing edge was given by multiplying a coefficient to the profile. It is

$$z_m = c_m\, z_p \qquad \text{(eq. 2.8.5)}$$

The coefficient c_m is given from a diagram (see [Stewart et al, 1960, Fig. 7]). Stewart et al [1960] gave the breakdown of the total losses which is with profile loss (called the kinetic-energy loss in the paper) 0.55, and the endwalls and trailing edge loss (called mixing loss in the paper) 0.25 and 0.20 respectively.

This model in principle can be used in subsonic conditions. Shock loss was not considered. The details of blade geometries for the experiments were not given in this paper. This model looks a bit rough and simple. However the model gave an example of how to derive the loss model from the analysis of boundary layer characters from experiments.

2.9 Baljé & Binsley

Baljé & Binsley [1968] gave a loss model which is expressed as a function of blade angles, blade height, blade pitch, blade trailing edge thickness and tip clearance. They mentioned that this method can be used in optimization of turbines over a wide range of possible operating conditions, however no specific limitations of this range was introduced by the authors.

Total Loss Coefficient

The total losses were splitted into profile loss, endwall loss, tip clearance loss and disk friction loss (see eq. 2.9.1).

$$z = z_p + z_e + z_{Tl} + z_{pa} \qquad \text{(eq. 2.9.1)}$$

Profile Loss

The profile loss is a function of blade pitch, outlet blade angle and boundary layer displacement and momentum thickness (see eq. 2.9.2). In principle, it was defined as the ratio of the boundary layer momentum thickness to the free flow passage.

$$z_p = 1 - \frac{\dfrac{\cos^2 l_2 (1 - d^* - q^* - \frac{t_e}{t})^2}{(1 - d^* - \frac{t_e}{t})^2} + \sin^2 l_2 (1 - d^* - \frac{t_e}{t})^2}{1 + 2\sin^2 l_2 \left[(1 - d^* - \frac{t_e}{t})^2 - (1 - d^* - q^* - \frac{t_e}{t}) \right]} \qquad \text{(eq. 2.9.2)}$$

In equation 2.9.1, λ_2 are the blade inlet and outlet angles defined by Baljé & Binsley [1968]: $\lambda_1 = (\alpha'_1 - 90^0)$. The blade inlet angle is $\lambda_2 = (90^0 - \alpha'_2)$. $\mathbf{t_e}$ in equation 2.9.1 is the trailing edge thickness.

This profile loss model was derived from the turbulent boundary layer equation for arbitrary pressure gradients [Sieverding, 1985]. The main assumption made in this model is that the total boundary layer growth on the blade surface can be reasonably well predicted using a linear variation of the velocity along the mean camber line. This assumption was justified on the basis of comparative calculations showing that the total boundary layer growth calculated in this way was essentially the same as the one using a more realistic trapezoidal blade velocity distribution. From integration of the assumed linear velocity distribution along the blade camber line, Baljé & Binsley [1968] gave simple correlations for calculating boundary layer displacement thickness and momentum thickness on blade surfaces with following equations:

$$q^* = \frac{q}{b_B} \frac{b_B}{l} \frac{l}{t \sin l_2} \qquad \text{(eq. 2.9.3)}$$

$$d^* = H_{bl} q^* \qquad \text{(eq. 2.9.4)}$$

$$\frac{q}{b_B} = \begin{cases} 0.0021 \left[\dfrac{1 - (\sin l_2 / \sin l_1)^{4.5}}{1 - \sin l_2 / \sin l_1} \right]^{0.8} & \mathrm{Re} = 2x10^5 \\ 0.0021 \left[\dfrac{1 - (\sin l_2 / \sin l_1)^{4.5}}{1 - \sin l_2 / \sin l_1} \right]^{0.8} Cr & \mathrm{Re} / = 2x10^5 \end{cases} \qquad \text{(eq. 2.9.5)}$$

$$Cr = \frac{71.0}{(\log_{10} \mathrm{Re})^{2.58}} + 1 - \tanh(1.96508 \log_{10} \mathrm{Re} - 8.51713)$$

$$\frac{b_B}{l} = \begin{cases} 0.7221988 + 0.005047357 (l_1 - l_2) & (l_1 - l_2) > 55 \\ 1.0 & (l_1 - l_2) <= 55 \end{cases} \qquad \text{(eq. 2.9.6)}$$

Endwall Loss

The endwall loss was given as a function of the flow deflection angle (λ_1-λ_2), the acceleration ratio ($\sin\lambda_2$/ $\sin\lambda_2$), aspect ratio and the initial boundary layer thickness.

$$z_e = K_e \frac{l}{H}\{\left[0.0388(\frac{\sin l_2}{\sin l_1}) + 0.08)(1+\frac{l_1 - l_2}{100})\right] + 0.0003371\left[10(\frac{\sin l_2}{\sin l_1} + 0.08)\right]^{1.5+\frac{l_1-l_2}{160}}\} \quad \text{(eq. 2.9.7)}$$

In the foregoing equation K_e is initial boundary layer coefficient, it can be calculated with

$$K_e = \begin{cases} 0.3 & stator \\ 0.3 + \tanh(2.857 z_{eN}) & rotor \end{cases} \quad \text{(eq. 2.9.8)}$$

The equation means that K_e can be chosen to be 0.3 for stator while for rotor the influence of the of the boundary layer from previous stator is concerned.

Tip Clearance Loss

The tip clearance loss given by Baljé & Binsley [1968] is based on the principle in which the tip leakage losses are functions of a blade loading parameter and the ratio of tip clearance to blade height, as well as solidity. It can be calculated with the tip clearance, blade height, cascade diameter, blade chord, mean flow angle and inlet and outlet blade angles as the following equation:

$$z_{Tl} = 0.0696 \tanh(13\frac{t}{l})\frac{l}{D}\frac{D}{H}\sin a_m(\cot l_2 - \cot l_1) \quad \text{(eq. 2.9.9)}$$

Baljé & Binsley [1968] showed that Reynolds number based on the blade camber line affects the profile loss coefficient because the momentum thickness will vary when the Reynolds number changes. The correction of the boundary layer momentum thickness as the effect of Reynolds number was given by them. The critical Reynolds number, at which laminar separation can no longer be avoided, was given as 1.5×10^4 for rotors and 4×10^4 for stators by Baljé & Binsley [1968, p.346]. No Reynolds number effect was assumed for the endwall and tip clearance losses.

2.10 Zehner

Zehner [1980] gave a loss model for calculating the off-design profile loss in axial turbines. The model is based on the turbine cascade characteristics, i.e. the loss coefficient is a

function of the cascade geometry and various parameters of flow, especially the incidence, Reynolds number and Mach number.

Off-design Profile Loss

An important cascade geometry parameter given by Zehner is:

$$g = \frac{f}{t}\sqrt{g(a'_{in} + a'_{out})} \qquad \text{(eq. 2.10.1)}$$

In the foregoing, **f** is the curvature height of the blade camber line i.e. the distance from the highest point on the camber line to the chord line. This parameter represents how much the blade turn, curvature and lean related to the pitch. The small **g**, for example g=0.1, signifies a cascade consisting of airfoil-like profiles with low deflection while bigger **g**, for example g=1.0, a cascade with profiles with a high degree of deflection.

The off-design profile loss was give in the following equation.

$$z_p = 1 - (1 - z_{p(i=0)})e^{-a(\Delta i^*)^b} \qquad \text{(eq. 2.10.2)}$$

in this equation, $z_{p(1=0)}$ is the profile loss on design point. Zehner [1980] used Traupel's model, which has been introduced in section 2.2, to calculate this loss in his application. **Di** is non-dimensional function of the incidence. It is calculated with

$$\Delta i^* = i \Big/ (180 - a'_{in}) \qquad \text{(eq. 2.10.3)}$$

a and **b** in equation 2.10.2 are coefficients related to the cascade geometry character, which are calculated with

$$a = \begin{cases} 2.587 - 0.426g - 1.216g^2 & i > 0 \\ 0.446 + 3.82g - 2.899g^2 & i < 0 \end{cases} \qquad \text{(eq. 2.10.4)}$$

$$b = \begin{cases} 4.175 + 10.802g - 13.881g^2 & i > 0 \\ 2.413 + 10.38g - 10.116g^2 & i < 0 \end{cases} \qquad \text{(eq. 2.10.5)}$$

Zehner [1980] used the Traupel's model to calculate secondary and tip leakage losses.

2.11 Moustapha

A loss model for predicting profile loss and secondary loss at off-design points was given by Moustapha et al [1990].

Off-design Profile Loss

The incidence losses are shown, by Moustapha et al [1990], to be a function of leading edge diameter, pitch, aspect ratio and channel convergence.

$$\Delta f^2 = \begin{cases} 0.778\times10^{-5}\,x' + 0.56\times10^{-7}\,x'^2 + 0.4\times10^{-10}\,x'^3 + 2.054\times10^{-19}\,x'^6, & 800 > x' > 0 \\ -5.1734\times10^{-6}\,x' + 7.6902\times10^{-9}\,x'^2, & 0 > x' > -800 \end{cases} \quad \text{(eq. 2.11.1)}$$

$$x' = \left(\frac{d}{t}\right)^{-1.6} \left(\frac{\cos\alpha'_{in}}{\cos\alpha'_{out}}\right)^{-2} i \quad \text{(eq. 2.11.2)}$$

Δf^2 is the variation of kinetic energy loss coefficient created by the incidence at off-design positions. Foregoing equations show that the off-design profile loss will be affected mainly by the incidence, leading edge diameter, and blade turning. Comparing with the off-design loss models given by Ainley/Mathieson, Craig/Cox and Zehner, the leading edge diameter of the blades is considered as an important factor in this loss model. The kinetic energy loss coefficient can be converted to the pressure loss efficient with

$$Y = \frac{\left[1 - \frac{g-1}{2} M_{out}^2 \left(\frac{1}{f^2} - 1\right)\right]^{\frac{-g}{g-1}} - 1}{1 - \left(1 + \frac{g-1}{2} M_{out}^2\right)^{\frac{-g}{g-1}}} \quad \text{(eq. 2.11.3)}$$

Off-design Secondary Loss

In addition to the traditional secondary loss models described in the sections above, Moustapha et al [1990] noted that the secondary loss would vary with the incidence and introduced the concept of the off-design secondary loss, which is mainly associated with incidence, leading edge diameter and blade turning. It is calculated with

$$\frac{Y_S}{Y_S^*} = \begin{cases} \exp(0.9x'') + 13x''^2 + 400x''^4, & 0.3 > x'' > 0 \\ \exp(0.9x''), & 0 > x'' > -0.4 \end{cases} \quad \text{(eq. 2.11.4)}$$

$$x'' = \frac{i}{180 - (\alpha'_{in} + \alpha'_{out})} \left(\frac{\cos\alpha'_{in}}{\cos\alpha'_{out}}\right)^{-1.5} \left(\frac{d}{l}\right)^{-0.3} \quad \text{(eq. 2.11.5)}$$

The loss model given by Moustaph et al[1990] are just for calculation of off-design losses. When applying this model, it is recommended that the Kacker/Okapuu loss model is used to calculate the losses on design point. The two loss models have the same application range.

2.12 Ito

Ito et al [1980] gave a model for predicting film cooling loss by modifying the model given by Hartsel [1972].

Film Cooling Loss

In this approach, it is assumed that mixing layers are postulated to adjoin the blade surfaces with thickness larger then the boundary layer.

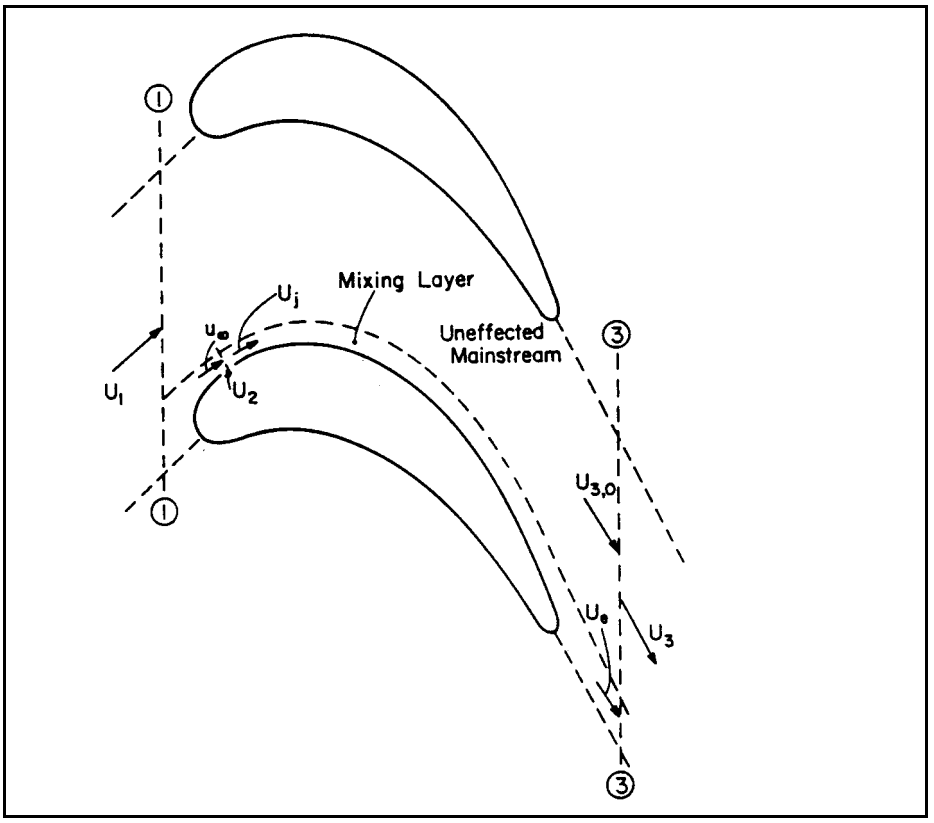

Fig. 2.12.1: *Sketch of flow illustrating film cooling mixing in a turbine row Ito et al [1980, p. 967]*

In 2.12.1, the mixing layer is sketched on the suction side. A similar layer occurs also along the pressure side. The rest of the flow is supposed not affected by the injected coolant flow. The analysis for the various layers is one dimensional. The fluid in the mixing layer expands isentropically from the upstream velocity U_1 to the velocity u_∞ approaching the point of injection. The coolant injected with the velocity U_2 mixes with the fluid in the mixing layer at constant pressure. The resulting uniform velocity is U_j. After mixing, the fluid in the mixing layer continues to expand isentropically to the exit section 3 in the figure reaching the velocity U_e. The unaffected main stream expands isentropically from the upstream velocity U_1 to the exit velocity $U_{3,0}$ in the exit cross section 3 in the figure. The two stream mix at constant pressure and resulting uniform velocity is U_3.

By employing the conservation of mass, momentum and energy in the mixing layers on the blade surfaces, the pressure loss coefficient for the film cooling is

$$Y_{fc} = 1 - \frac{(1+FR)\left(1+FR\frac{c_{p,f}}{c_{p,1}}\right)}{\left(1+FR\frac{R_f}{R_1}\right)\left(1+FR\frac{c_{p,f}}{c_{p,1}}\frac{T_f}{T_1}\right)}\left[\frac{1+\frac{(FR+s)}{(1-s)}\frac{U_e}{U_{3,0}}}{1+\frac{FR+s}{1-s}}\right]^2 \qquad \text{(eq. 2.12.1)}$$

$$\frac{U_e{}^2}{U_{3,0}{}^2} = \frac{\left(1+\frac{FR}{s}\frac{R_f}{R_1}\right)\left(1+\frac{FR}{s}\frac{c_{p,f}}{c_{p,1}}\frac{T_f}{T_1}\right)}{\left(1+\frac{FR}{s}\right)\left(1+\frac{FR}{s}\frac{c_{p,f}}{c_{p,1}}\right)}\left[1-\left(\frac{u_\infty}{U_{3,0}}\right)^2\right]+\left(\frac{u_\infty}{U_{3,0}}\right)^2\left[\frac{\left(1+\frac{FR}{s}\frac{U_2}{U_{3,0}}\right)}{\left(1+\frac{FR}{s}\right)}\right] \qquad \text{(eq. 2.12.2)}$$

where FR is the ratio of coolant to main flow and σ is ratio of mass flow in mixing layer to total mainstream mass flow before mixing and the subscript **f** represents the parameters of coolant.

Additional assumptions for this model are: the pressure through the blade row is a constant, i.e. $p_1=p_3$; the area of cross section in mixing layers is a constant; flows in mixing layers are incompressible.

Ito et al [1980] compared the loss predicted with this model with experimental results. The agreement was good. But the limitations for this approach are: small coolant ratio, FR<=0.03; just one hole for the coolant flow through on the blade surface.

2.13 Lakshminarayana

Lakshminarayana [1996] gave a model for calculating the film cooling loss in turbines. This model was developed from the one given by Kollen and Koschel [1985].

Film Cooling Loss

The analysis of this model was based on the same flow sketch as shown in Fig. 2.12.1 by Ito et al [1980] except assuming that the flow is compressible through the blade passage and mixing layers on blade surfaces. The enthalpy loss coefficient given in this model is (notation of parameters are the same as the section above, referenced to Fig. 2.12.1)

$$\boldsymbol{z}_{fc} = 1 - \frac{(1+FR)U_3^2}{U_{3,0}^2 + FRU_{fi}^2} \qquad \text{(eq. 2.13.1)}$$

$$U_3 = \frac{A}{2} - \sqrt{\frac{A}{4} - \frac{2g}{g+1}RT_{c3}} \qquad \text{(eq. 2.13.2)}$$

$$A = \frac{2g}{g+1}\left[\frac{1-s}{1+c}U_{3,0} + \frac{s+c}{1+c}U_j + \frac{p_3 A_3}{\dot{m}_{in}(1+c)}\right] \qquad \text{(eq. 2.13.3)}$$

where FR is the ratio of coolant to main flow, σ is ratio of main mass flow in mixing layer to total mainstream mass flow before mixing, A_3 is the area normal to axial flow velocity at section 3 in Fig. 2.12.1, χ is ratio of coolant to main flow in mixing layers and the subscript **f** represents the parameters of coolant.

$$T_{c3} = \frac{1-s}{1+c}T_{c1} + \frac{s+c}{1+c}T_{ce} \qquad \text{(eq. 2.13.4)}$$

U_{fi} is the ideal coolant velocity at the same pressure as the mixed gases. It is derived by assuming an isentropic expansion of the coolant flow from the injection point to station 3.

$$U_{fi} = \sqrt{\frac{2g}{g-1}RT_{cf}\left[1-\left(\frac{p_3}{p_{cf}}\right)^{(g-1)/g}\right]} \qquad \text{(eq. 2.13.5)}$$

It was noted by Lakshminarayana [1996] that, to use this model, an inviscid calculation is needed to predict $U_{3,0}$, A_3, U_j and $p_{3,0}$.

Like the model given by Ito [1980], this model is derived also from assuming that there is one hole for the coolant flow though on the blade surface.

2.14 A Development of Film Cooling Loss Calculation in Turbines

The cooling in turbines involve increased aerodynamic losses, in addition to the conventional losses, and decreased efficiency. In view of the complexity of the geometry and numerous parameters involved, a systematic method is yet to evolve for the prediction of cooled turbine efficiency. A few efforts have been made by, for example Ito et al [1980] and Lakshminarayana [1996] as shown before, to calculate film cooling losses in turbines. The similar models were also introduced by Hartsel [1972], Kollen and Koschel [1985] and Denton [1983]. All these models need local flow and geometrical parameters to calculate the loss. But it seems difficult to use these methods to estimate overall film cooling loss through a blade row in the preliminary process of turbine optimisation because the local parameters in the blade passage are unknown before the blade profiles are finally determined. Development of a simple method for predicting overall cooling loss in turbine row is needed. In this section, an effort is made by author to develop a method for approximately predicting overall film cooling loss in a turbine blade row.

Shapiro [1953] made an analysis in one dimensional complex flow in the most general condition. A compressible flow comes through a varied cross section channel with exchange of mass (injected secondary flow and evaporation), heat and power with out side. He employed the conservation of mass, momentum and energy through control surfaces in the

flow field and derived a group of equations which show the relationship of all flow parameters. Fig. 2.14.1 shows the sketch of the 1D mixing flows.

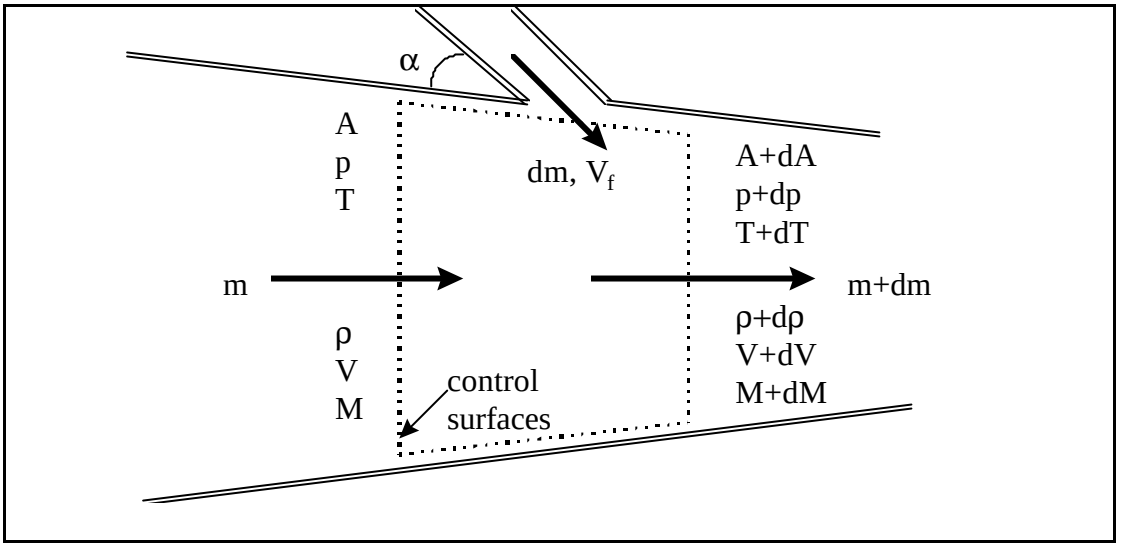

Fig. 2.14.1 *Sketch of one dimensional mixing flows*

After neglecting the variation of specific heat, the derivative of entropy with respect to other parameters is

$$ds = c_p\left[(1+\frac{g-1}{2}M^2)\frac{dT_c}{T_c}+\frac{g-1}{2}M^2\left(4f\frac{dx}{D}+\frac{dX}{\frac{1}{2}gpAM^2}-2f\frac{dm_c}{m}\right)+(g-1)M^2\frac{dm_c}{m}\right] \quad \text{(eq. 2.14.1)}$$

where **f** is the coefficient of friction between the gas and wall, dX is drag force of liquid droplets when the injected flow is liquid, A is area of cross section in the flow channel, ϕ is ratio of injected flow velocity to the main flow velocity along the stream line direction, dm_c is the derivative of the injected mass flow to control volume.

$$f = \frac{V_f}{V}\cos a \quad \text{(eq. 2.14.2)}$$

where V is main flow velocity, V_f is coolant flow velocity and α is the angle between the flows.

By employing equation 2.14.1 to a turbine blade passage, dm_c is considered as the derivation of coolant mass flow injected into the main flow. Thus in the equation, the first item represents the entropy increase due to the stagnation temperature variation caused by the heat exchange between the main flow and injected coolant flow. This variation of entropy is not caused by the irreversibility in the cooling process. So the first item can be neglected from the equation. The entropy increase due to the friction between the gas and blade surface has been taken account into the profile loss which is introduced earlier. So the second item in the equation can be taken away. The drag force dX=0, because there are not liquid droplets in

the coolant flow. Then derivative of entropy for irreversibility due to the cooling flow injected in the turbine blade passage is

$$ds = c_p(g-1)M^2(1-f)\frac{dm_c}{m_g} \qquad \text{(eq. 2.14.3)}$$

Shapiro [1953] also gave relationships among other parameters. For examples:

$$\frac{dM^2}{M^2} = -\frac{2\left(1+\frac{g-1}{2}M^2\right)}{1-M^2}\frac{dA}{A} + \frac{\left(1+gM^2\right)\left(1+\frac{g-1}{2}M^2\right)}{1-M^2}\frac{dT_c}{T_c} + \frac{2\left(1+gM^2-fgM^2\right)\left(1+\frac{g-1}{2}M^2\right)}{1-M^2}\frac{dm_c}{m_g} \qquad \text{(eq. 2.14.4)}$$

$$\frac{dT_c}{T_c} = \frac{dT}{T} + \frac{\frac{g-1}{2}M^2}{1+\frac{g-1}{2}M^2}\frac{dM^2}{M^2} \qquad \text{(eq. 2.14.5)}$$

$$\frac{dT}{T} = \frac{(g-1)M^2}{1-M^2}\frac{dA}{A} + \frac{\left(1+gM^2\right)\left(1+\frac{g-1}{2}M^2\right)}{1-M^2}\frac{dT_c}{T_c} + \frac{\left(fgM^2-gM^2-1\right)(g-1)M^2}{1-M^2}\frac{dm_c}{m_g} \qquad \text{(eq. 2.14.6)}$$

$$\frac{dV}{V} = -\frac{1}{1-M^2}\frac{dA}{A} + \frac{\left(1+\frac{g-1}{2}M^2\right)}{1-M^2}\frac{dT_c}{T_c} + \frac{\left(1+gM^2-fgM^2\right)}{1-M^2}\frac{dm_c}{m_g} \qquad \text{(eq. 2.14.7)}$$

In detailed performance calculation, turbine blade geometrical parameter are known. So the variation of passage cross section area, dA/A, along the stream line is known. The cooling flow velocity, V_f, and variation of the injected cooling flow, dm_c/m_g, along the stream line can also be determined if detailed information concerning the coolant are known, such as mass flow, inlet parameter, number and location of the holes. Then the entropy variation over a blade row can be acquired by solving the 1D equations 2.14.3-7 numerically along the middle-stream from inlet to outlet of the blade row.

If the distribution of Mach number, M(x), and flow velocity, V(x), are known and the cooling holes on blades are also known, for an example there are total n holes on the blade surfaces in the passage. Assuming that $\mathbf{c_p}$ and $\mathbf{g}$ are constants and the coolant velocity from every hole is the same value, the entropy over the blade row may be calculated as:

$$s_{out} - s_{in} = c_p(g-1)\sum_{i=1}^{n} M(x_i)^2\left(1-\frac{V_{fi}}{V(x_i)}\cos\alpha\right)\frac{(\Delta m_f)_i}{m_{in}+\sum_{k=0}^{i-1}(\Delta m_f)_k} \qquad \text{(eq. 2.14.8)}$$

where $(\Delta m_f)_i$ is the mass flow of coolant through the hole i. The Mach number and velocity distribution, M(x) and V(x), can approximately be determined from a 2D inviscid calculation over the blade row without cooling.

In the preliminary process of turbine design and optimisation when the mean line prediction is performed, the detailed blade shape and information about the coolant, such as the distribution of coolant mass flow and holes on surfaces, are unknown. In this case, a more simple method is needed to give overall losses with correct trends and reasonable values. Denton [1993] suggested to use Shapiro's entropy calculate method. However the detailed information concerning how to apply it in turbine blade rows is limited.

For this purpose, assuming that the coolant is continuously and uniformly injected into the passage from the inlet to outlet of the blade row, one can try to integrate equation 2.14.3 and have

$$s_{out} - s_{in} = c_p(g-1)\int_{in}^{out} M^2(1-f)\frac{d\dot{m}}{\dot{m}} \qquad \text{(eq. 2.14.9)}$$

where the Mach number, M, and velocity ratio, ϕ, are complex functions of mass flow $\dot{m}$. It is impossible to obtain an analytical result from this integration.

If assuming that there are an average Mach number, $\overline{M}$, and velocity ratio, $\overline{f}$, which are not functions of the mass flow, equation 2.14.9 can be simplified and integrated

$$\begin{aligned} s_{out} - s_{in} &= c_p(g-1)\overline{M}^2(1-\overline{f})\int_{in}^{out}\frac{d\dot{m}}{\dot{m}} \\ &= c_p(g-1)\overline{M}^2(1-\overline{f})\ln\left(\frac{\dot{m}_{out}}{\dot{m}_{in}}\right) \end{aligned} \qquad \text{(eq. 2.14.10)}$$

where $\dot{m}_{in}$ and $\dot{m}_{out}$ are the mass flows at the blade row inlet and outlet respectively. There is a relation

$$\dot{m}_{out} = \dot{m}_{in} + \dot{m}_f \qquad \text{(eq. 2.14.11)}$$

where $\dot{m}_f$ is the total mass flow of coolant injected through the blade row. Finally, the entropy creation over the blade row due to the film cooling is

$$s_{out} - s_{in} = c_p(g-1)\overline{M}^2(1-\overline{f})\ln\left(1+\frac{\dot{m}_f}{\dot{m}_{in}}\right) \qquad \text{(eq. 2.14.12)}$$

In order to obtain the average Mach number and velocity ratio to use this equation, a generic rectangular velocity distribution on blade surfaces can be assumed. It is assumed that the velocity on the suction surface is a constant and equal to the blade row exit velocity and that the velocity on the pressure surface is also a constant and has a value which is lower than the inlet velocity. The assumed velocities on blade surfaces produce an actual tangential force which corresponds to the aerodynamic load coefficient. This concept of rectangular velocity distribution has been used by Zweifel [1946], Stewart et al [1960], Baljé and Binsley [1968] and Denton [1990, 1993] for estimating the blade boundary layer conditions in profile loss calculation. If the rectangular velocity distribution is assumed, the average Mach number and velocity on the middle stream line can be calculated

$$\overline{M} = \frac{\overline{M}_{ss} + \overline{M}_{ps}}{2} = \frac{M_{out} + M_{in} - \Delta M}{2} \qquad \text{(eq. 2.14.13)}$$

$$\overline{V} = \frac{\overline{V}_{ss} + \overline{V}_{ps}}{2} = \frac{V_{out} + V_{in} - \Delta V}{2} \qquad \text{(eq. 2.14.14)}$$

Neglecting the variation of the coolant velocity, the velocity ratio is

$$\overline{f} = \left(1 - \frac{V_f}{\overline{V}} \cos a\right) \qquad \text{(eq. 2.14.15)}$$

After using equation 2.14.12 to both stator and rotor (when using it for rotor, relative values of Mach number and velocity should be taken), the entropy due to film cooling in the two blade rows will be calculated respectively. Then the sum of the entropy from the two rows will be used for computing stage efficiency.

The development of this film cooling loss prediction method (see equation 2.14.8, for example) shows that the Mach number is a significant parameter for calculating the losses. For the same amount of coolant mass flow, the cooling losses could be very different if comparing the case when coolant is injected near the leading edge where the Mach number is low with that when it is added at the trailing edge where the Mach number could be very high. The ratio of coolant to main flow is also a significant parameter for film cooling loss calculation. The results show that the increase of the ratio is almost proportional to the diminution of the efficiency. Equation 2.14.12 is based on the assumption of continuous and uniform coolant injected into the blade row. In practise, the coolant might be added more at the leading edge than the trailing edge because, in principle, cooling is more needed near the leading edge where gas has lower velocity and higher temperature compared with downstream.

This film cooling loss estimating method has been applied to the performance prediction of a high temperature and pressure cooled turbine with the ratio of coolant to main mass flow 0.16 for the stator and 0.09 for the rotor. The results showed that, after adding this method to the loss models of Kacker/Okapuu and Moustapha/Kacker, the trends of simulated performances with the combined models have better agreement with the trend of experimental data compared with the results without the cooling losses. The predicted stage efficiency values are also improved to about 2-2.5% units lower than the experiments, which are closer to the experiments than the corresponding predicted results without the cooling losses. (See in Chapter 4.)

It is noted that the development of the film cooling loss in this section is for coolant addition through holes or slots in the blade or endwall surfaces and does not apply to coolant ejection through the trailing edge where the change of base pressure must be included in the analysis. In fact, coolant ejection through the trailing edge can increase the base pressure and so be beneficial. An investigation of the cooling ejection at the trailing edge was given by Denton and Xu [1989].

2.15 Summary of the loss models

General characters of the loss models described above are summarised here. To make it simple, the emphasis is put on the main parts of the loss components: the secondary losses, tip leakage losses, cooling losses and profile losses which are two dimensional losses consisting of the shock loss, trailing edge loss and basic profile loss (the losses associated with the friction between the flow and blade surfaces). In Appendix 3, all parameters used in the loss models introduced in this chapter are listed in several tables which can be references to this summary.

Design profile losses

The profile losses at the design condition are caused by the viscous and turbulent dissipation in the boundary layer on the blade surfaces (it used to be called basic profile loss or friction loss) and in the mixing of flow at the trailing edge. The boundary layer condition on the blade surface is the key factor for influencing the losses. The boundary layer condition depends mainly on pitch/chord ratio, Mach number, Reynolds number, turbulence level, surface roughness and the blade shape including the blade chord, inlet and outlet angles, camber angles, stagger angle, thickness etc. The loss models for predicting design profile losses can be classified into two group, one is mainly based on the test data and the another from the semi-analysis of the physics of the flow losses.

Soderberg, Traupel, Ainley/Mathieson, Dunham/Came, Kacker/Okapuu and Craig/Cox are models which are made from extensive tests on linear turbine cascades and turbine stages. Soderberg gave a simple model of profile loss which is just a function of blade deflection with a correction of Reynolds number (see equation 2.1.1 and 2.1.2). Traupel and Craig/Cox presented their loss models with a series of diagrams respectively. Traupel correlated his profile loss with blade inlet and outlet angles, pitch, roughness, trailing edge thickness and Mach and Reynolds numbers, while Craig/Cox correlated with the inlet and outlet flow angle, ratio of pitch to camber line length, pitch to blade back radius ratio, contraction ratio of blade channel, trailing edge thickness and Mach and Reynolds numbers. Ainley/Mathieson developed the profile loss model which depends on the pitch/chord ratio, inlet and outlet flow angles, blade maximum thickness and trailing edge thickness. This model was modified by Dunham/Came with adding the terms related to Mach number and Reynolds number. Kacker/Okapuu developed finally this model by restructuring it and adding a Mach number correction factor which is a function of the inlet and outlet Mach number. Comparing these different models, it can be seen that blade inlet and outlet angles have been taken into account in every one, blade roughness was only considered in the Traupel model, the blade maximum thickness was the parameter used only by Ainley/Mathieson and Craig/Cox used the geometrical parameters of the pitch to blade back radius ratio and the contraction ratio of blade channel which were not applied in the other models.

Stewart, Baljé/Binstey and Denton models are based on the fact of the physical origin of losses. They were established by means of applying boundary layer theories, basic thermodynamic equations and simplified equations of the conservation of mass, momentum and energy. From a theoretical analysis of the entropy generation in the boundary layer, Denton developed the method to predict the loss associated with the friction in the boundary

layer on blade surfaces which is integrated with the area of blade surfaces, dissipation coefficient and flow velocity on the surfaces. The mixing loss at the blade trailing edge was given by Denton by means of applying the conservation of momentum at the trailing edge region. In this calculation, the throat width of the blade passage, trailing edge thickness, base pressure and displacement and momentum thickness of the boundary layer on blade surfaces at trailing edge are needed. In Denton's profile loss models, empirical correlations have to be used to predict base pressure at blade trailing edge and displacement and momentum thickness of the boundary layer which can not be calculated analytically. Furthermore, the velocity distributions on blade surfaces have to be known or assumed in using the Denton model. Stewart derived that the profile loss is proportional to the ratio of deficiency of momentum in the boundary layer to the ideal momentum in free-stream flow. In this model, the loss is calculated with chord, pitch, trailing edge thickness, outlet blade angle and displacement and momentum thickness. Baljé/Binstey developed Stewarts' model by using Truckenbrodt's turbulent boundary layer equation for arbitrary pressure gradients. The main assumption made in this model is that the total boundary layer growth can be reasonably well predicted using a linear variation of the velocity along the mean camber line. This variation of velocity was justified with test data. From this assumption the displacement and momentum thickness can be predicted when this model is used.

Off-design profile losses

Because of the difficulty in analytically calculating the boundary layer separation on the blade surface, the models for predicting the off-design profile losses are mainly made from empirical correlations. A few of off-design profile loss models were given by Ainley/Mathieson, Craig/Cox, Moustapha and Zhner. The incidence is the most important parameter to predict the off-design profile loss. This parameter was taken into account by all of these models. In the Ainley/Mathieson and Craig/Cox models, the stall incidence angle was used. This stall incidence angle was defined as the incidence at which the profile loss is twice the minimum profile loss and was mainly correlated to the pitch to chord ratio and the inlet and outlet blade angles. A large pitch to chord ratio and a high turning of blade will result easily in the flow separation on the blade surface, therefore the stall incidence angle will be small. In addition, in the Craig/Cox model the contraction ratio was also considered. This implies the influence of the flow acceleration on the boundary layer separation. In the Moustapha model, besides the incidence and blade inlet and outlet angles, the ratio of leading edge diameter to the pitch was considered as a important parameter together, which gives the influence from the leading edge diameter on the flow separation. In the Zhner model, the pitch, incidence angle, inlet and outlet blade angles, stagger angle and blade camber line curvature were used.

Secondary losses

Although a lot of effort has been made to understand the flow pattern associated with secondary losses, it is still difficult to know adequately the magnitude of the losses. All models described in this chapter for calculating the secondary losses are based on the experiments.

Ainley/Mathieson calculated the secondary losses with the loading factor which is just a function of inlet and outlet flow angles. From the review of new secondary loss data, Dunham/Came modified this model with adding the terms of aspect ratio and influence of upstream boundary layer which is simplified as a constant. Kacker/Okapuu developed the Dunham/Came model by modifying the term of aspect ratio and adding the Mach number correction factor which is a function of the inlet and outlet Mach number. Finally, Moustapha modified the Kacker/Okapuu model on off-design points by considering the incidence angle and the ratio of leading edge diameter to chord. In this group of models, the secondary losses were assumed to be proportional to the strength of the secondary vortex. The derivation of the relation between the secondary vorticity and the secondary loss coefficient was given by Lakshminarayana [1996]. In such calculations, the secondary loss coefficients are mainly the function of flow angles which implies the velocity triangles will affect very much the losses. It is noted that the pitch/chord ratio, which also affects the blade loading, has not been taken account into this group of loss models.

Baljé/Binstey gave the secondary loss as a polynomial of blade inlet and outlet angles. This model considers that the secondary loss coefficient depends only on velocity triangles which affects the blade loading. Stewart proposed the secondary loss associated with the end wall boundary layer shin friction, obtained by increasing the profile loss. The blade loading caused by flow angles was not considered in this model.

Traupel and Craig/Cox give the secondary losses which correlate to more parameters. Traupel structured the secondary loss as a function of blade pitch/span ratio, blade pitch/chord ratio, profile loss, inlet and outlet flow angles and the ratio of inlet and outlet flow velocity which implies that the correlation does account for compressibility effects. The secondary loss in the Craig/Cox model was calculated with a linear function of basic secondary loss and the factors of Reynolds number and aspect ratio. The basic secondary loss was correlated with blade pitch/chord ratio, ratio of inlet and outlet flow velocities and the lift parameter which is a function of the inlet blade angle and outlet flow angle. The influence of the upstream flow boundary layer on the secondary losses is not considered in the Traupel and Craig/Cox models, but compressibility and the blade loading caused by both the velocity triangles and pitch/chord ratio are considered. Unlike the Traupel model, there is not direct relationship between the profile and secondary losses in the Craig/Cox model.

Denton analysed the secondary losses, called the endwall losses in his paper, by studying the origin of the entropy generation from the flow at turbine endwalls. He described that about 2/3 of it comes form entropy generation in the annulus wall boundary layers within, upstream of and downstream of the blade row. This part of the secondary losses can be calculated with equation 2.7.14-19. The further part comes from mixing loss of the ratio of inlet boundary layer thickness to span which, he thinks, is an unknown function of blade load and turning. A third component of the secondary losses is the loss associated with the secondary kinetic energy which is of the order of ¼ of the total secondary losses. He noted that this proportion will depend on the inlet boundary layer thickness and skew and on blade turning and blade loading but there are no simple theories relating the loss to any of these factors. Other contributions to secondary losses may come from local flow separations and from thicknening and premature fraction of the blade surface boundary layer as a result of the secondary flow. No simple models were given by Denton for predicting such loss components. He believed that in all the situation is too complex and too dependent on details of the flow and geometry

for simple quantitative prediction to be made and the main hope in the near future is that the loss can be quantified by 3D Navier-Stokes solutions.

Tip leakage losses

Ainley/Mathieson, Dunham/Came and Kacker/Okapuu gave tip leakage losses by generally simulating the tip leakage vortex and determine the induced drag of the vortex on the blade. The models are inviscid and incompressible. It was firstly done by Ainley/Mathieson to adapt the model for secondary loss calculation with influence of tip clearance. The loss becomes a function of the flow inlet and outlet angles and the ratio of tip clearance to blade height (see equation 2.3.8). Then Dunham/Came modified this model in the light of some later cascade data, which suggested a non-linear variation of tip leakage losses with the ratio of tip clearance to blade height (see equation 2.4.4). Kacker/Okapuu keept using the Dunham/Came model for shrouded blades but modified the structure of the model for unshrouded blades according to their new test data (see equation 2.5.12). To convert the resulting momentum deficiency into a total pressure loss, it is nessary to assume that the loss is distributed uniformly over the mass flow. Thus, these models implicitly predict the fully mixed-out value of the losses. However the measurements show that fully mixed-out conditions are approached further downstream [Yaras & Sjolander, 1996].

The tip clearance loss given by Baljé/Binsley is based on the test data and the principle in which the tip leakage losses are function of a blade loading parameter and the ratio of tip clearance to blade height, as well as solidity. It is calculated with the tip clearance, blade height, cascade diameter, blade chord, mean flow angle and inlet and outlet blade angles (equation 2.9.9). This model is similar to the model given by Ainley/Mathieson.

Denton developed a simple tip-leakage loss model from first principles, using a control-volume analysis for the mixing of the leakage jet with the passage flow. In this model, the tip clearance loss is calculated with the flow angles, tip clearance, blade height/chord ratio, flow velocities and leakage and main mass flow (see equation 2.7.12 and 2.7.13). To keep the resulting expression tractable, a number of simplifying assumptions were made. For example, it was assumed that the gap flow mixes with a uniform passage flow at constant pressure. The endwall shear stress was also omitted from the control-volume analysis.

Traupel gave the model for calculating shrouded blades as a function of the velocity ratio and the ratio of leakage jet to the main flow through the passage (see equation 2..2.9). This model seems like the model given by Denton (equation 2.7.12) which is based on the principle of the mixing. However the flow angles were not be considered, which implies that the part of loss caused from the different directions of the leakage and main flow is neglected. The model for calculating tip leakage loss for unshrouded blades given by Traupel is presented as a diminution of the cascade efficiency which has a linear function with the tip clearance (see equation 2.2.10). This model is based on turbine test results and similar to the tip leakage loss model given by Kacker/Okapuu (equation 2.5.12).

Craig/Cox expressed the tip leakage losses for shrouded blades as an efficiency diminution caused by the tip leakage loss (see equation 2.6.4) which is a function of the leakage

coefficient, the ratio of the clearance to throat areas and the efficiency when the clearance is zero. The leakage coefficient is mainly a function of the ratio of the inlet and outlet velocity at the tip region, which actually implies the static pressure drop over the blade row. This model is based on turbine test results.

Film cooling losses

All models for predicting film cooling loss are based on one dimensional flow in a blade passage with adding coolant. The models given by Ito et al [1980] and Lakshminarayana [1996] were development from the ones given by Hartsel [1972] and Kollen and Koschel [1985] respectively. In these models, it is assumed that the coolant is mixed with main flow in layers with a constant area of cross section on blade surfaces and the static pressure is a constant from upstream to downstream. It seems difficult to use these models to estimate overall film cooling loss of a blade row because some local parameters, for examples the main flow velocity at the hole and the ratio of the mixing layer to passage width, are needed. Lakshminarayana [1996] suggested that some inviscid calculations should be used together with the cooling loss modes for obtaining local parameters.

By analysing the entropy creation in the mixing of coolant with the main flow in a turbine blade passage by means of applying one dimensional conservation of mass, momentum and energy in a channel with injected additional flow, a development of the film cooling loss model is made by author for approximately estimating the overall film cooling loss in a turbine blade row. With equation 2.14.12, the overall film cooling loss in the blade row can be approximately predicted with coolant velocity, ratio of total coolant to inlet main mass flows and the average main flow velocity and Mach number. The average Mach number is a critical parameter in the calculation. It is suggested that a rectangular velocity distribution on blade surfaces is assumed in order to acquire the average Mach number and velocity with inlet and outlet parameters. If knowing the detailed cooling information, such as the location of coolant holes and distribution of coolant mass flow through each hole, and acquiring the Mach number and velocity distribution through the blade row by a 2D inviscid calculation, the entropy creation can be calculated with equation 2.14.8 in the analysis cases when the blade shapes have been estimated.

Some other loss models for predicting individual secondary and tip leakage losses

There are also many literature sources which are concerning the methods for predicting the individual loss components, especially secondary and tip clearance losses, in axial turbines. For example, the secondary loss model have been given by Ehrich & Detra [1954], Scholz [1954], Hawthorne [1955], Macdonald [1956], Markov [1958], Boulter [1962], Sharma & Butler [1987], Dunham [1970] and Okan & Gregory-Smith [1992], and the tip leakage models given by Hesselgreaves [1969], Lakshminarayana [1970], Yaras & Sjolander [1992], Cecco et al [1995], Kim & Chung [1997] and Wehner et al [1997]. It is not the objective of this thesis to discuss all these individual loss component models one by one here. However one can find some useful knowledge for understanding the losses better from these investigations on such individual loss components. Some information concerning these loss models can be found in Appendix 2.

3. TURBINE STAGES AND EXPERIMENTAL DATA USED FOR PERFORMANCE SIMULATIONS AND COMPARISON

In order to better understand the behaviour of the different loss models and properly use them, 5 turbine stages have been simulated with the loss models. The main geometrical parameters and working conditions are shown in this chapter. The experimental data on these turbines are shown and compared with the predicted results in detailed in chapter 4.

3.1 Turbine Stages 1 and 2

Turbine stages 1 and 2 are used for experimental studies of axial turbine stages in the test turbine system at the laboratory of Chair of Heat and Power Technology in the Department of Energy Technology, the Royal Institute of Technology. These two single stages have been used for research projects. Both of the stages have the same profile shape (see Fig. 3.1.1), but different blade spans. Turbine stage 1 has higher span than turbine stage 2. The main geometrical parameters for the stages are shown in table 3.1.1 and the nominal flow conditions are shown in table 3.1.2. Fig. 3.1.1 shows the blade profiles of the turbines with the flow triangles at nominal flow conditions.

Geometrical parameters	**Turbine Stage 1**		**Turbine Stage 2**	
	Stator	**Rotor**	**Stator**	**Rotor**
Number of blades	42	64	42	64
Span, **H**, [m] (whole chord)	0.024	0.025	0.033	0.034
Chord, **l**, [m]	0.041	0.026	0.041	0.026
Axial chord, $\mathbf{l}_x$, [m]	0.025	0.025	0.025	0.025
Solidity at midspan, **l/t**, [-]	1.44	1.39	1.40	1.36
Pitch at hub, $\mathbf{t}_{hub}$, [m]	0.0266	0.0174	0.0266	0.0174
Pitch at midspan, **t**, [m]	0.0284	0.0187	0.0291	0.0191
Pitch at tip, $\mathbf{t}_{tip}$, [m]	0.0302	0.0199	0.0316	0.0208
Stagger angle, $\boldsymbol{\gamma}$, [°]	52.3	20.8	51.0	20.8
Radius at midspan, $\mathbf{r}_m$ [m]	0.190	0.190	0.1945	0.1945
Aspect ratio, **H/l**, [-]	0.59	0.96	0.80	1.30
Hub-casing ratio, $\mathbf{r}_{hub}/\mathbf{r}_{tip}$, [-]	0.88	0.87	0.84	0.83

Table 3.1.1 *Main geometrical parameters of turbine stages 1 and 2.*

The experimental performance of the turbine stages were determined with measurements by aerodynamic probes, thermal coupes probes, flow orifice and torque meter. The detailed information concerning the measurements on the turbines has been given by Wei and Svensdotter [1995].

The accuracy of the experimental data in turbine stage 1 was analysed by Haghighi [1996]. In his report, the accuracy of the experimental stage efficiency is estimated as 1.1%. The accuracy of the experimental data in turbine stage 2 has the same level as one in stage 1 Hedlund [1999]. From the information measurement uncertainty and the method to estimate accuracy of experimental data introduced by Haghighi [1996], the accuracy of the experimental pressure loss coefficient in these turbine stages can be estimated as +/- 0.9%.

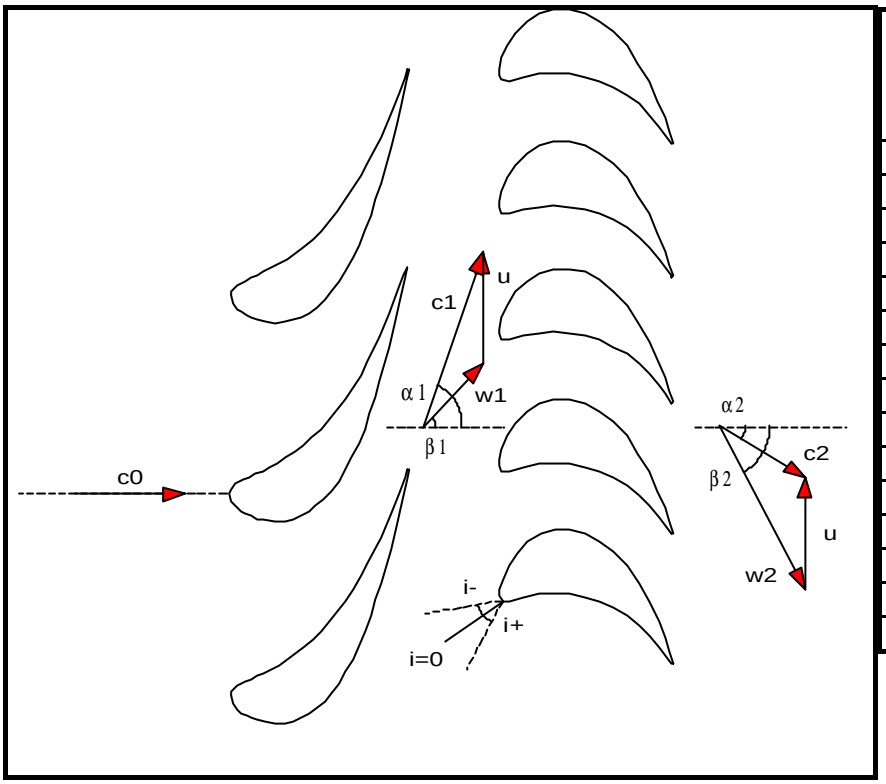

Fig. 3.1.1: *The test stage geometry at midspan.*

Nominal conditions at midspan	Stage 1	Stage 2
π, [-]	1.23	1.21
r, [-]	0.15	0.20
ν, [-]	0.56	0.55
c_0, [m/s]	37.6	38.3
α_0, [deg]	0.0	0.0
c_1, [m/s]	170.4	162.5
c_{1x}, [m/s]	43.6	43.4
w_1, [m/s]	74.1	69.3
α_1, [deg]	75.2	74.7
β_1, [deg]	54.0	51.8
c_2, [m/s]	47.7	43.5
c_{2x}, [m/s]	42.8	41.8
w_2, [m/s]	93.8	99.4
α_2, [deg]	-26.6	-16.0
β_2, [deg]	63.0	65.1

Table 3.1.2: *Nominal flow conditions for Turbine stages 1 and 2*

3.2 Turbine Stage 3

Turbine stage 3 used for the calculation is the first stage of an axial 4 stage test turbine of which the test data was published in the report Agard-AR-275 [Fottner, 1990, p. 365]. The test turbine is at the University of Hannover. The profiles of the blades are showed in Fig. 3.2.1. The turbine was basically designed to have the same blade sections in all stages at a given radius. The blading is of the free-vortex type with a 50% degree of reaction in the middle section of the last stage.

The turbine has a hub diameter of 270 mm. The outer casing is cylindrical except across the blading where it is conical. Tip clearances and labyrinth clearances can be estimated as 0.4 mm.

The accuracy of the experimental data in this turbine stage was estimated as +/- 0.8% [Fottner, 1990].

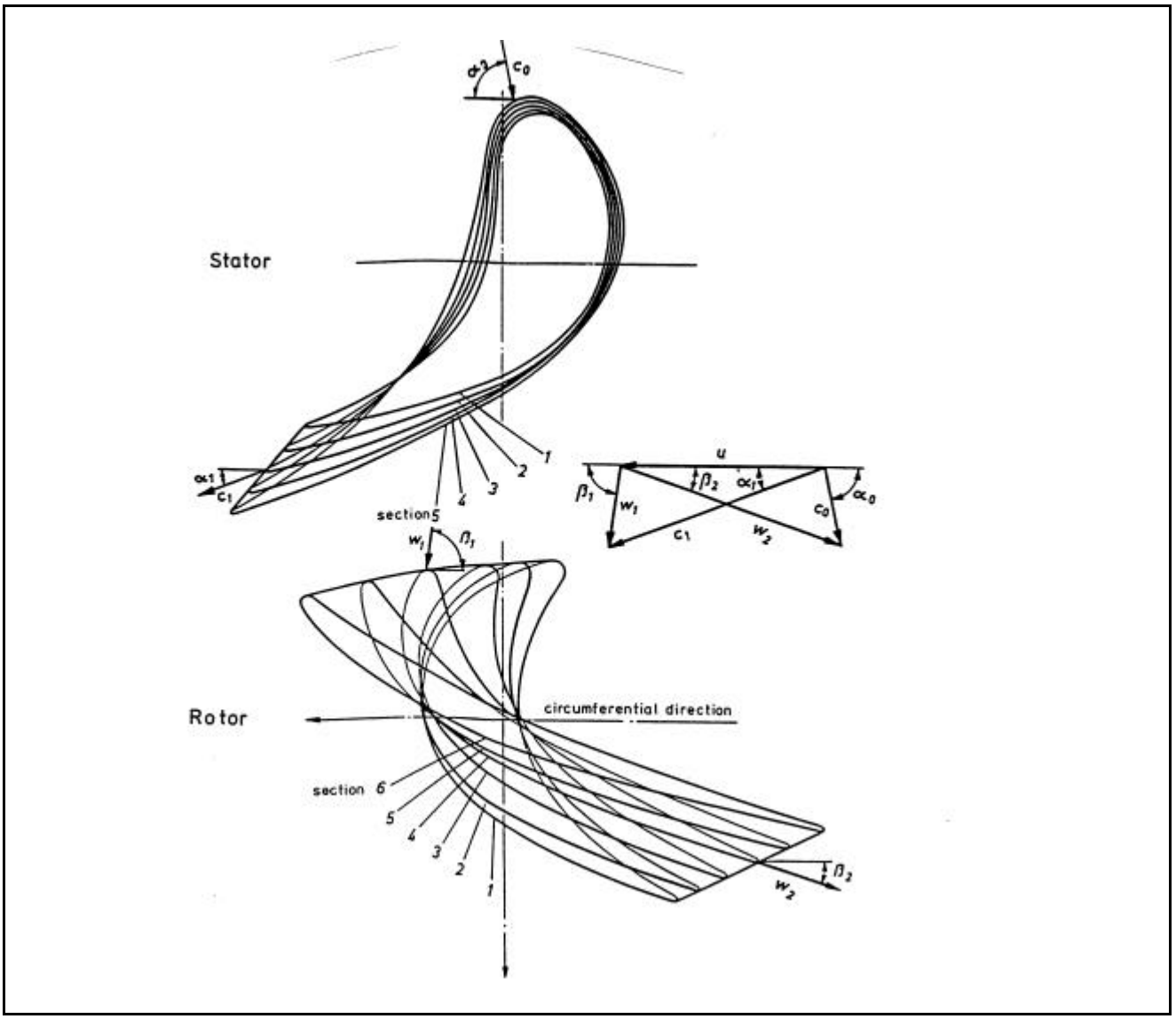

Fig. 3.2.1: *Blade profile of the turbine stage 3* [Fottner, 1990, p. 374].

The Nominal conditions given from the report Agard-AR-275 are listed in the table 3.2.1.

rotating speed	7500 rpm
air mass flow rate	7.8 kg/s
inlet pressure	2.600 bar
inlet temperature	413 K
outlet pressure	1.022 bar
outlet temperature	319 K
degree of reaction	0.5
hub/tip ratio at outlet	0.525

Table 3.2.1: *Nominal flow conditions for turbine stage 3*

3.3 Turbine Stages 4 and 5

Turbine stages 4 and 5 are from an aircraft engine which is a low-by-pass-ratio turbofan engine with afterburner. It is a small and powerful engine in the 80 kN thrust class.

Turbine stage 4 is the high pressure turbine stage in the engine. This stage works at high temperature, high pressure and transonic flow conditions with heavy cooling. The main mean line geometrical parameters in this turbine stage are shown in table 3.3.1.

Geometrical parameters	Stator	Rotor
Chord at middle span, [m]	0.057	0.035
Pitch/chord ratio at middle span	0.682	0.787
Solidity at middle span	1.466	1.271
Inlet blade angle at middle span, [^{o}]	0.0	36.5
Outlet blade angle at middle span, [^{o}]	71.0	58.5
Inlet blade span, [m]	0.0450	0.0421
Outlet blade span, [m]	0.0400	0.0448
Ratio of max. Blade thickness to chord	0.2688	0.2569
Ratio of trailing edge thickness to chord	0.0153	0.0584
Aspect ratio	0.70	1.25
Inlet hub/casing ratio	0.8464	0.8572
Outlet hub/casing ratio	0.8635	0.8480

Table 3.3.1 *Main geometrical parameters of turbine stage 4.*

Turbine stage 5 is the low pressure turbine stage in the engine and works at subsonic flow condition. Table 3.3.2 shows the main mean line geometrical parameters in this stage.

Geometrical parameters	Stator	Rotor
Chord at middle span, [m]	0.0550	0.0320
Pitch/chord ratio at middle span	0.6417	0.6622
Solidity at middle span	1.5584	1.5101
Inlet blade angle at middle span, [^{o}]	25.0	44.8
Outlet blade angle at middle span, [^{o}]	65.0	54.2
Inlet blade span, [m]	0.0620	0.0905
Outlet blade span, [m]	0.0770	0.0950
Ratio of max. Blade thickness to chord	0.1810	0.1666
Ratio of trailing edge thickness to chord	0.0171	0.0232
Aspect ratio	1.34	2.89
Inlet hub/casing ratio	0.7980	0.7202
Outlet hub/casing ratio	0.7345	0.7063

Table 3.3.2 *Main geometrical parameters of turbine stage 5.*

There are not direct experimental data for turbine stages 4 and 5. In chapter 4, predicted results will be compared with reference data on these stages. The reference data shown in chapter 4 were calculated and verified with engine global measurements by an aeroengine manufacturer [Johansson, 1999]. The accuracy of the reference data is not available.

4 RESULTS AND ANALYSIS OF TURBINE PERFORMANCE SIMULATION WITH DIFFERENT LOSS MODELS

The performance on the 5 turbine stages described in the chapter 3 have been simulated with different loss models. The main input data to the calculations are the stage inlet stagnation pressure and temperature, mass flow, turbine speed and geometric parameters of the stator and the rotor. These data are taken from experiments and the original design of the stage. Then the flow parameters at each section and the overall performance parameters of the stage are predicted row by row. The calculations are based on the principle of conservation of mass, momentum and energy over every blade row. In this approach, loss models have to be used to determine the entropy variation at each section in the turbine stage.

The loss models given by Ainley/Mathieson and Dunham/Came (AMDC), Kacker/Okapuu (K-O), Craig/Cox (C-C) and Moustapha/Kacker (M-K) have been used in the performance prediction on all these turbine stages. For stage 4 which is a special high temperature and high pressure cooled turbine stage, an additional film fooling loss model developed in Chapter 2 (see section 2.12.3) is also applied to predict the loss due to film cooling.

The study on turbine stage 1 is related to a specific pressure ratio, 1.23, with velocity ratio as a varied parameter from 0.20 to 0.73. The conditions are the same as the experiments. This range of velocity ratio covers the large off-design region, the incidence for the rotor blade row is approximately from $+18^0$ to -21^0 corresponding to this range of velocity ratio. For turbine stage 2, the pressure ratios are 1.18 to 1.23 and velocity ratio varies from 0.25 to 0.85. This range of velocity ratio covers the large off-design region, the incidence for the rotor blade row is approximately from $+18^0$ to -60^0. The predicted results were compared with the experimental results measured in the same operation range. The calculation on turbine stage 3 is related to a shaft speed 7500 rpm with mass flow as a parameter varied from 4.1 to 7.8 kg/s. The calculated results show that this range of mass flow variation covers a region of load ratio from about 0.6 to 1.1 and the incidence for the rotor blade row from $+8^0$ to -27^0. The simulation on stages 4 and 5 are corresponding to a series of experiments based on a real operation range of the aeroengine. For stage 4, the mass flow number is 0.65 and speed number varies from 380 to 390. For stage 5, the mass flow number varies from 1.43 to 2.19 and speed number from 141 to 350.

4.1 Performance Simulation on Turbine Stage 1

A comparison between predicted stage efficiencies and experimental data is shown in Fig. 4.1.1. The velocity ratio in Fig. 4.1.1 is equal to the blade speed divided by the square root of the isentropic enthalpy drop over the stage (see equation 4.1.1).

velocity ratio: $$n = \frac{u_2}{\sqrt{\Delta h_{is}}} \qquad \text{(eq. 4.1.1)}$$

The efficiency values predicted with the AMDC model were lower than the experimental results in all operating ranges. Fig. 4.1.1 shows that there is a gap between the experimental

and predicted results in the AMDC model, the difference is about 5% units near the design point and 5-8% units on the off-design points. This result generally agrees with the results in [Sieverding, 1985, Fig. 7 & 33] and [Tremblay et al, 1990], i.e. the AMDC loss, comparing with other models, could overestimate the profile loss and secondary loss. This is because that the data base for establishing this models was based on the experiments of old blade profiles. However the trend of the efficiency distribution in AMDC model agrees well with the trend in experiments, i.e. the gap between these two curves in Fig. 4.1.1 keeps almost same value in the most of the operation region except at the ends of the curves where the turbine runs in heavy off-design conditions. The AMDC off-design profile model gives more overestimated losses at the large +/- incidence positions. This can clearly be seen in the detailed analysis of loss distribution in the next section.

It can be seen from Fig. 4.1.1 that the efficiency values predicted in the Craig/Cox loss model agrees well with the experimental value, about 1% unit higher than the experimental results, near the design point. But as the operation point moves towards off-design directions, this model gives lower efficiency than the experimental values. Similar with the AMDC models, the Craig/Cox off-design profile loss model also predicts too high loss at the large incidence angles. Craig/Cox loss model gives a sharp decrease of the efficiency at the lowest velocity ratio point (highest off-design point with positive incidence) in Fig. 4.1.1. This can clearly be seen in the loss distribution later. Fig. 4.1.1 also shows that the gap between the experimental efficiency and predicted efficiency in the Craig/Cox model is larger at the end of highest velocity ratio, negative incidence, than at the end of lowest velocity ratio, positive incidence. This is because the tip leakage loss in the Craig/Cox model increases when the incidence moves from negative to positive. This will be analysed in detail in the next section.

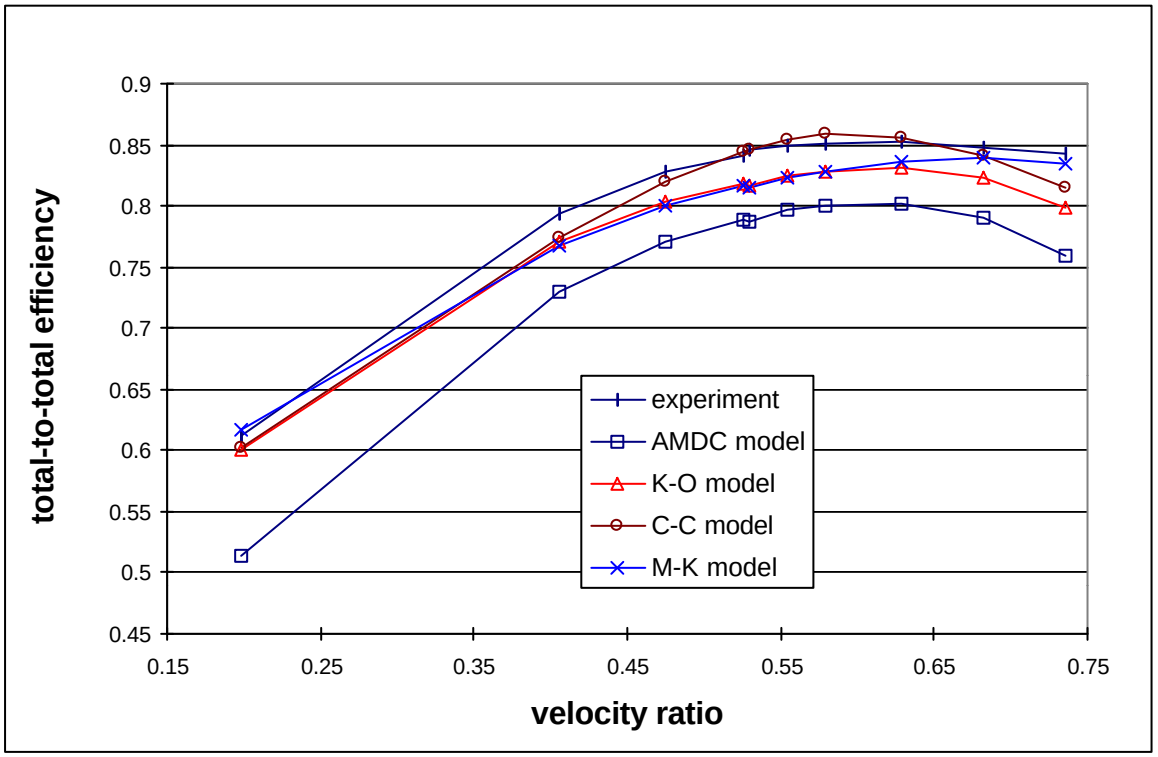

Fig. 4.1.1: *Total-to-total efficiency on turbine stage 1*

Predicted results in the Kacker/Okapuu loss model in Fig. 4.1.1 show a similar trend along the operation region compared with the results in the AMDC model, because the calculating

methods of the off-design profile loss and main part of the design profile loss is the same in these two models. However the Kacker/Okapuu model was modified to predict less losses than the AMDC model. The detailed analysis of the different loss models will be given in the next section.

In comparing the efficiency values predicted in Kacker/Okapuu loss model with the results predicted in Mustapha/Kacker model, we can see that they agree well in the operation region near the design points. This is because that the Moustapha/Kacker method is based on the method of Kacker/Okapuu except some improvement in off-design loss prediction. The loss prediction near the design point from these two methods are very close to each other. However, there is a difference between the values of these two models in the region at far off-design positions. This is caused mainly by the difference of the off-design profile and secondary losses calculation methods in those two models. The Moustapha/Kacker model predicts less total losses than the Kacker/Okapuu model in the high incidence points. The difference of this will be analysed in the following.

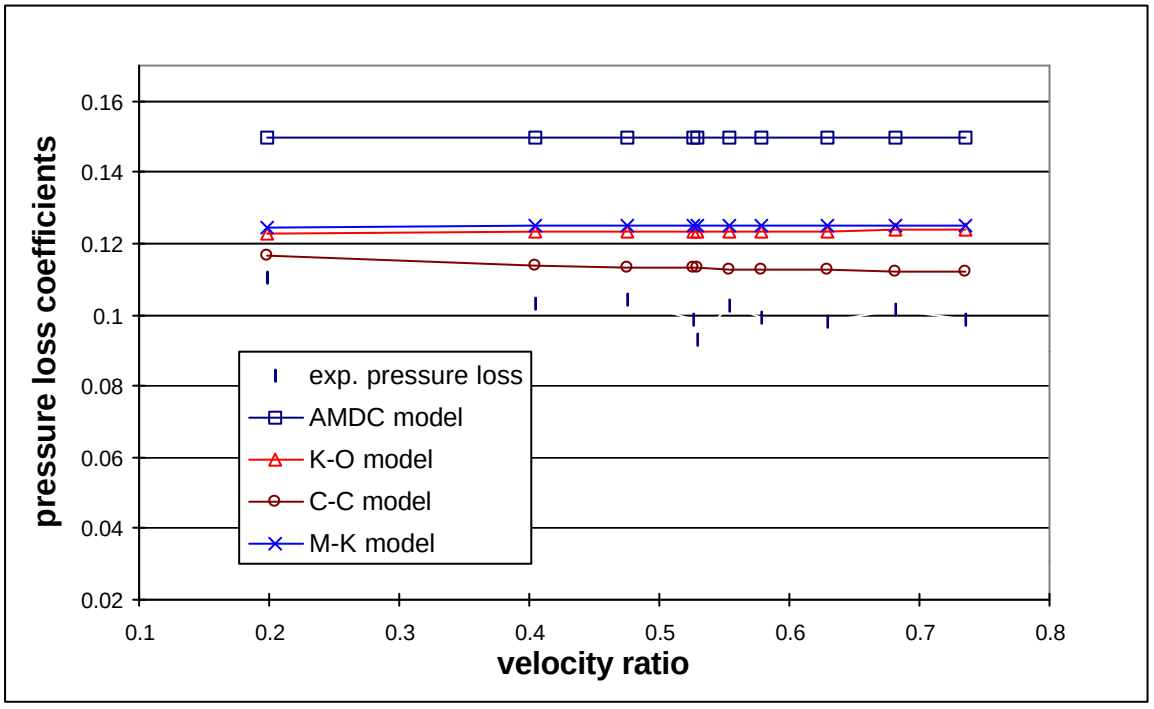

Fig. 4.1.2: *Experimental and predicted pressure loss coefficients in the stator row of turbine stage 1*

Fig. 4.1.2 shows the distribution of the experimental and predicted total loss coefficients predicted for the stator. The inlet flow angle to the stator is not changed for these test cases, i.e. the incidence to the stator is zero and only design point losses were calculated. All models give almost constant values of losses over the stator. The AMDC model is the one which gives most overestimated losses, about 1/3 higher than the experimental results and ¼ higher than the losses predicted in the models of K-O, C-C and M-K. This agrees with the research results by Sieverding [1985, Fig. 7 & 33] and Tremblay et al [1990]. In comparing the equation 2.3.3 for the AMDC model with the equation 2.5.3 for the K-O and M-K models, it can be see that AMDC models give about 1/3 higher profile loss than other models. This is the main reason why the losses by AMDC model are highest.

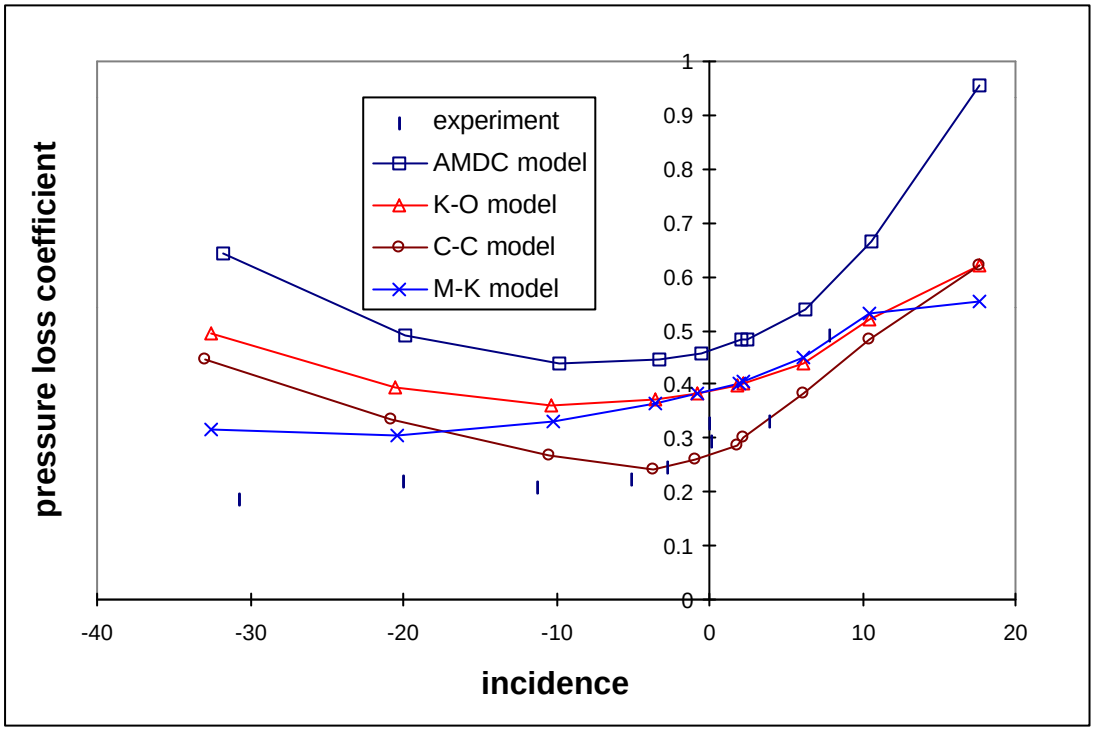

Fig. 4.1.3: *Total losses coefficients in the rotor row of turbine stage 1*

It is more interesting to see the total pressure loss on the rotor row, in Fig. 4.1.3. Due to the change of the velocity triangles, the incidence angle to the rotor is different for these test cases. Similar to the results in the stator, the AMDC model gives highest loss, about 30% higher than the experimental values at the design point, compared with other models. The losses predicted in the AMDC model increase more sharply in the region of positive incidence than in the region of the negative incidence because both the secondary and tip leakage losses increase when incidence rises. The gap between the loss predicted in the AMDC model and the experimental results in the negative incidence region becomes large and large as the operating point moves to the negative incidence direction. This is because the rapid increase of the off-design profile loss predicted in the AMDC model. The distribution of total loss predicted in the K-O model has a similar shape as the loss from the AMDC model, because the K-O model use the same off-design profile loss calculation method as the AMDC model, but with the level reduced about ¼ lower than AMDC loss. In the region of incidence over 10 degree, the K-O loss increases more smoothly than the AMDC loss because the reduction of the secondary loss in the K-O model at the point of negative degree of reaction. The M-K model gives almost the same level of the results near the design point as the model of K-O because the two models use the same methods for calculating the losses of the design point. The loss predicted in the M-K model increases more smoothly when the incidence is over 10 degrees than the other models because the reduction of the secondary loss at the point of negative degree of reaction and because its smooth increase of off-design profile loss. In the region of the negative incidence, the total loss decreases when the incidence moves toward to the negative direction. This is the same trend as the experimental results and different with the loss distribution in other loss models. It is because the off-design profile predicted in the M-K model has very smooth increase with the variation of the incidence. In the region of negative incidence, this smooth increased off-design profile loss could not compensate the decrease of the secondary and tip leakage losses. Therefore the total loss reduces along the negative incidence direction. The loss predicted in the C-C model agrees well with the experimental results near the design point

and in the region of positive incidence. But it increases more rapidly than the experimental results in the negative incidence region. This is mainly because the leakage loss given by the C-C model has a different trend with other models.

In order to understand the physical principle for the behaviour of the loss models, it is interesting to investigate the detailed breakdown of the loss components in the rotor row. These results are shown in Fig 4.1.4 - Fig. 4.1.7.

Fig. 4.1.4 shows the losses predicted in the AMDC models. All calculation equations have been discussed in chapter 2. The profile loss give the lowest value near the zero incidence, which is calculated with equation 3.2.2. When the incidence increases or decreases from the zero incidence point, the profile loss will increase, which is calculated in the off-design correlation shown in Fig. 2.3.4. The off-design profile loss is a 2-D loss (blade-to-blade section) and associated with the flow separation on the blade surfaces. From the principle of flow dynamics, it mainly has the relationship with the incidence, i, Reynolds number, Re, Mach number, M, pitch/chord ratio and inlet and outlet blade angles. In the AMDC model, the off-design profile loss was correlated with the ratio of the incidence angle to the stall incidence angle that was defined as the incidence angle at which the profile loss is twice of the minimum profile loss (see Fig. 2.3.4). The stall incidence angle was correlated with the blade pitch/chord ratio and the ratio of inlet and outlet blade angles. The high incidence angle and large absolute value of the ratio of the blade inlet to outlet angles (which imply the high turning of the blade shape) will easily induce flow separation on the blade surfaces and give a small stall incidence angle therefore produce high off-design profile loss.

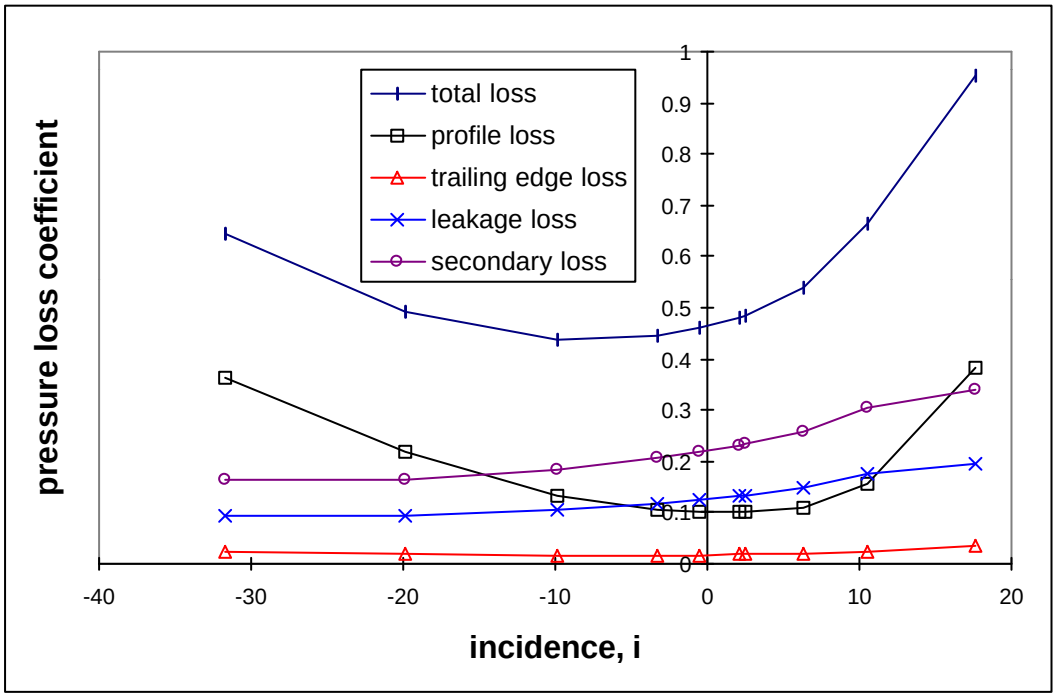

***Fig. 4.1.4**: Breakdown of losses in the rotor of stage 1calculated with AMDC loss models*

As discussed in chapter 1, the secondary loss is mainly caused by the boundary layers on the endwalls and their interaction with the flow in the blade row passage. The loss has the main relationship with the thickness of the inlet endwall boundary layer, blade load, and blade shape. In the AMDC model, the secondary loss is mainly considered as a function of blade loading which is in terms of blade inlet and outlet angles (see equation 2.4.3). In this model,

the inlet boundary layer and blade shape were also correlated by simplifying to a constant and chord/height ratio in equation 2.4.3. From the predicted results in Fig. 4.1.4, the secondary loss rises with the increase of the incidence angle. This is because that when incidence increases, the difference between flow inlet and outlet angles becomes large, flow has high turning and blade loading increase. Therefore the secondary loss becomes large. The trend of this results agrees well with the experiments by Perdichzzi & Dossena [1992], who found that increasing the incidence angle, the region interested by secondary flows extends progressively towards the midspan, i.e. the vortices of the two half parts of the flow channel reach the midspan and interact with each other, as a consequence the overall secondary loss undergoes a huge increase.

Fig. 4.1.4 shows that the tip leakage loss over the rotor row rises when the incidence increases. In the AMDC model, the tip clearance loss was mainly correlated with the tip clearance and blade load (see equation 2.4.4). In the predicted results on the turbine stage 1 shown in Fig. 4.1.4, the tip clearance does not change among the operation points. When incidence increases, difference between inlet and outlet flow angles become large and blade loading increase, which results in high tip leakage loss.

The total losses predicted in the AMDC model are shown in Fig. 4.1.4. The losses are the sum of the profile loss, secondary loss and tip leakage loss and multiplied by the correction of Reynolds number and trailing edge shape (see equation 2.4.1). In this application of subsonic flow turbine, the loss component caused by trailing edge is very small compared with the profile, secondary and tip leakage losses and is just about 4% of the total losses in this model. The minimum total loss is at the point at which the incidence is about -10 degree. The losses increase more sharply in the region of positive incidence than the region of the negative incidence because both the secondary and the tip leakage losses increase when incidence rises.

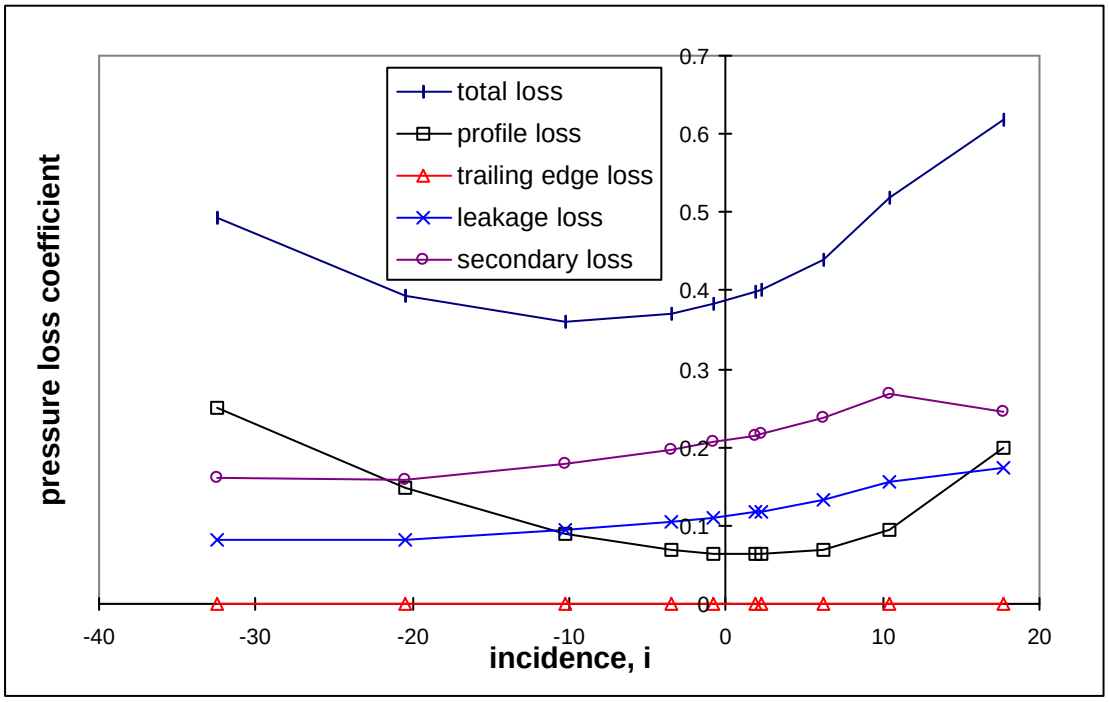

***Fig. 4.1.5**: Breakdown of losses in the rotor of stage 1 calculated with Kacker/Okapuu loss models*

Fig. 4.1.5 shows the losses predicted in the K-O models. The profile loss at the zero incidence point is calculated with equation 2.5.4, which is the same as the design point profile loss calculated in the AMDC model. When the incidence increases or decreases from the zero incidence point, the profile loss will increases, which is calculated as same as the off-design correlation from the AMDC model shown in Fig. 2.3.4. The final profile loss in the K-O model is calculated with equation 2.5.3. In comparing this profile loss with the profile loss in the AMDC model shown in Fig. 4.1.4, it is seen that both curves of the losses have the same trend, however the K-O profile loss is about 1/3 lower than the profile loss in the AMDC model. This can be noted by comparing equation 2.5.3 with the equation 2.3.3. The K-O model takes 1/3 lower profile loss, in equation 2.5.3, than the AMDC model in order to regulate the overestimated profile loss in the AMDC model, equation 2.3.3.

The secondary loss in the K-O model is calculated with equation 2.5.8. Based on the AMDC model, this loss is correlated to the blade loading, which is in terms of blade inlet and outlet angles, as well as the blade height/chord ratio and inlet and outlet Mach number. From the predicted results in Fig. 4.1.5, the secondary loss rises with the increase of incidence. This is because that when incidence increases, the difference between flow inlet and outlet angles becomes large, flow has high turning and blade loading increases. Therefore the secondary loss becomes large. This trend is the same as the one from the result of secondary loss calculated in the AMDC model shown in Fig. 4.1.4. It can be seen from Fig. 4.1.5 that the secondary loss at the point of highest incidence angle falls down, which is different with the AMDC model in Fig. 4.1.4. This is because that in the K-O model the secondary loss is considered as a function of channel flow acceleration by correlating to the Mach number correction factor K_p (see equation 2.5.5 and 2.5.8). K_p depends on the outlet Mach number and ratio of inlet and outlet Mach numbers. When the outlet Mach number is larger than 0.2, K_p mainly depends on the ratio of inlet and outlet Mach numbers. Higher acceleration over the blade row leads to smaller ratio of inlet to outlet Mach numbers and larger value of K_p. This implies the relative higher loss. It is noted, from experimental data, that this ratio of Mach number increases with the raising of incidence. It is also known, from the test data, that at the operation point of highest positive incidence the turbine runs with negative degree of reaction and the rotor relative inlet Mach number is even larger than the outlet Mach number, which means that flow decelerates though the rotor row. Thus the ratio of the inlet and outlet Mach number is close to unity and K_p decreases. Therefore the secondary loss calculated with equation 2.5.8 is reduced at this operating point. Table 4.1.1 shows some experimental parameters inlet and outlet the stator and rotor in the stage respectively (Reynolds number is based on the outlet velocity and blade chord and parameters for the rotor are relative values). A comparison of the parameters for calculating losses involved in these loss models are showed in Table 4.1.2.

The tip leakage loss calculated in the K-O model, with equation 2.5.13, is mainly correlated with the tip clearance and blade load. Fig. 4.1.5 shows that the tip leakage loss over the rotor row rises when the incidence increases. When incidence increases, difference between inlet and outlet flow angles become large and blade loading increases, which results in a high tip leakage loss.

The total loss predicted in the K-O model is shown in Fig. 4.1.5. The loss is the sum of profile loss, trailing edge loss, secondary loss and tip leakage loss and multiplied by the correction of Reynolds number (see equation 2.5.1). In this application of subsonic flow turbine, the loss component caused by trailing edge is very small and negligible compared with the profile,

secondary and tip leakage losses. The minimum total loss is at the point on which the incidence is about -10 degree. The loss increase more sharply in the region of positive incidence than the region of the negative incidence because both the secondary and tip leakage losses increase with the rise of the incidence angle. The distribution of total loss predicted in the K-O model has the similar shape as the loss from the AMDC model but with the level about ¼ lower than AMDC loss. In the region of incidence over 10 degree, the K-O loss increases more smoothly than the AMDC loss because of the discount of the secondary loss in the K-O model at the point of negative degree of reaction as mentioned above.

Velocity ratio **Parameters**	0.20	0.40	0.47	0.53	0.55	0.58	0.63	0.68	0.73
Stator									
incidence [^{o}]	0.0	0.0	0.0	0.0	0.0	0.0	0.0	0.0	0.0
inlet velocity [m/s]	40.7	38.3	38.0	37.5	37.3	37.2	37.1	36.6	36.5
outlet velocity [m/s]	191.7	176.7	174.7	171.7	170.6	170.2	168.6	166.7	165.2
ratio of inlet to outlet velocity	0.212	0.217	0.218	0.218	0.219	0.219	0.219	0.219	0.221
inlet Mach number	0.115	0.108	0.107	0.106	0.105	0.105	0.105	0.103	0.103
outlet Mach number	0.557	0.511	0.505	0.496	0.493	0.492	0.487	0.481	0.477
ratio of inlet to outlet Mach number	0.206	0.211	0.212	0.214	0.213	0.213	0.216	0.214	0.216
Re x 10^5	4.945	4.559	4.508	4.429	4.401	4.392	4.350	4.302	4.262
Rotor (relative values)									
incidence [^{o}]	15.0	7.8	4.0	0.0	-2.7	-5.1	-11.2	-20.0	-30.8
inlet velocity [m/s]	155.2	105.2	90.8	79.3	74.2	70.1	60.9	52.8	46.3
outlet velocity [m/s]	86.2	96.2	95.7	93.0	93.7	93.8	93.2	91.2	91.7
ratio of inlet to outlet velocity	1.801	1.094	0.949	0.853	0.792	0.747	0.653	0.579	0.505
inlet Mach number	0.453	0.305	0.264	0.230	0.215	0.203	0.176	0.153	0.134
outlet Mach number	0.249	0.279	0.278	0.270	0.272	0.273	0.271	0.265	0.267
ratio of inlet to outlet Mach number	1.819	1.093	0.950	0.852	0.790	0.744	0.649	0.577	0.502
Re x 10^5	1.410	1.575	1.566	1.521	1.534	1.535	1.525	1.493	1.501

***Table 4.1.1**: Experimental flow parameters of turbine stage 1*

Losses	**AMDC Model**	**K-O Model**	**C-C Model**	**M-K Model**
Profile loss, design	α'_{in}, α_{out} , t/l, t'_{max}/l,	α'_{in}, α_{out} , t/l, t'_{max}/l,	α_{in}, α_{out}, t/b_B, t'/t, o/t,	α'_{in}, α_{out} , t/l, t'_{max}/l,

	M_{out},	M_{out}, M_{in}/M_{out}, p_{in}/p_{out}, r_h/r_t	M_{out}, t/r_e, $(\cos\alpha_{in}/\cos\alpha_{out})$	M_{out}, M_{in}/M_{out}, p_{in}/p_{out}, r_h/r_t
Profile loss, off-design	i, α_{out}, $\alpha'_{in}/\alpha_{out}$, t/l	i, α_{out}, $\alpha'_{in}/\alpha_{out}$, t/l	i, α'_{in}, α'_{out}, t/b_B, $(\cos\alpha_{in}/\cos\alpha_{out})$,	i, d/t, $(\cos\alpha'_{in}/\cos\alpha'_{out})$,
Secondary loss	H/l, α'_{in}, α_{in}, α_{out},	H/l, α'_{in}, α_{in}, α_{out}, M_{out}, M_{in}/M_{out},	H/l, α_{in}, α_{out}, t/b_B, v_{in}/v_{out}, b_B/H	H/l, α'_{in}, α'_{out}, α_{in}, α_{out}, M_{out}, M_{in}/M_{out}, i, d/l,
Tip clearance loss	τ/H, α_{in}, α_{out}, l/H, z	τ/H, α_{in}, α_{out}, l/H, z	A_k/A_t, $\zeta_{\pi=0}$, h_{in}, h_{out}, w_{out}, w_{in}/w_{out}	τ/H, α_{in}, α_{out}, l/H, z

Table 4.1.2 *: Parameters involved in the loss models.*

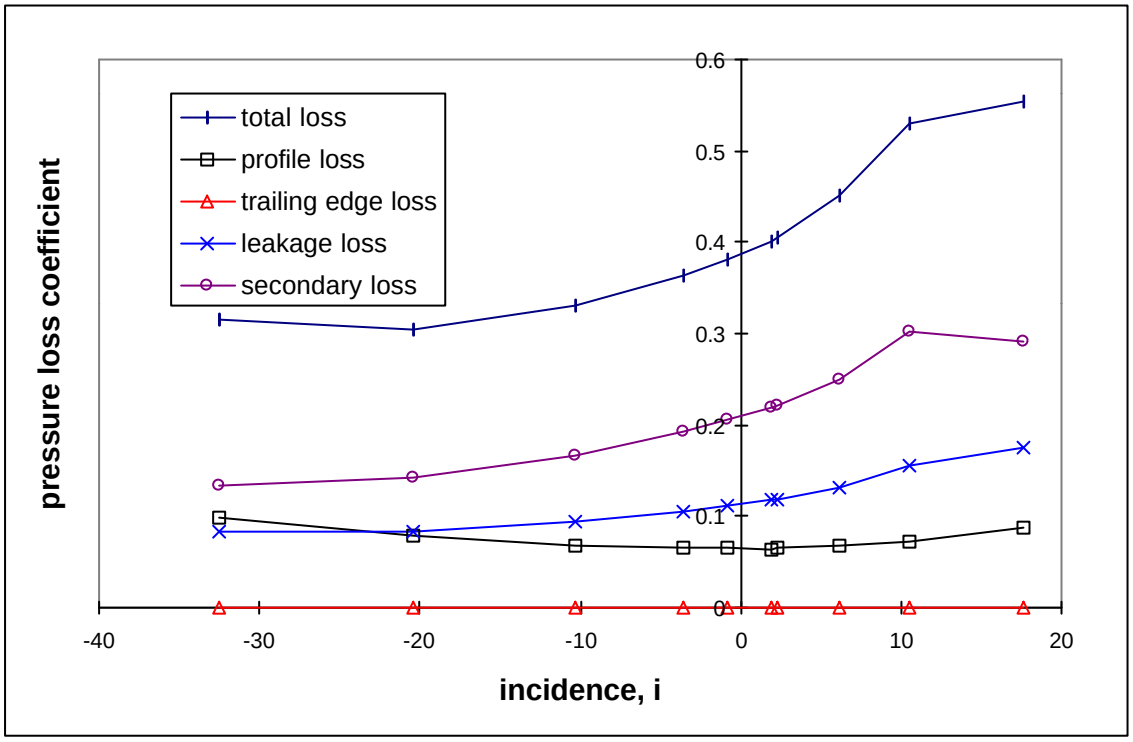

Fig. 4.1.6*: Breakdown of losses in the rotor of turbine stage 1 with Moustapha/Kacker loss models*

The losses over the rotor row predicted in the Moustapha/Kacker (M-K) model are shown in Fig. 4.1.6. The profile loss at the design point in this model is calculated in the same way as the K-O model. It can be seen that the profile loss value at zero incidence point in Fig. 4.1.6 is the same level as the loss in Fig. 4.1.5, which is calculated with equation 2.5.4. and 2.5.3. Unlike the AMDC and K-O model, the off-design profile loss in the M-K model is calculated with a 6-order polynomial (see equation 2.11.1), which is correlated to the incidence, ratio of the blade inlet and outlet angles and the leading edge diameter (see also equation 2.11.3). It is obvious, from this correlation, that high incidence angle, large leading edge diameter and big ratio of blade outlet/inlet angles (which imply the high turning of the blade shape) will easily induce flow separation on the blade surfaces and therefore produce high off-design profile loss. By comparing the distribution of the off-design loss in this calculation in Fig. 4.1.6 with the losses in Fig. 4.1.4 and 4.1.5, it can be seen that the profile loss in M-K model increases more smoothly than the losses in AMDC and K-O models when the incidence rises or reduces from the design point. It is perhaps because the M-K off design profile loss model was calibrated against the test data based on the more advanced blade types than those used with the AMDC model.

The secondary loss calculated in the M-K model is separated into the loss at the design point and the loss at the off-design points. The secondary loss at the design point in the M-K model is calculated with equation 2.5.8, which is the same as the secondary loss calculation method in the K-O loss model. It can be seen that the design point secondary loss in the M-K model is correlated to the blade loading, which is in terms of blade inlet angle and flow inlet and outlet angles, as well as the blade height/chord ratio and inlet and outlet Mach number. The secondary loss at off-design point in the M-K model is calculated with a 4-order polynomial (see equation 2.11.4), which is correlated to the incidence, blade inlet and outlet angles and the leading edge diameter (see also equation 2.11.5). In this model, the influence of incidence on the secondary loss was considered in order to compensate the under-predicted secondary loss by K-O model for cascades having low aspect ratio when operated at large positive incidence [Moustapha et al, 1990, p273]. The M-K model gives the secondary loss with a similar trend to the secondary loss calculated in the K-O model in Fig. 4.1.5. However, although the two models predict almost a same level of the secondary loss at the design point, the M-K model gives a little higher secondary loss in the positive incidence region and lower loss in the negative incidence region compared with the K-O model. The loss from M-K model is about 18% higher, when the incidence is 18 degree, and 16% lower, when the incidence is -32 degree, than the loss from the K-O model. This is done by use of equation 2.11.4, which was the aim for Moustapha et al [1990] to modify this secondary loss calculation from the K-O model.

The method for calculating the tip leakage loss in the M-K model in Fig. 2.1.6 is exactly as the same as the method used in the O-K model in Fig. 2.1.5 because the same method were used in these two models. It is not needed to make special discussion of this loss component.

The total losses predicted in the M-K model is shown in Fig. 4.1.6. The structure for calculating this total loss is as same as the one used in K-O loss model. Because of the different methods for calculating the off-design and secondary losses, the M-K model gives the minimum total loss at the -20 degree of incidence. In the positive incidence region, the M-K model gives the total loss with a similar trend to the AMDC and K-O models except that after the incidence is over than 10 degree the loss from M-K model increases more smoothly than other models. This is because of the smooth distribution of the off-design profile loss in this region given by the M-O model. In the region of the negative incidence, the total loss decreases with the reduction of the incidence. This is different with the loss distribution in other loss models. It is also because the off-design profile predicted in the M-K model has very smooth increase with the variation of the incidence. In the region of negative incidence, this smooth increase of off-design profile loss could not compensate the decrease of the secondary and tip leakage losses. Therefore the total loss reduces along the negative incidence direction.

The losses calculated in the C-C model are shown in Fig. 4.1.7. The profile loss in this model is a main function of a basic profile loss corrected by multiplying factors of Reynolds number, incidence and trailing edge, the effect of Mach number, suction trailing side curvature and trailing edge thickness (see equation 2.6.2). The basic profile loss is correlated with the pitch/(axial chord) ratio, contraction ratio and lift parameter which is a function of the inlet blade angle and outlet flow angle (see Fig. 2.6.1 and 2.6.2). On the off-design points, the profile loss will increase depending on the incidence angle and the install incidence angle (see Fig. 2.6.3) that was defined as the incidence angle at which the profile loss is twice of

the minimum profile loss. The stall incidence depends on the blade shape. Craig/Cox gave the stall incidence with a series of correlations of the blade inlet angle, outlet angle, ratio of pitch to camber line and the contraction ratio of the blade passage. High turning of blade, high ratio of pitch to camber line and low contraction ratio which leads to low flow acceleration through blade passage, will easily induce flow separation on the blade surface and therefore produce high off-design profile loss. In comparing the profile loss distribution in the C-C models in Fig. 4.1.7 with the loss in the other loss model, it can be seen that the C-C model gives more rapid increase of the off-design profile loss, especially in the region of positive incidence, than others. This is because the too small value of the stall incidence angle was given in this model. Similar results has been found by Shu et al [1985].

The secondary loss in the C-C model was calculated with a linear function of basic secondary loss and the factors of Reynolds number and aspect ratio (see equation 2.6.3). The basic secondary loss was correlated with blade pitch/chord ratio, ratio of inlet and outlet flow velocities and the lift parameter which is a function of the inlet blade angle and outlet flow angle. In this correlation, high velocity ratio, pitch/chord ratio and lift parameter imply the low flow acceleration, high pitchwise pressure gradient and high blade load therefore give high secondary loss. In Fig. 4.1.7, the secondary loss calculated in the C-C model increases when the incidence rises. This is due to the increase of the lift parameter at the high incidence. When incidence increases, the difference between flow inlet and outlet angles becomes large, flow has high turning and blade loading increases. Therefore the secondary loss becomes large. The physical reason of this trend is as the same as the secondary losses predicted in other models discussed above.

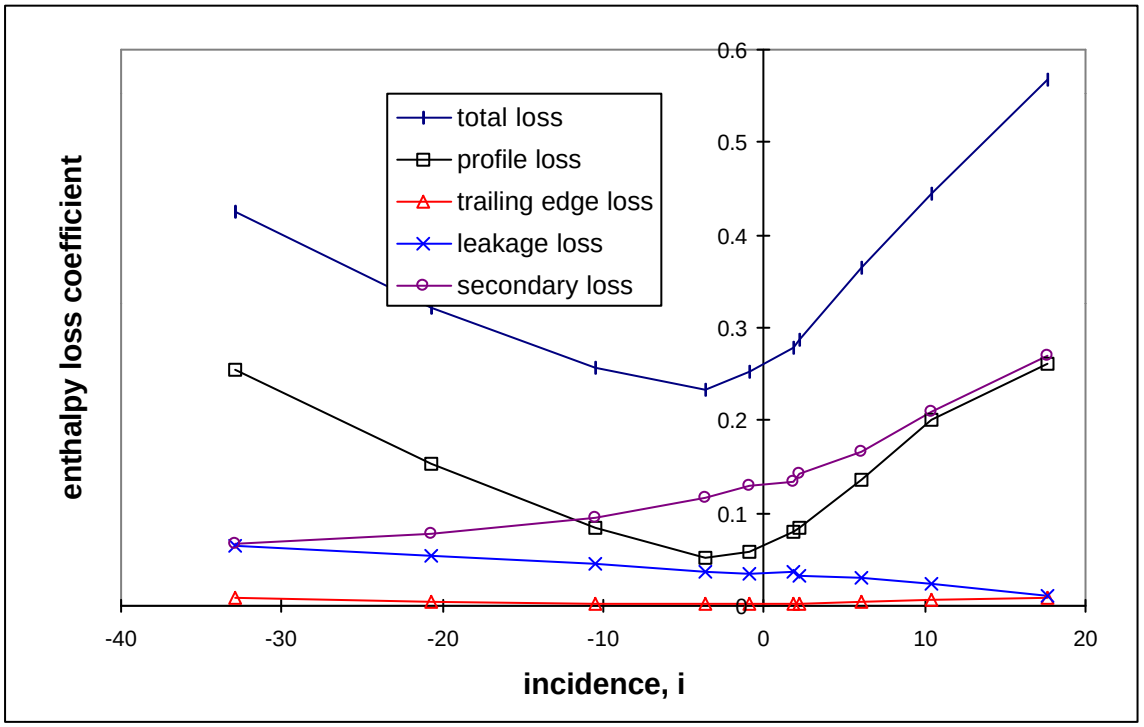

***Fig. 4.1.7**: Breakdown of losses in the rotor of turbine stage 1 calculated with Craig/Cox loss models*

The tip leakage loss in the C-C models is calculated with equation 2.6.4, in which the diminution of the efficiency caused by the tip leakage loss is a function of the leakage coefficient, ratio of the clearance to throat areas and the efficiency when the clearance is zero. The leakage coefficient in the equation is a main function of the ratio of the inlet and outlet

velocity at the tip region. When the ratio is small, the leakage coefficient will be large. This ratio actually implies the static pressure drop over the blade row. The small inlet and outlet velocities ratio means the high acceleration of the flow and large static pressure drop over the blade, which will drives more leakage flow through the clearance area and causes large tip clearance loss. The large inlet and outlet velocities ratio, for example when the ratio is close to unity, indicates the low acceleration of the flow and small static pressure drop. The mass flow through the leakage will be small therefore the tip leakage is small. This is the reason why the tip leakage loss predicted in the C-C model in Fig. 4.1.7 decreases when the incidence rises. With the operating point with low negative incidence, the inlet flow velocity is much smaller than the outlet velocity. The flow has high acceleration and the static pressure drop over the rotor is also high and the tip clearance loss in this model is large. As the operating point is shifted toward the positive incidence direction, the ratio of inlet and outlet flow velocities become large and static pressure drop over the rotor decreases, which leads to the tip leakage loss reducing.

The total loss in the C-C model is the sum of profile loss, trailing edge loss, secondary loss and tip leakage loss. It can be seen that from Fig. 4.1.7 the minimum loss is at the incidence about -3 degree which is given by the lowest profile loss. The loss increases when the operating points is shifted from the minimum loss point. It increases more sharply when the incidence moves toward to the positive direction because both the profile and secondary losses rise rapidly in this direction. Compared with the results from the other loss models, the total loss predicted in the C-C model increases more rapidly in the negative incidence region. This is mainly because the contribution of the tip leakage loss which increases with the reduction of the incidence angle.

Concluding remarks for the loss prediction in turbine stage 1

The C-C model gives the loss closest to the experimental results for the stator and on and near the design point for the rotor, but over predict the loss in the negative incidence region. The AMDC model is the one which most overestimate the losses in the whole operation range while the K-O model has the similar trend of the loss distribution with the AMDC model but lower loss level. In the operation range of negative incidence, only M-K model has the same trend of the total loss distribution as the experimental results.

Following remarks will be given on the behaviour of every loss components:

Profile loss:
All the models are based on experimental data and are correlated mainly with the blade inlet and outlet angles and pitch/chord ratio (C-C model takes the ratio of pitch to camber line instead). In the AMDC, K-O, and M-K models, the ratio of blade maximum thickness to the pitch was taken into account while the pitch to blade back radius ratio was considered in the C-C model as a blade shape parameter which influences the flow boundary layer statues on the blade surface. The flow acceleration in the blade passage was considered in the K-O and M-K models by taking the ratio of inlet and outlet Mach number while in the C-C model by using the contraction ration which is the ratio of the inlet and throat widths. The incidence is the most important parameter to predict the off-design profile loss. This parameter was taken into account by all the models. In the AMDC and C-C models, the stall incidence angle was

taken as a parameter to predict the off-design loss and this stall incidence angle was mainly correlated to the pitch to chord ratio and the inlet and outlet blade angles. In addition, in the C-C model the contraction ratio was also considered. In the M-K model, besides the incidence, the ratio of leading edge diameter to the pitch was considered as an important parameter together with the blade inlet and outlet angles. The results show that the AMDC and C-C models (the K-O model has the same methods to predict the off-design profile loss with the AMDC model) give rapid increase of off-design profile loss, especially in the negative incidence region. It seems that the high predicted off-design profile loss come from the too small calculated stall incidence angle. Compared with these, the M-K model give much smoother increase of off-design profile loss.

Secondary loss:

In all of these models, the secondary losses were considered as a main function of the blade aspect ratio and load (in the term of lift parameter in the C-C model) which is correlated with flow turning over the blades. Besides this, the influence of the flow acceleration on the secondary loss was also considered in the K-O, C-C and M-K models by correlating the inlet and outlet flow velocity in the C-C model and inlet and outlet Mach numbers in the K-O and M-K models. In most of the operation ranges, all models give the same trend of the secondary losses. But at the highest positive incidence point where the degree of reaction is near to zero, the secondary losses from the K-O and M-K models decrease while the loss from C-C model keeps increasing. This is because of the different way in treating flow acceleration in the models. In the C-C model, the basic secondary loss increases with the rise of the inlet to outlet flow velocity ratio. In the K-O and M-K models, the coefficient K_p reduces, which leads to the decrease of the losses, with the rise of the inlet to outlet Mach number ratio. It is also noted that the pitch to chord ratio was taken into account as a parameter for secondary loss prediction in the C-C model but not in the other models. The incidence and the ratio of blade leading edge diameter to chord ratio were considered in the secondary loss calculation in the M-K model. Compared with the K-O model, the M-K model gives the same level of the loss at design point but higher loss in the positive incidence region and lower loss in the negative region. The difference level of the losses between these two models can be about 16-18% at the ends of the operation range.

Tip leakage loss:

In the AMDC, K-O and M-K models, the tip leakage loss was calculated by correlating mainly to the aspect ratio, the ratio of tip clearance to blade span and the blade load which is a function of flow turning. The tip leakage loss predicted with these models rises versus the increase of the incidence angle. In the C-C model, the tip leakage loss is calculated by diminishing an amount of variation of the blade efficiency from the blade efficiency when tip clearance is zero. By converting this equation to the tip leakage loss coefficient, it is a function of the clearance to throat areas ratio, inlet and outlet velocity and the non-clearance loss which is the sum of the profile and secondary losses. The tip leakage loss predicted with the C-C model rises versus the decrease of the incidence angle. This is a completely different trend compared with the losses predicted in the AMDC, K-O and M-K models.

4.2 Performance Simulation on Turbine Stage 2

A comparison between predicted stage efficiencies and experimental data for turbine stage 2 is shown in Fig. 4.2.1. The velocity ratio in Fig. 4.2.1 is defined as same as that in stage 1 (see equation 4.1.1). The calculations on turbine stage 2 were performed at the condition of pressure ratio from 1.18 to 1.23 and velocity ratio from 0.25 to 0.85. This operation range covers the large off-design region. The incidence angle for the rotor blade row varies approximately from $+18^0$ to -60^0 corresponding to this range of velocity ratio. Compared with stage 1, the flow conditions on this stage do not change significantly and the most of the geometrical parameters of this stage are also same. The only difference between these two stages is that stage 2 has 25% higher aspect ratio than stage 1. This can be seen in chapter 3.

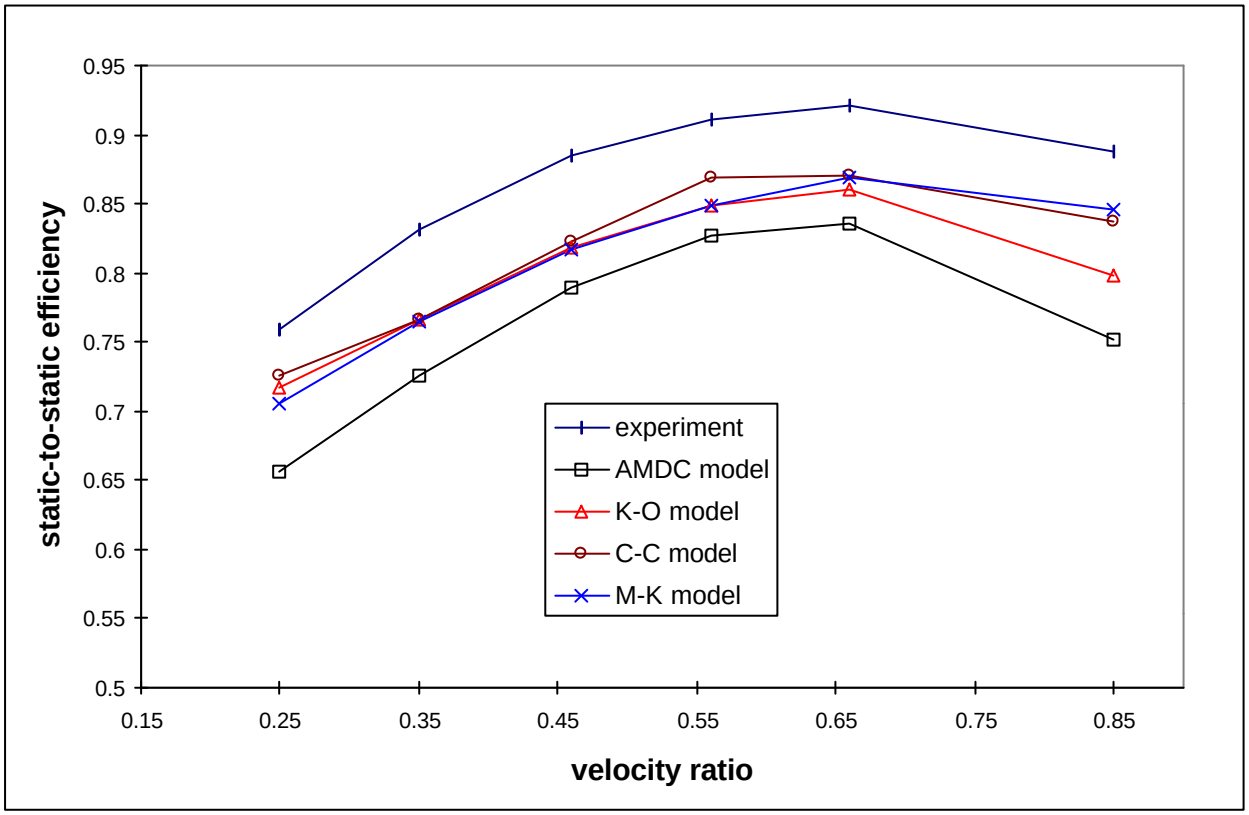

Fig. 4.2.1: Static-to-static efficiency on turbine stage 2

The distribution of static-to-static stage efficiency on turbine stage 2, predicted with various loss models, is shown in figure 4.2.1. It can be seen from Fig 4.2.1 that the predictions from all methods give the same trend of the efficiency as the experimental results. The predicted results are lower than the experimental data. In comparing with the results predicted on stage 1 in Fig. 4.1.1, it is shown that the gap between the predicted and experimental results in stage 2 is larger than that in stage 1. However it is noted that the experimental results of the efficiency from turbine stage 2 have a measurement error about 1-1.5% percent higher than the measurements on stage 1 [Hedlund, 1997]. The measurement error seems mainly exists in the rotor. This can be seen from following analysis of the losses over the rotor. The difference between the measurements in the two turbine stages is indicated with error bars in Fig. 4.2.1. In this calculation, the AMDC method still predicts the lowest efficiency which means highest losses in the stage predicted with this method. That is the same as the earlier

predictions in stage 1. The Craigh/Cox method gives the results which are closer to the experimental data than the other methods in the region near the design operation, velocity ratio from 0.45 to 0.65. In the region of low velocity ratio from 0.25 to 0.45 (the region of positive incidence to the rotor), the K-O, C-C and M-k models give close efficiency which is about 3-5% units lower than the experiments. In the region of high velocity ratio from 0.65 to 0.85 (in corresponding to the region of negative incidence to the rotor), the C-C and M-k models keep the same trend with the about 5% units lower that the experiments. The K-O model has the loss decreasing more rapidly than those in the M-K and C-C models in this high velocity ratio region.

Fig. 4.2.2 shows the distribution of total loss coefficients predicted from the stator compared with the experiments. For all of these test cases, the inlet flow angle to the stator is not changed, that means the incidence to the stator is zero and only design point losses were calculated. The predicted loss coefficients in these loss models keep almost in constants because of the non-change of the incidence. The AMDC model most overestimates losses which are about 1/3 higher than the experimental results and about ¼ higher than the losses predicted in the models of K-O, C-C and M-K, around 0.1 in this stage. In comparing the results in this turbine stage with the corresponding results of turbine stage 1 shown in Fig. 4.1.2, it can be seen that total loss coefficient over the stator of stage 2 are 10% lower by the C-C model and 20% lower by the AMDC, K-O and M-K models than the loss values of stage 1. By comparing the experimental results between the two stages, it is found that the total loss in stage 2 is 15% lower than that in stage 1. The decrease of the losses in stage 2 is because this turbine stage a higher span to chord ratio than stage 1, except the same blade profiles in the two turbine stages, which leads to lower secondary loss.

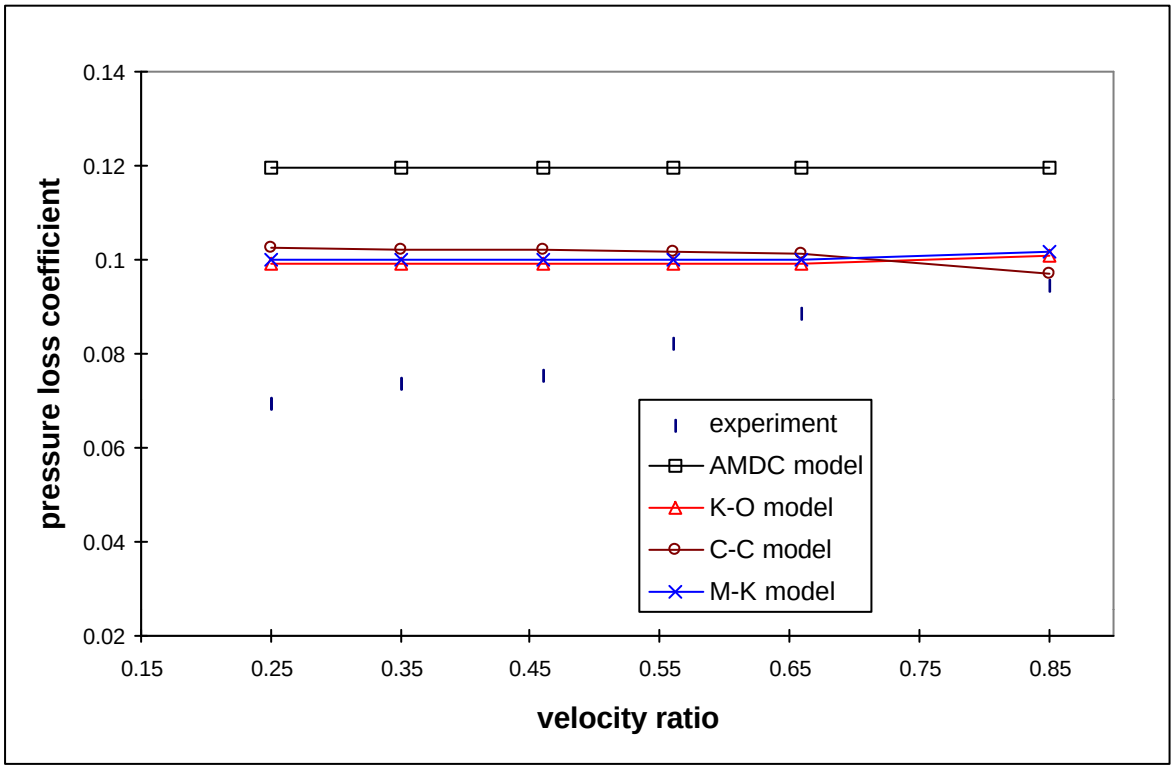

Fig. 4.2.2: *Pressure loss coefficient over the stator of turbine stage 2*

Fig. 4.2.3 shows the total pressure loss, on the rotor row, distributed along the design and off-design operating points. The results in this turbine stage are similar to the corresponding

results in turbine stage 1. The AMDC model gives highest loss comparing with others. The distribution of total loss predicted in the K-O model has the similar shape to the loss from the AMDC model but with the level about ¼ lower than AMDC loss as the same as the results in turbine stage 1. The M-K model give the almost same level of the results near the design point as the model of K-O. The loss predicted in the C-C model is closest to the experimental results near the design point and in the region of positive incidence and increases more rapidly than the experiments in the negative incidence region. Compared with the corresponding total losses over the rotor in turbine stage 1 shown in Fig. 4.1.3, the predicted losses in all these models are about 15-30% lower but the experimental results is 2/3 lower. Compared with the loss reduction in the stator from turbine stage 1 to stage 2, it seems that the 2/3 reducing of rotor loss in the experiments is too much, which is the reason why the error bars exist for the experimental stage efficiency in Fig. 4.2.1.

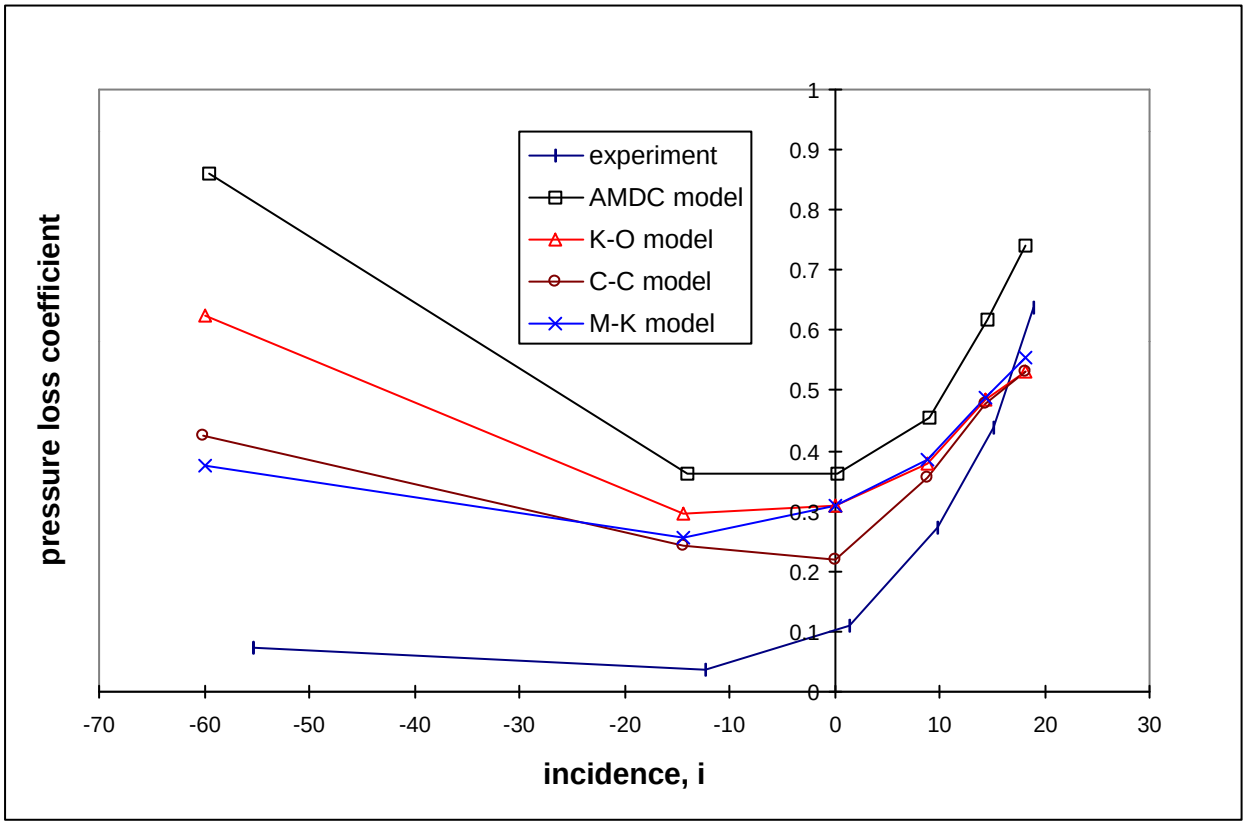

Fig. 4.2 3: *Total loss coefficient over the rotor of turbine stage 2*

It is of interest to look though the detailed breakdown of the loss components in the rotor row, shown in Fig 4.1.4 - Fig. 4.1.7, to further understand the physical principle for the behaviours of the loss models.

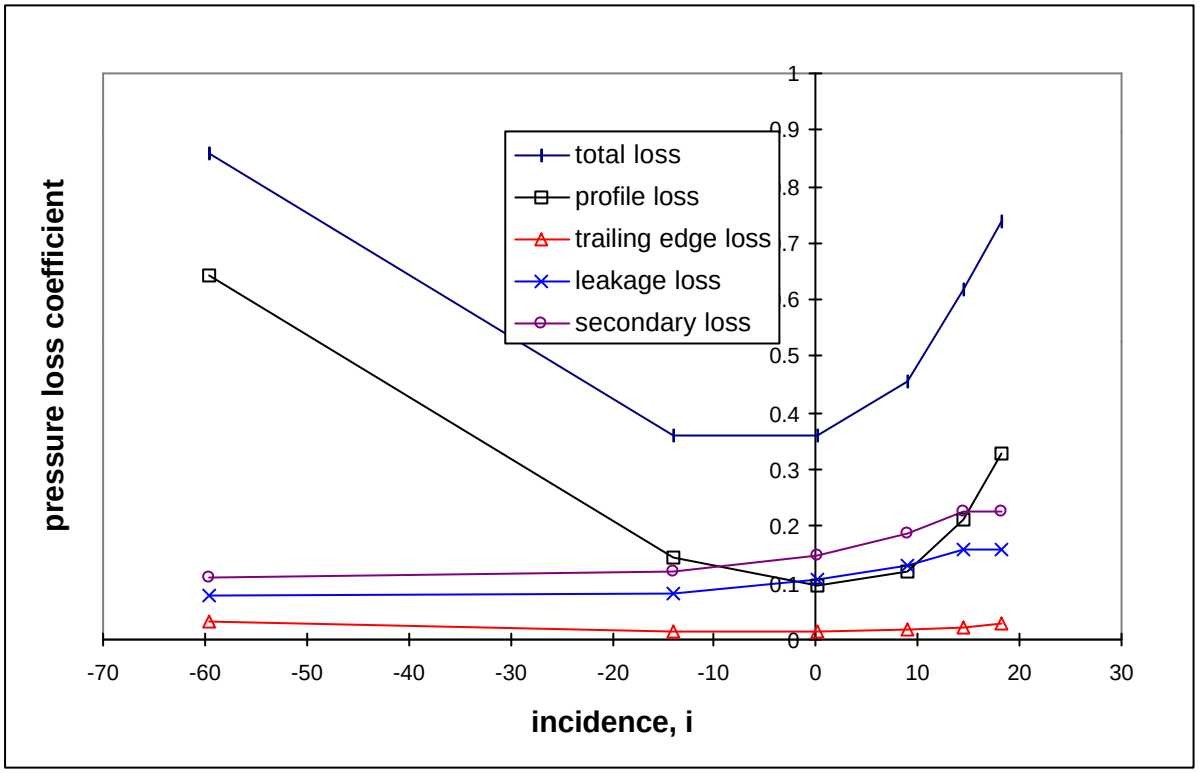

Fig. 4.2.4: *Breakdown of losses in the rotor of turbine stage 2, calculated with the AMDC models*

Fig. 4.2.4 shows the losses predicted in the AMDC models. The profile loss predicted in the AMDC model has the same trend as the corresponding results from turbine stage 1. Compared with the rotor loss breakdown in turbine stage 1 shown in Fig. 4.1.4, it can be seen that the levels of profile loss do not change in the corresponding region. This means the span to chord ratio variation in turbine stage 2 do not affect to the profile loss prediction in the AMDC model. The profile loss is due to the blade boundary layers and its separation on blade surface through viscous and turbulent dissipation. It is considered a two dimensional loss, on blade to blade section, and correlated with the blade geometrical parameters on this 2D section. The correlation of the profile loss has no relationship with the aspect ratio, which can be seen from all equations for calculating profile loss presented in Chapter 2. In this application of a preliminary turbine design process, the overall losses are predicted with mean line method, which means the parameters at the mean radius are used and radial variation of the parameters are neglected. If blades need to be stacked with varied geometrical parameters along the radius in the further process of the turbine design, the profile loss must be calculated in different radial section then integrated in order to have a more precise overall result.

Form the predicted results in Fig. 4.2.4, the secondary loss has a trend as the same as the results in turbine stage 1. Compared with the rotor loss breakdown in stage 1 shown in Fig. 4.1.4, it can be seen that the levels of the secondary loss is about 30-35% lower in the rotor of turbine stage 2 in the corresponding region. This is caused by the increase of the blade span to chord ratio in turbine stage 2. It is obvious that, when the aspect ratio is small, there will be the risk of the interaction between the secondary vortex on at two endwalls and the secondary losses will be large.

Fig. 4.2.4 shows that the tip leakage loss predicted in the AMDC model over the rotor row rises when the incidence increases. In the AMDC model, the tip clearance loss was mainly

correlated with the tip clearance and blade load (see equation 2.4.4). This trend of the tip leakage loss is the same as the corresponding results in turbine stage 1. Compared with the rotor loss breakdown in turbine stage 1 shown in Fig. 4.1.4, it can be seen that the levels of the tip leakage loss are about 15-25% lower in the rotor of turbine stage 2 in the corresponding region. This is caused by the increase of the blade span to chord ratio in turbine stage 2, which leads to the ratio of the tip clearance to the blade chord lower than the one in stage 1 therefore the loss becomes lower (see equation 2.4.4).

The total loss predicted in the AMDC shown in Fig. 4.2.4 has the same trend as the loss predicted in turbine stage 1. The level of the total loss in the corresponding operation range is about 15-30% lower than total profile loss predicted on turbine stage 1. This is because of the decrease of the secondary and tip leakage losses due to the 25% increase of the aspect ratio in turbine stage 2.

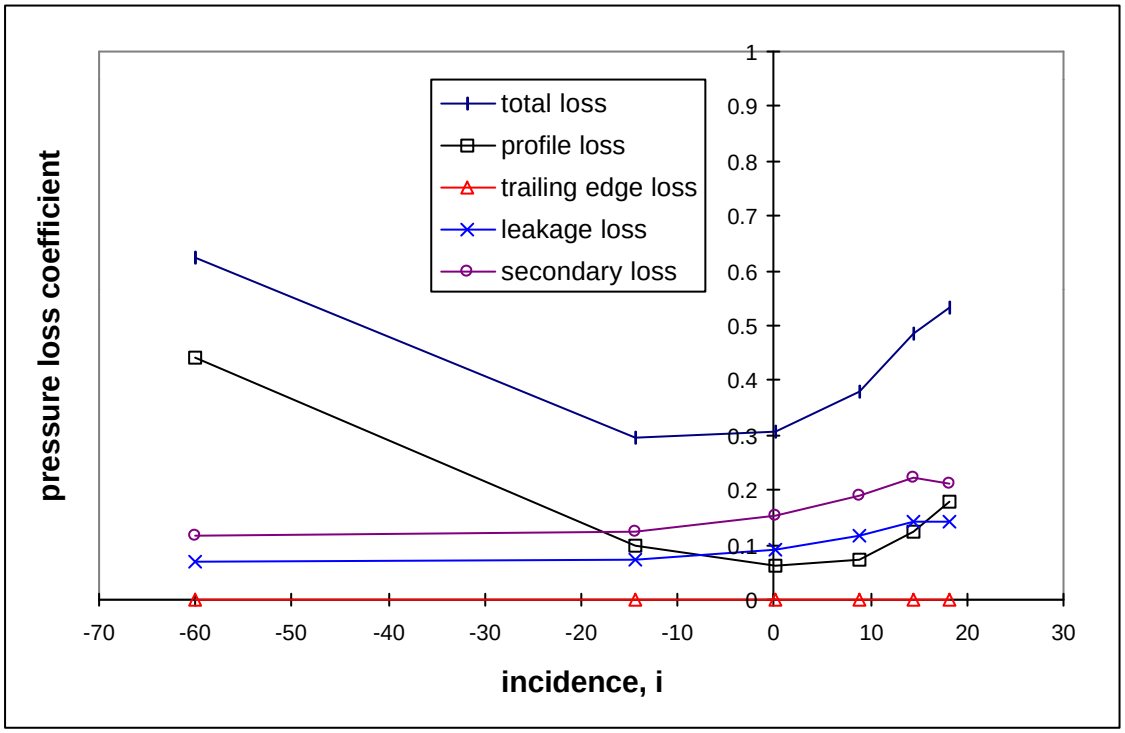

Fig. 4.2.5: *Breakdown of losses in the rotor of turbine stage2 with the Kacker/Okapuu model*

Fig. 4.2.5 shows the losses predicted in the K-O models. In comparing this profile loss with the profile loss in the AMDC model shown in Fig. 4.2.4, it is seen that the both curves of the losses have the same sharp, however the K-O profile loss is about 1/3 lower than the profile loss in the AMDC model. The K-O model takes 1/3 lower profile loss than the AMDC model in order to regulate the overestimated profile loss in the AMDC model (see equation 2.5.3 and 2.3.3). Compared with the rotor loss breakdown in stage 1 shown in Fig. 4.1.4 predicted in the same model, the levels of profile loss predicted in stage 2 do not change in the corresponding region. The reason is the same as the AMDC model.

The secondary and tip leakage losses predicted on turbine stage 2 in the K-O model shown in Fig. 4.2.5 has the same trend as the corresponding losses in turbine stage 1. Compared with the rotor loss breakdown in turbine stage 1 shown in Fig. 4.1.5, the levels of the secondary loss predicted in this model is about 15-30% lower and the tip leakage loss is about 15-25% lower in the rotor of turbine stage 2 in the corresponding region due to the

increase of the aspect ratio. The reason is the same as the secondary and tip leakage losses predicted in the AMDC model.

The total loss predicted in the K-O model is also shown in Fig. 4.2.5. It has the same trend as the total loss in turbine stage 1 predicted in this model. Like the prediction in the AMDC model, the total rotor loss of turbine stage 2 predicted in the K-O model is about 15-25% lower than the corresponding loss in turbine stage 1 because the aspect ratio in turbine stage 2 is 25% higher than that turbine stage 1, which leads to the decrease of the secondary and tip leakage losses.

The losses over the rotor row predicted in the Moustapha/Okapuu (K-O) model are shown in Fig. 4.2.6. All these losses have the same trends as the ones of the corresponding losses predicted in turbine stage 1. Similar to the losses predicted in the AMDC and K-O models, the M-K model gives lower secondary and tip leakage losses in turbine stage 2 than the corresponding losses in turbine stage 1 due to the increase of the aspect ratio. The secondary loss is about 15-30% lower and the tip leakage loss about 15-25% lower in turbine stage 2 than those in turbine stage 1. This leads to the rotor total loss of turbine stage 2 predicted in the M-K model is about 15-25% lower than the loss in turbine stage 1.

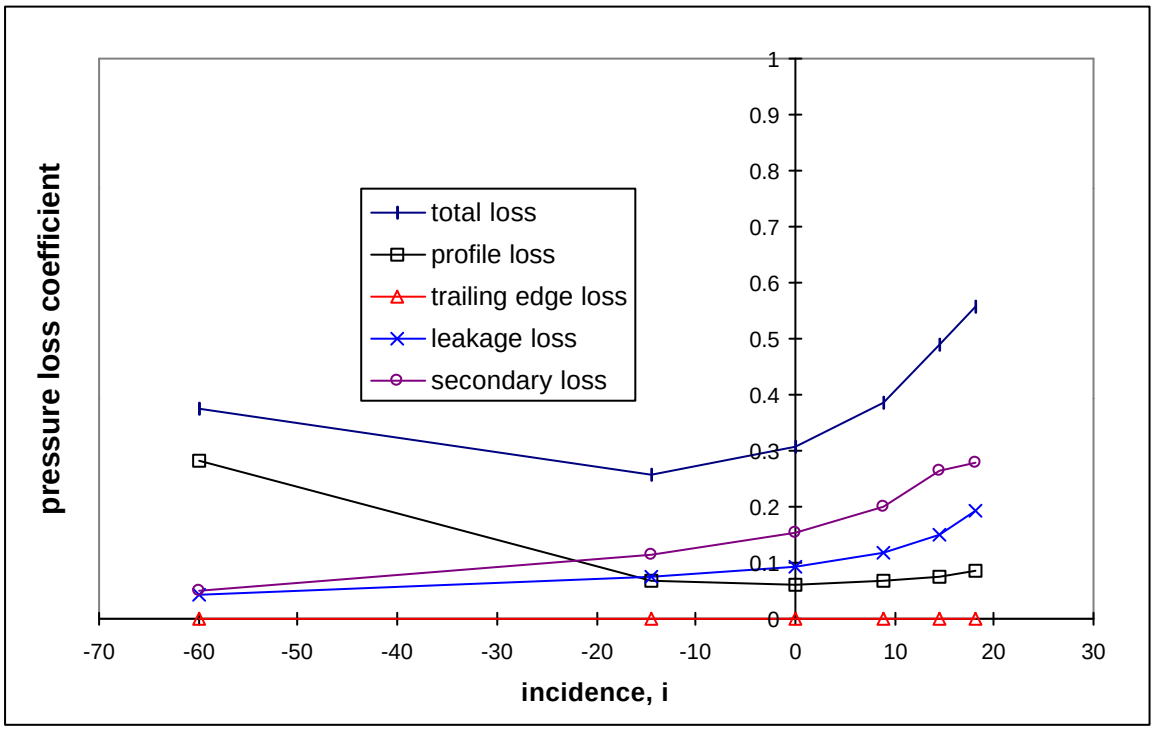

Fig. 4.2.6: *Breakdown of losses in the rotor of turbine stage 2 with the Moustapha/Kacker model*

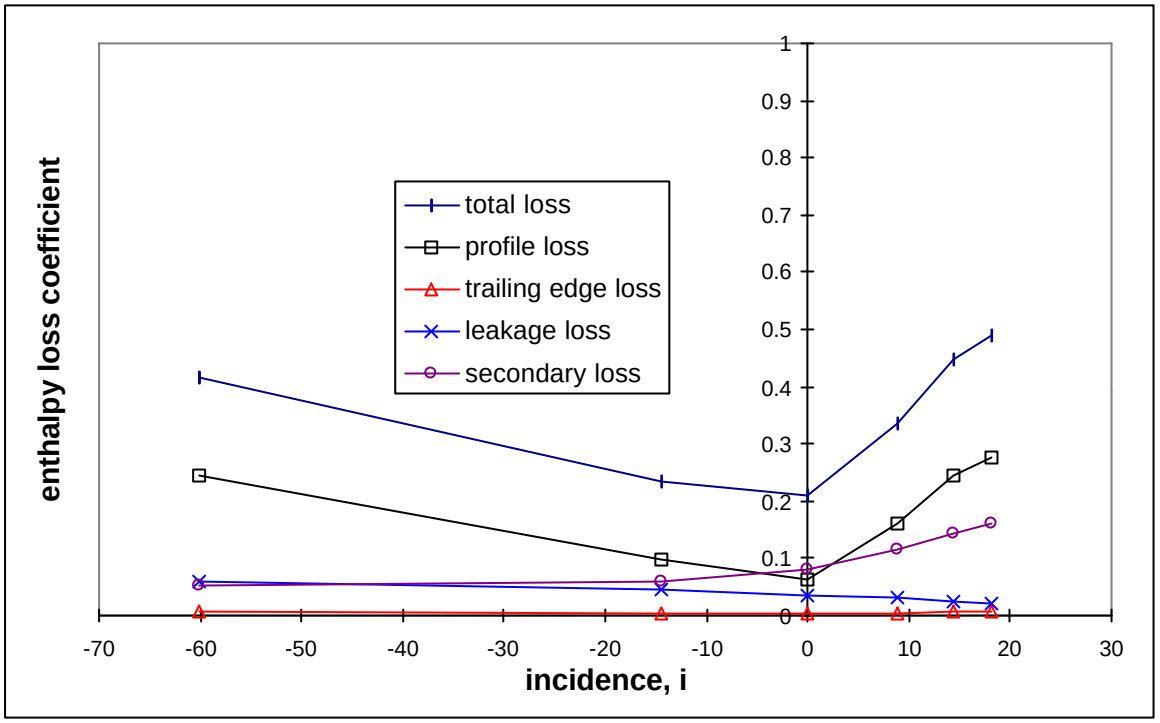

Fig. 4.2.7: *Breakdown of losses in the rotor of turbine stage 2 calculated with the Craig/Cox model*

The losses calculated in the C-C model in the turbine stage 2 are shown in Fig. 4.2.7. All these losses predicted in the C-C model have the same trends as the ones in turbine stage 1. Like the other loss models, the increase of the blade span to chord ratio does not affect the profile loss in this model. The total rotor loss of turbine stage 2 is about 15-30% lower than the total loss in turbine stage 1 along the operation range. This is due to the decrease of the secondary and tip leakage losses caused by the increase of the aspect ratio in turbine stage 2.

Table 4.2.1 shows some experimental parameters, such as the inlet and outlet velocities and Mach numbers and Reynolds number, for the stator and rotor in turbine stage 2. These parameters are significant to the prediction the losses in the turbine with these models. Compared Table 4.2.1 with Table 4.1.1 for stage 1, it can be seen that the variation of parameters is not significant between the parameters in these two stages.

Concluding remarks for the loss prediction in turbine stage 2

All the models give the similar trends of losses on turbine stage 2 with the corresponding trends of the results predicted in stage 1 because the flow conditions do not change significantly and most of the geometrical parameter are also same, except the aspect ratio, in comparing with the stage 1. The profile losses predicted on the rotor of stage 2 in these models have the same level compared with the corresponding losses predicted in stage 1. For the stator, the 25% increase of the aspect ratio in stage 2 causes a significant reduction of secondary losses in the rotor predicted in all these models (secondary losses reduced 13-35% by the AMDC model, 15-40% by the C-C model and 15-30% by the K-O and M-k models respectively) and about 15-25 reduction of the tip leakage losses predicted in the AMDC, K-O and M-K loss models in the corresponding operating range. The tip leakage loss predicted in the C-C model is not affected significantly by this variation of the aspect

ratio. Therefore the total losses in the rotor of stage 2 predicted in the models decrease about 15-25% by the K-O and M-K models and 15-30% by the AMDC and C-C models compared with the corresponding results from the rotor of stage 1. In the stator, the total losses decrease about 10% predicted by the C-C model and 20% by the every one of the other models compared with the losses in the stator of stage 1 because of the 25% increase of the aspect ratio in stage 2 which causes the decrease of the secondary loss.

Velocity ratio **parameters**	0.25	0.35	0.46	0.56	0.66	0.85
Stator						
incidence [^{o}]	0.0	0.0	0.0	0.0	0.0	0.0
inlet velocity [m/s]	39.4	39.1	38.7	38.2	37.9	30.4
outlet velocity [m/s]	176.5	172.4	170.0	167.3	165.2	125.4
ratio of inlet to outlet velocity	0.223	0.227	0.228	0.228	0.229	0.242
inlet Mach number	0.113	0.112	0.111	0.109	0.109	0.087
outlet Mach number	0.518	0.506	0.498	0.490	0.484	0.364
ratio of inlet to outlet Mach number	0.218	0.221	0.223	0.222	0.225	0.239
Re x 10^5	4.554	4.447	4.386	4.318	4.264	3.235
Rotor (relative values)						
incidence [^{o}]	19.0	15.1	9.9	1.5	-12.2	-55.3
inlet velocity [m/s]	137.4	114.4	93.5	73.8	57.1	34.2
outlet velocity [m/s]	100.7	95.9	93.6	96.5	98.1	74.7
ratio of inlet to outlet velocity	1.364	1.193	0.999	0.765	0.582	0.458
inlet Mach number	0.403	0.335	0.274	0.216	0.167	0.099
outlet Mach number	0.294	0.281	0.274	0.283	0.289	0.218
ratio of inlet to outlet Mach number	1.371	1.192	1.000	0.763	0.578	0.454
Re x 10^5	1.649	1.569	1.532	1.578	1.605	1.222

Table 4.2.1: *Some experimental flow parameters of turbine stage 2*

4.3 Performance Simulation on Turbine Stage 3

The calculation on turbine stage 3, the fist stage of the Hannover turbine, was performed and compared against the test data on 4 cases, one design point with mass flow 7.8 kg/s and 3 off-design points with mass flow 6.5, 4.6 and 4.1 kg/s (see [Fottner, 1990]). All the test cases are run with turbine shaft speed 7500 rpm. The calculated results show that this range of mass flow variation covers a region of load coefficient from about 0.6 to 1.1 and the incidence for the rotor blade row from $+8^0$ to -27^0. Table 4.3.1 shows the main stage parameters for these run cases. The load and flow coefficients are defined as equation 4.3.1 and 4.3.2 respectively.

Load coefficient: $$y = \frac{h_{co} - h_{c2}}{u_2^{\,2}} \qquad \text{(eq. 4.3.1)}$$

Flow coefficient: $$j = \frac{c_{2x}}{u_2} \qquad \text{(eq. 4.3.2)}$$

Run cases	mass flow (kg)	shaft speed (rpm)	load coefficient	flow coefficient
1 (design point)	7.8	7500	1.09	0.43
2	6.5	7500	0.95	0.40
3	4.6	7500	0.71	0.34
4	4.1	7500	0.59	0.32

Table 4.3.1: *Main stage parameters of run cases for turbine stage 3*

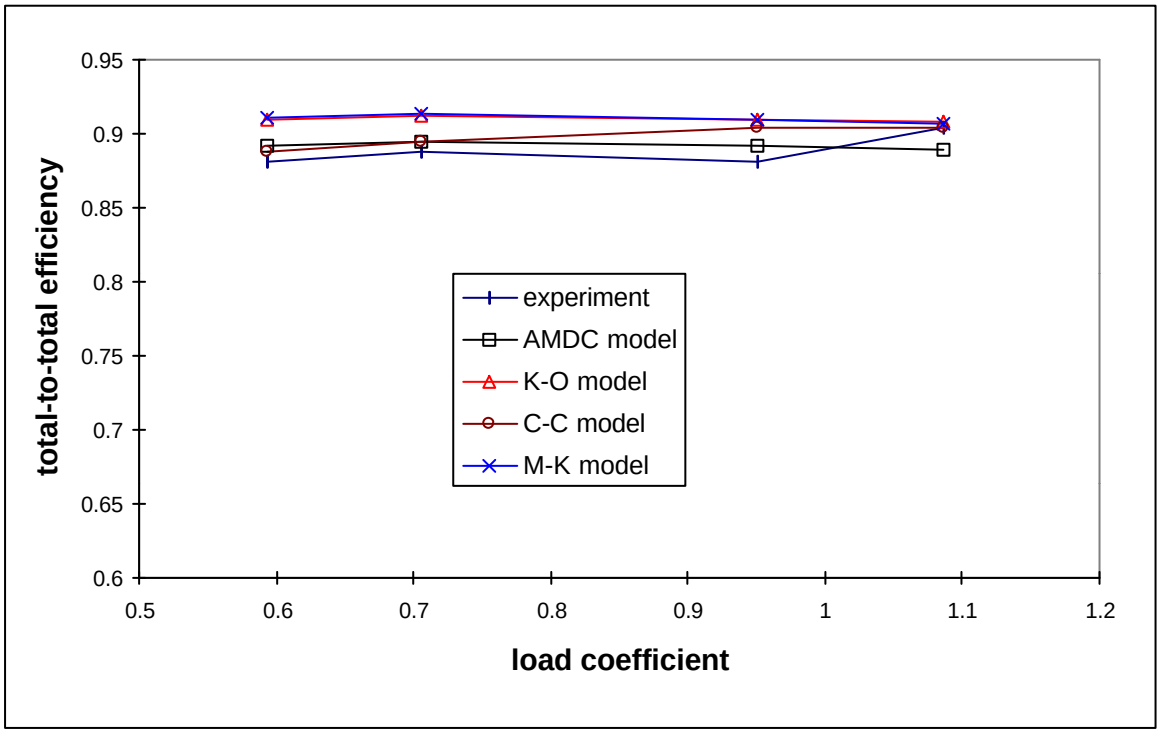

Fig. 4.3.1: *Total-to-total efficiency on turbine stage 3*

Fig. 4.3.1 shows the calculated and experimental results of total-to-total efficiency over the turbine stage 3. It shows that the K-O, M-K and C-C loss models agree well with the experimental results at the design point while the AMDC model gives lower values than those, which indicates that the AMDC model overestimates the losses at this point. When the operating point moves to the off-design region, where the load coefficient is low, all the models seem to underestimate the losses, even the AMDC model. This is because the losses at the hub wall are under-predicted. It has been introduced in chapter 3 that turbine stage 3 was designed as a free vortex stage. In the free vortex turbine, the tangential velocity is prescribed to vary inversely with the radii, and the blading is designed accordingly (see Fig. 3.2.1). This usually results in low degree of reaction and very large tangential velocity and flow turning near the hub, and the blading is highly twisted because both the inlet and exit flow angles as well as stagger angles vary considerably along the radius. Therefore the hub wall losses are likely to be higher in the free vortex turbine blading. The degree of reaction may even become negative. The calculations described in this chapter were performed on mean line which means all flow and geometrical parameters, including the blade angles, were taken at the mean radius. With this mean radius parameters, the losses, especially the losses on off-design points, at the hub wall are underpredicted.

Fig. 4.3.1 shows that the experimental efficiency at the load coefficient 0.95 seems too low. It is doubtful if the measurements error at this point is larger than at other operating points. Along this operation region, the efficiency values predicted in the C-C model decreases with the reduction of the load coefficient, which is the same trend as the experimental results. But the values predicted with the AMDC, K-O and M-K models are almost constant in the whole operation region. The reasons for the different trend of the predicted results in the loss models can be seen from the following analysis of the loss breakdown.

It is of interest to see why the loss models give different trends of performance along the operation region. Because the incidence to the stator row is not changed versus the variation of the operating point, the losses over the stator predicted in every model are constant along the operation region. The key factor which influence the different behaviours of the performance trends of the stage is the distribution of the rotor losses predicted in the various loss models.

There is no measurements on the section between the stator and rotor in this turbine. So the experimental results are insufficient for having loss coefficients for the stator and rotor and it is impossible to make detailed comparison between the experimental and predicted losses in each blade row.

Fig. 4.3.2 shows the losses predicted over the rotor of turbine stage 3 predicted in the AMDC models. It should be aware that all these 4 run cases were operated on the significantly different mass flow. So the Mach number changes much in these cases. Table 4.3.2 shows that the variation of the Mach number among the operation range could be 20%. One can not simply compare the loss distribution predicted in this turbine stage with the corresponding results in the turbine stages 1 and 2 which run in condition of non significant change of Mach number. The profile loss shown in Fig. 4.3.2 slightly increase versus the reduction of the incidence angle. The variation of the profile loss is more smooth than the profile loss predicted in the rotor of turbine stages 1 and 2 in the corresponding incidence angle region. The main reason for this is because the different profile of the blades. Turbine stage 3 is a

stage designed with 50% reaction of degree while turbine stages 1 and 2 are stages with blades close to impulse profile. The losses in an impulse blade, where turning angles are higher, are higher than those of a reaction turbine. Another reason could be the different Mach number for the running cases in turbine stage 3. In turbomachine blade row, profile loss are proportional to Mach number. In the operating range of turbine stage 3, the Mach number decreases toward to the negative direction of the incidence (see Table 4.3.2). Therefore the profile losses on the high negative incidence points increase slowly from the losses on the points near the design position.

Parameters	**Stator**				**Rotor** (relative values)			
Flow coefficient	0.32	0.34	0.40	0.43	0.32	0.32	0.40	0.43
inlet mass flow [m/s]	4.1	4.6	6.5	7.8	4.1	4.6	6.5	7.8
incidence [°]	-5.0	-5.0	-5.0	-5.0	-27.3	-21.8	1.9	8.4
inlet velocity [m/s]	46.1	47.8	55.4	57.9	50.2	50.0	54.7	57.9
outlet velocity [m/s]	119.2	123.8	145.8	153.0	115.1	125.9	141.2	153.3
ratio of inlet to outlet velocity	0.387	0.386	0.380	0.378	0.436	0.397	0.387	0.378
inlet Mach number	0.122	0.126	0.141	0.144	0.134	0.133	0.141	0.146
outlet Mach number	0.317	0.328	0.376	0.386	0.310	0.337	0.368	0.391
ratio of inlet to outlet Mach number	0.385	0.384	0.375	0.373	0.432	0.395	0.383	0.373
Re x 10^5	3.083	3.202	3.765	3.951	2.723	2.979	3.341	3.627

Table 4.3.2: *Some calculated flow parameters of turbine stage 3*

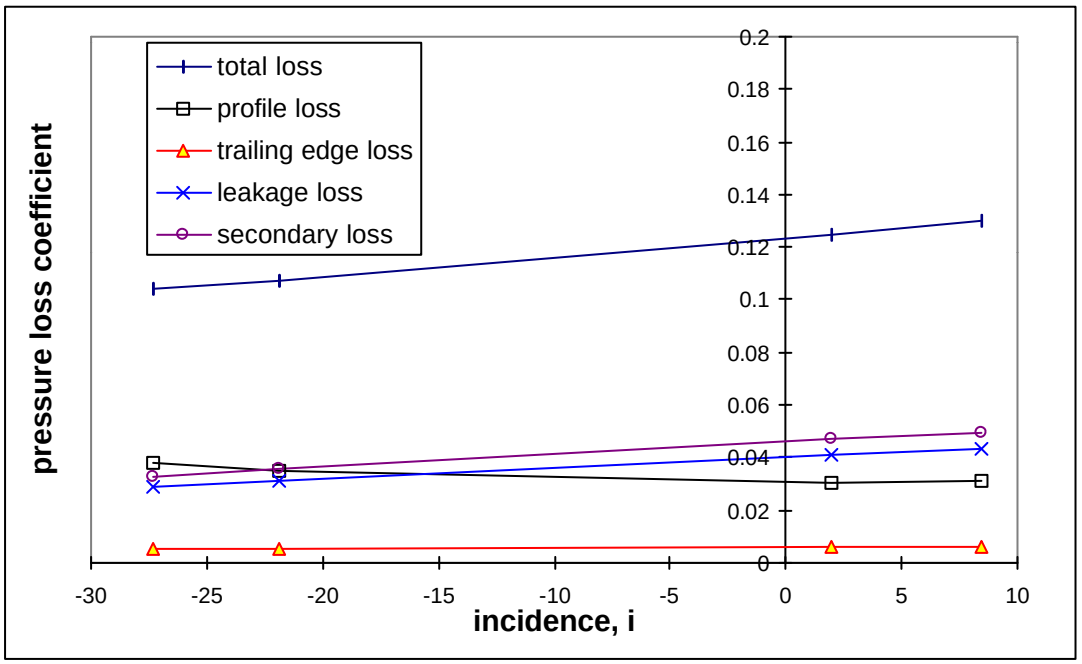

Fig. 4.3.2: *Breakdown of losses in the rotor of turbine stage 3, calculated with the AMDC model*

The secondary and tip leakage losses predicted in the AMDC model shown in Fig. 4.3.2 have upward trend when the incidence angle increases. This is the same trend with the predicted results in turbine stage 1 and 2. All these loss components lead to that the total loss predicted in the AMDC model in Fig. 4.3.2 has the upward trend with the increase of the incidence angle on the whole operation region. At the nominal condition, the level of this loss decrease about 1/3 compared with the corresponding loss in turbine stage 3 shown in Fig. 4.2.4.

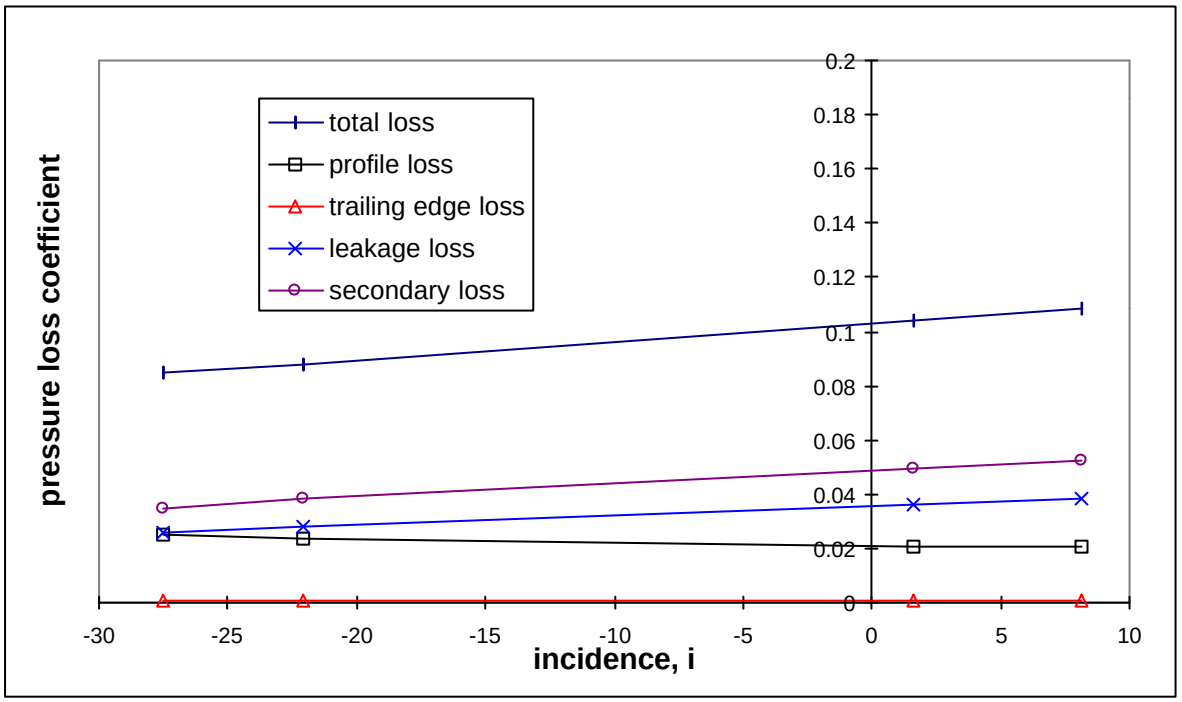

Fig. 4.3.3: *Breakdown of losses in the rotor of turbine stage 3, calculated with the Kacker/Okapuu model*

The losses predicted in the K-O and M-K models over the rotor of turbine stage 3 are shown in Fig. 4.3.3 and 4.3.4 respectively. The losses predicted in these two models have the same trend with the losses predicted in the AMDC model shown in Fig. 4.3.2.

Similar as the results in other turbines, the level of the profile loss predicted in these models are about 1/3 lower than the profile loss in the AMDC model. This leads to the total losses in these models are 1/5 lower than the total loss predicted in the AMDC model. Compared with the corresponding losses predicted in the impulse stage, turbine stage 2, the K-O and M-K models give about 1/3 lower losses on the rotor of this reaction turbine stage in the nominal flow condition.

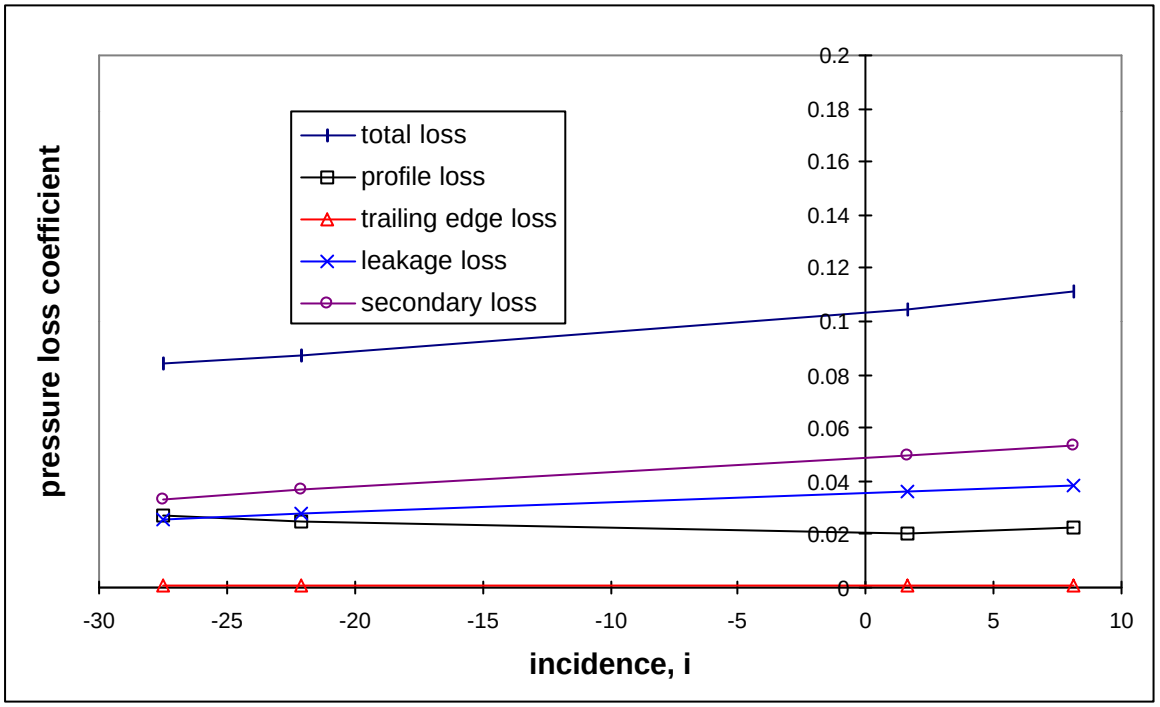

Fig. 4.3.4: *Breakdown of losses in the rotor of turbine stage 3, calculated with the Moustapha/Kacker model*

Fig. 4.3.5 shows the losses predicted in the C-C model over the rotor of turbine stage 3. Like the other models, the C-C model gives a more smooth variation of the profile loss compared with the loss predicted in turbine stage 2. The level of the profile loss predicted in this turbine stage is also lower than the loss predicted in turbine stage 2.

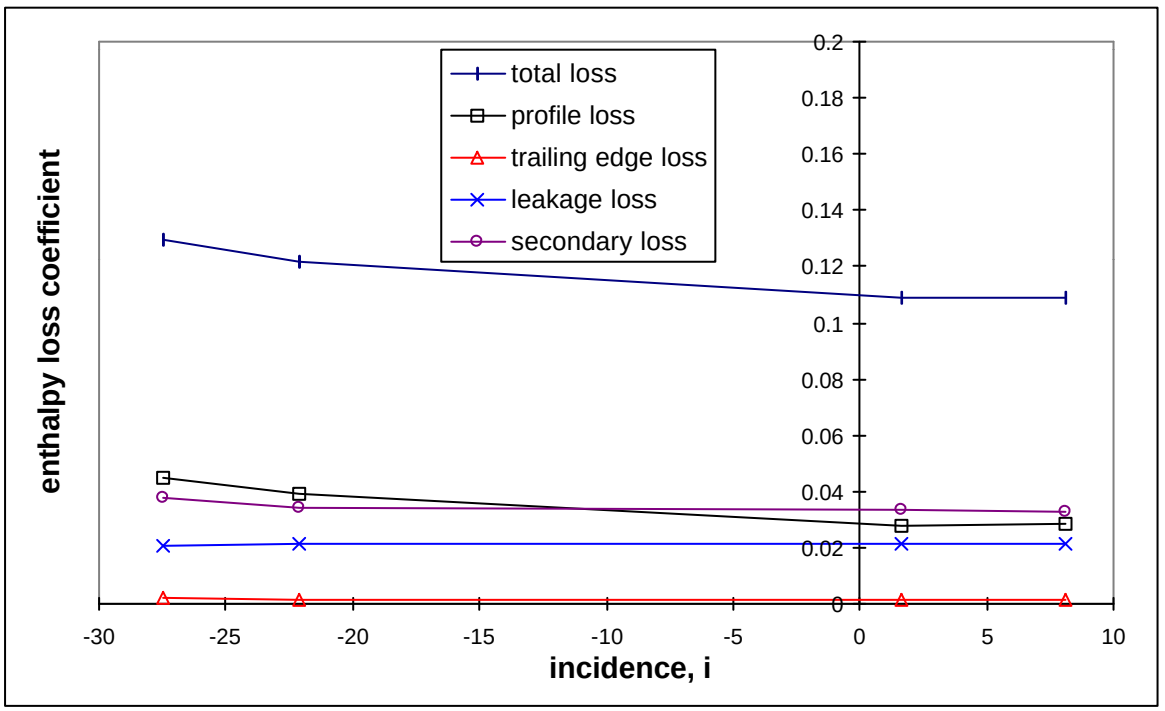

Fig. 4.3.5: *Breakdown of losses in the rotor of turbine stage 3, calculated with the Craig/Cox model*

In Fig. 4.3.5, the secondary loss predicted in the C-C model has a slight downward trend when the incidence angle increases. This trend is completely different from the results predicted with the other models in this turbine stage and the results in the C-C model in

turbine stage 2. This is because in the C-C model, the secondary loss is correlated with not only the blade load and inlet and outlet blade angles but also the ratio of inlet and outlet velocity. In this model, the basic secondary loss increases with the rise of the inlet to outlet flow velocity ratio because the high ratio indicate the relative weak acceleration of the flow though the blade channel and possibly poor boundary layer condition on the endwalls. This will cause the stronger secondary vorticity and higher losses. The running cases for calculation in this turbine stage are operated with reducing the mass flow from the design point to the off-design points. This is a different trend from turbine stage 1 and 2 above, which are run with change of shaft speed while the mass flow does not change significantly. By comparing Table 4.3.2 with Tables 4.1.1 and 4.2.1, it can be seen that the inlet to outlet velocity ratio to the rotor has upward trends with the increase of incidence for turbine stage 1 and 2 but a downward trend with the increases of incidence degree for turbine stage 3. In the operation cases of turbine stage 3 shown in Fig. 4.3.5, the ratio of inlet to outlet velocity is about 1/3 on the design point and ½ on the off-design point where the incidence is -27 degree. This means that the flow has lower acceleration though the rotor blade passage on the off-design points , where the mass flow and load coefficient are low, than the flow on the design point. Therefore the secondary loss is higher resulting from this weak flow acceleration. This factor is not taken into account by the other loss models.

Unlike the other models, the tip leakage loss predicted in the C-C model on the rotor of turbine stage 3 shown in Fig. 4.3.5 does not change very much because it is not correlated with the blade load and angles. This loss has a very slight decrease at the off-design point with negative incidence degree. This is also because the tip leakage loss in the C-C model is a function of the inlet to outlet velocity ratio (see equation 2.6.4). When the ratio is small, the leakage coefficient will be large. This actually implies the static pressure drop over the blade row. The small inlet and outlet velocities ratio means the high acceleration of the flow and large static pressure drop over the blade, which will drive more leakage flow through the clearance area and causes large tip clearance loss. The large inlet and outlet velocities ratio indicate the low acceleration of the flow and small static pressure drop. The mass flow through the leakage will be small therefore the tip leakage is small.

The loss components predicted in the C-C models in Fig. 4.3.5 leads to the total loss over the rotor of turbine stage 3 has a downward trend when the incidence degree increases. This trend is different with the results predicted in the other models. This distribution of the losses results in the same trend of the stage efficiency given by C-C model as the experimental results, which is a different from the results given by the other models shown in Fig. 4.3.1. Compared with the corresponding losses in the impulse stage, turbine stage 2, C-C model gives about ½ lower losses in this reaction turbine stage.

Concluding remarks for the performance prediction in turbine stage 3

In this turbine stage, the AMDC, K-O and M-K models predict about 1/3 lower and C-C model ½ lower total losses than the corresponding losses in the turbine stage 2 which is with impulse blades.

The profile losses over the rotor of this turbine stage predicted in all these models have a more smooth distribution versus the incidence angle compared with the corresponding losses over the rotor of turbine stage 1 and 2 which are the stages with impulse blades in the rotors.

For the free vortex blading like turbine stage 3, the losses are underpredicted in all these models, especially at the off-design operating points, because the high losses at the hub wall caused by the blading of free vortex are underestimated by using the parameters at mean line.

The C-C model gives the same trend of the performance as the experimental results. But the AMDC, K-O and M-K models have different trends. The reason is because the C-C model has a different method to calculate the secondary loss than the other models. In the C-C model, the ratio of the inlet to outlet flow velocity to the blade row is taken into account to calculate the secondary loss and the loss is proportional to the ratio. This ratio physically implies the flow acceleration through the blade and the condition of the boundary layer and secondary vorticity as well as the losses at the endwall. This ratio varies significantly in the running cases for turbine stage 3 and is not considered in the same way in the other loss models.

4.4 Performance Simulation on Turbine Stages 4 and 5

In this section, the performance of turbine stages 4 and 5 are firstly simulated with the loss models of AMDC, Kacker/Okapuu, Moustapha/Kacker and Craig/Cox witch are the conventional models without concerning the losses associated with cooling. Then the performance of turbine stage 4, which is a high temperature and high pressure cooled stage, is investigated with an additional developed film cooling loss method introduced in Chapter 2 (see section 2.14). All these simulations are compared against the reference data.

For turbine stage 4, there are 7 run cases in a range of the mass flow from 47.3 to 6.0 kg/s and the shaft speed from 10428 to 16795 rpm.

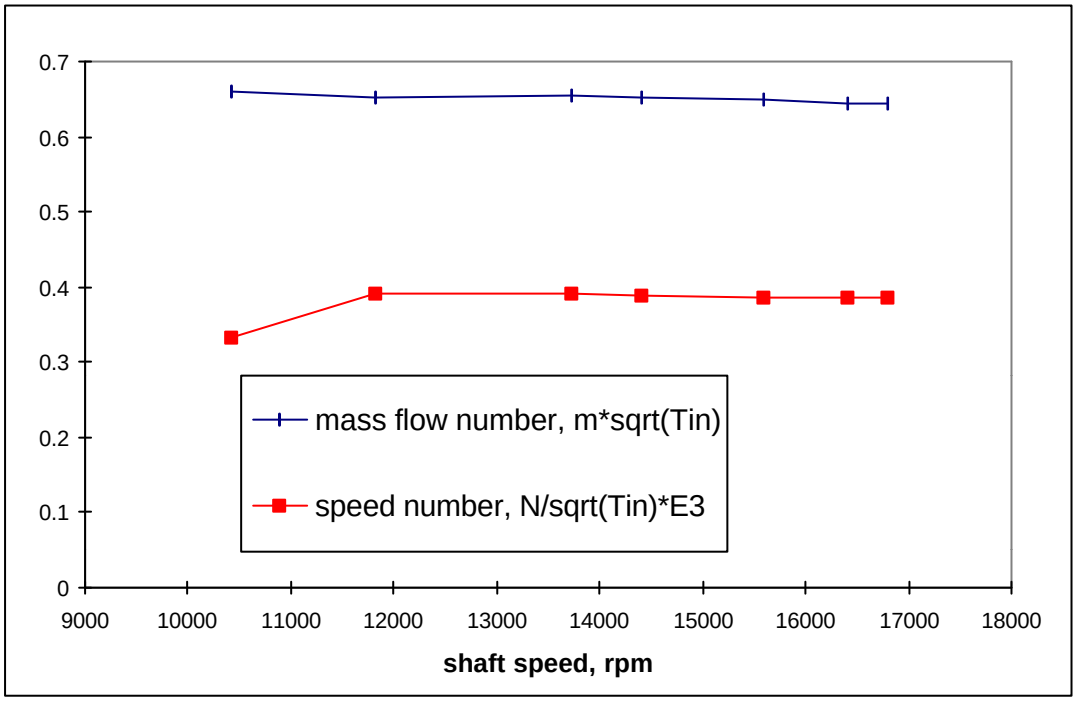

***Fig. 4.4.1**: Working condition of turbine stage 4, reference data*

Fig. 4.4.1 shows the working conditions for the reference data, speed and mass flow numbers, in the operating range of the shaft speed. The speed number, defined as $N/\sqrt{T_{oin}}$ which is multiplied by 10^{-3}, and mass flow number, defined as $\dot{m}\sqrt{T_{oin}}/p_{oin}$, are the parameters commonly used for turbomachinery. $\dot{m}$ is the mass flow and T_{oin} and p_{oin} are the inlet stagnation temperature and pressure respectively. The mass flow number in Fig. 4.4.1 stays constant in the whole operating range while the speed number decrease in the run case which the engine is operated at the lowest mass flow and shaft speed. This implies that the velocity triangles in the stage are similar at the most operating points, except the point with the lowest speed, because of the reduction of both mass flow and shaft speed. At the lowest speed operating point, the velocity triangles is different compared with the other points because the shaft speed drops more rapidly than the mass flow. This leads to the blade speed, u, becomes smaller relatively in the velocity triangle and the flow into the rotor turns to more positive incidence direction.

Turbine stage 4 works in the condition of high temperature and pressure after the combustion chamber. Strong cooling is needed for this stage, especially on the stator blades. The ratio

of cooling flow to the main flow are about 16% for the stator and 9.7% for the rotor. In a cooled turbine, several streams of air are undergoing a similar thermodynamic cycle. The main flow, expanding through a stator and rotor has loss associated with frictional effects, such as the profile, trailing edge, secondary and tip leakage losses described before as well as the loss due to the cooling. The definition of the stage efficiency in such cooled turbine is not as simple as the normal definition of the efficiency shown in Chapter 1, which is for conventional non-cooled turbines. There are several definitions of efficiency in the open literature for cooled turbines. The definition used by Lakshminarayana [1996] is probably the most appropriate for a modern turbine. This efficiency is defined as followings:

$$h_{tt} = \frac{\dot{m}_p (\Delta h_o)_p + \sum_j \dot{m}_j (\Delta h_o)_j - (\Delta h_o)_{cp}}{\dot{m}_p (\Delta h_o)_{ip} + \sum_j \dot{m}_j (\Delta h_o)_{ji}} \qquad \text{(eq. 4.4.1)}$$

where $\dot{m}_p$ is the primary air of the mainstream flow, $\dot{m}_j$ is the mass flow of the jth cooling stream, $(\Delta h_o)p$ is the actual enthalpy drop of the primary air, and $(\Delta h_o)_j$ is the actual enthalpy drop of the jth cooling stream. $(\Delta h_o)_{cp}$ is the power required to pump the coolant. This is the work done to accelerate the tangential velocity of the rotor coolant at the rotor entry to the blade mean line velocity. The denominator represents the ideal power developed by the primary air $(\Delta h_o)_{ip}$ and the secondary air $(\Delta h_o)_{ji}$, respectively.

To calculate the efficiency with equation 4.4.1, the details of the coolant must be known. As a preliminary analysis of the cooled turbine, industries used to apply a more simple definition of the efficiency. This efficiency is defined as [Lundbladh, 1998]:

$$h_{tt} = \frac{(1 - \frac{T_{c3}}{T_{c2}})}{(1 - \frac{p_{c3}}{p_{c2}})^{\frac{g-1}{g}}} \qquad \text{(eq. 4.4.2)}$$

where T_{c2} and p_{c2} are the stagnation temperature and pressure between the stator and rotor and T_{c3} and p_{c3} are the stagnation temperature and pressure after the rotor. Unlike the normal efficiency definition for the non-cooled turbines, the stage inlet stagnation temperature and pressure are replaced by the rotor inlet stagnation temperature and pressure, T_{c3} and p_{c3}, in equation 4.4.2. From principles of thermodynamics, with using equation 4.4.2, it is simplified that the constant mass flow expand through the stator and then cooled after the stator and that the cooling in the rotor is neglected. It is must be assuming, with this equation, that the heat exchange process between the coolant and main flow in the stator is performed in a constant pressure and the heat is

$$q \cong c_p (T_{c1} - T_{c2}) \qquad \text{(eq. 4.4.3)}$$

where T_{c1} is the stagnation temperature at inlet of the stator. This heat must be not considered as a part of work output from the turbine stage. This is why T_{c2} is taken in equation 4.4.2 instead of T_{c1}. It is argued that the equation seems more reasonable if p_{c1} is used instead of p_{c2}. However there would be not significant influence on comparing the

predicted performance against reference data if both of these from the same definition of equation 4.4.2.

The calculation on turbine stage 5, a low pressure turbine stage after stage 4, was performed and compared against the reference data. The run cases are corresponding to the cases used in the calculation of turbine stage 4, total 7 run cases with the range of the mass flow from 51.9 to 6.6 kg/s and the shaft speed from 12714 to 3900 rpm. Unlike turbine stage 4, the inlet flow to turbine stage 5 is not always in the axial direction. The input of the inlet flow to turbine stage 5 was taken from the predicted results at the outlet of turbine stage 4.

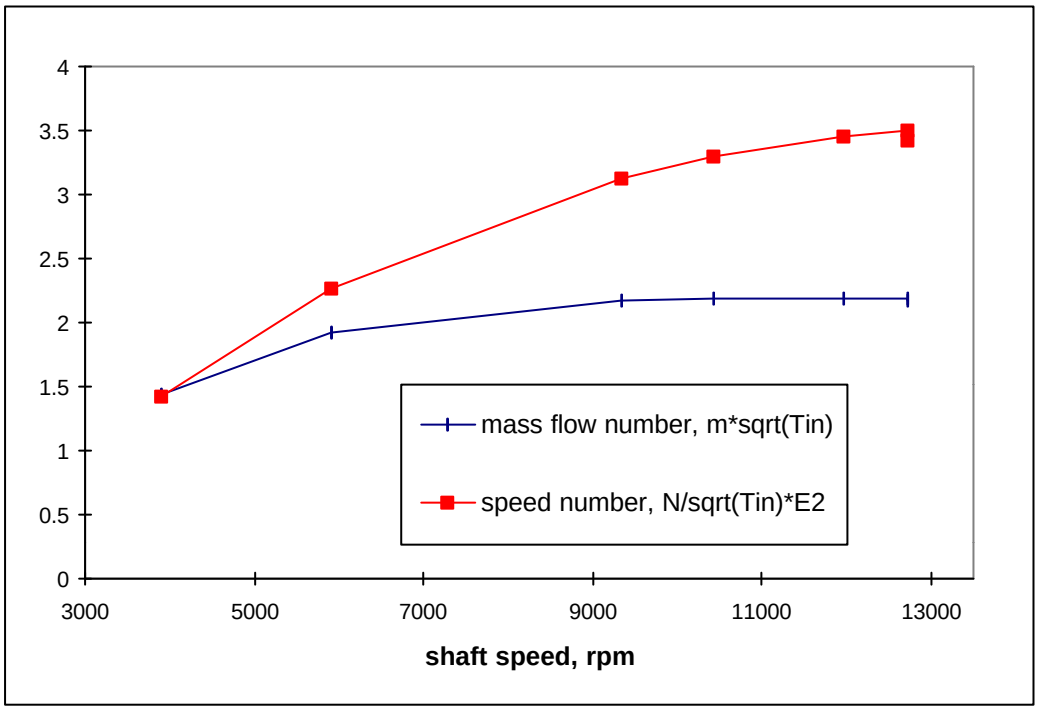

***Fig. 4.4.2**: Working condition of turbine stage 5, reference data*

Fig. 4.4.2 shows the reference working conditions, speed and mass flow numbers, on the operating range of shaft speed. The speed number and mass flow number are the same definitions used in turbine stage 4 in Fig. 4.4.1. There is no cooling for turbine stage 5. The efficiency in this turbine is calculated as the same definition in Chapter 1.

4.4.1 Performance Without Cooling Loss Prediction

Fig. 4.4.1.1 shows the predicted results and reference data of the total-to-total stage efficiency. Both predicted results and reference data are based on the definition of efficiency calculated in equation 4.4.2.

It can be seen from Fig. 4.4.1.1 that the trends of the stage efficiency given by all these models are similar to the trend of reference data. The trends of the predicted values agree well to the reference data from 13700 to 16800 rpm in the operating range. At the points the speed smaller than 11800 rpm, the reference data reduces more rapidly than the predicted values. The reason for this will be explained together with looking of the results of pressure ratio later. All these models underestimate the losses therefore the values of predicted

efficiency in Fig. 4.4.1.1 are higher than the reference data. The AMDC model gives 2-5% units, the C-C model 1-3% units and K-O and M-O models about 5-8% units higher than the reference data. It seems that the results from the AMDC and C-C models are closer to the reference data than others. However it should be noted that all these models are created for predicting the losses in non-cooled turbines and there is no method for calculating the cooling loss in any of these models. So one can not say that the AMDC and C-C models predict the performance more reasonably. The performance with concerning cooling loss will be calculated and discussed in the next section.

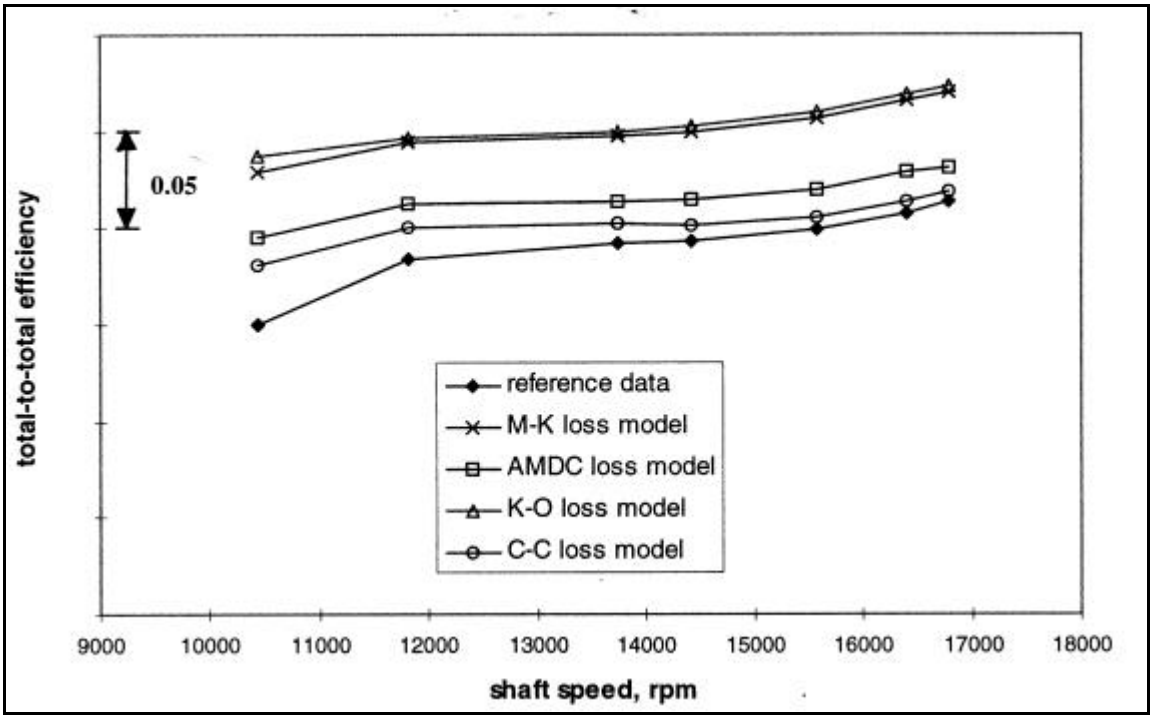

***Fig. 4.4.1.1**: Reference and predicted data of total-to-total efficiency on turbine stage 4*

The predicted results and reference data for the stagnation pressure ratio over the turbine stage 4 are shown in Fig. 4.4.1.2. Trends of the pressure ratio predicted in all these models are the same as the trend of the reference data. The reference data of pressure ratio is closer to the results predicted in the AMDC and C-C models than to the results in the K-O and M-K models. This is corresponding to the results of stage efficiency shown in Fig. 4.4.1.1.

It can be seen from Fig. 4.4.1.2 that the predicted pressure ratio are closer to the reference data at the points of low speed than at the high speed. This seems a contrary trend to the results of efficiency shown in Fig. 4.4.1.1 in which the agreement between the predicted and reference values is poorer at operating points with low speed than at those with high speed. This is because the efficiency was calculated from the parameters including the predicted stagnation pressure ratio and the efficiency is more sensitively affected by calculated errors at the low pressure ratio than the high pressure ratio points. This can be proved as followings.

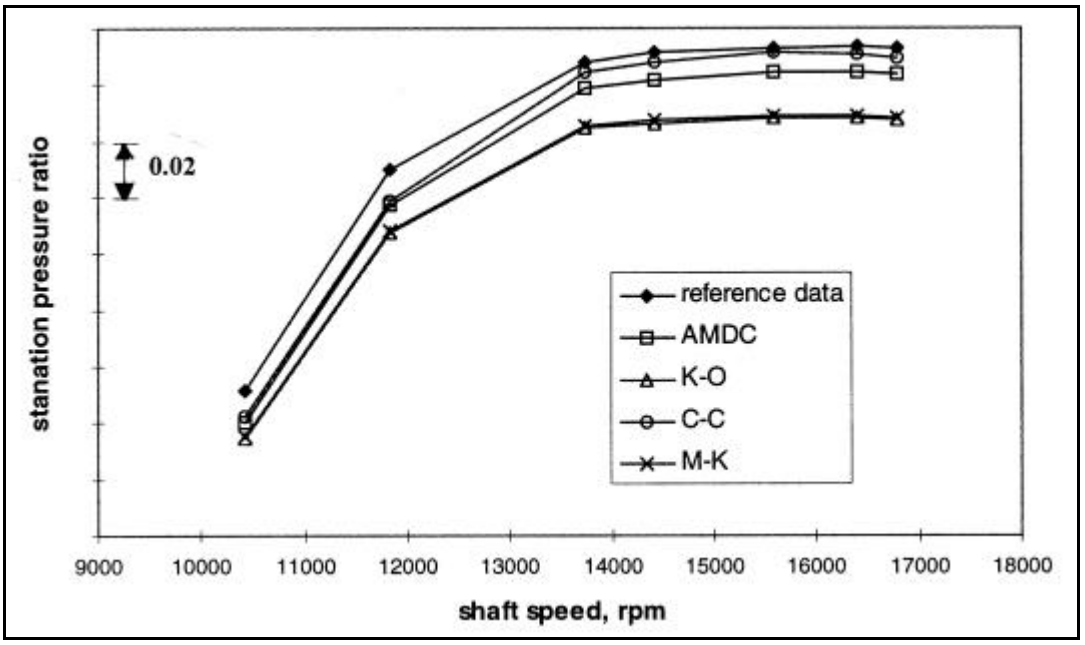

Fig. 4. 4.1.2: *Reference and predicted stagnation pressure ratio over turbine stage 4*

In equation 4.4.2, if assuming the pressure ratio PR=p_{o2}/p_{o3} and the efficiency is just a function of PR, by making derivative of the efficiency with respect to PR, we get

$$\frac{dh_{tt}}{h_{tt}} = \frac{g-1}{g}\frac{1}{(PR)^{\frac{1-g}{g}}-1}\frac{d(PR)}{PR}, \qquad PR>1 \qquad \text{(eq.4.4.1.1)}$$

Approximately, $$\frac{\Delta h_{tt}}{h_{tt}} = \frac{g-1}{g}\frac{1}{(PR)^{\frac{1-g}{g}}-1}\frac{\Delta(PR)}{PR}, \qquad PR>1 \qquad \text{(eq. 4.4.1.2)}$$

It is obvious from equation 4.4.1.2 that the same relative error of pressure ratio, Δ(PR)/PR, will give larger relative error of the efficiency, $\Delta\eta_{tt}/\eta_{tt}$, when the pressure ratio PR is smaller.

It is found that the efficiency was affected significantly by the variation of the ratio of specific heats, γ. In principle, the ratio of specific heat varies with the temperature and composition of the working medium. In gas turbines, this ratio can be considered as a function of the temperature and fuel/air ratio FA:

γ=f(T, FA) (eq.4.4.1.3)

In the earlier predictions in the test turbines, the working medium is air and the ratio of specific heats was chosen to be varied slightly with the variation of temperature in the different run cases. However the running cases used in this turbine stage are the simulation of the engine which is operated in different real working conditions that are corresponding to the fly situation of the aircraft. Both temperature and fuel/air ratio vary significantly among these running cases. Fig. 4.4.1.3 shows the variation of the fuel/air ratio in the operation region of turbine stage 4.

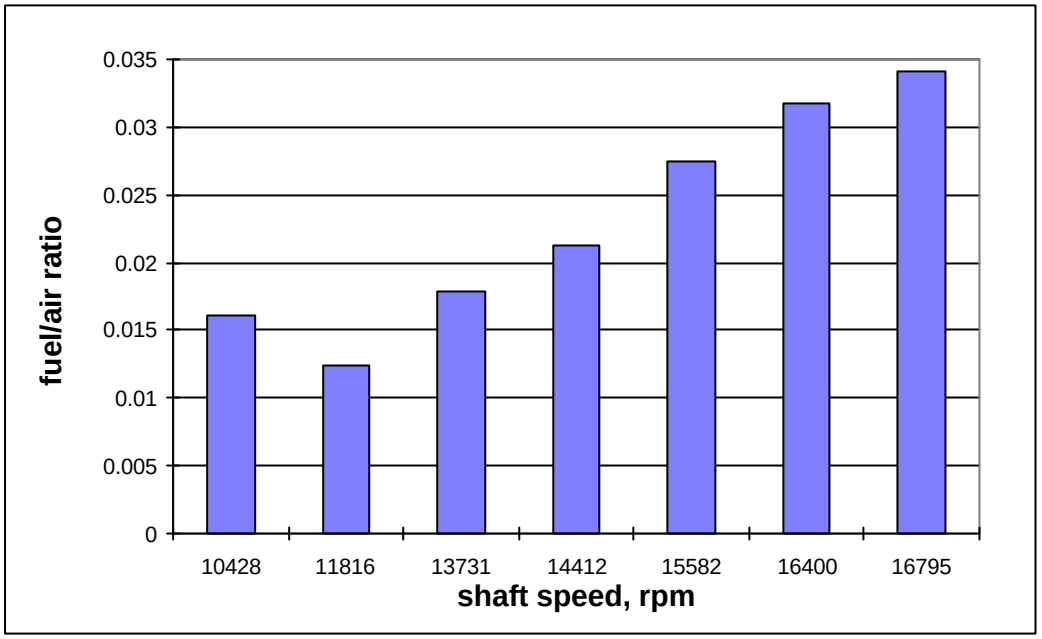

Fig. 4.4.1.3: *Variation of fuel/air ratio in the operation of turbine stage4*

It can be seen from Fig. 4.4.1.3 that the variation of the fuel/air ratio is large in the operation region. For example, from the case1 to case 6, the ratio changes about 47%.

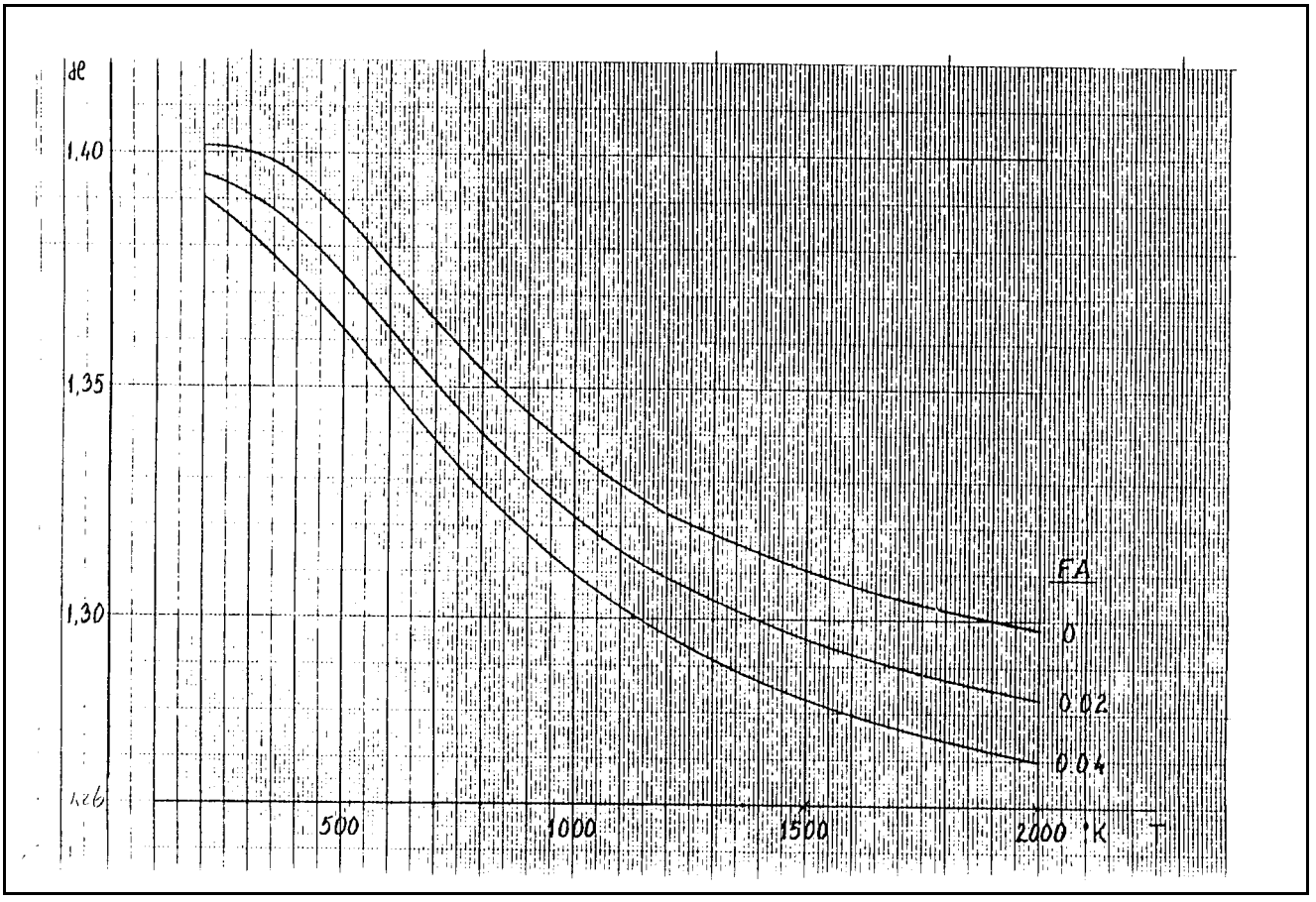

Fig. 4.4.1.4*: Relationship between the ratio of specific heats and temperature and fuel/air ratio*

The figure in Fig. 4.4.1.4 shows curves on which the ratio of specific heats varies versus both the temperature and fuel/air ratio. In this figure, κ is the ratio of specific heats. This figure

covers the variation range of fuel/air ratio and temperature, where turbine stage 4 is operated. Both reference and predicted stage efficiencies shown in Fig. 4.4.1.1 are based on this relationship between κ and T and FA. In the prediction, the reference temperature for determining the ratio of specific heats was chosen as the temperature between the stator and rotor. From this figure, it can be seen that ratio of specific heats varies more against the fuel/air ratio when the temperature is high. This implies that influence on the stage performance from the variation of the ratio of specific heats is stronger in the high temperature turbines.

A test calculation was made to see how much the variation of the ratio of specific heats affects on the stage efficiency. The results of this test calculation is shown in Fig. 4.4.1.5.

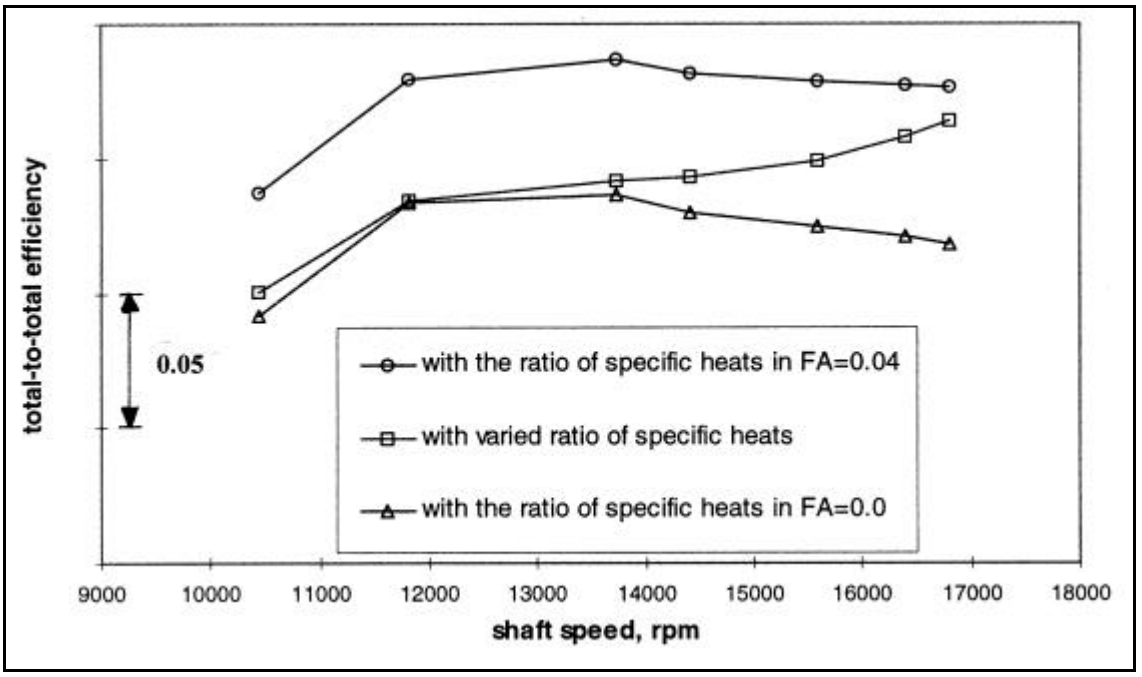

Fig. 4.4.1.5: *Comparison of the reference data of stage efficiencies determined with different ratio of specific heats on turbine stage 4*

The efficiency was calculated with the equation 4.4.2. The parameters of temperatures and pressures used for calculation are taken from the reference data. For every run case, these parameters are identical as calculating with different specific heat ratio. As showing in Fig. 4.4.1.5, the circles and triangles represent the efficiencies determined with the ratios of specific heats when the fuel/air ratio is a constant of 0.04 and 0.0 respectively and the squares are the reference data of efficiencies as same as the one shown in Fig. 4.4.1.1, which are determined with the ratio of specific heats as the variation of fuel/air ratio. It is shown that the difference of the efficiency between the ratio of specific heats considered as constant fuel/air ratio 0.04 and 0.00 respectively can be 6% units higher although the same pressures and temperatures are used and that the results with the constant fuel/air ratio have complete different trends in comparing with the results with the true variation of fuel/air ratio. From this analysis, it can be noted that the variation of the ratio of specific heats due to not only the change of the temperature but also the change of the fuel/air ratio must be considered in the performance prediction on high temperature turbines with large variation of fuel consumption.

It is also of interest to see if the variation of the ratio of specific heats due to the change of the fuel/air/ ratio can give any influence on the loss coefficient when these loss models are used to predict the performance in this turbine stage. The loss calculations with varied ratio of specific heats due to the change of the fuel/air ratio in every model were performed. Fig. 4.4.1.6-9 show some examples of the rotor loss calculation with the varied ratio of specific heats due to the change of fuel/air ratio.

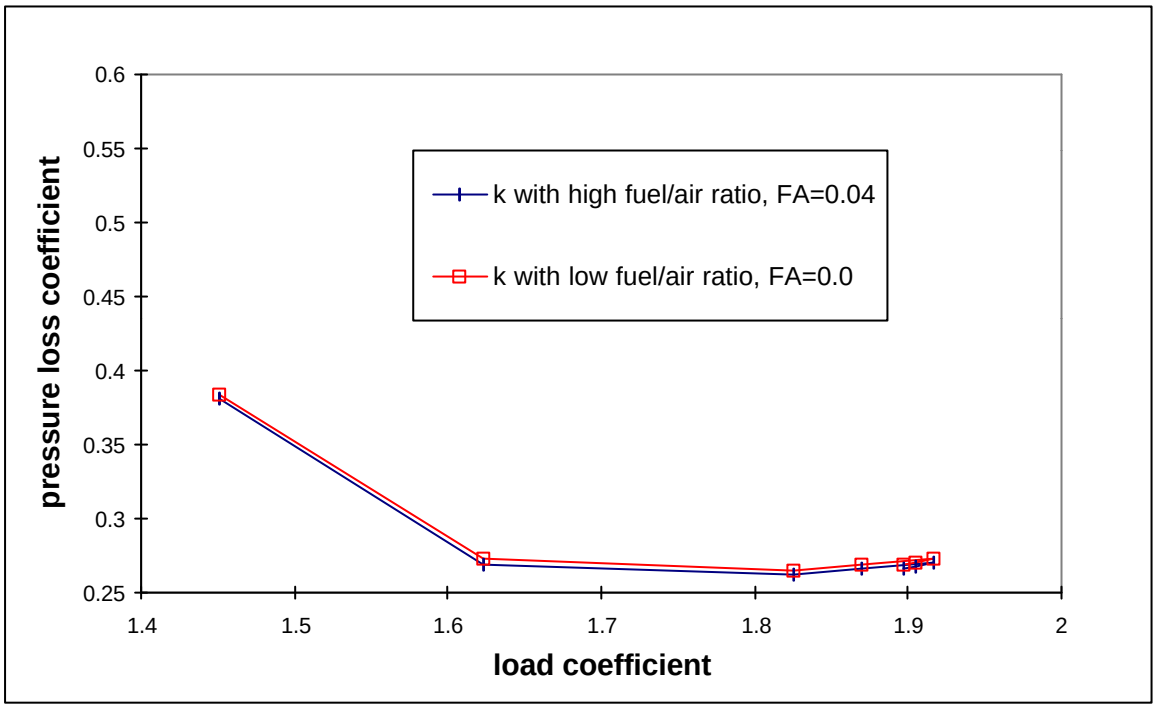

Fig. 4.4.1.6: *Comparison of the rotor loss coefficient predicted in the AMDC model with different ratio of specific heats due to the change of fuel/air ratio on turbine stage 4*

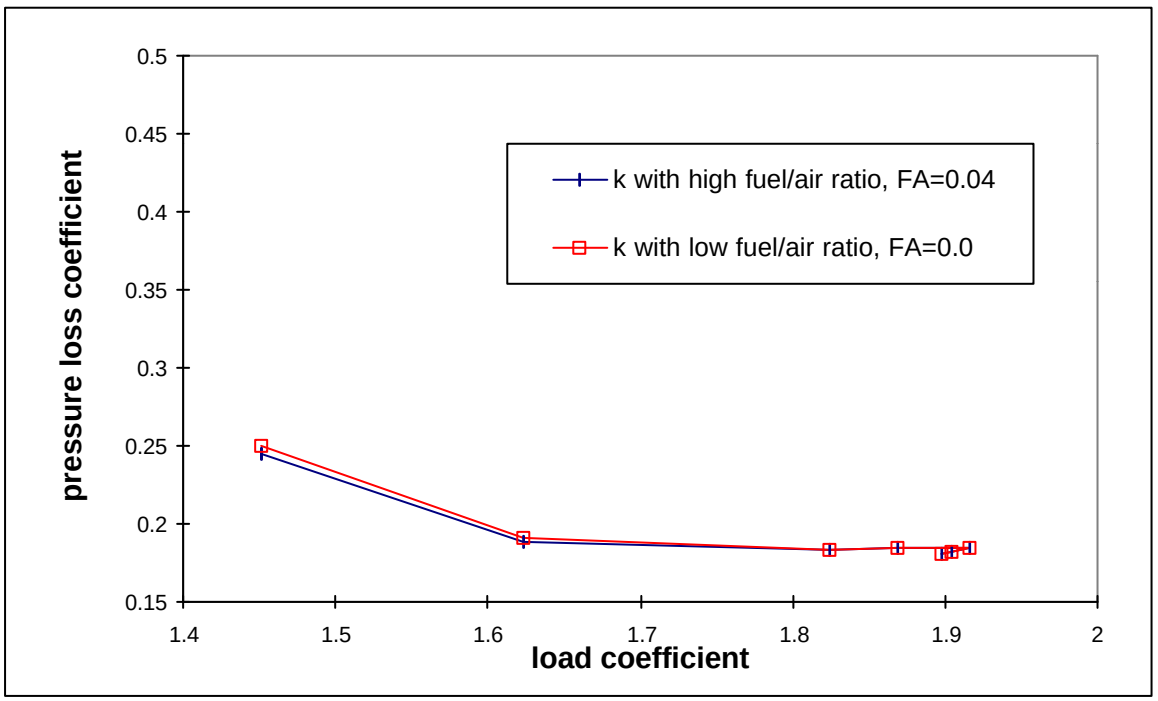

Fig. 4.4.1.7: *Comparison of the rotor loss coefficient predicted in the Kacker/Okapuu model with different ratio of specific heats due to the change of fuel/air ratio on turbine stage 4*

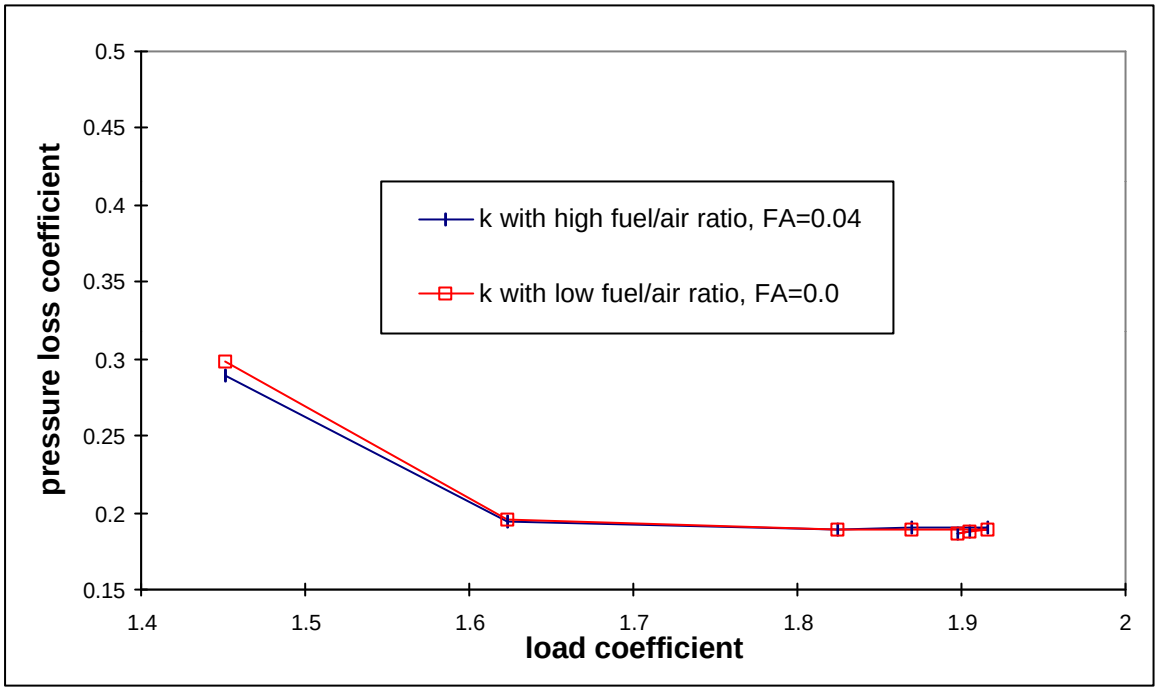

Fig. 4.4.1.8: *Comparison of the rotor loss coefficient predicted in the Moustapha/Kacker model with different ratio of specific heats due to the change of fuel/air ratio on turbine stage 4*

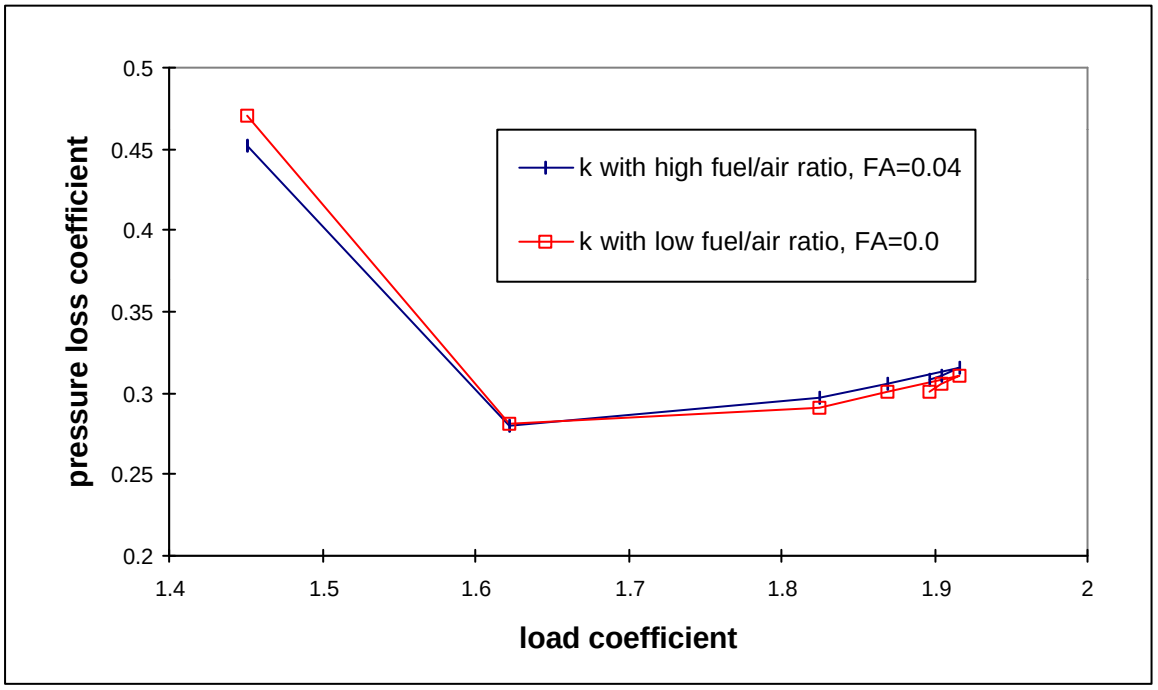

Fig. 4.4.1.9: *Comparison of the rotor loss coefficient predicted in the Craig/Cox model with different ratio of specific heats due to the change of fuel/air ratio on turbine stage 4*

The loss coefficients predicted in the AMDC and K-O models, shown in Fig. 4.4.1.6 and 4.4.1.7 respectively, have very small changes when different ratios of specific heats due to variation of fuel/air ratio are used. There are slight changes in the loss coefficients predicted in the M-K and C-C models, shown in Fig. 4.4.1.8 and 4.4.1.9 respectively, especially in the high off-design operating point with low load coefficient.

The ratio of specific heats does not directly affect on the loss coefficient because this parameter is not taken account into the formulas for calculating losses in the loss models employed in these applications. This can be seen from looking at the details of the equations for calculating losses in these models described in chapter 2. However, in some loss models, inlet or outlet parameters, such as pressures, velocities as well as Mach numbers, are needed for correlating losses. Because these parameters would be affected by the ratio of specific heats, it will give a certain indirect influences on the calculation of loss coefficient. This indirect influence on the loss calculation seems not very significant but much depending on the structure of the loss calculation in each individual model.

Fig. 4.4.1.10 shows the predicted and reference data of total-to-total efficiency on turbine stage 5 which is the low pressure and uncooled turbine stage. The total-to-total efficiency is defined as the same as one introduced in Chapter 1.

It can be seen from the figure that the efficiencies predicted from all these models have the same trend as the reference data. The predicted values agree well with the reference data on the high load and high pressure ratio operations which are close to the design points. In comparing with results in turbine stage 4 shown in Fig. 4.4.1.1, the efficiency predicted in this stage is much closer to the reference data because there is not much cooling losses in this stage. The gaps between the predicted results and reference data become bigger as the operating point moves toward to the low load, low pressure ratio and off-design direction. This is mainly because the efficiency is more sensitively affected by calculated errors at the low pressure ratio, which has been discussed earlier .

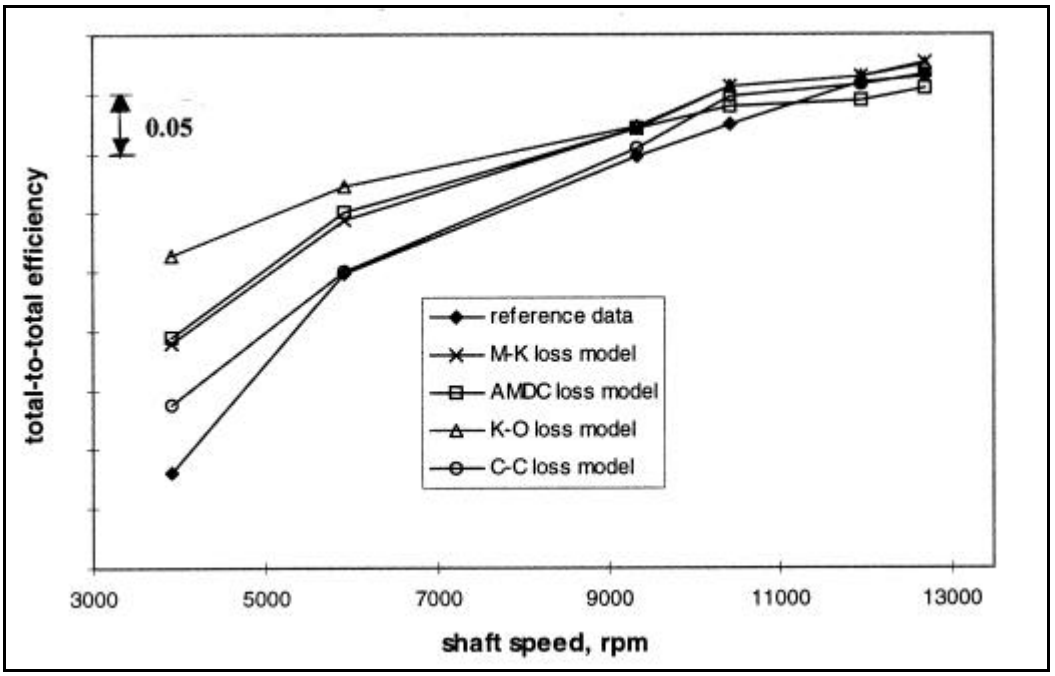

***Fig. 4.4.1.10**: Reference data and predicted results of total-to-total efficiency on turbine stage 5*

The predicted results and reference data of the stagnation pressure ratio over turbine stage 5 are shown in Fig. 4.4.1.11. The pressure ratios predicted in all these models agree very well with the reference data in all operating points.

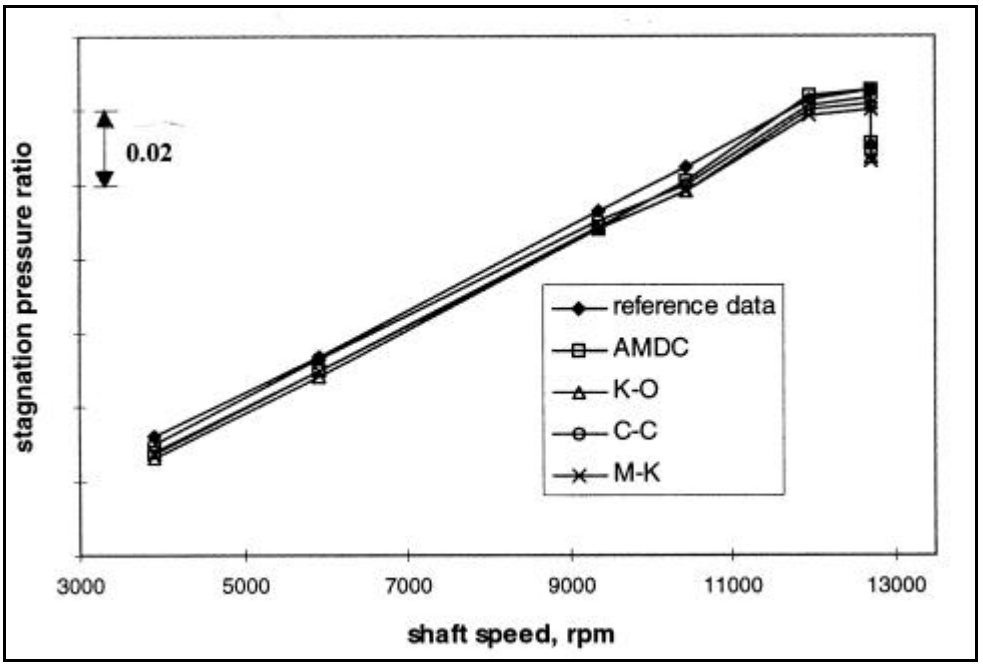

Fig. 4. 4.1.11: *Stagnation pressure ratio over turbine stage 5*

Because there have been insufficient experimental results for determining loss coefficients for the stator and rotor, it is impossible to make detailed comparison between the experimental and predicted losses in each blade row for turbine stages 4 and 5.

Concluding remarks

The loss models predict the performance of turbine stages 4 and 5 with the same trend as the reference data. The agreement between the trend of predicted and reference data of the efficiency are poor in the run cases with low pressure ratio because the efficiency is more sensitively affected by calculated errors at the low pressure ratio than the high pressure ratio points.

All models predict higher efficiency than the reference data in cooled stage turbine stage 4 because the lack of cooling loss calculation in the models. The AMDC and Craig/Cox models seem to give close results to the reference data because of the fortuity of overestimated non-cooled turbine losses.

The variation of specific heat with both temperature and fuel/air ratio affects very much on the calculation of stage efficiency on the high temperature and heavy cooled turbine stage although it does not give a significantly direct influence on the calculation of the loss coefficient in the models.

4.4.2 Performance With Additional Cooling Loss Prediction on Turbine Stage 4

Turbine stage 4 is a high temperature and high pressure stage with heavy cooling. The cooling technique employed in this stage is mainly film cooling method as described before. The cooling air, taken from the exit of the high pressure compressor stage before the burner,

is injected into the main flow through small holes on the blade surfaces and on the endwalls [Johansson,1999]. A thin layer of the cool air is formed and it insulates the blade from the hot gas stream. The ratios of the coolant air to the inlet main flow are 16% and 9% for the stator and rotor respectively. In the previous section, the performance results predicted with the loss models showed that the loss models give higher efficiency than the reference data in turbine stage 4. This is because the models, such as AMDC, K-O C-C and M-K loss models, employed in this application do not consist of cooling loss calculation. According to the literature by Lakshminarayana [1996, p. 694-700], 16% cooling mass flow ratio can cause 5% decrease of efficiency in the term of film cooling turbine stage.

In this section, an effort is made to supplement cooling losses to performance of turbine stage 4. The development film cooling prediction method introduced in Chapter 2 (see section 2.14) is used in this application. Entropy creations due to the film cooling losses in the stator, $\Delta s_{fc,N}$ and rotor, $\Delta s_{fc,R}$, of the stage were calculated with equation 2.14.12 respectively. Then the diminution of the stage efficiency associated with the film cooling losses is calculated with

$$\Delta h_{tt} = \frac{T_{c2}(\Delta s_{fc,N} + \Delta s_{fc,R})}{c_p \Delta T_{cis}} \qquad \text{(eq. 4.4.2.1)}$$

where ΔT_{cis} is the isentropic stagnation temperature drop over the stage.

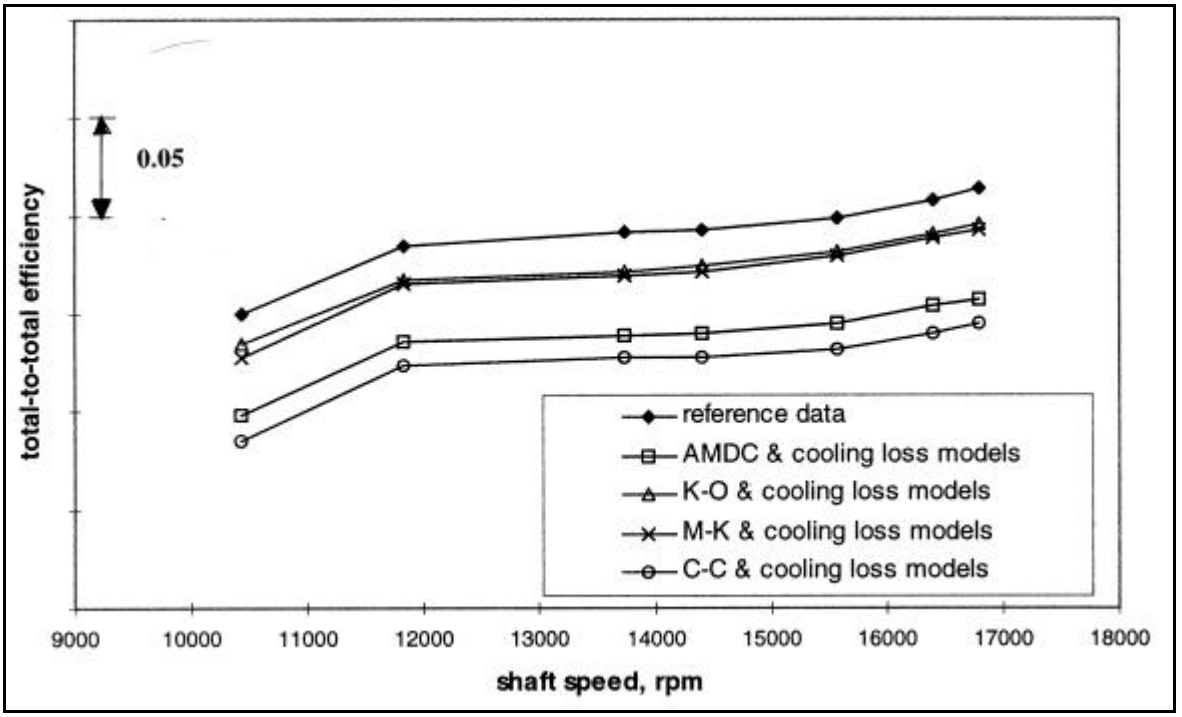

Fig. 4.4.2.1: *Comparison of performances of turbine stage 4 between reference and predicted data with cooling losses*

Fig. 4.4.2.1 shows the new results of the turbine stage 4 stage efficiency predicted by adding the film cooling model to the AMDC, M-K, K-O and C-C models. By comparing this with the results without concerning the cooling losses in Fig. 4.4.1.1, It can be found that, after adding the cooling loss prediction, the trends of simulated performances with the models have better agreement with the trend of reference data in the operating range although the models seem

overestimate the losses. The AMDC or C-C models with cooling loss prediction give about 5.5-6.5% units lower efficiency than the reference data because the AMDC and C-C models overestimate the non-cooled losses as shown in Fig. 4.4.1.1. The results predicted with the K-O or M-K model with the cooling loss prediction is about 2-2.5% units lower than the reference data in Fig. 4.4.2.1, which has better agreement with the reference data than the results without concerning the cooling losses as shown in Fig. 4.4.1.1.

It seems that the model given by author for predicting overall film cooling losses in equation 2.14.12 overestimates the losses. This is perhaps because following reasons.

- The model is derived from an assumption that the coolant is mixed well with the main flow in a small control volume (see section 2.14). But in fact it is difficult for the two flows to mix very well in the blade channel.
- The model, equation 2.14.12, is based on the assumption of continuous and uniform coolant injected into the blade row. In practise, the coolant might be added more near the leading edge than the trailing edge because, in principle, cooling is more needed near the leading edge, where gas has lower velocity and higher temperature compared with the downstream. The cooling losses are low when the mach number and velocity are low.
- In cooled turbine blades, there used to be an amount of coolant which ejects to the downstream of the blade row through the trailing edge where the base pressure must be changed by this ejected coolant. In fact, coolant ejection through the trailing edge can increase the base pressure and so be beneficial, which is not considered in this model. An investigation of the cooling ejection at the trailing edge was given by Denton and Xu [1989].

A precise prediction of film cooling losses can only be made by calculating the losses locally, for example by using equation 2.14.3-7 or 2.14.8 after knowing the details of the information of coolant and the flow parameters at each cooling hole in blade rows.

In equation 2.14.12, the parameters are used for calculating the entropy creation caused by the film cooling are Mach number, main flow velocity, coolant velocity, angle between the main flow and coolant and the mass flow ratio of overall coolant to main flow. It is of interest to investigate the influences from these parameters on the film cooling losses. Fig. 4.4.2.2-6 show the results of the diminution of the stage efficiency affected by the variation of such parameters. This investigation is based on the film cooling calculation in the stator row of turbine stage 4, at the run case with 16795 rpm, by changing one of these parameters, in the range of +/-60%, and keeping the others as constants.

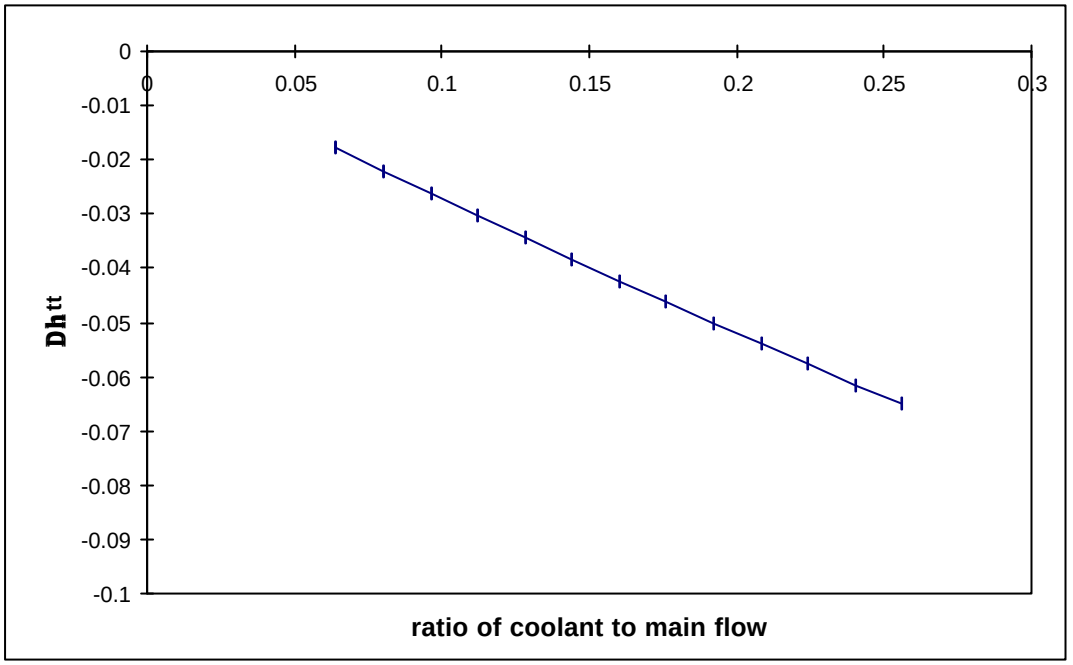

Fig. 4.4.2.2: *Test calculation results of the stage efficiency diminution, due to cooling loss in the stator, versus varied ratio of coolant to main flow*

Fig. 4.4.2.2 shows the change of diminution of the stage efficiency on turbine stage 4 with the variation of coolant to main flow ratio. It can be seen that when the flow ratio change from 0.06 to 0.26, the diminution of the efficiency varies from 1.7% to 6%.

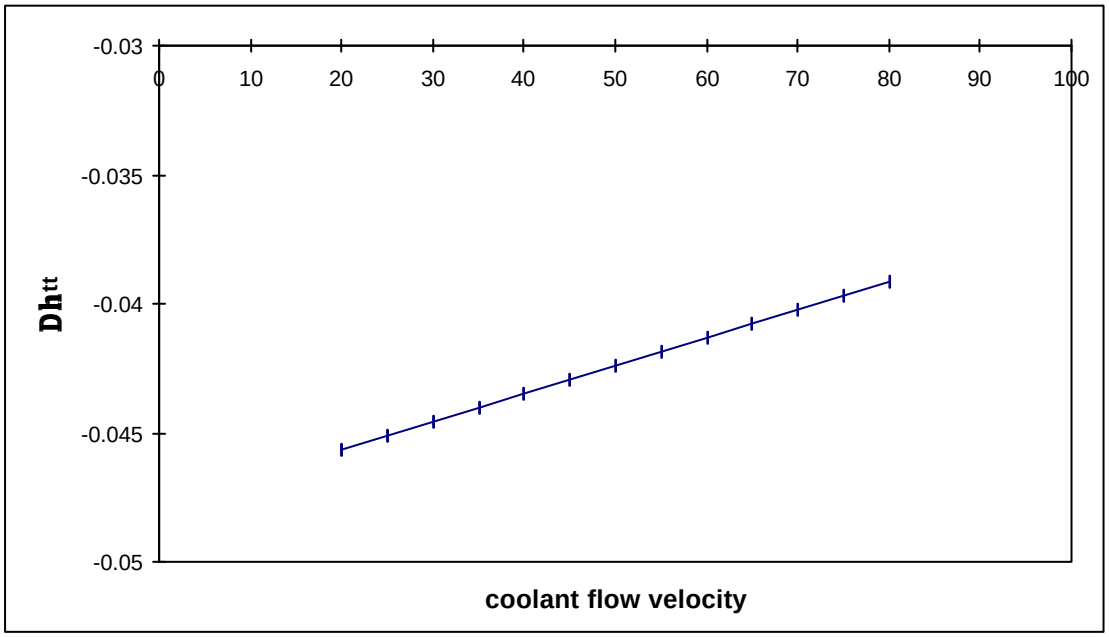

Fig. 4.4.2.3: *Test calculation results of the stage efficiency diminution, due to cooling loss in the stator, versus variation of coolant flow velocity*

From Fig. 4.4.2.3, it can be seen that when the coolant flow velocity changes from 20 to 80 m/s, the diminution of the efficiency varies from 4.5% to 3.9%.

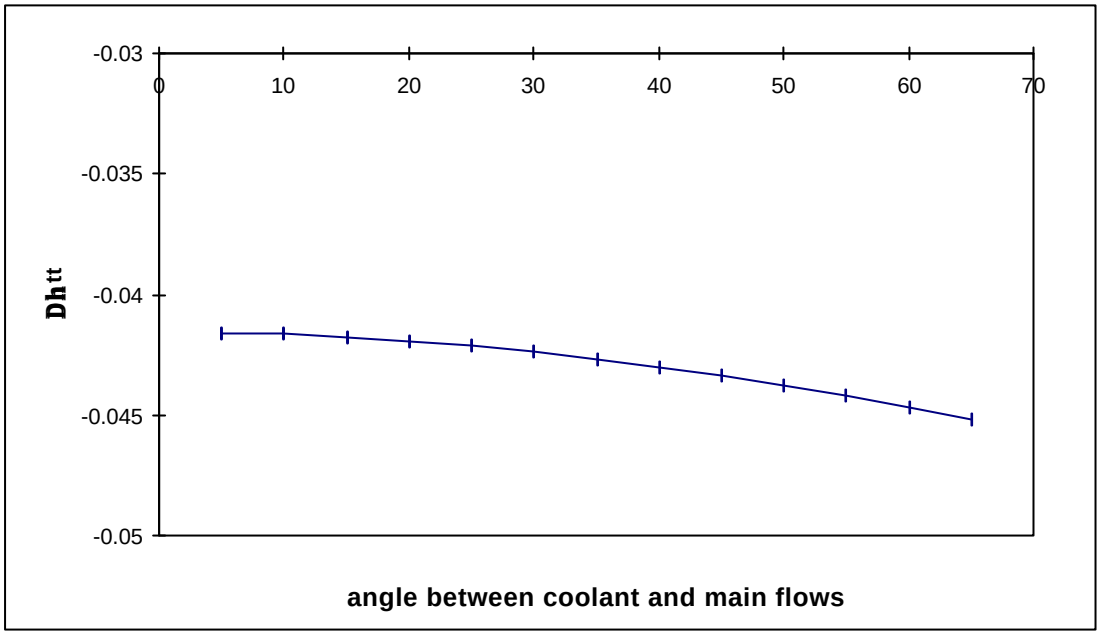

Fig. 4.4.2.4: *Test calculation results of the stage efficiency diminution, due to cooling loss in the stator, versus variation of angle between coolant and main flows*

Fig. 4.4.2.4 shows the variation of diminution of the stage efficiency on stage 4 with the change of the angle between coolant and main flows. It can be seen that when the angle ratio changes from 5^o to 65^o, the diminution of the efficiency varies from 4.1% to 4.5%.

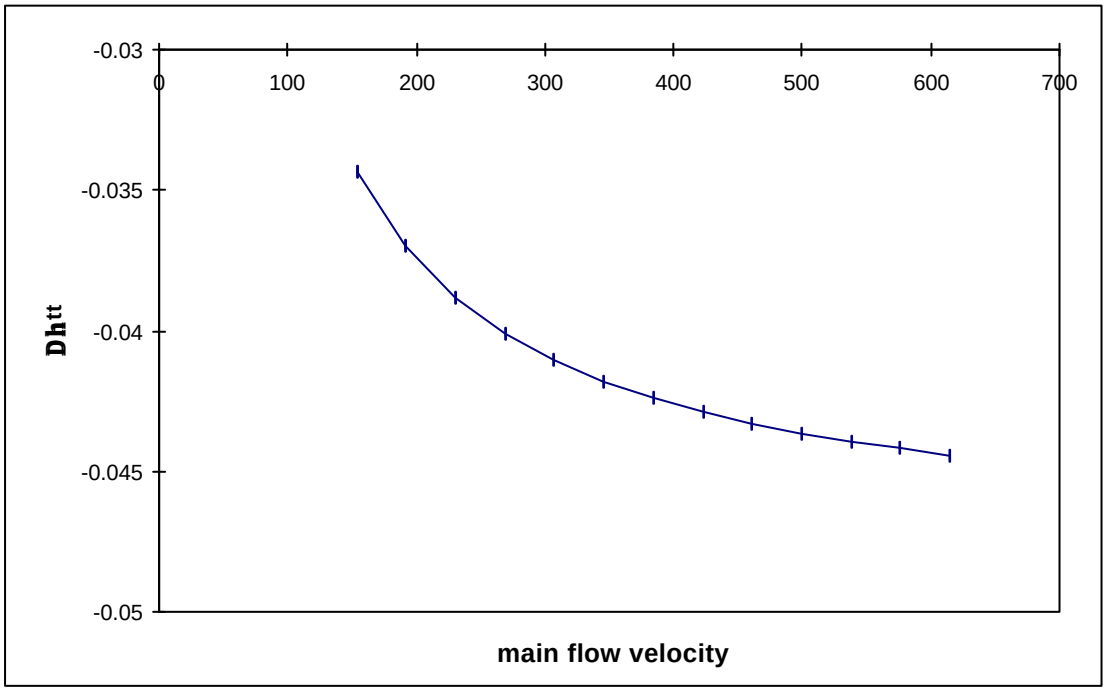

Fig. 4.4.2.5: *Test calculation results of the stage efficiency diminution, due to cooling loss in the stator, versus variation of main flow velocity*

From Fig. 4.4.2.5, it is seen that the diminution of the efficiency is not linear with the variation of main flow velocity. When the main flow velocity increases from 390 to 614 m/s, the diminution of the efficiency rise from 4.2% to 4.4%. But when the velocity decreases from 150 to 390 m/s, the diminution of efficiency is from 3.4% to 4.2%.

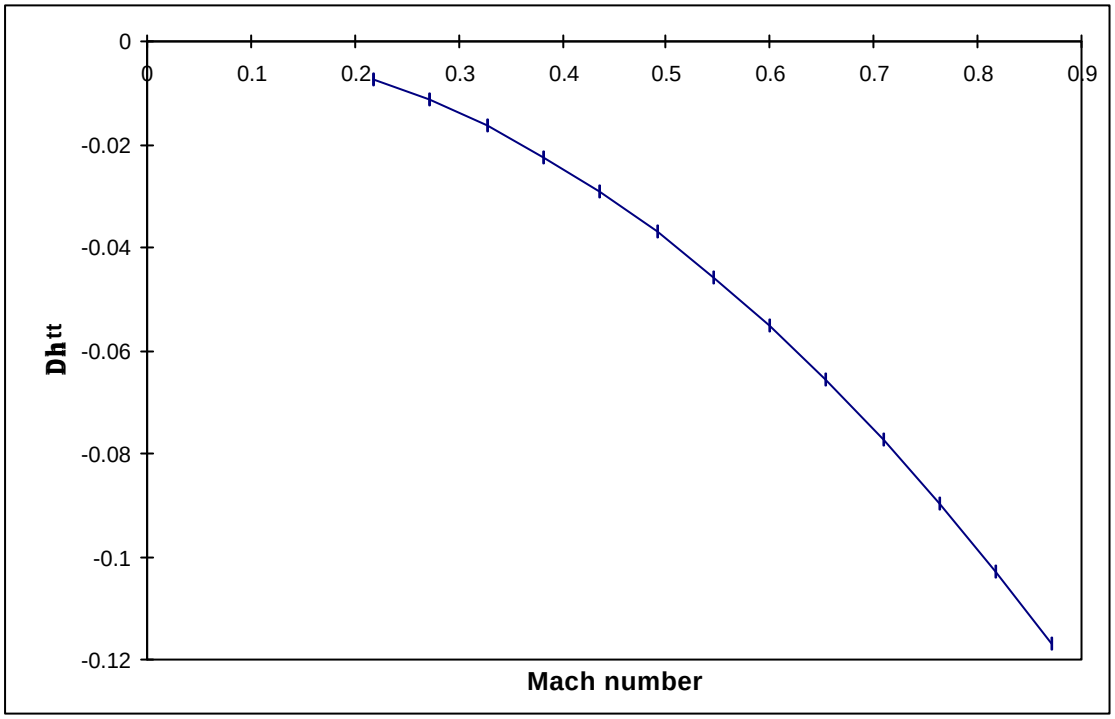

Fig. 4.4.2.6: *Test calculation results of the stage efficiency diminution, due to cooling loss in the stator, versus variation of Mach number*

Fig. 4.4.2.6 shows the change of diminution of the stage efficiency on turbine stage 4 with the variation of Mach number. When the Mach number increases from 0.22 to 0.55, the diminution of the efficiency rises from 0.7% to 4.5%. When the Mach number decreases from 0.55 to 0.88, the diminution of the efficiency is from 4.5% to 11.7%.

These results show that the Mach number will significantly affect the cooling losses, especially when the Mach number is higher than 0.6. This implies that the film cooling loss will change more significantly in supersonic turbines than in subsonic turbines. It also implies that the loss will be high when the hole for injection of coolant is on surfaces near the trailing edge where Mach number is higher compared with the place at upstream. The ratio of coolant to main flow is also a significant parameter for film cooling loss calculation. The results show that the increase of the ratio is almost proportional to the diminution of the efficiency.

Concluding Remarks

The film cooling loss method developed by author has been applied on the performance prediction of turbine stage 4 as a supplement to the loss models of AMDC, Kacker/Okapuu, Craig/Cox and Moustapha/Kacker. Results showed that, after adding the cooling loss prediction, the trends of simulated performances with the combined models have better agreement with the trend of reference data, compared with the results without concerning the cooling losses in the previous section, although the overall combined loss models seem overestimate the losses. The stage efficiency values predicted with the Kacker/Okapuu or Moustapha/kacker model together with the cooling loss prediction are about 2-2.5% units lower than the reference data, which are closer to the reference data than the corresponding predicted results without the cooling losses.

5. AN ANALYSIS OF OPTIMUM PITCH/CHORD RATIO WITH DIFFERENT LOSS MODELS

In this chapter, an aerothermodynamic performance simulation is made on turbine stage 1 with different loss models. The simulation revealed distributions of losses versus the variation of pitch/chord ratios. The aims of this work are to further understand the significance of the loss models and to investigate the behaviours of the models on the pitch/chord ratio variation in the turbines.

In the preliminary design of turbomachinery, pitch/chord ratio is one of the critical geometrical parameters. From the profile loss point of view, if the pitch between blades is made relatively small, the fluid tends to receive a good amount of guidance from the blades, but the friction losses between the flow and blade surfaces will be very high because of the increase in blade numbers, and the machine will be heavy and more costly. On the other hand, with the same blades spaced well apart, friction losses are small but, because of poor fluid guidance, the losses resulting from flow separation are higher. Early turbine designers widely employed Zweifel load number to make a preliminary estimation of the optimum pitch/chord ratio. This has been well introduced by many authors, for example Dixon [1989], Horlock [1966], Cohen et al [1990] and Baljé & Binsley [1968]. However, with the use of the Zweifel number, the optimum of the profile loss only is taken into account and the secondary and tip leakage losses are not involved. In many cases, the secondary and tip leakage losses also have significant influence on the variation of the pitch/chord ratio. This has been found through many experimental investigations, for example by Hodson & Domin [1987], Perdichizzi et al [1997], Bindon [1991] and Cehen et al [1990]. It is interesting to see the variation in optimum value of pitch/chord ratio by making a detailed estimate of stage performance predicted by considering the total losses, mainly profile loss, secondary loss and tip leakage loss, in both stator and rotor.

The Zweifel optimum lift coefficient has been presented in equation 2.1.4, in Chapter 2.1. Zweifel [1945] suggested that the optimum lift coefficient based on the tangential loading should be approximately 0.8. It is so called the Zweifel load number which has been used to give preliminary optimum pitch/number in turbine design. In according to this coefficient, the pitch/chord ratio for the stator and rotor of turbine stage 1 are calculated and listed in Table 5.1. The blade inlet and outlet angles and the original pitch/chord ratios for the stator and rotor of turbine stage 1 are also shown in the table.

	Stator	Rotor
inlet angle, [^{0}]	0.0	54.0
outlet angle, [^{0}]	75.2	63.0
original pitch/chord ratio	0.69	0.72
pitch/chord ratio from the Zweifel coefficient	0.99	0.54

Table 5.1*: Some geometrical parameters of turbine stage 1*

In Table 5.1, the Zweifel coefficient gives a quite different results from the original pitch/chord ratio. Compared with the original pitch/chord ratio, the stator pitch/chord ratio from the Zweifel coefficient is higher but the rotor ratio is much lower. Especially, the stator pitch/chord ratio from the Zweifel load number is unreasonable high. From the comparison,

it can be seen that the Zweifel coefficient has limitations in real application of the turbine design.

In this work, an analysis of the pitch/chord ratio optimisation on turbine stage 1 was made by means of stage performance prediction with different loss models which include the main loss components, profile, secondary and tip clearance losses. The main input data to the calculations are the stage inlet stagnation pressure and temperature, mass flow, turbine speed and geometric parameters of the stator and the rotor. These data are taken from experiments and the original design of the stage. Then the flow parameters at each section and the overall performance parameters of the stage are predicted row by row. The calculations are based on the principle of conservation of mass, momentum and energy over every blade row. In this approach, loss models have to be used to determine the entropy variation at each section in the turbine stage. The loss models given by Ainley/Mathieson and Dunham/Came (AMDC), Kacker/Okapuu (K-O) and Craig/Cox (C-C) have been used in this application.

The calculation was performed firstly on the nominal condition with original pitch/chord ratio. Then calculations were made by changing the pitch/chord ratio of the stator and the rotor respectively while all other flow and geometry data were kept constant. The range in which the pitch/chord ratio varies is from 0.3 to 0.9. This gave distributions of total loss and each individual loss components for the stator and rotor respectively, as well as the stage efficiency, according to the pitch/chord ratio. The optimum pitch/chord ratio points corresponding to the minimum total loss for the stator and rotor respectively were clarified. A detailed analysis of the predicted performance on this turbine stage was made. The behaviours from different loss models were also analysed and compared.

From the performance calculation of the turbine stage, total loss coefficients and each individual loss component over the stator and the rotor are obtained. The distribution of the losses and the optimum point of the pitch/chord ratio can be found.

Fig 5.1 and 5.2 show the total loss coefficient calculated over the stator and the rotor respectively. From the figures, we can see that the AMDC model gives higher losses than the K-O and C-C models. For the stator, the optimum pitch/chord ratio predicted in the AMDC, K-O and C-C loss models was the same, about 0.6. For the rotor, the predicted ratio in the AMDC and K-O models were about 0.5 while the ratio predicted in the C-C model was about 0.65. The predicted optimum pitch/chord ratios for both the stator and the rotor are smaller than the original, 0.69 for the stator and 0.72 for the rotor. However, the pitch/chord ratio evaluated by total losses predicted over the stator and the rotor is not very critical. In the large region around the optimum pitch/chord ratio, the total losses do not vary much. The predicted variation of total loss is no higher than 1.8% of the optimum value in the region of pitch/chord ratio from 0.55 to 0.70 for the stator and 0.45 to 0.75 for the rotor. It is noted that the original pitch/chord ratios were chosen at near the upper limit of these low loss regions. It is reasonable to consider using as few blades as possible in the design to reduce the weight of the real machine.

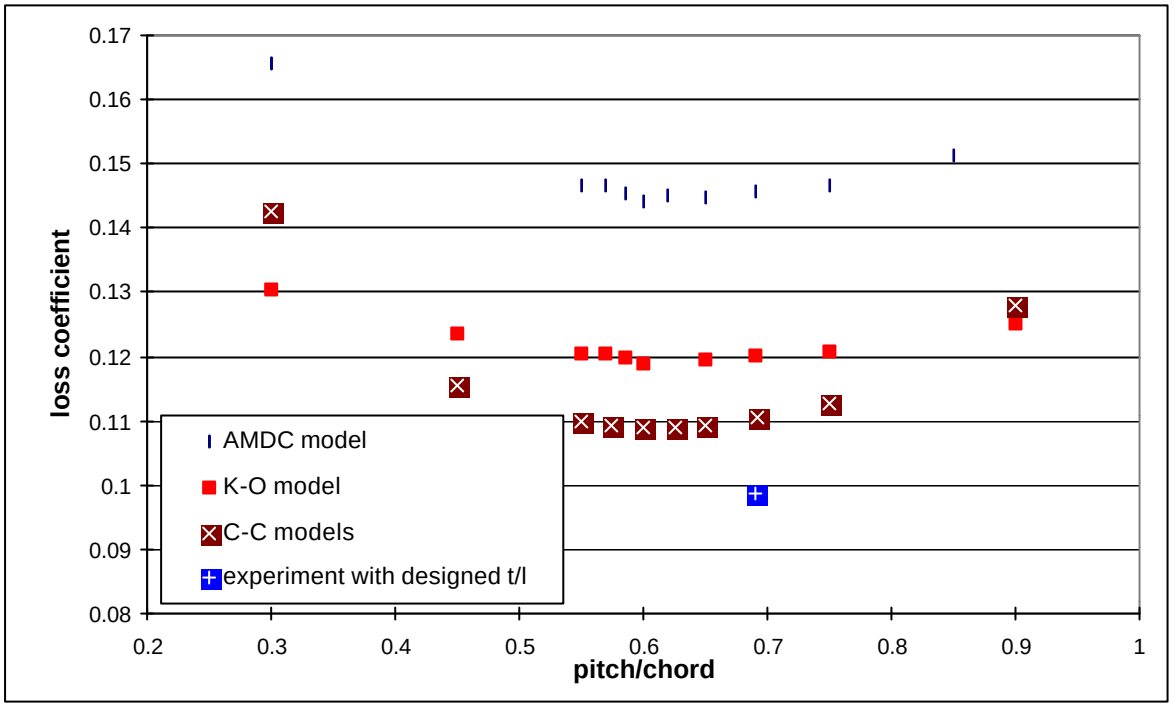

Fig. 5.1: *Stator total loss versus pitch/chord ratio*

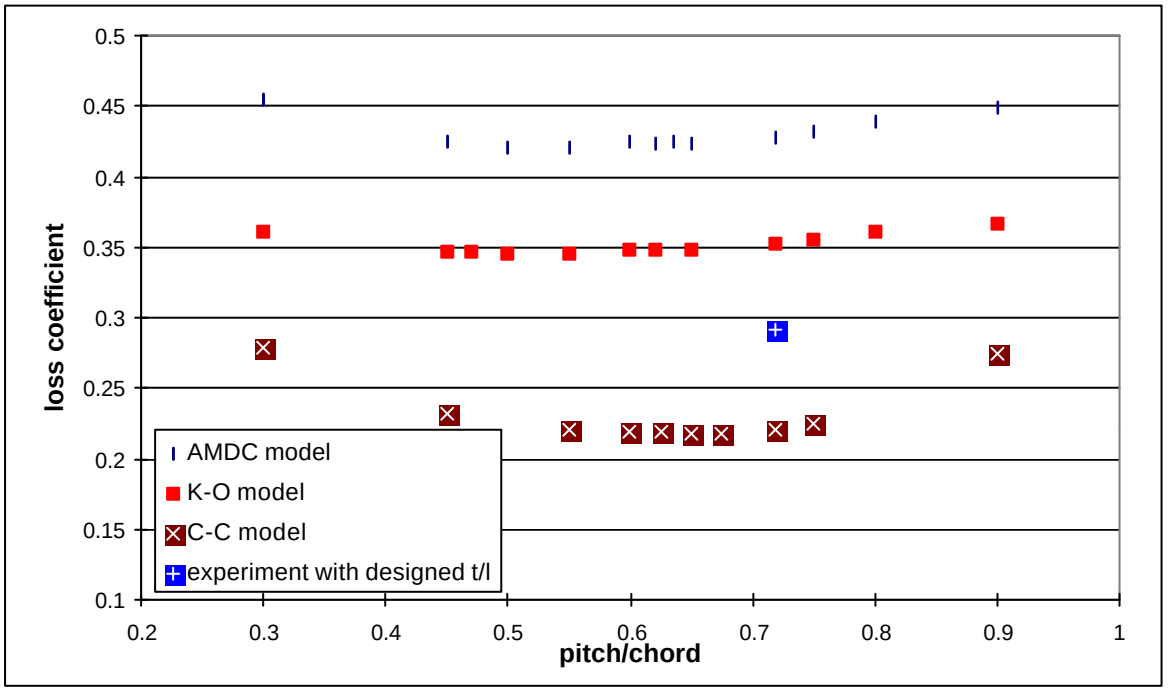

Fig. 5.2: *Rotor total loss versus pitch/chord ratio*

Compared the low loss regions with the pitch/chord ratios from the Zweifel in Table 5.1, it is seen that the ratio, 0.99, for the stator given by Zweifel load number is out of the low loss region predicted in the loss models. This shows that the Zweifel coefficient with the number of 0.8 is not valid for such stator with high outlet angle. In corresponding to the low loss region from the loss models in Fig. 5.1, the Zweifel load coefficient is from 0.45 to 0.57.

The results of the low loss region from various loss models in the rotor are slightly different. From Fig. 5.1, it can be seen that the low loss regions in the AMDC and K-O models are a little larger than the corresponding region in the C-C model. The C-C model gives the

lowest loss point which is at the larger pitch/chord ratio than the ones given by AMDC and K-O models. The reason for this slight difference is the different behaviours of the models for individual loss components. This can be seen from the following analysis of loss breakdown in Fig. 5.3 and Fig. 5.4.

Fig. 5.3 and 5.4 show the predicted stator and rotor profile loss respectively. The profile losses have minimum values, which are the result of, in principle, the balance of the energy loss associated with friction on the blade surface and the loss associated with unguided separation. Compared with the total loss, the results of profile loss have narrower low loss regions. In the stator, the lowest loss point is at pitch/chord ratio 0.6 in the AMDC and K-O loss models and at 0.75 in the C-C model, shown in Fig. 5.3. In the rotor, the point is at 0.5 of pitch/chord ratio in the AMDDC and K-O models and at 0.75 in the C-C model.

The results show different optimum values of pitch/chord ratio based on the profile loss predicted by various loss models. The AMDC and K-O models have the lowest profile loss based on the models derived form Fig. 2.3.1 and 2.3.2. Fig. 2.3.1 is the correlation of the profile loss based on the profile with inlet flow in axial direction, that is, the same inlet condition as the stator. Fig. 2.3.2 represent the loss correlation of the impulse blade row which is similar to the rotor with a small degree of reaction ($\alpha'_{in}=54^0$ and $\alpha'_{out}=63^0$). The C-C loss model gave the lowest profile loss at a pitch/chord ratio about 0.75 for both the stator and rotor which seems similar to the optimum pitch/chord ratios between the impulse and reaction blades if the C-C profile loss model is applied.

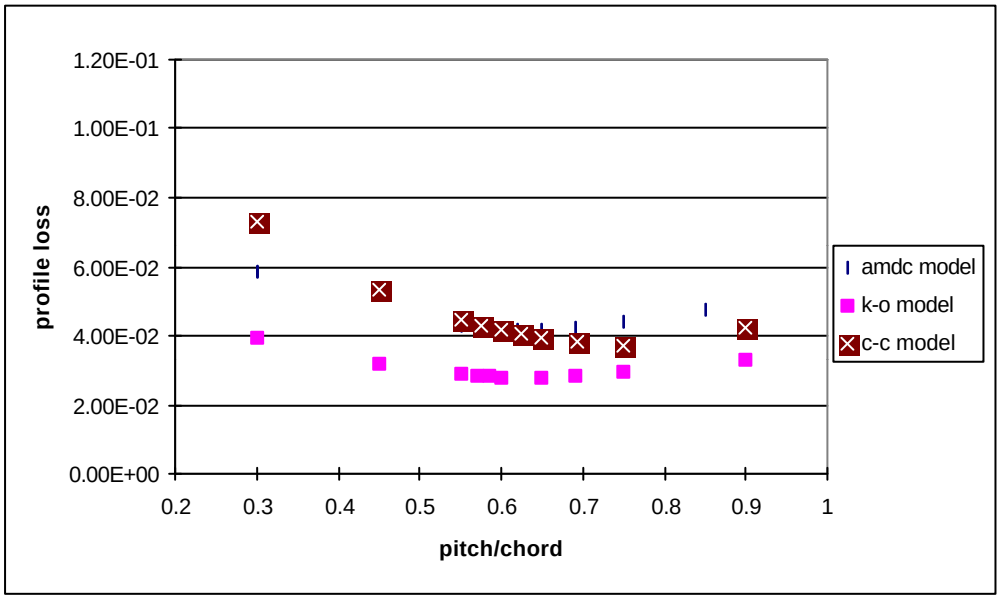

Fig. 5.3: *Stator profile loss versus pitch/chord ratio*

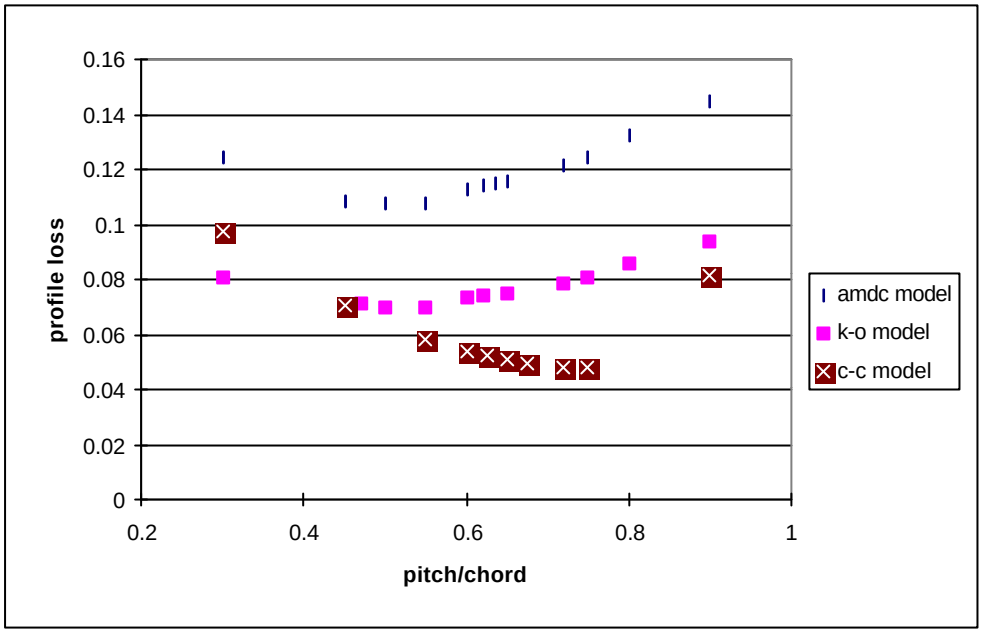

Fig. 5.4: *Rotor profile loss versus pitch/chord ratio*

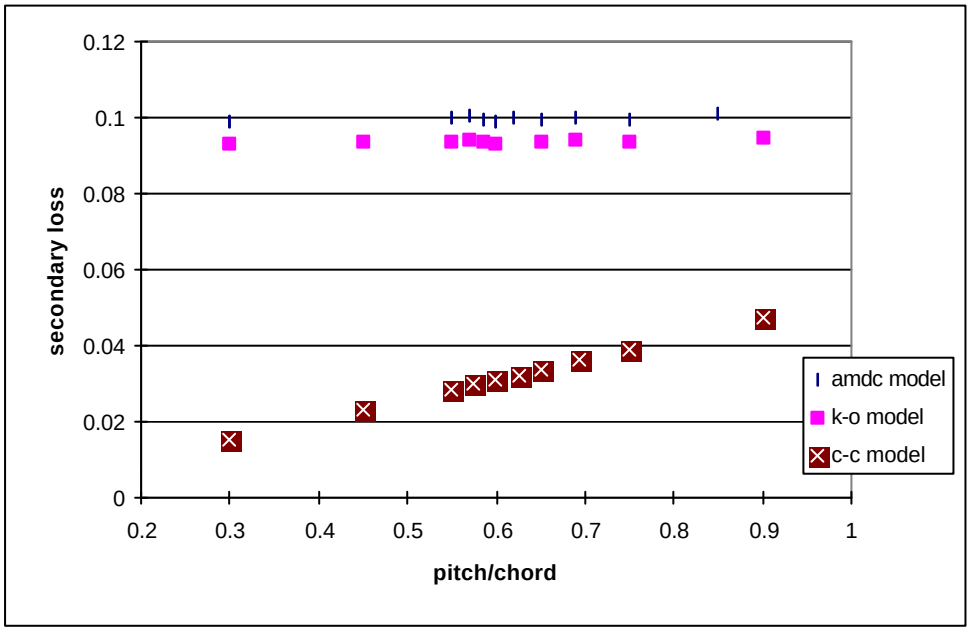

Fig. 5.5: *Stator secondary loss versus pitch/chord ratio*

Fig. 5.5 shows the secondary loss predicted over the stator. It should be noted that the secondary loss predicted in various loss models had significantly different behaviours. It can be found that the secondary losses predicted in the AMDC and K-O models were almost constant along the variation of pitch/chord ratio while the loss predicted in the C-C model rises with increase in pitch/chord ratio. This is because the influence of the pitch/chord variation on the secondary loss is not taken into account in the final secondary loss models of the AMDC and K-O (see equations 2.3.4 and 2.5.8). In these equations, the secondary losses are main functions of only aspect ratio and flow angles. However, the C-C secondary loss model is a function of flow angles, aspect ratio, ratio of inlet to outlet velocity as well as the pitch/chord ratio (see Fig. 2.6.7). From cascade aerodynamics, it is known that when the pitch/chord ratio rises, the pitchwise pressure gradient in between blades increases. This increased pitchwise gradient will strengthen the secondary flow

and the secondary loss will increase. In Fig. 5.5, the results of the secondary loss predicted with the C-C loss model exhibit a reasonable trend.

Fig. 5.6 shows the results of predicted secondary losses over the rotor. The trends of the losses from the different models in the rotor are the same as the corresponding trends in the stator. The values of the secondary loss in the rotor are, on average, higher than those in the stator. This is because the rotor has a higher blade turning than the stator. This leads to higher blade load and higher secondary flow and hence higher secondary loss.

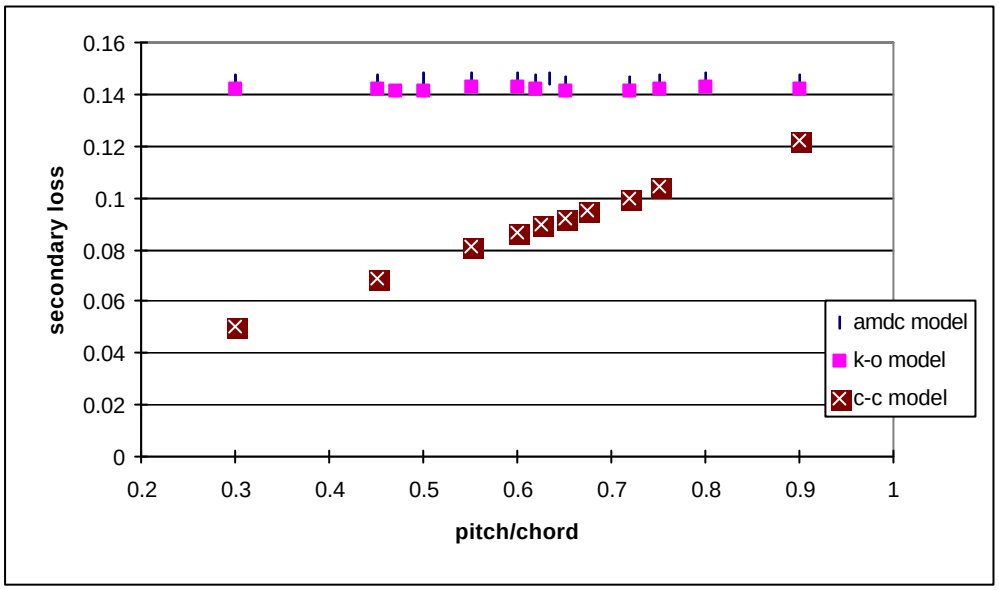

Fig. 5.6: *Rotor secondary loss versus pitch/chord ratio*

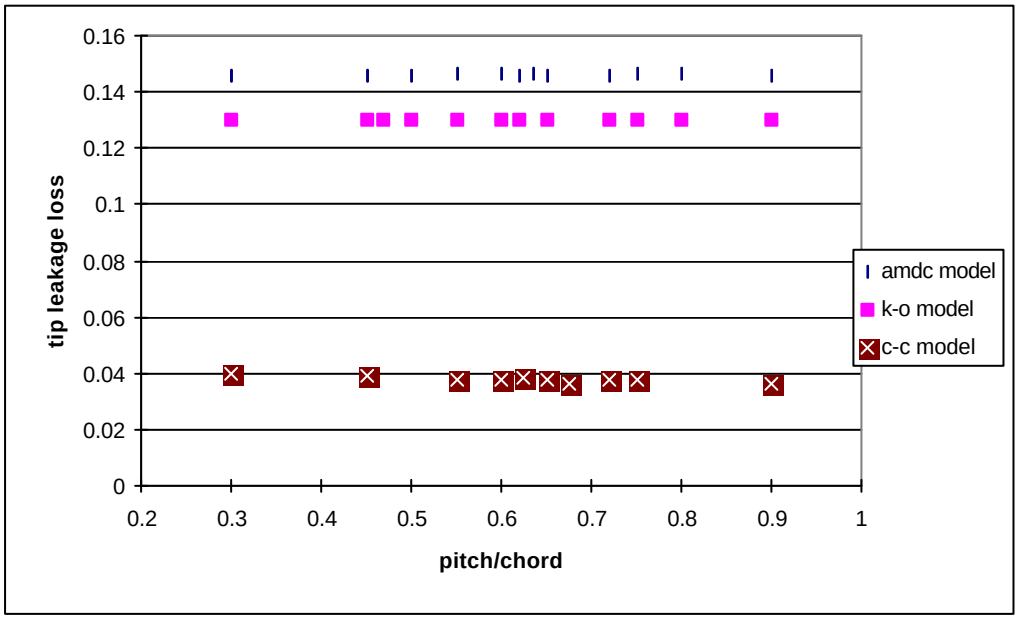

Fig. 5.7: *Rotor tip leakage loss versus pitch/chord ratio*

The predicted tip leakage for the rotor is shown in Fig. 5.7. This loss is kept almost constant when the pitch/chord ratio is varied. This is because the turbine stage is shrouded and the tip leakage over a shrouded turbine cascade depends mainly on the pressure over

the rotor cascade and the inlet and outlet flow angles. None of these parameters change significantly when only the pitch/chord ratio is varied.

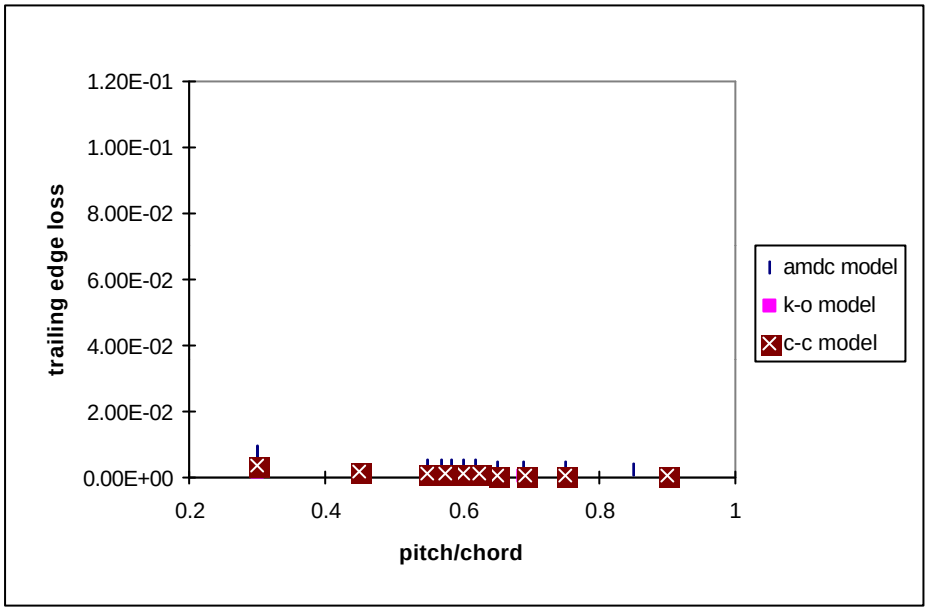

Fig. 5.8: *Stator trailing edge loss versus pitch/chord ratio*

Fig. 5.8 and 5.9 show the predicted trailing edge loss for the stator and the rotor respectively. It can be seen from the figures that the predicted trailing edge losses increase while the pitch/chord ratio decreases because the relative blockage to the flow free stream at the trailing edge increases when the pitch/chord ratio decreases. The trailing edge loss is a small percentage compared with the other loss components in this flow condition of the turbine. Therefore, it does not play important roles in the pitch/chord variation in this case. However, we should be aware that the trailing edge loss should not be neglected in supersonic flow.

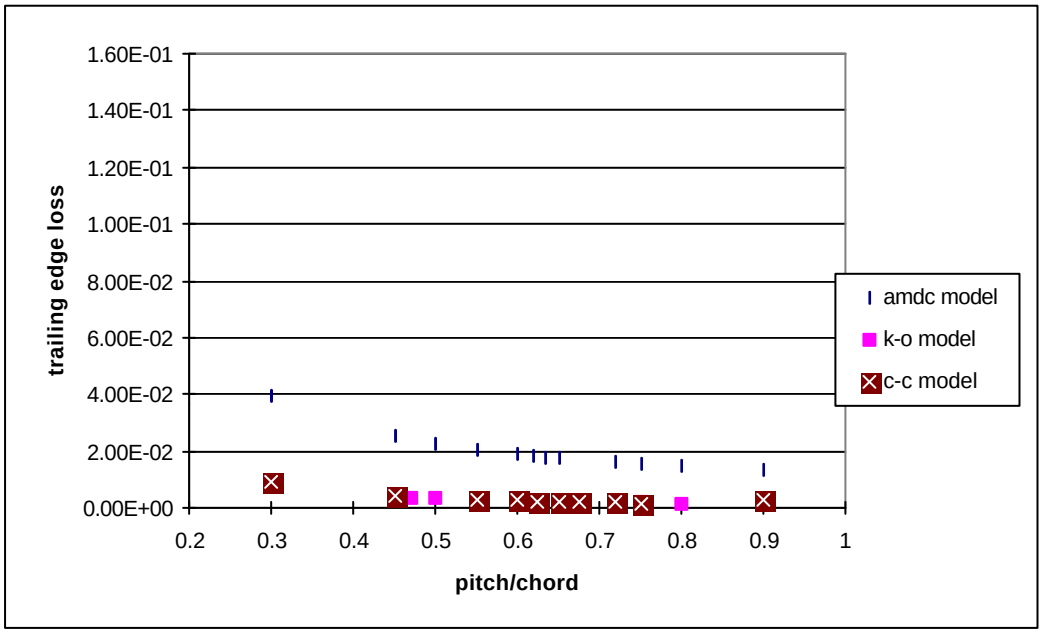

Fig. 5.9: *rotor trailing edge loss versus pitch/chord ratio*

Concluding Remarks

From the performance prediction on the test turbine stage with the AMDC, K-O, and C-C loss models, it can be seen that the pitch/chord ratio evaluated by total losses predicted over the stator and the rotor is not very critical. In a large region of the pitch/chord ratio, 0.55-0.70 for the stator and 0.45-0.75 for the rotor, the total losses do not vary much. The total losses significantly increase when the pitch/chord ratio are out of these regions. The original designed pitch/chord ratio of the stator and rotor in the turbine stage are located at near the upper limits of the lowest total loss regions. It is seem that this design was a good compromise between optimum losses and reduced weight and cost. The stator optimum pitch/chord ratio given by the Zweifel number (see Table 5.1) is far out of the low loss region from the loss models. It is proved that the Zweifel number (when the Zweifel coefficient is equal to 0.8) is not valid for obtaining the optimum pitch/chord ratio for such stator blade with a high outlet angle.

The ranges of these lowest loss regions by these 3 loss models are slightly different. It seems not giving a significant difference to use any one of them to obtain the optimum pitch/chord ratio through a prediction of the total loss.

6. CONCLUSIONS

It is not the purpose of this thesis to establish what is the best loss model for axial turbines, such a comparison can be done only being at one's disposal a very large number of tests results over real turbines operating in a wide range of conditions. However, following points concerning the behaviours of loss models can be made according to the studies and discussions in previous chapters. These points might hopefully be useful for turbine simulation and optimisation with the loss models.

Conclusions on overall performances:

In the performance predictions of the impulse turbine stages, all the AMDC, Kacker/Okapuu, Moustapha/Kacker and Craig/Cox loss models give the same trend of losses as, however overestimated, the experiments. Craig/Cox model gives the loss closest to the experimental results on and near the design point, but over predict the loss in the off-design region. The AMDC model is one which most overestimate the losses in the whole operation range. It was found that when the span/chord ratio increases about 25% in such type of stage, the total losses in the stator decrease about 10% by the Craig/Cox model and 20% by the every one of the other models while the total losses in the rotor decrease about 15-25% by the K-O and M-K models and 15-30% by the AMDC and C-C models in the corresponding operating range.

For the free vortex blading like turbine stage 3, it was found that the losses are underpredicted in all the models, especially on the off-design operation points, because the high losses at the hub wall caused by the blading of free vortex are underestimated by using the parameters at mean line.

It was found that the loss models predict the performances in turbine stages 4 and 5 with the same trend as reference data. All these models predict higher efficiency than the reference data in turbine stage 4, which is the high pressure stages of a aeroengine with a cooling, because the lack of cooling loss calculation in the models. The AMDC and Craig/Cox models seem to give close results to the reference data because of the fortuity of overestimated uncooled turbine losses.

It was found that the variation of specific heat with both temperature and fuel/air ratio could give a significant error on the calculation of stage efficiency on the high temperature and heavy cooling turbine although it does not give a significantly direct influence on the calculation of the loss coefficient in the models. Results showed that the errors on the calculation of stage total-to-total efficiency, caused just by the variation of fuel/air ratio from 0.0 to 0.04, was up to 7% on the operating range.

From a analysis of optimum pitch/chord ratios in turbine stage 1 calculated with the loss models, it was found that the pitch/chord ratio evaluated by total losses is not very critical. All these models gave similar low loss regions of pitch/chord ratios in which the total losses do not change significantly. The regions covers the original pitch/chord ratios for the stator and rotor respectively. Compared the results with the ratios calculated with Zweifel load

number, it was found that the Zweifel load number is not valid for the stator which is with high outlet blade angle. The results showed that there will be no significant difference between these loss models if they are employed to obtain the optimum pitch/chord ratio in turbine optimisation process.

An effort for developing a simple method to predict overall film cooling loss approximately in a turbine blade row was made based on analysing 1D equation of mass, momentum and energy conservation in mixing flows. This method has been applied on the performance prediction of turbine stage 4 as a supplement to the loss models of AMDC, Kacker/Okapuu, Craig/Cox and Moustapha/Kacker. Results showed that, after adding the cooling loss prediction, the trends of simulated performances with the combined models have better agreement with the trend of reference data, compared with the results without concerning the cooling losses in the previous section, in the operating range although the overall combined loss models seem overestimate the losses. The stage efficiency values predicted with the Kacker/Okapuu or Moustapha/Kacker model together with the cooling loss prediction are about 2-2.5% units lower than the reference data, which are closer to the reference data than the corresponding predicted results without concerning the cooling losses.

Conclusions on loss component predictions:

Design profile loss:
All the models are based on the experimental data and are correlated mainly with the blade inlet and outlet angles and pitch/chord ratio (Craig/Cox model takes the ratio of pitch to camber line instead). In AMDC, Kacker/Okapuu, and Moustapha/Kacker models, the ratio of blade maximum thickness to the pitch was taken into account while the pitch to blade back radius ratio was considered in the Craig/Cox model as a blade shape parameter which influences the flow boundary layer statues on the blade surface. The flow acceleration in the blade passage was considered in the Kacker/Okapuu and Moustapha/Kacker models by taking the ratio of inlet and outlet Mach number while in the Craig/Cox model by using the contraction ration which is the ratio of the inlet and throat widths. The AMDC model has most overestimated results while the Kacker/Okapuu and Moustapha/Kacker models give about 1/3 lower losses than the AMDC model.

Off-design profile loss:
The incidence is the most important parameter to predict the off-design profile loss. This parameter was taken into account by every model. In the AMDC and Craig/Cox models, the stall incidence angle was taken as a parameter to predict the off-design loss and this stall incidence angle was mainly correlated to the pitch to chord ratio and the inlet and outlet blade angles. In addition, in the Craig/Cox model the contraction ratio was also considered. In the Moustapha/Kacker model, besides the incidence, the ratio of leading edge diameter to the pitch was considered as an important parameter together with the blade inlet and outlet angles. From the application of these loss models, It was found that the AMDC and Craig/Cox models gave rapid increase of off-design profile loss, especially in the negative incidence region. It seems that the high predicted off-design profile loss come from the too small calculated stall incidence angle. Compared with these, the results showed that the Moustapha/Kacker model gave much smoother increase of off-design profile loss.

Secondary loss:

In all of these models, the secondary losses were considered as a main function of the blade aspect ratio and load (in term of list parameter in the Craig/Cox model) which is correlated with flow turning over the blades. Besides this, the influence of the flow acceleration on the secondary loss was also considered by correlating the inlet and out let flow velocity in the Craig/Cox model and inlet and outlet Mach number in the Kacker/Okapuu and Moustapha/Kacker models. From the applications of these loss models, it was found that the losses predicted in all these models increased versus the rises of the blade load. But at the highest positive incidence point where the degree of reaction is near to zero, the secondary losses from the Kacker/Okapuu and Moustapha/Kacker models could decrease. This is because that in the Kacker/Okapuu and Moustapha/Kacker models, the coefficient K_p reduces, which lead to the decrease of the losses, with the rise of the inlet to outlet Mach number ratio. In the Craig/Cox model, the ratio of the inlet to outlet flow velocity to the blade row is taken into account to calculate the secondary loss and the loss is proportional to the ratio. This ratio physically implies the flow acceleration through the blade and the condition of the boundary layer and secondary vorticity as well as the losses at the endwall. These different behaviours of the loss models can lead to different results when they are employed for turbine design and simulation in the cases of such flow conditions. The results showed that all these models give reasonable trend of the secondary loss reductions as the increase of blade aspect ratios, but the losses reduce in different levels by the various loss models depending on the blade geometrical parameters. For axial entry stator blades, the reduction of the secondary losses due to the 25% increase of the aspect ratio are about 10% by the Craig/Cox model, 27% by the AMDC model and 24% by the Kacker/Okapuu and Moustapha/Kacker models. For impulse rotor blades, the reduction of the losses at the design point due to the 25% increase of the aspect ratio are about 36% by the Craig/Cox model, 30% by the AMDC model and 25% by the Kacker/Okapuu and Moustapha/Kacker models.

Tip leakage loss:

In the AMDC, Kacker/Okapuu and Moustapha/Kacker models, the tip leakage loss were calculated with correlating mainly the aspect ratio, the ratio of tip clearance to blade span and the blade load which is a function of flow turning. In the Craig/Cox model, the tip leakage loss is a function of the clearance to throat areas ratio, inlet and outlet velocity and the non-clearance loss which is the sum of the profile and secondary losses but no relation with the aspect ratio and blade load. The predicted results showed that, for impulse rotor blades, the reduction of the tip leakage losses due to the 25% increase of the aspect ratio are about 15-25% by the AMDC, Kacker/Okapuu and Moustapha/Kacker models. From the application of these loss models, it was found that the tip leakage loss predicted in the Craig/Cox model could have a complete different trend with the losses predicted in the AMDC, Kacker/Okapuu and Moustapha/Kacker models. The results showed that the tip leakage losses from the AMDC, Kacker/Okapuu and Moustapha/Kacker models have a upward trend with the increase of the incidence while the tip leakage loss from the Craig/Cox model might have a downward trend, which depends to the ratio of inlet to outlet velocities. It should be noted that the different behaviours of these loss models can possibly lead to different results when they are employed for machine design and simulation in some cases when the tip leakage loss

has a large percentage in the total loss, such as a turbine with high blade load, low aspect ratio and high ratio of the tip clearance to blade span.

7. PROPOSALS FOR FUTURE WORK

In order to optimise and simulate turbines well, loss models, especially off-design loss models, are need to be revised and updated to reflect recent trends in turbine design. This can only be done when a large number of detailed tests results over recent blade cascades and turbine stage operating in a wide range of conditions.

Improvement of the physical understanding of the flow in turbines is needed for predicting losses more correctly:

- turbulent and transition in the boundary layer on blade surface for predicting design profile loss
- separation of the boundary layer on blade surface for predicting off-design profile loss
- characters of the 3D boundary layer on endwalls for predicting secondary and tip leakage losses
- characters of the secondary vortex for predicting the secondary and tip leakage losses
- mechanisms of mixing between coolant and main flow in cooled turbine blade rows

BIBLIOGRAPHY

Ainley, D. G.; Mathieson, G. C. R.; 1951
"A Method of Performance Estimation for Axial-Flow Turbines"
British Aeronautical Research Council, R&M 2974

Atkins, M. J; 1987
"Secondary losses and end-wall profiling in a turbine cascade," *Cambridge C255/87*

Baljé, O. E.; Binsley, R. L.; 1968
"Axial Turbine Performance Evaluation. Part A - Loss-Geometry Relationhsip"
Journal of Engineering for Power, Oct. 1968, p341-348

Baljé, O. E.; Binsley, R. L.; 1968
"Axial Turbine Performance Evaluation. Part B - Optimization with and without constraints"
Journal of Engineering for Power, Oct. 1968, p348-360

Bindon, J. P., 1989
"The Measurement and Formation of Tip Clearance Loss,"
ASME, Journal of Turbomachinery, July 1989, Vol. 111, p 257-263.

Bindon, J. P.; 1991
"The Microflows Within the Tip Clearance Gap of An Unshrouded Axial Turbine", International Journal of Turbo and Jet Engines, 8, 55-74 (1991)

Boulter, R. A.; 1962
"The Effect of Aspect Ratio on the Secondary losses in a Cascade of Impulse Turbine Blades," unpublished Pamertrada Report, (quoted in reference [Dunham, 1970])

Boyle, B. J.; 1993
"Prediction of Surface Roughness and Incidence Effects on Turbine Performance"
ASME 93-GT-280

Bölcs, A.; 1993
"Turbomachines Thermiques",
Laboratoire de turbomachines et de Termique Appliquée, Département de Mécanique,
École Polytechnique Fédérale de Lausanne

Cohen, H.; Rogers, GFC.; Saravanamutto, HIH.; 1996
"Gas Turbine Theory", 4th Edition, ISBN 0-582-23632

Craig, H. R. M.; Cox, H. J. A.; 1970
"Performance Estimation of Axial Flow turbines," *Proc. Instn. Mech. Engrs. 1970-71, Vol. 185 32/71*

Dejc, M. E.; Trojanovskij, B. M.; 1973

"Untersuchung und Berechnung axialer Turbinenstufen," *VEB Verlag Technik Berlin 1973*

Denton, J. D.; 1987
"Loss Mechanisms in Turbomachines," *MechE 1987-6, C260/87*

Denton, J. D.; 1990
"Entropy Generation in Turbomachinery," *Whittle Lab. Cambridge University*

Denton, J. D.; 1993
"Loss mechanisms in Turbomachinery," *ASME, 93-GT-435*

Denton, J. D.; 1994
"Axial turbine aerodynamic design", Lecture note for an advanced course on Turbomachinery Aerodynamic, *University of Cambridge, UK*

Denton, J. D.; Xu, L.; 1989
"The Trailing Edge Loss for Transonic Turbine Blades," *ASME, 89-GT-278, 1989*

Dixon, S. L:, 1989
"Thermodynamics of Turbomachinery," *Pergamon press plc. ISBN o-08-022722-8*

Dunham, J.; 1970
"A review of Cascade Data on Secondary losses in Turbines"
Journal Mechanical Engineering Science, Vol. 12, No. 1, 1970

Dunham, J.; 1996
"Compressor Off-Designe Performance Prediction Using an Endwall Model,"
ASME 96-GT-62

Dunham, J.; Came, P. M.; 1970
"Improvements to the Ainley-Mathieson Method of Turbine Performance Prediction"
ASME, 70-GT-2

Ehrich, F.; Detra, R.; 1954
"Transport of the Boundary Layer in Secondary Flow", *Journal of Aeronautical Sciences, Vol. 21, pp. 136-138,* (quoted in reference [Dunham, 1970])

Franus, D. J.; 1994
"The World Gas Turbine Industry Production Trends and Key Factors"
For the 1994 ASME Turbo Expo-Land, Sea & Air, The Hague, The Netherlands
By Forecast International, USA

Farn, C. L.; Whirlow, D. K.; Chen, S.; 1991
"Analysis and Prediction of Transonic Turbine Blade Losses," ASME 91-GT-183

Fottner, L.; 1990

"Test Cases for Computational of Internal Flows in Aero Engine Components",
Agard AR-275

Gregory-Smith, D. G.; Graves, C. P.; Walsh, J. A.; 1988
"Growth of Secondary Losses and Vorticity in an Axial Turbine Cascade", 87-GT-114

Haghighi, A.; 1996
"Analytical Study of the Mass flow and Efficiency Calculation and its Accuracy for the Test Turbine at HPT/KTH, Technical Report HPT/KTH 96-01, Division of Heat and Power Technology, Royal Institute of Technology, Stockholm Sweden

Hartsel, J. E.; 1972
"Prediction of Effects of Mass -Transfer Cooling on the Blade Row Efficiency of Turbine Aerofoils," AIAA paper, 72-11, (quoted in reference [Denton, 1993])

Hawthorne, W. R.; 1955
"Some Formular for the Calculation of Secondary Flow in Cascades"
A.R.C. Report No. 17519, (quoted in reference [Dunham, 1970])

Hedlund, L.; 1999
Private communication, ABB-STAL

Hodson, H. P; Dominy, R. G.; 1986
"The Off-Design Performance of a Low-Pressure Turbine Cascade", ASME, 86-GT-1887

Horlock, J. H.; 1966
"Axial flow turbine," *Butterwoth Published 621-154*

Hubner; J.; Fottner, L.; 1996
"Influnce of tip-Clearance, Aspect ratio, Blade Loading, and Inlet Boundary layer on Secondary Losses in Compressor Cascades," ASME 96-GT-505

Håll, U.; 1990
"Program Report Turbine Performance," *Report from CTH*

Ito, S.; Eckert, E. R. G.; Goldstein, R. J.; 1980
"Aerodynamic Loss in a Gas Turbine Stage with Film Cooling"
Journal of Engineering for Power, Oct. 1980, Vol. 102

Johansson, T.; 1999
Private communication, Volvo Aero Corporation

Kacker, S. C.; Okapuu, U.; 1982
"A mean Line Prediction Method for Axial Flow turbine Efficiency", *ASME, 81-GT-58*

Kind, R. J.; Serjak, P. J.; Abbott, M. W. P.; 1996

"Measurements and Prediction of the Effects of surface Roughness on profule losses and Deviation in turbine Cascade", 96-GT-203

Klein, A.; 1966
"Untersuchungen uber die Einfluss der Zuströmgrenzschicht auf die Sekundärströmung in den Beschaufelungen von Axialturbinen," Forsch. Ing., Ba 32, Nr. 6.
(quoted in reference [Lakshminarayana, 1996])

Kollen, O.; Koschel, W.; 1980
"Effect of Film Cooling on the Aerodynamic Performance of a Turbine Cascade,"
AGARD CP 227, (quoted in reference [Lakshminarayana, 1996])

Kroon, R. P.; Tobiasz, H. J.; 1971
"Off-Design Performance of Multistage Turbines",
Journal of Engineering for Power, Jan. 1971

Lakshminarayana, B.; 1970
"Methods of Predicting the tip Clearance Effects in Axial Flow Turbomachinery"
ASME, Journal of Basic Engineering, Sep. 1970

Lakshminarayana, B.; 1996
"Fluid Dynamics and Heat Transfer of Turbomachinery," ISBN 0-471-85546-4

Langston, L. S.; 1980
"Crossflow in a Turbine Cascade Passage," J. Eng. Power, Vol. 102, p. 866

Langston, L. S.; Nice, M. L.; Hooper, R. M.; 1977
"Three-Dimensional Flow Within a Turbine Passage," J. Eng. Power, Vol. 99, p. 21-28

LeGrives, E.; 1986
"Cooling Techniques for Modern Gas Turbines," Chapter 4 in Topics in Turbomachinery Technology (D. Japikse, ed.), Concepts ETI, Inc., Norwich, VT.
(quoted in reference [Lakshminarayana, 1996])

Ludbladh, A.; 1998
Private communication, Volvo Aero Corporation

Macchi, E.; 1985
"Design Limits, Basic parameter Selection and Optimisation Methods in Turbomachinery Design", Thermodynamics and Fluid Mechanics of Turbomachinery, , No. 97B, Vol. 2,

Macchi, E.; Perdichizzi, A.; 1981
"Efficiency Prediction for Axial-flow Turbine Operating with Nonconventional Fluids"
J. of Engineering for Power, Oct. 1981, Vol. 103

Moustapha, S. H.; Kacker, S. C.; Tremblay, B.; 1990
"An Improved Incidence Losses Prediction Method for Turbine Airfoils"

ASME 89-GT-284

Mukhtarov, M. Akrichakin, V. I.; 1969
“Procedure of Estimating Flow Section Losses in Axial Flow Turbines When Calculating their Characteristics, ” teploenergetika, vol. 16, No. 7, p. 76-79

Nikolos, I. K.; Douvikas, D. I.; Papailiou, K. D.; 1996
“Modelling of the Tip Clearance Losses in Axial Flow Machines,” ASME 96-GT-72

Okan, M. B.; Gregory-smith, D. G.; 1992
"A simple method for estimating secondary losses in turbines at the preliminary design stage," ASME 92-GT-294

Perdichizzi, A.; Savini, M.; Dossena, V.; 1997
“Secondary Flow Investigations in Turbine Cascades”, in Turbomachinery Fluid Dynamics and Heat Transfer, ISBN: 0-8247-9829-5, 1997

Schobeiri, T.; Abouelkheir, M.; 1992
"Row-by- Row Off-Design Performance Calculation Method for Turbines"
Journal of Propulsion and Power, Vol. 8, No. 4, July Aug. 1992

Scholz, N.; 1954
“Secondary flow losses in Turbine Cascades,” J. aero. Sci. 1954 21, 707
(quoted in reference [Dunham, 1970])

Shapiro, A. H.; 1953
“The Dynamics and Thermodynamics of Compressible Fluid Flow,” Vol. 1 & 2
The Ronald Press, New York

Sharma, O. P.; Butler, T. L.; 1987
“Predictions of Endwall Losses and Secondary Flow in Axial flow Turbine Cascades”
Journal of Turbomachinery, Apr. 1987, Vol. 109

Shu, J.; Liu, D.; Ren, S.; 1985
“An Investigation of internal Efficiency Calculation of the Steam Turbine Flow Path”
Zhongguo Dianji Gongcheng Xuebao, Vol. 5, No. 4, Nov. 1985

Sieverding, C. H.; 1984
"Recent Progress in the Understanding of basic Aspects of Secondary Flow in Turbine Blade Passages," ASME 84-GT-78

Sieverding, C. H.; 1985
“Axial Turbine Performance prediction Methods,” *NATO ASI Series. No. 97B, Vol. 2*

Smith, S. F.; 1965
“A Simple Correlation of Turbine Efficiency,” J. of the Royal Aeronautical Society, Jun. 1965

Soderberg, C. R.; 1949
Unpublished notes, Gas Turbine Laboratory, Massachusetts Institute of Technology
(quoted in reference [Dixon, 1989])

Stewart, W. L.; Whitney, W. J.; Wong, R. Y.; 1960
"A study of Boundary-Layer Characteristics of Turbomachine Blade Rows and Their Relation to Over-All Blade Loss," *Transactions of the ASME, September 1960*

Tremblary, B.; Sjolander, S. A.; Moustapha, S. H.; 1990
"Off-Design Performance of a Linear Cascade of Turbine Blades," ASME 90-GT-314

Traupel, W.; 1977
"Termische Turbomaschinen Zweiter Band Geländerte Betriebsbedingungen, Regelung, Mechanische Probleme, Temperaturprobleme"
Springer-Verlag Berlin heidelberg New York 1977

Wei, N.; Svensdotter, S.; 1995
"Investigation of the Flow Trough an Axial Turbine Stage," *Licentiate Thesis*
Chair of Heat and Power Technology, KTH, ISRN KTH/KRV/R-95/1-SE

Wei, N. 1996
"Utveckling av metoder för analys och optimering av motorsystem, Status Report 01.04.96 - 30.06.96", KTH/HPT 96-06

Wei, N.; Fransson, T.; 1998
"An Analysis of Optimum Pitch/Chord Ratio in an Axial Turbine Stage with Different Loss Models," Proceeding of The 3rd International Conference on Pumps and Fans, Beijing, Oct. 1998, p. 121

Yamamoto, A.; 1988
"Interaction Mechanisms Between Tip Leakage Flow and the Passage Vortex in a Linear Turbine Rotor Cascade," J. Of Turbomachinery, Vol. 110, July 1988, p. 329

Yamamoto, A.; 1989
"Endwall Flow/Loss Mechanisms in a Linear Turbine Cascade," ASME 88-GT-235

Yaras, M. I.; Sjolander, S. A.; 1992
"Prediction of tip-leakage losses in axial turbines," Transaction of the ASME, Vol. 114, Jan. 1992

Zehner, P.; 1980
"Calculation of four-Quadrant Characteristics of Turbines," ASME 80-GT-2

Zweifel, O.; 1945
"The spacing of Turbomachine Blading, Especially with Large Angular Deflection,"
Brown Boveri Rev., 32 (1945) 12, (quoted in reference [Horlock, 1966])

Zweifel, O.; 1946
“Optimum Blade Pitch for Turbomachines with Special Reference to Blades of Great Curvature,” The Engineers’ Digest, Vol. 7, November, 1946, p. 358-360
(quoted in reference [Baljé and Binsley, 1968])

APPENDIX 1

Equations from Loss Models

Authors	Correlation Formulae	Remarks
Soderberg [1949]	Total loss: $z = \left(\frac{10^5}{R_e}\right)^{1/4} \left[\left(1+x^*\right)\left(0.993+0.075\frac{l}{H}\right)-1\right]$, Re =$10^5$ $x^* = 0.04+0.06\left(\frac{e}{100}\right)^2$, $t'_{max}/l=0.2$ and $H/l_x=3$	Design point input data needed: Re, l, H, ε
Traupel [1977]	Total loss: $\zeta = \zeta_p + \zeta_f + \zeta_r$ Profile loss (design point): $\zeta_p = \chi_R \chi_M \zeta_{p0} + \zeta_{Te} + \zeta_c$ ζ_{p0} --- the basic profile loss see Traupel [1977, Fig. 8.4.5] χ_R --- the Reynolds number correction factor based on the influence of Reynolds number and surface roughness, see Traupel [1977, Fig. 8.4.6] χ_M --- the Mach number correction factor, see Traupel [1977, Fig. 8.4.5] ζ_{Te} --- the trailing edge loss, see Traupel [1977, Fig. 8.4.5] ζ_c --- the Carnot shock loss which appears in a fluid that is undergoing a sudden expansion, for example after the trailing edge. $z_c = \left\langle \frac{\Delta_a}{1-\Delta_a} \right\rangle^2 \sin^2 a_{out}$ $\Delta_a = \frac{t'}{t\sin\left(90^0 - a_{out}\right)}$ Rest losses: $z_r = \frac{z_p}{z_{p0}} F \frac{t}{H} + z_a$ H/t>=$(H/t)_k$ $z_r = \frac{z_p}{z_{p0}} \frac{F}{(H/t)_k} + z_a + A\left(\frac{l}{H} - \frac{l/t}{(H/t)_k}\right)$ H/t<$(H/t)_k$ F – see Traupel [1977, 8.4.8] $z_a = \frac{c_f \cdot d}{\sin\left(90^0 - a_{out}\right)\cdot h}$ h – highs of cascade casing δ_a – gaps between cascades critical blade length: $(l/t)_k = \begin{cases} 7\sqrt{z_p} & stator \\ 10\sqrt{z_p} & rotor \end{cases}$ Tip leakage loss: Shrouded blades:	Design point only input data needed: α_{in}, α_{out}, Re, V_{in}, V_{out}, ν, l, t, t', H, u, D, Δh,

	$\zeta_{Tl} = \begin{cases} 2\cdot(1-R_H)\cdot m_N \cdot \left[1-\left(\dfrac{n-n(a_0*)}{n(a_0*)}\right)^2\right] & stator \\ m_N \cdot \left[1-\left(\dfrac{n-n(b_1*)}{n(b_1*)}\right)^2\right] & rotor \end{cases}$ Unshrouded blades: $\Delta h_{Tl} = K_d \dfrac{(t-0.002\,l)D}{HD_m}$ Fan loss: see Traupel [1977, Fig. 8.4.7]	
Ainley & Mathieson [1951]	Total losses: $Y = (Y_p + Y_S + Y_{Tl})\,\chi_{Te}$ χ_{Te} – see Ainley & Mathieson [1951, Fig. 9] Profile loss (design point): $Y_{P(i=0)} = \left\{Y_{P(\alpha'_{in}=0)} + \left(\dfrac{\alpha'_{in}}{\alpha_{out}}\right)^2\left[Y_{P(\alpha'_{in}=\alpha_{out})} - Y_{P(\alpha'_{in}=0)}\right]\right\}\left(\dfrac{t'_{max}/l}{0.2}\right)^{\frac{\alpha'_{in}}{\alpha_{out}}}$ $Y_{P(a'_{in}=0)}$ and $Y_{P(a'_{in}=a_{out})}$ see Ainley & Mathieson [1951, Fig. 4] Off-design profile loss: $Y_p = \chi_i\, Y_{P(i=0)}$ χ_i – see Ainley & Mathieson [1951, Fig. 7 & 8] From [Håll, 1990]: $\zeta_i = \begin{cases} 1+i_{rat}^2(0.0625 i_{rat}+0.575) & i_{rat}<0.0 \\ 1+i_{rat}^2(1.111 i_{rat}-0.111) & i_{rat}>0.0 \end{cases}$ $i_{rat} = i/i_{stall}$ $i_{stall} = i_{ref} + \Delta i_s$ Secondary loss: $Y_S = l4\left(\tan a_{in} - \tan a_{out}\right)^2\left(\dfrac{\cos^2 a_{out}}{\cos a_m}\right)$ λ -- see Ainley & Mathieson [1951, p. 26] $\alpha_m = \tan^{-1}[(\tan\alpha_{in} + \tan\alpha_{out})/2]$ Tip leakage loss: $Y_{Tl} = \begin{cases} 0.47\dfrac{t}{h}4\left(\tan a_{in} - \tan a_{out}\right)^2\left(\dfrac{\cos^2 a_{out}}{\cos a_m}\right) & shrouded \\ 0.5\dfrac{t}{h}4\left(\tan a_{in} - \tan a_{out}\right)^2\left(\dfrac{\cos^2 a_{out}}{\cos a_m}\right) & unshrouded \end{cases}$ τ -- radial tip clearance h -- annulus height (equals blade height if radial tip clearance is zero)	Valid for: t´/t=0.02 Re=2x105 M<=0.6 H/l>=2 Design and Off-design points i_{stal} – stall incidence i_{ref} – reference incidence (when t/l=0.75) [Ainley & Mathieson, 1987, Fig. 7] Δi_s – correction of stall incidence [Ainley & Mathieson, 1987, Fig. 7] input data needed: α_{in}, α_{out}, α'_{in}, t'_{max}, M_{out}, l, τ, H, t, t', i
Dunham & Came [1970]	Total loss:	Modified from the Ainley & Mathieson models

	$$Y = \left[\left(Y_P + Y_S\right)\left(\frac{R_e}{2\times10^5}\right)^{-0.2} + Y_{Tl} \right] \boldsymbol{c}_{Te}$$ χ_{Te} – same as Ainley & Mathieson model Profile loss: $$Y_P = \left[1+60\left(M_{out}-1\right)^2\right] \boldsymbol{c}_i Y_{P(i=0)}$$ χ_i and $Y_{p(i=0)}$ – same as Ainley & Mathieson model Secondary loss: $$Y_S = 0.0334\left(\frac{l}{H}\right)\left[4\left(\tan\alpha_{in}-\tan\alpha_{out}\right)^2\right]\left(\frac{\cos^2\alpha_{out}}{\cos\alpha_m}\right)\left(\frac{\cos\alpha_{out}}{\cos\alpha'_{in}}\right)$$ Tip leakage loss: $$Y_{Tl} = \begin{cases} 0.47\frac{l}{h}\left(\frac{\boldsymbol{t}}{l}\right)^{0.78} 4\left(\tan\boldsymbol{a}_{in}-\tan\boldsymbol{a}_{out}\right)^2\left(\frac{\cos^2\boldsymbol{a}_{out}}{\cos\boldsymbol{a}_m}\right) & stator \\ 0.37\frac{l}{h}\left(\frac{\boldsymbol{t}}{l}\right)^{0.78} 4\left(\tan\boldsymbol{a}_{in}-\tan\boldsymbol{a}_{out}\right)^2\left(\frac{\cos^2\boldsymbol{a}_{out}}{\cos\boldsymbol{a}_m}\right) & rotor \end{cases}$$	Design point Off-design points are calculated same as [Ainley & Mathieson, 1987] input data needed: α_{in}, α_{out}, α'_{in}, t'_{max}, M_{out}, l, τ, H, t, t', i
Kacker & Okapuu [1982]	Total loss: $Y = \chi_{Re} Y_p + Y_S + Y_{Tl} + Y_{te}$ $$\boldsymbol{c}_{\mathrm{Re}} = \begin{cases} \left(\frac{\mathrm{Re}}{2\times10^5}\right)^{-0.4} & \mathrm{Re} \le 2\times10^5 \\ 1.0 & 2\times10^5 > \mathrm{Re} < 10^6 \\ \left(\frac{\mathrm{Re}}{10^6}\right)^{-0.2} & \mathrm{Re} > 10^6 \end{cases}$$ Profile loss: $$Y_P = 0.914\left(\frac{2}{3}K_P \boldsymbol{c}_i Y_{P(i=0)} + Y_{shork}\right)$$ $$Y_{P(i=0)} = \left\{ Y_{P(\alpha'_{in}=0)} + \left|\frac{\alpha'_{in}}{\alpha_{out}}\right|\left(\frac{\alpha'_{in}}{\alpha_{out}}\right)\left[Y_{P(\alpha'_{in}=\alpha_{out})} - Y_{P(\alpha'_{in}=0)}\right]\right\}\left(\frac{t'_{max}/l}{0.2}\right)^{\frac{\alpha'_{in}}{\alpha_{out}}}$$ $$K_p = 1-1.25\left(M_{out}-0.2\right)\left(\frac{M_{in}}{M_{out}}\right)^2 \quad \text{for } M_{out} > 0.2$$ $$Y_{shock} = 0.75\left(M_{in,H}-0.4\right)^{1.75}\left(\frac{r_H}{r_T}\right)\left(\frac{p_{in}}{p_{out}}\right)\frac{1-\left(1+\frac{\gamma-1}{2}M_{in}^2\right)^{\gamma/\gamma-1}}{1-\left(1+\frac{\gamma-1}{2}M_{out}^2\right)^{\gamma/\gamma-1}}$$ $$M_{in,H} = M_{in}\left(1+K\left|\frac{r_H}{r_T}-1\right|^{2.2}\right)$$ χ_i – same as Ainley & Mathieson model Secondary loss: $$Y_S = 0.04\left(\frac{\tau}{H}\right)\chi_{AR}\left[4\left(\tan\alpha_{in}-\tan\alpha_{out}\right)^2\right]\left(\frac{\cos^2\alpha_{out}}{\cos^3\alpha_m}\right)\left(\frac{\cos\alpha_{out}}{\cos\alpha_{in}}\right)\left[1-\left(\frac{t_x}{H}\right)^2(1-K_P)\right]$$	Valid for DCA and MCA profiles and transonic flow. Design point Off-design points are calculated same as [Ainley & Mathieson, 1987] input data needed: α_{in}, α_{out}, α'_{in}, t'_{max}, M_{out}, l, τ, H, t, r_t, l_x, t', o, i

	$$c_{AR} = \begin{cases} 1 - 0.25\sqrt{2 - H/l} & for \quad H/l \le 2 \\ 1 & for \quad H/l > 2 \end{cases}$$ Tip leakage loss: Shrouded blades: $$Y_{Tl} = 0.37 \frac{l}{h} \left(\frac{t'}{l} \right)^{0.78} 4 \left(\tan \alpha_{in} - \tan \alpha_{out} \right)^2 \left(\frac{\cos^2 \alpha_{out}}{\cos \alpha_m} \right)$$ $\tau' = \tau / (\text{number of seals})^{-0.42}$ Unshrouded blades: $$\Delta h_{tt} = 0.93 \left(\frac{r_T}{r_m} \right) \left(\frac{1}{H \cos \alpha_{out}} \right) h_{tt,0} \, \Delta t$$	
Denton [1993]	Total loss: $$z = z_{Bb} + z_{Te} + z_{Tl} + z_{Eb} + z_{shock}$$ Profile loss: $$z_p = \frac{T_2}{\frac{1}{2} \rho V^2} \sum_s^p h \, C_s \int_0^1 \frac{C_d \rho V^3}{T} d(x/C_s)$$ Trailing edge loss: $$z_{Te} = -\frac{C_{pb} t'}{t \cos \alpha_{out}} + \frac{2\theta}{t \cos \alpha_{out}} + \left(\frac{\delta^* + t'}{t \cos \alpha_{out}} \right)^2$$ $$C_{pb} = (p_b - p_{in}) / (p_{c,in} - p_{in})$$ p_b (base pressure) -- can be calculated with Sieverding correlation θ and δ^* --- can be obtained with the relation by Baljé & Binsley [1968] Tip leakage loss: Shrouded blades: $$z_{Tl,R} = 2 \frac{\rho_2 V_2}{\rho_m V_m} \left(1 - \frac{\tan \beta_1}{\tan \beta_2} \sin \beta_2 \right)$$ Unshrouded blades: $$z_{Tl,R} = 1.5 \frac{t \, c}{H \, t \cos \alpha_2} \int_0^1 \left(\frac{V_s}{V_2} \right)^3 \left(1 - \frac{V_p}{V_s} \right) \sqrt{\left(1 - \left(\frac{V_p}{V_s} \right)^2 \right)} \; d(l/c)$$ Endwall loss (excluding secondary flow loss): $$z_{end} = \frac{T_2}{\frac{1}{2} \rho V^2} 0.25 \int_0^{c_x} \frac{C_d}{T} \frac{(V_s^4 - V_p^4)}{(V_s - V_p)} \rho y \; dx$$ Shock loss:	input data needed: α_{in}, α_{out}, t, C_d, C_S, H, l, p_b, t', o, V_{in}, V_{out}, τ, δ^*, θ, r_t

	$\zeta_{shock} = \frac{T_{out}}{\frac{V_{out}^2}{2}} C_v \frac{2g(g-1)}{3(g+1)^2}\left(M_{in}^2-1\right)^3$	
Craig & Cox [1970] (The most formulas are given by Håll [1990])	Total loss: $\zeta = \zeta_P + \zeta_S + \zeta_A$ Profile loss: $\zeta_P = \chi_R \chi_{Te} \chi_i \zeta_{P0} + \Delta\zeta_{P,M} + \Delta\zeta_{P,Se} + \Delta\zeta_{P,Tt}$ $\zeta_{p0} = \{\frac{t}{b_B}\cos\alpha_{out}(66.899F_L + 37.614C_R - 4.3348F_L^2 - 1.8038F_L C_R + \frac{497.93}{F_L} - \frac{114.37}{C_R} - 175.12)\}^{-1}$ $F_L = \frac{t}{b_B}(-1.3477*10^{-4}\alpha_{in}^2 + 2.956*10^{-3}\alpha_{in}\alpha_{out} - 3.0693*10^{-3}\alpha_{out} + 0.2535\alpha_{in} - 0.46384\alpha_{out} - 5.4895)$ $C_R = 1.0659 + 2.6963(1-\frac{\cos\alpha_{out}}{\cos\alpha_{in}})^2 - 1.1074(1-\frac{\cos\alpha_{out}}{\cos\alpha_{in}})\frac{t}{b_B} + 0.87386(1-\frac{\cos\alpha_{out}}{\cos\alpha_{in}})$ $b_B \approx l\frac{(\alpha_{in}-\alpha_{out})/2}{\sin(\alpha_{in}-\alpha_{out})/2}$ *parabola formate* $\chi_R = \begin{cases}1 & \mathrm{Re} > 10^5 \\ (\mathrm{Re}/10^5)^{0.055\log(\mathrm{Re})-0.54} & \mathrm{Re} < 10^5\end{cases}$ $\chi_{Te} = \{1 + 10.389(\frac{t'}{t})^2 + 0.074(\frac{t'}{t})\alpha_{out}$ $\Delta\zeta_{P,M} = \frac{o/t + t'/t}{2}(M_{out}-1)^2$ $\Delta\zeta_{P,Se} = -0.10699 + 0.1832(\frac{t}{r_e})^2 + 0.35665\frac{t}{r_e}M_{out} + 0.015552M_{out}^2 - 0.42797\frac{t}{r_e} + \frac{0.093753}{M_{out}}$ $\Delta\zeta_{P,Tt} = 1160(\frac{t'}{2})^3$ Off-design factor in profile loss: $\chi_i = 1 + (\frac{i-i_{min}}{i_{stal}-i_{min}})^2$ $i_{+stal} = i_{+bas} + i_{+sb} + i_{+CR}$ $i_{+bas} = 5.4188*10^{-3}\alpha_{in}\alpha_{out} - 4.9035*10^{-3}\alpha_{in}^2 - 0.017844\alpha_{out}^2 + 0.064328\alpha_{in} - 2.3766\alpha_{out} - 989.22/\alpha_{out} - 73.611$	Design and Off-design points F_L – blade lift parameter C_R – contraction ratio b_B – profile backbone length (camber length) r' – downstream radius F_i – incidence range ratio i_{min} – minimum loss incidence i_{+stal} – positive stall incidence i_{-stal} -- negative stall incidence input data needed: α_{in}, α_{out}, α'_{in}, t, H, l, t', o, e, M_{out}, V_{in}, V_{out}, r_t, i

$$i_{+sb} = 99.6 + 43.443(\frac{t}{b_B})^2 + 0.814\frac{t}{b_B}a_{out} + 6.9491*10^{-3}a_{out}^2 - 108.07\frac{t}{b_B} - 17.937\frac{b_B}{t} + \frac{198.35}{a_{out}}$$

$$i_{+CR} = 106.27 + 16.793C_R - 0.068C_R a_{out} - 71.466C_R + 0.182a_{out} - 46.293/C_R$$

$$i_{-stal} = i_{-bas} + i_{-sb}$$

$$i_{-bas} = 0.01267a_{in}^2 + 8.77*10^{-3}a_{in}a_{out} + 0.38352a_{in} - 0.30745_{out} - 18.587$$

$$i_{+sb} = 27.025 + 0.25632\frac{t}{b_B}a_{out} - 0.30139a_{out} - 25.88\frac{b_B}{t}$$

$$i_{\min} = \frac{i_{+atall} + F_i(i_{-stal})}{1+F_i}$$

$$F_i = 0.055759 + 1.0076*10^{-4}a_{in}(\frac{t}{b_B}) - 0.35031(\frac{t}{b_B})^2 - 0.012319a_{in} + 1.6388(\frac{t}{b_B})$$

Secondary loss:

$$\zeta_S = \chi_R \chi_{AR} \zeta_{S0}$$

$$z_{S0} = 0.0032F_L + (0.0288 + 0.0148F_L)(\frac{V_{in}}{V_{out}})^2$$

$$c_{AR} = \frac{b_B}{r_t - r_h}(1 - 0.1\frac{b_B}{r_t - r_h})$$

Tip leakage loss:

$$\Delta h_{Tl} = F_k \frac{A_k}{A_t} h_{t=0}$$

Annulus loss:

$$z_A = 0.025 + 2.9(0.85 - \frac{r_t^2 - r_h^2}{r'^2_t - r'^2_h})^2$$

Tip leakage loss:

$$\Delta h_{Tl} = F_k \frac{A_k}{A_t} h_{Tl=0}$$

Zhner [1980], and Petrovic & Riess [1995]	Total loss: same as [Traupel, 1977] Profile loss (design point): same as [Traupel, 1977] Profile loss (off-design points): Zehner model $z_p = 1-(1-z_{p(i=0)})e^{-a(\Delta i^*)^b}$ a=f_1(c, g), b=f_2(c, g) $g = \frac{f}{t}\sqrt{g(a'_{in}+a'_{out})}$ $\Delta i^* = i/(180-a'_{in})$ (from [Schobeiri & Abouelkheir, 1991]) $a = \begin{cases} 2.587-0.426g-1.216g^2 & i>0 \\ 0.446+3.82g-2.899g^2 & i<0 \end{cases}$ $b = \begin{cases} 4.175+10.802g-13.881g^2 & i>0 \\ 2.413+10.38g-10.116g^2 & i<0 \end{cases}$ Secondary loss: (same as Traupel, 1977] $z_r = \frac{z_p}{z_{p0}} F \frac{t}{H} + z_a$ $F = 0.0158\frac{V_{in}}{V_{out}}(a'_{in}+a'_{out})^{0.5} + 10^{-13}(a'_{in}+a'_{out})^5 \left[7.2(\frac{V_{in}}{V_{out}})^6 + 1.0\right]$ Tip leakage loss: same as [Traupel, 1977]	Use for through flow calculations Δi^* -- non-dimensional function of the incidence
Steewart et al [1060]	Total loss: $z = z_p + z_e + z_m$ Profile loss: $z_P = 1.8\frac{\frac{q}{l_c}\frac{l_c}{t\cos a_{out}}}{1-\frac{t'+d^*}{t\cos a_{out}}}$, $\frac{q}{l_c} = \frac{0.003}{1-1.4D_t}$ Endwall loss: $z_e = (1+\frac{t\cos g}{H})\, z_p$ Trailing edge mixing loss: $z_m = c_m\, z_p$	
Baljé & Binsley	Total loss:	

[1968]

$$z = z_p + z_e + z_{Tl} + z_{pa}$$

Profile loss (including trailing edge loss):

$$z_p = 1 - \frac{\dfrac{\cos^2 l_2 (1 - d^* - q^* - \frac{t_e}{t})^2}{(1 - d^* - \frac{t_e}{t})^2} + \sin^2 l_2 (1 - d^* - \frac{t_e}{t})^2}{1 + 2\sin^2 l_2 \left[(1 - d^* - \frac{t_e}{t})^2 - (1 - d^* - q^* - \frac{t_e}{t}) \right]}$$

$$q^* = \frac{q}{b_B} \frac{b_B}{l} \frac{l}{t \sin l_2} \quad , \qquad d^* = H_{bl} q^*$$

$$\frac{q}{b_B} = \begin{cases} 0.0021 \left[\dfrac{1 - (\sin l_2 / \sin l_1)^{4.5}}{1 - \sin l_2 / \sin l_1} \right]^{0.8} & \mathrm{Re} = 2x10^5 \\ 0.0021 \left[\dfrac{1 - (\sin l_2 / \sin l_1)^{4.5}}{1 - \sin l_2 / \sin l_1} \right]^{0.8} Cr & \mathrm{Re} / = 2x10^5 \end{cases}$$

$$Cr = \frac{71.0}{(\log_{10} \mathrm{Re})^{2.58}} + 1 - \tanh(1.96508 \log_{10} \mathrm{Re} - 8.51713)$$

$$\frac{b_B}{l} = \begin{cases} 0.7221988 + 0.005047357(l_1 - l_2) & (l_1 - l_2) > 55 \\ 1.0 & (l_1 - l_2) <= 55 \end{cases}$$

Endwall loss (endwll BL + secondary flow losses):

$$z_e = K_e \frac{l}{H} \{ \left[0.0388 (\frac{\sin l_2}{\sin l_1}) + 0.08) (1 + \frac{l_1 - l_2}{100}) \right] + 0.0003371 \left[10 (\frac{\sin l_2}{\sin l_1} + 0.08) \right]^{1.5 + \frac{l_1 - l_2}{160}} \}$$

$$K_e = \begin{cases} 0.3 & stator \\ 0.3 + \tanh(2.857 z_{eN}) & rotor \end{cases}$$

Tip leakage loss (unshrouded):

$$z_{Tl} = 0.0696 \tanh(13 \frac{t}{l}) \frac{l}{D} \frac{D}{H} \sin a_m (\cot l_2 - \cot l_1)$$

Disk friction loss:

Partial admission losses (ζ_{pa}):

Stager angle calculation:

if $\lambda_2 > (422.4465 - 7.993716\lambda_1 + 0.05545262 \lambda_1^2 - 0.000133964 \lambda_1^3)$:
$\gamma = 15.293 + 0.333845\lambda_1 - 0.0006696744 \lambda_1^2 + 0.4413227 \lambda_2 + 0.000266053\lambda_1^2 + 0.001201732\lambda_1 \lambda_2$
otherwise: $\gamma = \tan^{-1}[(2/(\cot \lambda_1 - \cot \lambda_2)]$

Design point only

$\lambda_1 = (\alpha'_1 - 90^0)$
$\lambda_2 = (90^0 - \alpha'_2)$
(tangential direction at pressure surface is the reference direction, i.e the angle turn from the pressure to suction surface)
deflection = $\lambda_1 - \lambda_2$

$H_{bl} = \delta/\theta$
boundary layer shape factor
(H=1.7 for turbulent flow [Denton, 1993, p. 9])

t_e – blade trailing edge thickness projection on plane of wheel
b_B—blade camber line
l -- chord

input data needed:
$\alpha'_{in}, \alpha'_{out}$, t, t', l_c, l, H, α_{in}, α_{out}, τ, D_t,

Moustapha et al [1990]	Off-design profile loss: $\Delta f^2 = \begin{cases} 0.778\times10^{-5}x' + 0.56\times10^{-7}x'^2 + 0.4\times10^{-10}x'^3 \\ \quad + 2.054\times10^{-19}x'^6 \quad for \quad 800 > x' > 0 \\ -5.1734\times10^{-6}x' + 7.6902\times10^{-9}x'^2 \quad for \quad 0 > x' > -80 \end{cases}$ $x' = \left(\frac{d}{t}\right)^{-1.6}\left(\frac{\cos\alpha'_{in}}{\cos\alpha'_{out}}\right)^{-2} i$ $Y = \frac{\left[1-\frac{g-1}{2}M_{out}^2\left(\frac{1}{f^2}-1\right)\right]^{\frac{-g}{g-1}}-1}{1-\left(1+\frac{g-1}{2}M_{out}^2\right)^{\frac{-g}{g-1}}}$ $\frac{Y_S}{Y_S^*} = \begin{cases} \exp(0.9x'') + 13x''^2 + 400x''^4, & 0.3 > x'' > 0 \\ \exp(0.9x''), & 0 > x'' > -0.4 \end{cases}$ $x'' = \frac{i}{180-(\alpha'_{in}+\alpha'_{out})}\left(\frac{\cos\alpha'_{in}}{\cos\alpha'_{out}}\right)^{-1.5}\left(\frac{d}{l}\right)^{-0.3}$	off-design loss calculation only

APPENDIX 2

General Information for Loss Models

Author	T/C	Types of losses	DP/ODP	Application Range	Notes
Ainley & Mathieson, 1951	T	TT=PR+SE+TL+TR	DP+ODP		
Baljé & Binsley, 1968	T	TT=PR+SE+TL	DP		
Boulter, 1962	T	SE			
Craig &Cox, 1970	T	TT=PR+SE+AN+OL	DP+ODP	Re<=2x10^6; ASP<=4	
Cecco et al, 1995	T	TL			
Denton, 1987, 1990, 1993	T/C	TT=PR+SE+TL+TR	DP		
Dunham, 1970		SE	DP		
Dunham & Came, 1970	T	TT=PR+SE+TL+TR	DP+ODP		
Ehrich & Detra, 1954		SE	DP		
Farn et al, 1991	T	TT		trns	Nu
Hawthorne, 1955		SE			
Kacker & Okapuu, 1982	T	TT=PR+SE+TL+TR	DP+ODP	Re<=10^6; ASP<=2; sbs+sps	
Kim & Chung, 1997	T	TL			
Kroon & Tobiasz, 1971	T	TT	DP+ODP	subsonic	
Lakshminarayana, 1970		TL			
Li & Ni, 1987	T	SE			
Martelli & Boretti, 1988	T	TT			Nu
Macchi & Perdichizzi, 1981	T	TT	DP+ODP		
Moustapha et al, 1990	T	PR, SE	ODP	Re<=10^6; ASP<=2; sbs+sps	
Mukhtarov & Krichakin, 1969	T	TT=PR+SE+TL	DP+ODP		
Okan & Gregory-Smith, 1992	T	SE	DP		
Schobeiri & Abouelkheir, 1992	T	PR	ODP		
Scholz, 1954	T	SE			
Sharma & Butler, 1987	T	SE	DP		
Smith, 1965	T	TT	ODP	0.6 <= M <=1.0	
Soderberg, 1949	T	TT=PR+SE+TL	DP		
Steward et al, 1960	T	PR, RE	DP		
Traupel, 1977	T	TT=PR+RS+FA+TL+DS	DP		
Wehner et al 1997	T	TL			
Yaras & Sjolander, 1992	T/C	TL			
Zehner, 1980	T	PR	ODP		

AN --- annulus loss
ASP --- aspect ratio
C --- compressor
DP --- design point
DS --- disc loss
FA --- fan loss
M --- Mach number
Nu --- Numerical method
OL --- Other losses
ODP --- off-design point
PR --- profile loss
RS --- rest loss
Re --- Reynolds number
sbs --- subsonic flow
sps --- supersonic flow
SE --- secondary flow loss
T --- turbine
TL --- tip leakage loss
TR --- trailing edge loss
TT --- total losses

APPENDIX 3

Parameters Used in Loss Models

Table 1: Design Profile Losses

Model	Compre-ssible	inlet angle	outlet angle	pitch	blade chord	blade span	max. thickness	M_{out}	M_{in}	Re	camber length	throat width	tip radius	hub radius	suction surface curvature	trailing edge thickness	flow velocity inlet	flow velocity outlet	flow velocity distribution	boundary layer condition	base pressure
Soderberg [1949]		x (blade)	x (blades)							x											
Ainley & Mathieson [1951]		x (blade)	x (flow)	x	x		x									x					
Stewart et al [1960]			x (flow)	x	x						x					x	x	x		x	
Baljé & Binsley [1968]		x (blade)	x (blade)	x	x					x	x					x				x	
Craig & Cox [1970]	x	x (flow)	x (flow)	x				x		x	x	x			x	x					
Dunham & Came [1970]	x	x (blade)	x (flow)	x	x		x	x		x						x					
Traupel [1977]	x	x (flow)	x (flow)	x				x		x						x					
Kacker & Okapuu [1982]	x	x (blade)	x (flow)	x	x		x	x	x	x			x	x		x					
Denton [1993]			x (flow)	x	x	x						x					x	x	x	x	x

Table 2: Off-Design Profile Losses

Model	incidence	blade inlet angle	blade outlet angle	flow inlet angle	flow outlet angle	pitch	blade chord	flow outlet angle	camber length	throat width	stagger angle	camber line curvature height	leading edge diameter
Ainley & Mathieson [1951]	x	x				x	x	x					
Craig & Cox [1970]	x	x	x	x	x	x			x	x			
Zehner [1980]	x	x	x			x					x	x	
Moustapha et al [1990]	x	x	x			x							x

Table 3: Secondary Losses

Model	Compre-ssible	flow inlet angle	flow outlet angle	blade inlet angle	blade outlet angle	pitch	blade chord	blade span	flow acceleration parameter	stagger angle	inlet boundary layer coefficient	Re	camber length	inci-dence	M_{in}	M_{out}	leading edge diameter	profile losses	flow velocity inlet	flow velocity outlet	axial distance between cascades
Soderberg [1949]							x	x				x									
Ainley & Mathieson [1951]		x	x	x					x												
Stewart et al [1960]						x		x		x								x			
Baljé & Binsley [1968]				x	x		x	x			x										
Craig & Cox [1970]		x	x	x		x		x	x			x	x						x	x	
Dunham & Came [1970]		x	x	x			x	x	x		x	x									
Traupel [1977]	x	x	x			x	x	x				x						x	x	x	x
Kacker & Okapuu [1982]	x	x	x	x			x	x	x		x				x	x					
Moustapha [1990]	x	x	x	x	x		x	x	x		x			x	x	x	x				

Table 4: Tip Leakage Losses

Model	tip clearance	flow inlet angle	flow outlet angle	blade inlet angle	blade outlet angle	pitch	blade chord	blade span	degree of reaction	blade diameter	camber length	amount of seals	velocity ratio	contraction coefficient	pressure inlet	pressure outlet	velocity distribution	velocity inlet	velocity outlet
Soderberg [1949]	x									x									
Ainley & Mathieson [1951]	x	x	x					x											
Baljé & Binsley [1968]	x			x	x		x	x		x									
Craig & Cox [1970]	x							x										x	x
Dunham & Came [1970]	x	x	x				x	x				x							
Traupel [1977]	x	x	x			x	x	x	x	x		x	x	x	x	x		x	x
Kacker & Okapuu [1982]	x	x	x				x	x		x									
Denton [1993]	x	x	x			x	x	x			x	x		x	x	x	x	x	x

Department of Energy Technology
Division of Heat and Power Technology
Royal Institute of Technology
SE-100 44 Stockholm, Sweden
Tel: +46 8 790 7467 (secretary)
Email: secr@egi.kth.se